UNIVERSITÀ
DEGLI STUDI
DI PADOVA

Sede Amministrativa: Università degli Studi di Padova

Dipartimento di Scienze Chimiche

Scuola di Dottorato di Ricerca in Scienze Chimiche

Indirizzo: Scienze Molecolari

XXIII CICLO

Synthesis and use of rigid peptide scaffolds

Coordinatore: Ch.mo Prof. Maurizio Casarin

Supervisore: Ch.mo Prof. Claudio Toniolo

Dottorando: Matteo De Poli

31 gennaio 2011

Research is to see what everybody else has seen,
and to think what nobody else has thought.
Albert Szent-Györgi (1893-1986)

Science may set limits to knowledge,
But should not set limits to imagination.
Bertrand Russell (1872-1970)

Love hides in molecular structures.
Jim Morrison (1943-1971)

INDEX

ABSTRACT

To understand in detail very complex natural systems with different inter- and intramolecular interactions or to create nanosystems with interestingly new properties like molecular recognition and information storage, it is often necessary to design model compounds of reduced complexity with well defined geometry. In this Ph.D. thesis it was decided to apply the properties of C^{α}-tetrasubstituted α-amino acids to fold into particularly stable 3_{10}-helical structures for the design of rigid templates and foldamers to be utilized in different spectroscopic and 3D-structural studies as well as in organic syntheses.

1. New spectroscopic techniques and helical peptides

A) 2D IR. We have combined two-dimensional infrared (2D IR) spectroscopy and isotope substitutions to reveal the vibrational couplings between a pair of amide-I and amide-II modes that are several residues away but directly connected through a hydrogen bond in a helical peptide. This strategy is demonstrated on a 3_{10}-helical hexapeptide and its ^{13}C, ^{18}O and ^{15}N labelled isotopomers in $CDCl_3$. The isotope-dependent amide-I/II cross peaks clearly show that the second and fourth peptide linkages are vibrationally coupled as they are in proximity, forming a 3_{10}-helical turn. This study reveals that the combination of 2D IR and isotope labelling is a useful approach to achieve structural information with residue-level specificity (in collaboration with the group of prof. N.-H. Ge, University of California, Irvine).

B) VCD. Coupling between the amide linkages in a peptide or protein is the key physical property that gives vibrational spectra and circular dichroism sensitivity to secondary structures. By use of rational ^{13}C isotopic labelling, the amide I band for selected residues was effectively isolated in the synthesized hexa- and octapeptides having dominant 3_{10}-helical conformations. The frequency and intensity responses were measured with IR absorption, vibrational circular dichroism, and Raman spectroscopies and simulated with DFT-based computations. Band fitting the spectral components was used to determine coupling constants. The sequential amide coupling for 3_{10}- helices is weaker than for α-helices, but larger than poly-$(Pro)_n$ type-II helices (in collaboration with the group of prof. T.A. Keiderling, University of Illinois, Chicago)

2. C^{α}-Methyl proline: a unique example of split personality

C^{α}-Methyl-L-proline is one of the most conformationally constrained α-amino acid. In this work, we examined the tendency of a number of N^{α}-acyl dipeptide N'-alkylamides of the type RCO-(αMe)Pro-Xxx-NHR' or RCO-Xxx-(αMe)Pro-NHR', in which Xxx is L (or D)-Ala, Aib, or L (or D)-(αMe)Pro, long enough to fold into intramolecularly hydrogen-bonded γ- or β- turns. The results are compared with those obtained for the corresponding dipeptides based on Pro, a well-known turn-forming residue. We used FT-IR absorption, ^{1}H and ^{13}C NMR spectroscopies and X-ray diffraction for a detailed conformational analysis. We conclude that (αMe)Pro is able to explore both *trans*' and *cis*' ψ areas of the conformational space, but in (αMe)Pro the latter is overwhelmingly more populated, in marked contrast to the Pro preference. This finding is a clear indication that in (αMe)Pro the major 3D-structural determinant is the C^{α}-methyl group. The electronic circular dichroism signature of a peptide type-III' β-turn conformation is also proposed.

3. Macrocyclizations on helical peptides

By taking advantage of the research period spent in the groups of prof. R.H. Grubbs and prof. D.J. O'Leary (California Institute of Technology, Pasadena, and Pomona College, Claremont, California, respectively), we used the olefin metathesis reaction to build up the *first 3_{10}-helical bis-peptide bundle* (*ladder peptide*). In this chapter we report the synthesis and preliminary conformational characterizations of this large peptide macrocycle rich in Aib. In order to obtain an α-amino acid to be used as a linker in the preparation of the ladder peptide, we first evaluated the possibility of incorporating an allyl moiety into an α-amino acid side-chain without loss of optical activity. After having tried different approaches, Asp appeared to be best choice. The synthesis of the ladder peptide was accomplished *via* solution-phase methods and the RCM-derived macrocycle was subjected to conformational analysis with FT-IR absorption, NMR and ECD spectroscopies. Preliminary results suggest this cyclic peptide to be largely 3_{10}-helical, confirming the high propension of Aib-containing peptides to form ordered secondary structures. Two major confomers were detected by NMR in DMSO solution. A model involving a tilting motion between helices was tentatively proposed to account for this result, though further analyses are needed to confirm such hypothesis.

RIASSUNTO

Per comprendere in dettaglio sistemi naturali molto complicati, con diverse relazioni inter- ed intramolecolari, oppure per creare nuovi nanosistemi con proprietà quali il riconoscimento molecolare o la conservazione di informazioni è necessario poter progettare e sintetizzare molecole modello di complessità ridotta nonchè una struttura tridimensionale ben definita. In questa Tesi di Dottorato è stato deciso di applicare la capacità degli α-amminoacidi C^{α}-tetrasostituiti di formare strutture 3_{10}-elicoidali particolarmente stabili, al fine di disporre di peptidi rigidi utili per studi di tipo spettroscopico, conformazionale e per applicazioni in sintesi organica.

1. Nuovi tipi di spettroscopie e sistemi peptidici rigidi

A) 2D IR. La spettroscopia di assorbimento infrarosso a due dimensioni (2D IR), insieme alla marcatura isotopica hanno permesso di rivelare gli accoppiamenti vibrazionali esistenti tra i modi ammide-I e ammide-II di residui distanti tra loro ma direttamente connessi attraverso un legame a idrogeno. Questa strategia è stata dimostrata su un peptide elicoidale di tipo 3_{10} ed i suoi isotopomeri marcati con ^{13}C, ^{18}O e ^{15}N. Grazie ai picchi fuori diagonale, riconoscibili dalla marcatura isotopica, si è dimostrato che i modi ammide I e II del secondo e quarto legame peptidico sono accoppiati vibrazionalmente, in quanto formano un ripiegamento elicoidale stabile di tipo 3_{10}. Con questo studio si è messo in evidenza che il 2D IR unito ad una opportuna marcatura isotopica può essere un metodo utile per ottenere informazioni strutturali già a livello di singolo residuo (in collaborazione con il gruppo della prof.ssa N.-H. Ge, University of California, Irvine).

B) VCD. Gli accoppiamenti che si instaurano tra legami ammidici sono alla base della capacità della spettroscopia di assorbimento FT-IR o del dicroismo circolare elettronico di distinguere tra varie strutture secondarie di peptidi o proteine. Grazie all'uso della marcatura sito-specifica mediante ^{13}C, si è potuto isolare la banda dell'ammide I in spettri di esa- ed ottapeptidi aventi conformazione elicoidale di tipo 3_{10}. Frequenza ed intensità di tali assorbimenti sono state misurate attraverso spettroscopia Raman, assorbimento FT-IR e VCD e successivamente simulate con calcoli DFT. Le costanti di accoppiamento sono state ottenute grazie al *fitting* dei componenti delle bande spettrali.

L'accoppiamento sequenziale ottenuto per eliche di tipo 3_{10} è più debole di quello nelle α-eliche, ma maggiore di quello ottenuto per la poli-$(Pro)_n$ di tipo II (in collaborazione con il gruppo del prof. T.A. Keiderling, University of Illinois, Chicago).

2. C^{α}-metilprolina: un particolare caso di doppia personalità

La C^{α}-metilprolina è uno degli α-ammino acidi conformazionalmente più ingombrati. In questo lavoro si sono esaminate le preferenze conformazionali di un vasto numero di N^{α}-acil dipeptidi N'-alchilammidi del tipo RCO-(αMe)Pro-Xxx-NHR' o RCO-Xxx-(αMe)Pro-NHR' (con Xxx = L (o D)-Ala, Aib, oppure L (o D)-(αMe)Pro) sufficentemente lunghi per dare ripiegamenti di tipo γ o β stabilizzati da legami a idrogeno intramolecolari. I risultati ottenuti sono stati confrontati con quelli dei corrispondenti dipeptidi basati sulla Pro, residuo che notoriamente tende a dare tali ripiegamenti. Mediante le spettroscopie di assorbimento FT-IR, ^{1}H e ^{13}C NMR nonchè la diffrazione ai raggi X è stata condotta un'analisi strutturale dettagliata, grazie alla quale si desume che l'(αMe)Pro è in grado di esplorare entrambe le zone *trans*' e *cis*' dello spazio conformazionale. Tuttavia, quest'ultima zona è considerevolmente più popolata nel caso dell'(αMe)Pro, in netto contrasto con quanto accade per la Pro. Questo fatto è una indicazione piuttosto chiara del fatto che nell'(αMe)Pro è il metile sul C^{α} a dirigere le preferenze conformazionali di questo α-ammino acido. In base a tali risultati è stato proposto l'andamento caratteristico dello spettro ECD per un ripiegamento β di tipo III'.

4. Macrociclizzazioni su eliche peptidiche

In seguito al periodo trascorso in qualità di *visiting student* presso il gruppo di ricerca dei proff. R.H. Grubbs e D.J. O'Leary (California Institute of Technology e Pomona College, rispettivamente) si è voluto esplorare l'uso della reazione di metatesi olefinica nella costruzione del primo fascio bis-peptidico 3_{10}-elicoidale (*ladder peptide*). In questo capitolo viene riportata la sintesi ed alcune prime indagini conformazionali di questo macrociclo peptidico ricco di residui di Aib. Nella prima parte del lavoro si è valutata la possibilità di inserire un'unità allilica in catena laterale di un α-ammino acido senza problemi di racemizzazione. Dopo vari tentativi, è stato scelto Asp come α-ammino acido avente funzione di *linker* nella preparazione del fascio peptidico. La

sintesi del *ladder* è proseguita con metodi in soluzione e il macrociclo ottenuto attraverso RCM è stato sottoposto a una prima analisi conformazionale in soluzione mediante assorbimento FT-IR, spettroscopia NMR e ECD. I risultati sinora ottenuti indicano che questo peptide tende ad assumere una conformazione elicoidale di tipo 3_{10} in soluzione, confermando quanto atteso per sequenze peptidiche ricche di Aib. Dall'analisi NMR, inoltre, si evince la presenza di un equilibrio tra due conformeri maggioritari in soluzione di DMSO. Nonostante siano necessari ulteriori dati per confermare tale ipotesi, si è tentato di spiegare tale effetto mediante l'instaurarsi di una rotazione reciproca tra le due eliche peptidiche.

ABBREVIATIONS

(αMe)Pro	=	C^{α}-methylproline
(αMe)Ser	=	C^{α}-methylserine
2D IR	=	two-dimensional infrared absorption
Ac	=	acetyl
Ac_2O	=	acetic anhydride
Aib	=	α-aminoisobutyric acid
Al	=	allyl
Ala	=	alanine
Asp	=	aspartic acid
Boc	=	*tert*-butyloxycarbonyl
Bzl	=	benzyl
COSY	=	correlation spectroscopy
DFT	=	density functional theory
DIPEA	=	N,N-di*iso*propylethylamine
DMAP	=	4-dimethylaminopyridine
DMF	=	N,N-dimethylformamide
DMSO	=	dimethylsulphoxyde
e.e.	=	enantiomeric eccess
ECD	=	electronic circular dichroism
EDC	=	N-ethyl-N'-(3-dimethylamino)propyl-carbodiimide
ESI	=	electron-spray ionization
Et_2O	=	diethyl ether
EtOAc	=	ethyl acetate
EtOH	=	ethanol
FT-IR	=	Fourier transform infrared spectroscopy
Gly	=	glycine
h(s)	=	hour(s)
H-bond	=	hydrogen bond
HFIP	=	1,1,1,3,3,3-hexafluoro-2-propanol
HOAt	=	1-hydroxy-7-azabenzotriazol
HOBt	=	1-hydroxybenzotriazol
HPLC	=	high performance liquid chromatography
HPLC-MS	=	HPLC coupled with mass spectrometry
Hse	=	homoserine
*i*Bu	=	*iso*butyl
*i*Pr	=	*iso*propyl
*i*PrCO	=	*iso*butiryl
FT-IR	=	Fourier transform infrared absorption
Leu	=	leucine
MeCN	=	acetonitrile
MeOH	=	methanol
MS	=	mass spectrometry
NMM	=	N-methylmorpholine
NMR	=	nuclear magnetic resonance
NOESY	=	nuclear Overhauser effect spectroscopy
OMe	=	methoxy
OSu	=	N-hydroxysuccinimide
O*t*Bu	=	*tert*-butoxy
*p*BrBz	=	4-bromobenzoyl
PE	=	petroleum ether

Piv	=	pivaloyl
ppm	=	parts per million
Pro	=	proline
RCM	=	ring-closing metathesis
Rf	=	retention coefficient
ROESY	=	rotating frame Overhauser effect spectroscopy
Ser	=	serine
TEA	=	triethylamine
TFA	=	trifluoroacetic acid
TFE	=	2,2,2-trifluoroethanol
THF	=	tetrahydrofuran
TLC	=	thin layer chromatography
$TMSCHN_2$	=	trimethylsilyldiazomethane
TOCSY	=	total correlation spectroscopy
UV-Vis	=	ultraviolet – visible spectroscopy
VCD	=	vibrational circular dichroism
Z	=	benzyloxycarbonyl

P.S. The chiral amino acids are in the configuration L (*S*) if not otherwise specified.

1. Introduction

The study of novel phenomena and processes at the molecular level provides useful information for the design of a wide range of tools, materials, devices and systems with unique characteristics. Nanostructured materials and nanodevices are irreplaceable in biomedical research and technologies because of their numerous and diverse applications[1]. To be able to synthesize and process complex nanomaterials with enhanced properties it is overwhelmingly important to prepare and to study structures of reduced complexity. Such model structures should be conformationally constrained in given conditions, such as solvent, temperature, pH, etc. This property is relevant for a correct assessment of the distances and relative orientations of the molecular groups or the functional parts studied. To this end, numerous pathways inspired by biological systems have been adopted, including the design of molecular rulers based on α-amino acids[2]. Peptides as self-assembling smart materials have an enormous potential. Sequence manipulations enable the design of a number of different structures that can be developed for many important applications, including tissue repair, miniaturized solar cells, and optical and electronic devices. Peptides offer attractive features, principally because of our acceptable knowledge of their ability to fold into specific structures, and of the rich chemistry with which their 3D-structure and function can be manipulated. Peptides also offer the ability to incorporate non-coded amino acids or non-peptidic moieties, which is a particularly valuable feature for the inclusion of function and/or smartness in the scaffold (i.e. a photoswitch or a non-peptide ligand). Notwithstanding the evident advantages of peptides for this purpose, it is not very easy to predict the structure of a peptide formed by proteinogenic α-amino acids. Another drawback of these amino acids is the requirement of rather long main-chain length for the formation and full development of a given polypeptide structure. The ability to form highly rigid and well developed 3_{10}-

helices by C^{α}-tetrasubstituted α-amino acids (**Fig. 1.1**) under appropriate conditions is very useful for creating short and precisely conformationally tunable peptide scaffolds.

Besides the classical α-helix, β-sheet and β-turn conformations, the 3_{10}-helix represents the fourth principal structural element occurring in globular proteins and has been described at atomic resolution in model peptides and in peptaibol antibiotics[3].

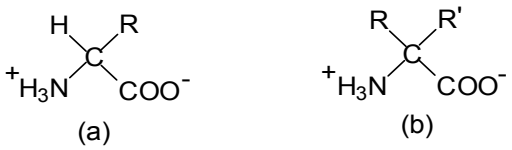

Fig. 1.1 Chemical structures of C^{α}-tri- (a) and (b) tetrasubstituted amino acids.

The helical conformations differ by the number of residues per turn, the pitch, the φ, ψ, ω torsion angles in the peptide backbone[4,5] (**Fig. 1.2**), and the number of the atoms in the *pseudo*-rings formed by the C=O···N-N intramolecular H-bonds.

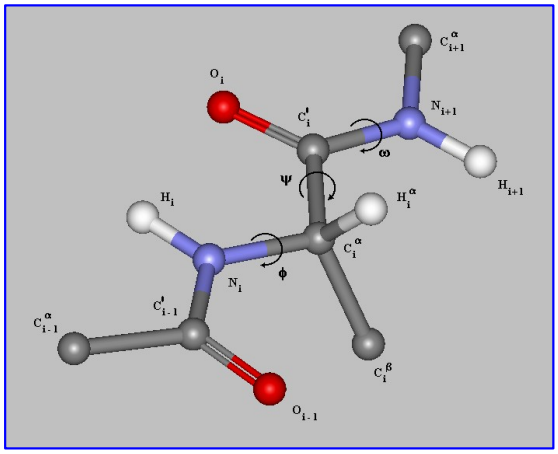

Fig. 1.2 Representation of a segment of polypeptide chain in the fully-extended conformation ($\phi_i = \psi_i = \omega_i = 180°$).

The α-helix is characterized by 3.63 residues per turn and it is stabilized by intramolecular H-bonds between the carbonyl group of a residue at position *i* and the

N-H group at the $i + 4$ position, forming the *pseudo*-rings of 13 atoms (α-turns or C_{13}-structures).[6] The 3_{10}-helical structure has 3.24 residues per turn. The intramolecular H-bonds are formed between the oxygen of the carbonyl group at position i and the N-H group at position $(i + 3)$ with the onset of *pseudo*-rings of 10 atoms (β-turns or C_{10}-structures) (**Table 1.1**). Thus, the average conformational parameters of the 3_{10}-helix are close to those of the α-helix, but the former helix is slightly tighter and more elongated (**Fig. 1.3**).

A 3_{10}-helix formed by C^{α}-trisubstituted (protein) α-amino acids is less stable than the α-helix due to the larger distortion of the H-bonds and some unfavorable van der Waals interactions.[7-9] Though the 3_{10}-helical structure would not be widespread, nevertheless it is not rare. The recent improvements in analytical techniques allowed to identify the 3_{10}-helical patterns in numerous natural proteins.[10-12] Some transmembrane channel-forming antibiotics, such as alamethicin, have a high content of 3_{10}-helices.[13]

A statistical analysis of the X-ray diffraction structures of 57 globular proteins revealed the presence of 71 3_{10}-helical motifs of different length. Interestingly, in most cases such structures were found at the N- and C-termini of α-helices; moreover, 3_{10} helices have been proposed as intermediates of the random coil – α transition process[14] and the 3_{10} structure is observed as picosecond intermediate in simulation studies of α-helix melting.[15,16]

Table 1.1 Structural parameters for the α- and 3_{10}-helical conformations.[6]

Parameter	3_{10}-Helix	α-Helix
Φ	-57°	-63°
Ψ	-30°	-42°
number of residues per turn	3.24	3.63
pitch	6.29 Å	5.67Å

The main β-turn patterns were classified by Venkatachalam[17] as types I, II, and III (**Fig. 1.4**), depending on the values of the φ, ψ torsion angles of the $(i + 1)$ and $(i + 2)$ residues (**Table 1.2**). Repeating type III β-turns leads to the formation of the right-handed 3_{10}-helical structure, while the other two types of β-turns are not helix forming.

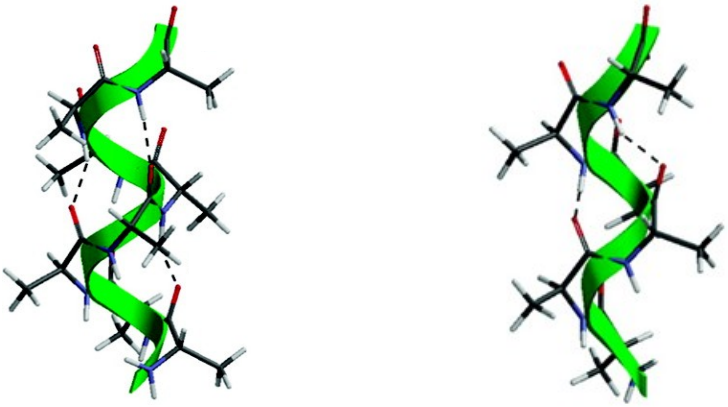

right-handed α-helix right-handed 3_{10}-helix.

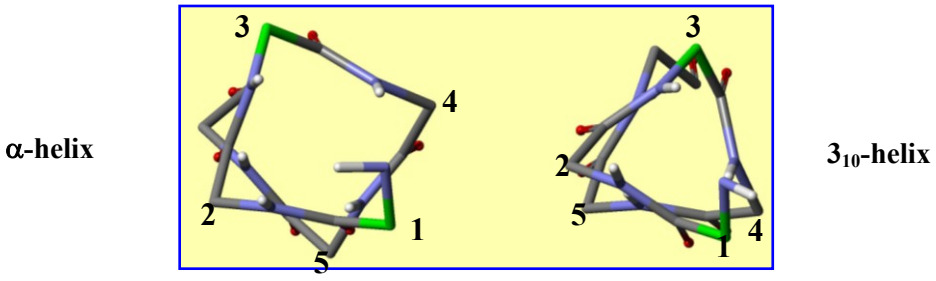

Fig. 1.3 Models of the α- and 3_{10}-helical conformations (*top*: side view; *bottom*: view along helix axis).

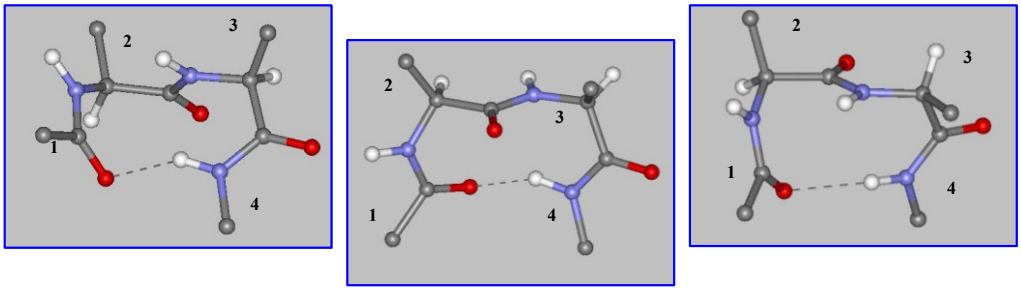

Fig. 1.4 Representation of the β-turn (type I, II and III) structure with the central amide bond in the *trans* conformation.

Table 1.2 Torsion angle values for the three types of β-turns

β-Turn	φ (*i* + *1*)	ψ (*i* + *1*)	φ (*i* + *2*)	ψ (*i* + *2*)
Type I	-60°	-30°	-90°	0°
Type II	-60°	+120°	+80°	0°
Type III	-60°	-30°	-60°	-30°

In contrast to the C^{α}-trisubstituted (protein) α-amino acids, the C^{α}-tetrasubstituted α-amino acids are extremely strong promoters of 3_{10}-helical structures. The study of the conformational preferences of the peptides rich in different C^{α}-tetrasubstituted amino acids and their possible applications have been the main subjects of the work of the research group headed by Prof. C. Toniolo (University of Padova) since 1980.[18-21]

C^{α}-Tetrasubstituted amino acids differ from protein amino acids by the substitution of the hydrogen at the α-carbon atom by an alkyl or an aryl group. The noticeable sterical hindrance induced by these substituents drastically limits the N-C^{α} and C^{α}-C' (φ and ψ torsion angles, respectively) bond rotations.[22,23]

In the case of the peptides containing the simplest C^{α}-tetrasubstituted α-amino acid (Aib, α-amino isobutyric acid) and protein amino acids as well, in the crystal state only helical structures of the α-, 3_{10}- or α/3_{10}-"mixed" type were found.[24,25] For the Aib-based oligopeptides also the second longest 3_{10}-helix known so far [(*p*BrBz-$(Aib)_{10}$-O*t*Bu)] was obtained in the Padova laboratory (**Fig. 1.5**). The main factors which bias the peptide conformational preference toward a specific type of helix are the length of the polypeptide chain, the Aib content, and the amino acid sequence. In general, the α-helix formation tends to be favored when the main chain is lengthened and the number of Aib residues is decreased. Very short peptides (up to 6 residues) with a large amount of Aib residues show a strong tendency for 3_{10}-helix formation.[26]

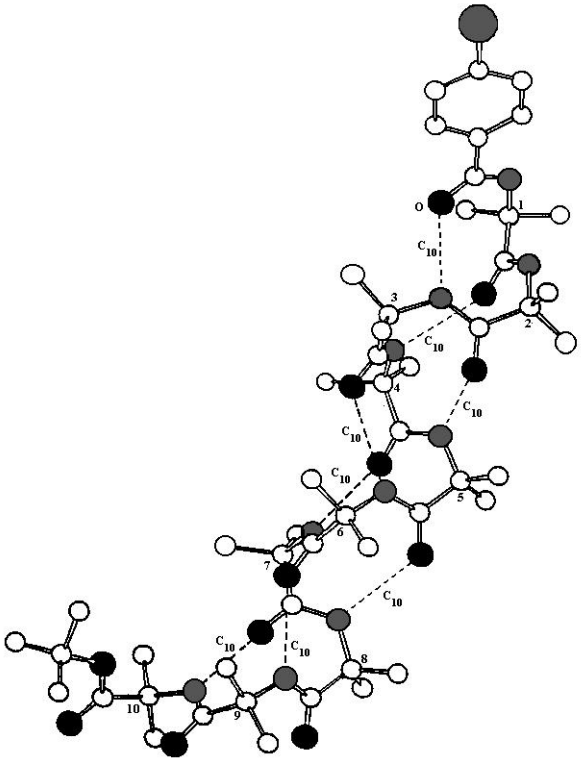

Fig. 1.5 X-ray diffraction structure of *p*BrBz-$(Aib)_{10}$-O*t*Bu
(intramolecular C=O···H-N H-bonds are shown as dashed lines).

Being achiral the Aib residue does not induce any preferred sense of spiralization in the peptide. As in the case of protein amino acids, in the peptides based on C^{α}-tetrasubstituted α-amino acids the helix sence is strongly influenced by the nature of side-chains. In the peptides containing C^{α}-tetrasubstituted α-amino acids with linear or β- or δ-branched side chains, the sense of spiralization follows the common rules of protein amino acids (L-residues induce a right-handed helix), while γ-branched side-chains tend to promote the opposite handedness. An exception is C^{α}-methyl isovaline (with one methyl and one ethyl side chain), which does not show any noticeable screw sense preference.

Highly ordered 3_{10}-helical structures are very promising tools for detailed studies of a variety of different biochemical and biophysical fundamental processes. In these cases, the rigid helices can be used as templates or spacers[27], which serve to direct and orient two or more labels into desired topologies.

In this Ph.D. thesis it was decided to apply the properties of C^{α}-tetrasubstitution in α-amino acids to form particularly stable 3_{10}-helical structures for different applications. In particular, they span from (*i*) their use as viable tools for the calibration of two new and promising spectroscopic techniques (2D IR and VCD), (*ii*) the estimation of the conformational preferences of foldamers based on one of the most sterically hindered C^{α}-tetrasubstituted α-amino acid (C^{α}-methyl-L-proline) and to (*iii*) their use as scaffolds for RCM-derived macrocyclizations.

2. New spectroscopic techniques and helical peptides

Infrared absorption spectroscopy is a widely used technique for determining the secondary structure and conformational changes of both short peptides and proteins.[28,29] It is based on the molecular vibration (and rotation) excited by the electromagnetic field in the region of infrared (IR) waves (with λ comprising the 780 nm – 2000 μm region). Characteristic bands found in the infrared absorption spectra of proteins and peptides include the amide I and amide II (**Fig. 2.1**)

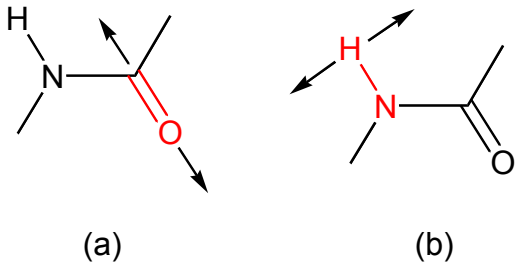

Fig. 2.1 Vibrational modes of the amide bond: amide I (a) and amide II (b).

These bands arise from the amide bonds that link the amino acids in a polypeptide. The absorption associated with the amide I band is caused by stretching vibrations of the C=O bond of the amide group, while overwhelmingly bending vibrations of the N-H bond lead to the absorption associated with the amide II band. Because both the C=O and the N-H bonds are involved in the H-bonding that takes place between the different elements of the peptide secondary structure, the locations of the amide I and amide II bands are sensitive to the conformation.[30-32]

The amide I band is the most studied protein vibration. Empirical frequency-structure correlations find that β-sheets have a strong absorption band at 1610-1640 cm^{-1} and a weaker band at 1680-1690 cm^{-1}. The α-helix and random coil structure are located at 1640-1650 and 1650-1660 cm^{-1}, respectively.[33,34] The origin of these band shifts is a strong coupling between individual amide I units, which gives rise to

delocalized or excitonic vibrational states that report on the symmetry and size of secondary structure.[29,32] While antiparallel β-sheets and aggregates give rise to distinct diagnostic amide I bands,[35] other secondary structures are poorly resolved in an amide I line shape with multiple contributions. The α-helical structure is predicted to have three IR active amide I modes, but their splittings are on the order of a few cm^{-1} and their detailed features are not resolvable.

The amide II vibration, due to its composition of N-H bend and C-N stretch, is predominantly known for its sensitivity to the protonation state of the peptide unit.[30] Despite early predictions of Miyazawa and Blout[36] that amide II would exhibit sensitivity similar to that of amide I, the amide II band is relatively unstructured and varies little with secondary structure. In the case of amide II', the congested nature of the linear IR spectrum make its use impractical as a structural diagnostic.

Therefore, most IR absorption conformational studies have been focused on the amide I band.[33,34] However, IR absorption spectroscopy is a low-resolution technique and it has the practical limitation of congested line shapes for studying peptides and proteins. It is limited to the determination of the *overall* secondary structural content and does not allow the distinction between different structures at the *residue* level.

Unlike traditional protein IR absorption spectroscopy, emerging methods in two-dimensional infrared (2D IR) spectroscopy are providing substantially more detailed methods for analyzing the structural and dynamical information content of amide vibrations.[28,35,37-44] 2D IR spreads IR transitions over two frequency axes and reveals cross peaks that quantify vibrational couplings and other correlations between vibrations. The combination of enhanced spectroscopic sensitivity and a new generation of structure-based amide spectroscopic models[37,45-48] is leading to a toolset that can be used for the quantitative study of time-dependent protein conformation.[49] This technique is one of a rapidly expanding class of new ultrafast coherent vibrational spectroscopies[50-53] that are finding broad use in studies of molecular structure and dynamics that probe peptides,[38] proteins,[28,35,42 ,54] DNA,[55] chemical exchange kinetics,[56,57] hydrogen bonding,[58,59] and rapidly initiated chemical reactions.[54,60,61]

Inspired by pulsed NMR techniques, 2D IR spreads a vibrational spectrum over two frequency axes to reveal vibrational couplings through cross peaks. A 2D IR spectrum correlates the frequency of vibrational excitation ω_1 (also called ω_τ or ω_{pump}) with the frequency of detection ω_3 (or ω_t or ω_{probe}). Diagonal peaks can be assigned to

chemically distinct normal vibrational modes or eigenstates. The presence and splitting of cross peaks characterizes the anharmonic couplings between vibrations. Connectivity, distance, or orientation between chemical bonds can be extracted by modeling vibrational couplings.[62] Positive and negative amplitude features in 2D IR spectra, corresponding to induced absorption or stimulated emission processes in the detection step, characterize the vibrational anharmonicity. Since the measurement is made with a picosecond or faster "shutter speed", it captures this structural information on a faster time scale than the evolution of most protein dynamics. 2D IR diagonal and antidiagonal line widths report on inhomogeneous and homogeneous broadening, respectively, and can be analyzed in more detail to describe variance in structural parameters.[63] From its first realizations, 2D IR has been applied to the amide I backbone vibrations of proteins,[37] and for extracting structural information about peptides and small molecules.[38,62] However, the use of multimode 2D IR spectroscopy that investigates cross-correlations between different amide vibrations opens entirely new possibilities for enhancing structural information in protein vibrational spectra.

Several spectroscopic techniques are useful for solving structures of biological molecules in solids, solutions, and membranes.[64] In fact, ECD and VCD techniques and 2D NMR measurements have successfully identified 3_{10}-helical structures of synthetic model oligopeptides in nonaqueous solution phases.[65-68] Because of insufficient time resolution, however, these techniques cannot discriminate between these two helices during the earliest steps of helix formation processes. Although time-resolved, linear-IR absorption spectroscopy can be performed on femtosecond and picosecond time scales, a diagnostic peak frequency of the amide I band is often ambiguous, especially for short 3_{10}- and α-helix structures.[69,70] The IR absorption peak frequency is influenced by several factors, including helical length, types of amino acid residues, structural deformation, and solvent exposure. An *ab initio* DFT study also shows that the amide I maximum in linear-IR spectra cannot be used to discriminate between 3_{10}- and α-helices.[71]

The 3_{10}-helix constitutes a small but significant percentage of secondary structural elements in proteins.[6,72] According to a general survey of protein structures, about 10% of all helices adopt the 3_{10}-helical conformation which is mainly observed at the termini of α-helices, in loops, and as connectors between β-strands and plays

important functional roles in several proteins.[73-75] Moreover, the 3_{10}-helix structure has recently been proposed as an intermediate in the folding of α-helices[14,72].

Two-dimensional IR spectroscopy is one of the most promising techniques for studying peptide conformation and 3_{10}- to α-helix transition, as shown in previous works from our group[76-78] conducted in collaboration with Prof. Nien-Hui Ge at the University of California, Irvine.

In the first case studied, an extensive set of 2D IR spectra of C^{α}-methylated homopeptides, Z-$(Aib)_n$-O*t*Bu (n = 3, 5, 8, and 10), in $CDCl_3$ was measured in the amide-I region. The 2D IR spectral patterns of the tripeptide are quite different from those of the longer peptides. The spectral signatures begin to converge at the pentapeptide and become almost the same for the octa- and decapeptide (**Fig. 2.2**), while the onset of the 3_{10}-helical secondary structure appears to already occur at the pentapeptide level.

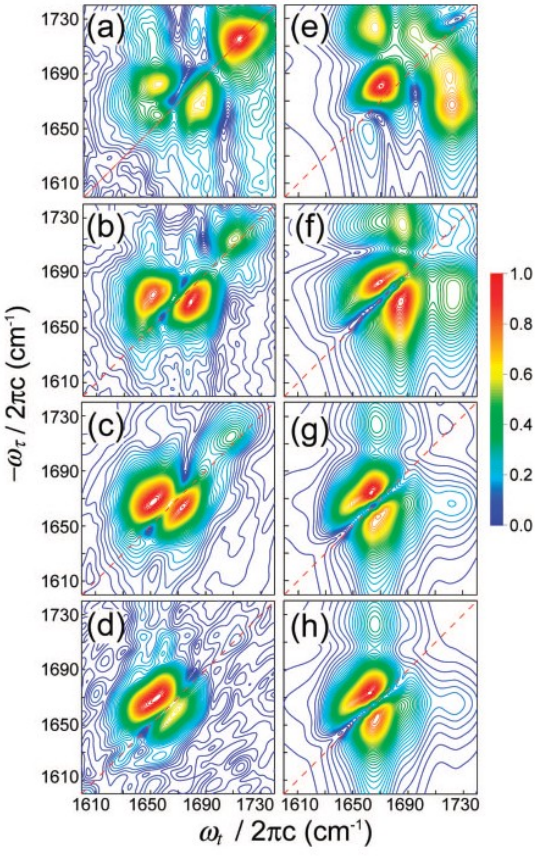

Fig. 2.2 Measured (a-d) and simulated (e-h) cross-peak patterns of Z-$(Aib)_n$-O*t*Bu in $CDCl_3$. n = 3 (a, e); 5 (b, f); 8 (c, g); and 10 (d, h).

In the second application, the solvent dependent,[67,72] 3_{10}- to α-helical conformational transformation of the homo-octapeptide Ac-[L-(αMe)Val]$_8$-O*t*Bu[79] is revealed by the use of 2D IR.

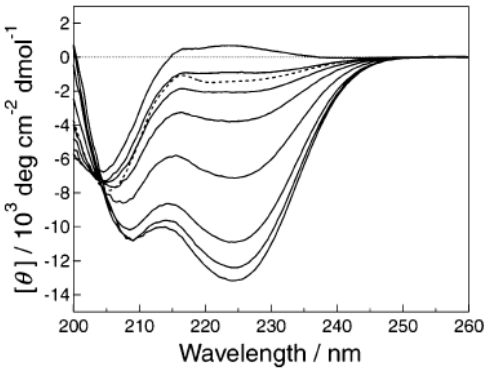

Fig. 2.3 Time-dependent ECD spectrum of Z-[L-(αMe)Val]$_8$-O*t*Bu in TFE solution.

The transition, which has also been followed by ECD (**Fig. 2.3**),[79] was detected by the different spectral signatures of 3_{10}- and α-helices in the amide I region. During the conformational change underwent by the peptide studied, its 2D rephasing spectrum evolves from an elongated doublet, characteristic of a distorted 3_{10}-helix, to a multiple-peak pattern, after becoming an α-helix (**Fig. 2.4**).

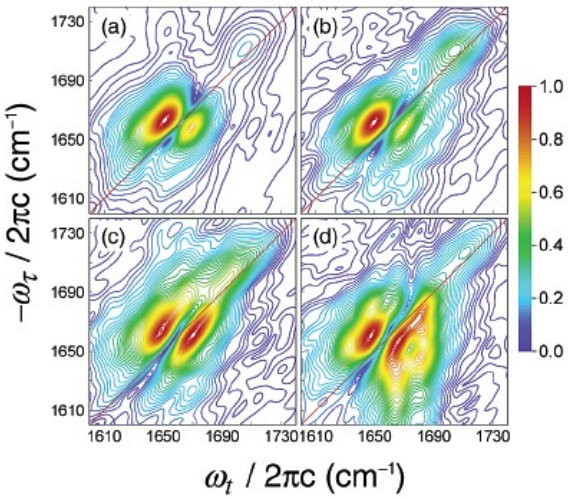

Fig. 2.4 2D IR absolute magnitude spectra of Z-[L-(αMe)Val]$_8$-O*t*Bu in different solvents: (a) $CDCl_3$; (b) TFE; (c,d) HFIP. The spectra in HFIP were measured (c) immediately and (d) 34 days after sample preparation.

These results makes 2D IR a powerful technique that can distinguish the subtle conformational differences between 3_{10}- and α-helices with a picosecond time resolution. The doublet cross-peak pattern is characteristic to the 3_{10}-helix structure but contains no residue-specific information.

To elucidate the intramolecular hydrogen bonding pattern and hence the difference between 3_{10}- and α-helix at the residue level, we decided to devise a strategy to directly probe the vibrational modes that are coupled through a specific C=O···H−N hydrogen bond using 2D IR on isotopically-labelled, rigid peptides in collaboration with the group headed by Prof. Ge.

Vibrational couplings between amide modes of peptide linkages are sensitive to the underlying structure, but direct probing of vibrational couplings between two hydrogen-bonded peptide linkages is not straightforward. In this chapter, we demonstrate achieving this task in a 3_{10}-helix through a combination of two-dimensional infrared (2D IR) spectroscopy and isotope editing (with ^{13}C, ^{15}N and ^{18}O) of amide-I and amide-II modes. The isotope-dependent cross-peaks can provide valuable information on local secondary structure, such as the formation of a single helix turn, important for studying protein folding processes.

In order to discern amide vibrational modes, we synthesized model peptides containing ^{13}C-, ^{15}N- and ^{18}O-labelled α-amino acids. Isotope substitution with $^{13}C=^{18}O$ proved to be useful in isolating a local amide-I mode[80], observing its couplings to other modes,[81,82] and probing local structure and dynamics. Isotope labelling the hydrogen bonding partner with N−D is the most intuitive choice, but it cannot be achieved in a site specific manner because of fast deuterium exchange. The amide-II mode is chosen as our reporter. ^{15}N labelling decreases the amide-II frequency of N-methylacetamide (NMA) in nitrogen matrix by 13−15 cm^{-1},[83] a sizable shift compared to typical line widths (~30 cm^{-1}). Only a recent few studies explored the couplings between the amide-I and amide-II modes in NMA and dipeptides,[80,82,84] but cross-peaks have yet to be observed for modes connected through an intramolecular hydrogen bond in peptides.

In this way, we were able to reveal intramolecular direct and site-specific coupling between hydrogen-bonded, labelled residues, detected by the appearance of off-diagonal peaks in the 2D IR spectrum.

2.1.1 Peptide synthesis and characterization

The criteria used for the design of the peptide sequences were the following:

- use of N- and C-termini protection to solubilize peptides in an organic solvent ($CDCl_3$);
- incorporation of many Aib units into the sequence, for supporting well formed 3_{10}-helical structure and achieving a narrow distribution of conformers of the peptide compounds.
- introduction of isotopic labelling in amino acids connected by an intramolecular hydrogen bond, their relative position in the main chain being *i*, (*i* + 3);
- hydrogen bond acceptors and donors are Leu ($^{13}C=^{18}O$) and Gly (^{15}N-H), respectively;
- evaluation of the 2D IR response on different peptide lenghts and helical content;
- *i*PrCO-(^{15}N)Gly-O*t*Bu (and its unlabelled, simple model counterpart) synthesis to experimentally determine the isotope shift of the amide-II mode due to ^{15}N labelling.

To this purpose, the following sequences were designed and synthesized:

(i) *unlabelled sequences*

*i*PrCO-Gly-O*t*Bu

Z-L-Leu-Aib-Ala-Gly-O*t*Bu

Z-Aib-L-Leu-Aib-Aib-Gly-Aib-O*t*Bu

Z-L-Leu-Aib-Aib-Gly-Aib-Aib-Aib-Aib-O*t*Bu

(ii) *labelled sequences*

*i*PrCO-Gly*-O*t*Bu

Z-L-Leu**-Aib-Ala-Gly*- O*t*Bu

Z-Aib-L-Leu**-Aib-Aib-Gly*-Aib-O*t*Bu

Z-Aib-L-Leu**-Aib-Aib-Gly-Aib-O*t*Bu

Z-L-Leu**-Aib-Aib-Gly*-Aib-Aib-Aib-Aib-O*t*Bu

Z-L-Leu**-Aib-Aib-Gly-Aib-Aib-Aib-Aib-O*t*Bu

Leu** = (1-^{13}C,^{18}O)-Leu; Gly* = (^{15}N)Gly

As regards the chemical synthesis (**Fig. 2.5**), the peptides were obtained by classical methods in solution, because sterically hindered C^{α}-tetrasubstituted amino acids do not allow using the faster solid-phase synthesis approach. A step-by-step method *via* EDC/HOBt[85] or HOAt[86] C-activation was used (in the case of segment condensation strategy, Aib-Aib bond formation was easily achieved *via* 5(4*H*)-oxazolone activation).

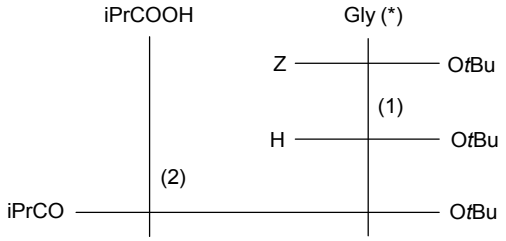

Fig. 2.5 (a) *i*PrCO-Gly-OtBu: (1) H_2, Pd/C; (2) EDC, HOBt, TEA

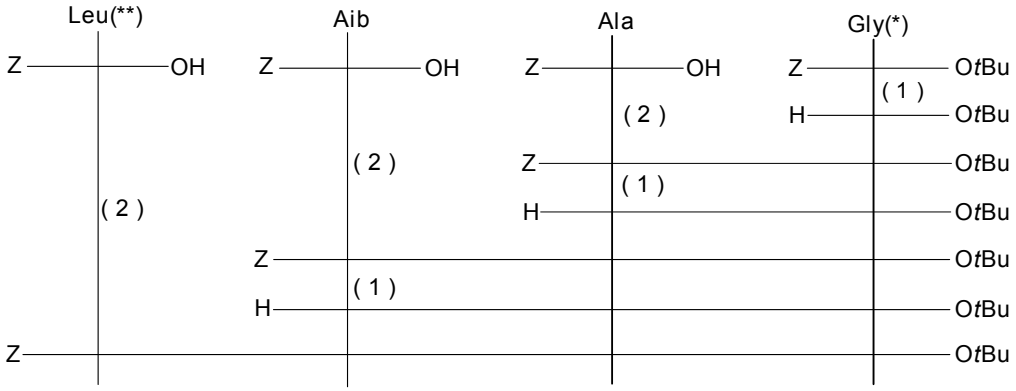

Fig. 2.5 (b) Tetrapeptide: (1) H_2, Pd/C; (2) EDC, HOAt or HOBt, DIPEA

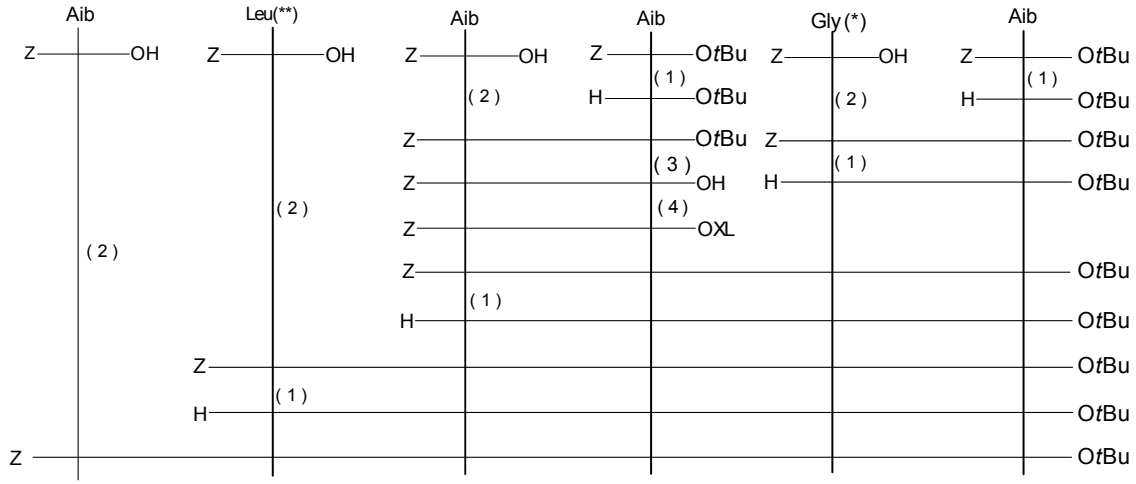

Fig. 2.5 (c) Hexapeptide (1) H_2, Pd/C; (2) EDC, HOAt/HOBt, DIPEA; (3) CF_3COOH; (4) EDC.

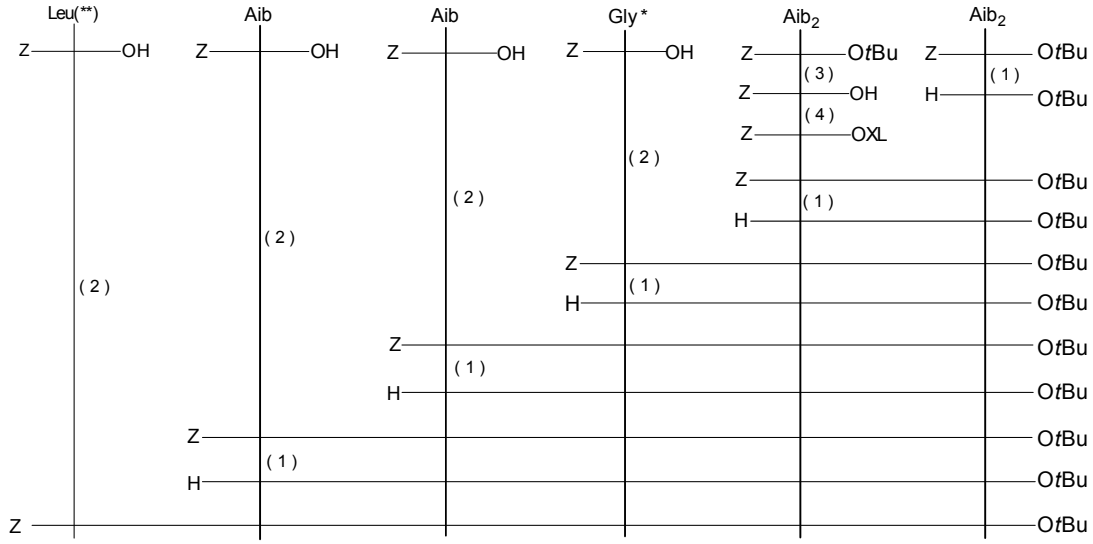

Fig. 2.5 (d) Octapeptide: (1) H_2, Pd/C; (2) EDC, HOAt or HOBt, DIPEA; (3) CF_3COOH; (4) EDC.

The (^{15}N)Gly and (1-^{13}C)Leu amino acids are commercially available (Cambridge Isotopes, Andover, MA) while ^{18}O labelling had to be introduced by treating (1-^{13}C)Leu with $H_2{}^{18}O$ in a strongly acidic environment at 60 °C for five days.[87] In this reaction, the carboxylic acid moiety is in equilibrium with its *ortho*-acid form, as seen in **Fig. 2.6**. Isotopic enrichment takes place for statistical reasons due to the presence of only $H_2{}^{18}O$ in the reaction medium.

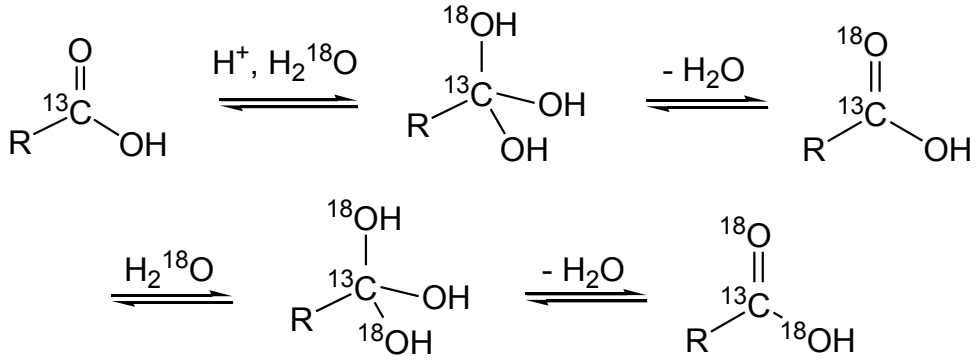

Fig. 2.6 Isotopic exchange equilibrium with $H_2{}^{18}O$

Gaseous hydrochloric acid (HCl) was bubbled directly into the amino acid-$H_2{}^{18}O$ mixture to avoid introducing any atmospherical water or ^{16}O contamination. Reaction yield was monitored by mass spectrometry, which detected the formation of

the two isotopically-enriched products (**Fig. 2.7**) in accordance to the literature procedure.[87]

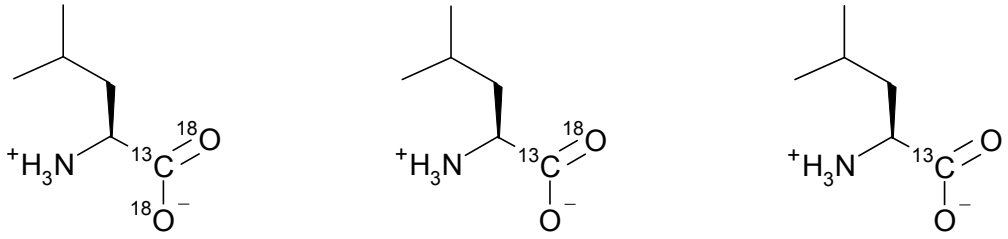

H-L-(1-^{13}C,^{18}O)Leu-^{18}OH **84.6%** | H-L-(1-^{13}C,^{18}O)Leu-OH **15.4%** | H-L-(1-^{13}C)Leu-OH **0.0%**

Fig. 2.7 Products distribution of the ^{16}O-^{18}O exchange reaction on L-Leu.

The labelled Leu was then N^{α}-protected and introducted in the peptide chain as described. In **Table 2.1** the ^{18}O isotopic enrichment of the various peptides synthesized is reported.

Compound	isotopic enrichment
Z-L-(1-^{13}C,^{18}O)Leu-^{18}OH	91.99%
Z-L-(1-^{13}C,^{18}O)Leu-Aib-Ala-(^{15}N)Gly-O*t*Bu (tetra)	94.06%
Z-L-(1-^{13}C,^{18}O)Leu-$(Aib)_2$-(^{15}N)Gly-Aib-O*t*Bu (hexa)	87.90%
Z-Aib-L-(1-^{13}C,^{18}O)Leu-$(Aib)_2$-Gly-Aib-O*t*Bu (hexa)	93.44%
Z-L-(1-^{13}C,^{18}O)Leu-$(Aib)_2$-Gly-$(Aib)_4$-O*t*Bu (octa)	94.22%
Z-L-(1-^{13}C,^{18}O)Leu-$(Aib)_2$-(^{15}N)Gly-$(Aib)_4$-O*t*Bu (octa)	94.40%

Table 2.1 Isotopic enrichment for the ^{18}O-labelled peptides

The results of a preliminary conformational investigation using FT-IR absorption,^{1}H NMR titration with the strongly hydrogen bond acceptor DMSO,[88,89] and 2D NMR suggest that in the structurally benign solvent $CDCl_3$ the longer peptides largely prefer a rigid, helical conformation, extensively stabilized by intramolecular C=O···H-N hydrogen bonds.

As far as the FT-IR absorption is concerned, structural information can be obtained by correlating the elongation of the peptide chain to the ratio of the two bands at 3360 and 3430 cm^{-1} (**Fig. 2.8**), assigned to free (solvated) and hydrogen-bonded N-H

stretching, respectively. Using the Mizushima's dilution technique,[90] we were able to demonstrate that intermolecular hydrogen bonding is negligible at 1 mM concentration in $CDCl_3$. As the number of aminoacids in the sequence increases (A → D), the intensity of the latter absorption band becomes bigger, supporting the hypothesis of a helical conformation in $CDCl_3$ solution, especially for the long peptides.

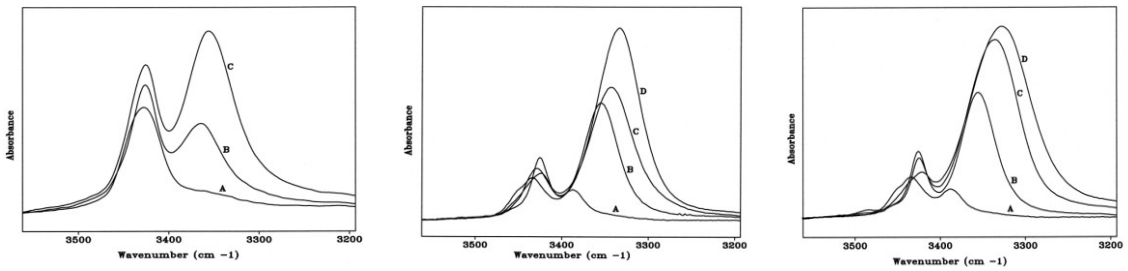

Fig. 2.8 FT-IR absorption spectra in the 3200-3550 cm^{-1} region of the unlabelled tetra-, hexa- and octapeptide and their shorter sequences (from left to right). Peptide concentration: 1 mM in $CDCl_3$.

As the peptide main-chain length is enhanced, the frequencies of the absorption maxima of the stretching bands of intramolecularly hydrogen-bonded peptide N-H and C=O groups (the latter absorption, amide I, is seen at 1690-1660 cm^{-1}) tend to decrease. These findings are in favor of the conclusion that a fully developed, stable, intramolecularly hydrogen-bonded structure is formed.[17,91-93]

However, it is not possible, at this point, to specify the type of intramolecular hydrogen bonding pattern adopted by the peptides (either 3_{10}- or α-helical). To assess this issue, a structural analysis was carried out by using ^{1}H-NMR spectroscopy.

Three kinds of 2D NMR experiments were performed on the peptides studied, each offering different and complementary information. COSY experiments highlight direct scalar coupling relations between nuclei (protons in case of ^{1}H NMR) generally less than three chemical bonds apart. TOCSY experiments allow the identification of spin systems (*i.e.*, groups of nuclei connected by scalar coupling relations). ROESY experiments, instead, are sensitive to the spatial proximity of the nuclei.

By combining the information extracted from the two-dimensional TOCSY spectrum[94-96] with the through-space connectivities of the $C^{\alpha}H(i)\rightarrow NH(i+1)$ and $NH(i)\rightarrow NH(i+1)$ types, as obtained from the ROESY experiments,[95] we were able to assign all of the proton resonances in $CDCl_3$ solution [**Fig. 2.10 (a-d)**]. Typical helical

cross-peaks are detected, like $d_{\alpha N}$ (i, i + 4) [distance between C^{α}_{i} proton and N_{i+4} proton], and $d_{\alpha N}$ (i, i + 2) [distance between C^{α}_{i} proton and N_{i+2} proton] (**Fig. 2.9**), but a clear demonstration of their actual conformation solely based on these data is not straightforward, as well as the discrimination between 3_{10}- or α-helical folding.

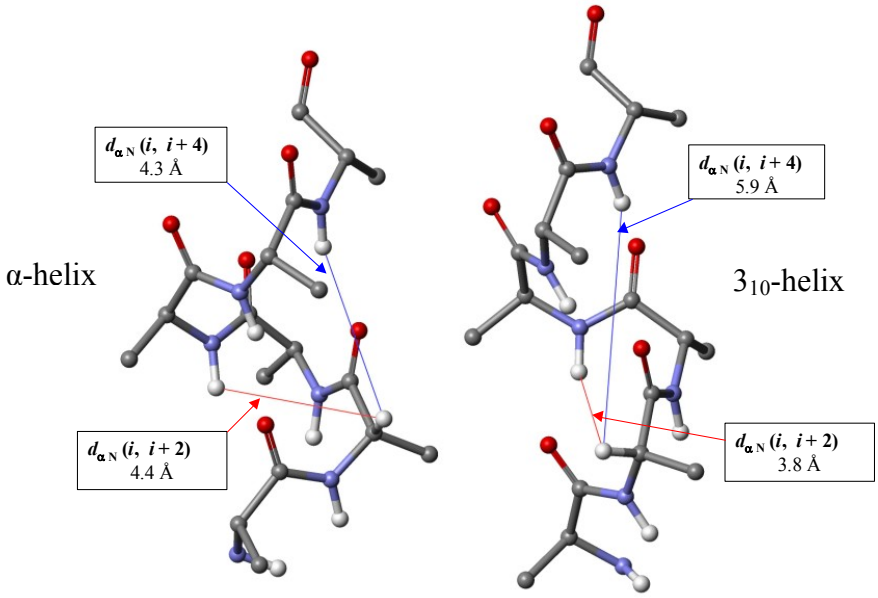

Fig. 2.9 Observable distances in the 3_{10}- and α-helical conformations by the NOE scalar coupling effect.

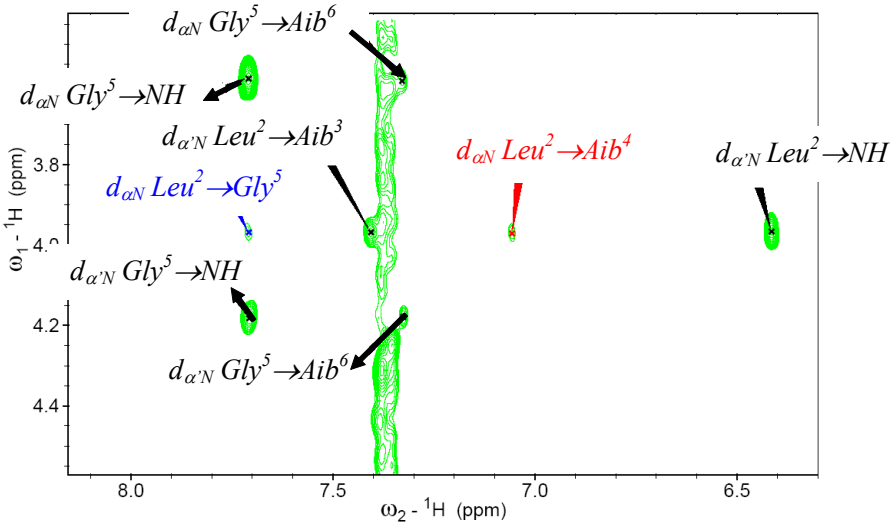

Fig. 2.10 (a) Portion of the 2D ROESY spectrum of Z-Aib-L-Leu-Aib-Aib-Gly-Aib-O*t*Bu in $CDCl_3$ solution. In red: $d_{\alpha N}$ (i, i + 2) 3_{10}-helical connectivities; in blue: $d_{\alpha N}$ (i, i + 3) 3_{10}/α-helical connectivities; in black: other connectivities

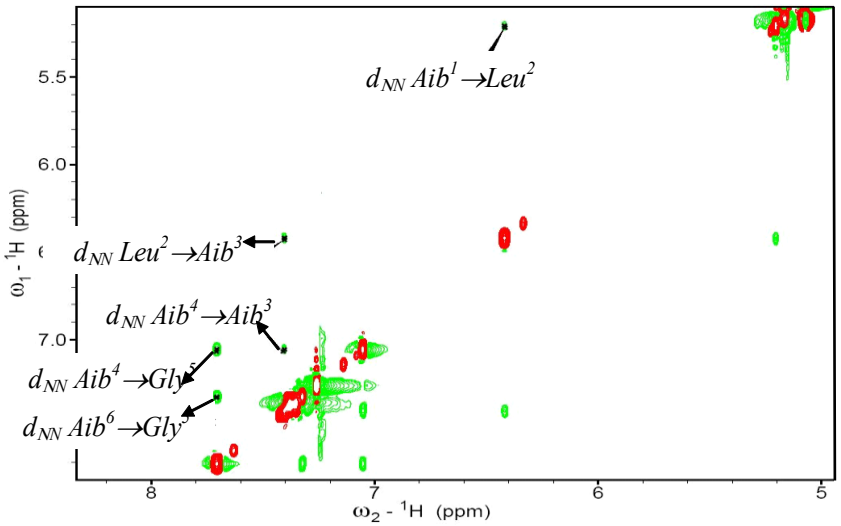

Fig. 2.10 (b) Portion of the 2D ROESY spectrum of Z-Aib-L-Leu-Aib-Aib-Gly-Aib-O*t*Bu in $CDCl_3$ solution: d_{NN} (i, i +1) connectivities are shown.

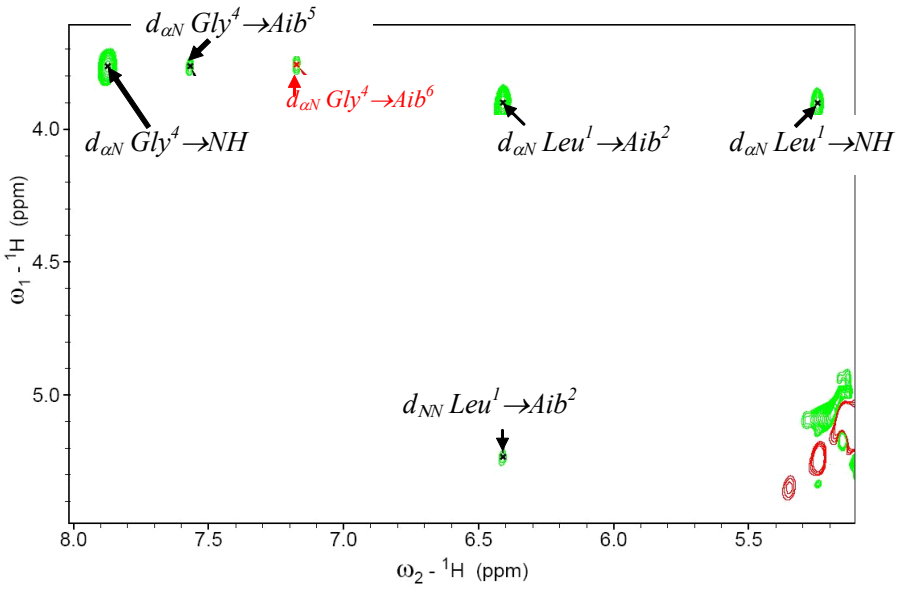

Fig. 2.10 (c) Portion of the 2D ROESY spectrum of Z-Aib-L-Leu-Aib-Aib-Gly-Aib-O*t*Bu in $CDCl_3$ solution. In red: $d_{\alpha N}$ (i, i + 2) 3_{10}-helical connectivites; in black: other connectivities.

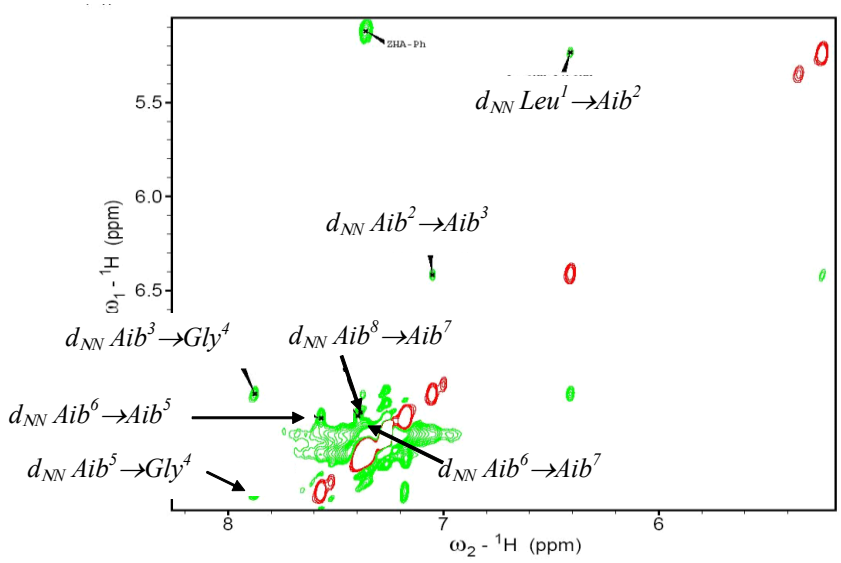

Fig. 2.10 (d) Portion of the 2D ROESY spectrum portion of Z-Aib-L-Leu-Aib-Aib-Gly-Aib-O*t*Bu in $CDCl_3$ solution: d_{NN} (i, i + 1) cross-peaks are shown.

Fig. 2.11 graphically describes the effect of adding DMSO on the NH chemical shifts in the ^{1}H-NMR spectra of the three (tetra-, hexa- and octa-) peptides in $CDCl_3$ solution. Such trends, with only the N(l)H and N(2)H protons significantly sensitive to DMSO, are those expected for standard 3_{10}-helical peptides. Our ^{1}H-NMR results indicate that all of the protons from N(3)H to the C-terminal NH proton of the hexa- and octapeptides in $CDCl_3$ solution are almost inaccessible to the perturbing agents and are therefore, most probably, intramolecularly hydrogen-bonded. The effect of DMSO on the tetrapeptide NH protons, on the other hand, appears to be more pronounced, indicating a reduced tendency to fold, probably related to its shorter main-chain length.

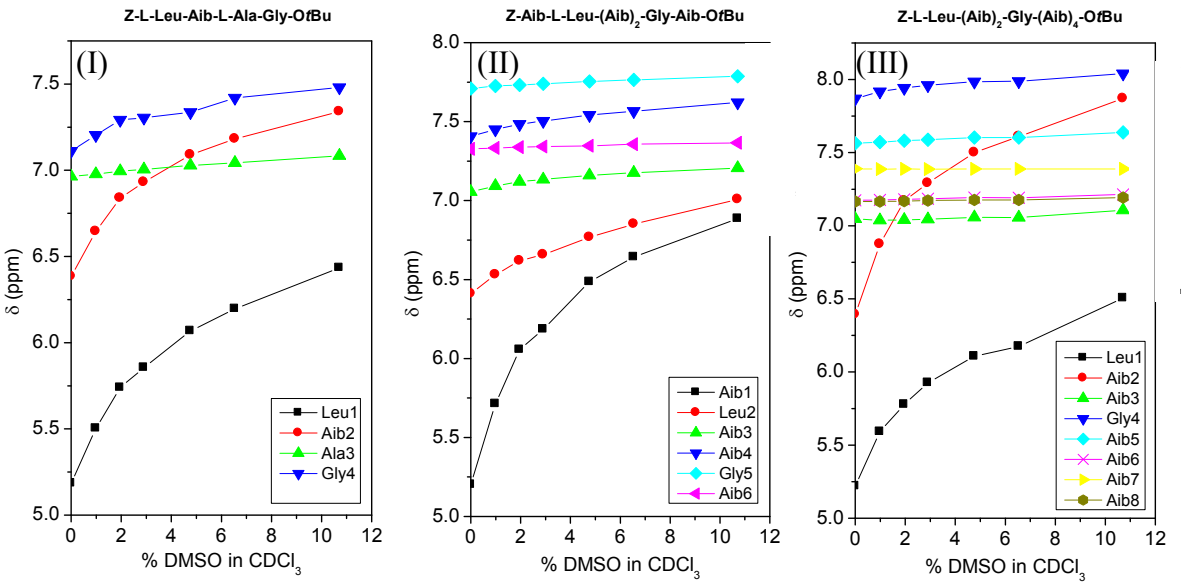

Fig. 2.11 Plots of NH chemical shifts in the ^{1}H-NMR spectra of: the tetrapeptide (I), hexapeptide (II), and octapeptide (III) as a function of increasing percentages of DMSO added to the $CDC1_3$ solution. Peptide concentration: 1 mM.

In view of the combined FT-IR absorption and ^{1}H-NMR observations, it is reasonable to conclude that the most populated structure adopted in $CDC1_3$ solution by the peptides is the 3_{10}-helix. This conclusion is more evident for the two longer hexa- and octapeptides.

Finally, a conclusive conformational analysis was possible on the crystal state structure of the unlabelled hexapeptide **1**, determined by single-crystal X-ray diffraction (Dr. Crisma, ICB-CNR, Padova unit), is illustrated in **Fig. 2.12**. Crystals were grown from EtOAc. Two independent peptide molecules (A and B) are present in the asymmetric unit. Both molecules are folded and stabilized by three intramolecular C=O···H-N H-bonds. Specifically, a C_{13} structure (α-turn) is observed between the Aib(4) N-H group and the Z-urethane carbonyl group, followed by two consecutive β-turns involving the Gly(5) and Aib(6) N-H groups as the donors, and the Leu(2) and Aib(3) carbonyl oxygens, respectively, as the acceptors. Overall, both molecules are mixed α-/3_{10}-helical in the crystal state. The main difference between them is found in their helical screw sense, which is right-handed in molecule A while left-handed in molecule B, despite the occurrence in their sequence of a single chiral residue (Leu) of

L- configuration. This is a rather uncommon but not unique observation in peptide crystallography.[97-99]

Anyway, the first β-turn, on the basis of the torsion angles adopted by the Aib(3) and Aib(4) residues at its corner positions, is quite close to the ideal type-III (III' in molecule B) type (which is the building unit of a regular 3_{10}-helix), whereas the following β-turn can be classified as belonging to the type-I (I' in molecule B) type. In addition to that, the first 3_{10}-helical β-turn is intramolecular stabilized by a H-bond between Leu(2) and Gly(5). This consideration is in aggreement with the results of 2D IR conformational analysis.

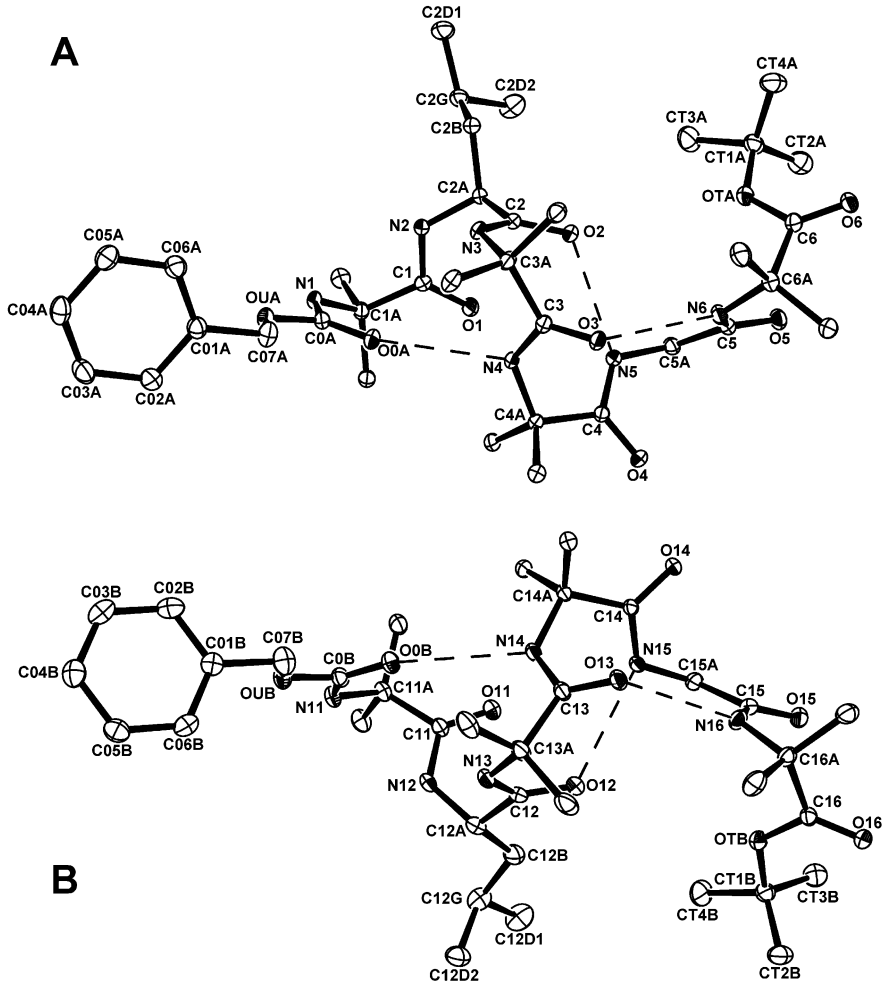

Fig. 2.12 X-ray structure of unlabelled hexapeptide **1**. A and B are the two independent molecules in the asymmetric unit.

2.1.2 2D IR analysis

On the basis of the previous conformational investigation on the peptides synthesized, the 2D IR analysis of the tetrapeptide is not particularly relevant, because of its tendency to fold only partially in $CDCl_3$ solution. The structural flexibility associated with this short peptide prevented us from achieving much clearer results other than those obtained with the conventional spectroscopic methods reported above. The octapeptide spectra as well are difficult to interpret. This compound has multiple peptide units, making it harder to observe the isotope shift from a single mode.

As regards the hexapeptide, on the other hand, the data collected are much more informative and give a little, but nevertheless attractive, picture of the possibilities opened by 2D IR for 3D-structural determination.

Figs. 2.13 and **2.14** show the linear IR absorption spectra (and the relative differences) of unlabelled (**1**), mono- (**1***) and double-labelled (**1****) hexapeptides in the regions covering the amide I/II modes.

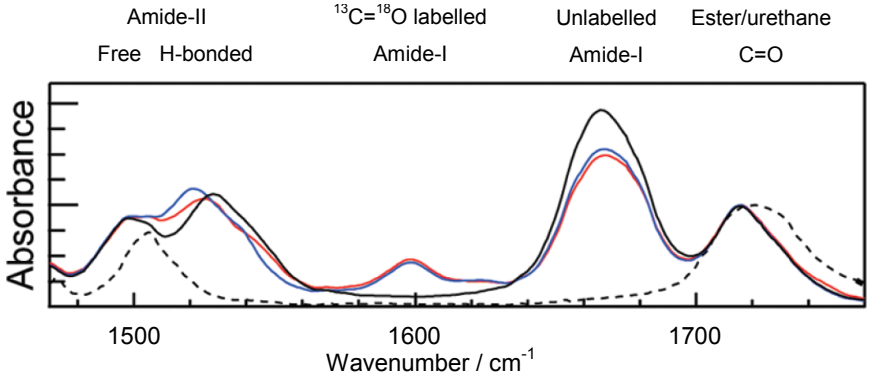

Fig. 2.13 Linear IR absorption spectra in the amide I/II regions of the three hexapeptides and Z-Aib-O*t*Bu (dashed black): unlabelled (**1**, solid black), mono-labelled at Leu $^{13}C=^{18}O$ (**1***, red) and double-labelled at Leu $^{13}C=^{18}O$ and at Gly ^{15}N (**1****, blue).

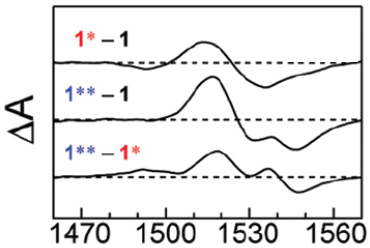

Fig. 2.14 Measured difference spectra between **1*** and **1**, **1**** and **1**, and **1**** and **1*** in the amide-II frequency region.

Two amide-II bands are observed at 1498 and 1528 cm^{-1}. Roughly speaking, the higher (lower) frequency band can be attributed to the vibrational exciton band of the hydrogen-bonded (free) amide-II mode.

The amide-II mode is known to exhibit a blue shift when the N-H group is hydrogen bonded.[96] If the hexapeptide forms a fully developed 3_{10}-helix, four out of the five peptide N-H groups will participate in intramolecular hydrogen bonding except for the first one near the N-terminus. The relative intensity of the two bands centered near 1520 cm^{-1} in **Fig. 2.13** is consistent with this picture when compared to the trend observed in the FT-IR absorption measurements of Z-$(Aib)_n$-O*t*Bu (n = 1, 2, 3, 5, 8, and 10) in $CDCl_3$, where the intensity of the higher frequency band increases with increasing n.[100,101] The spectrum of Z-Aib-O*t*Bu shows that the capping groups provide only small contributions to the spectral window of interest.

The $^{13}C{=}^{18}O$ labelling on the Leu residue of **1*** results in an amide-I peak at 1598 cm^{-1}, completely separated from the much stronger $^{12}C{=}^{16}O$ amide-I band (**Fig. 2.13**). The isotopes also affect the amide-II modes. As shown in the difference spectrum (**Fig. 2.14, 1*-1**), the intensity at 1536 cm^{-1} decreases and at 1514 cm^{-1} increases. Such a red shift of the higher frequency band indicates that the N-H group of the second peptide linkage is hydrogen bonded (to the urethane C=O group), as expected for a full 3_{10}-helix.

The double-labelled peptide **1**** has almost the same amide-I bands as **1***, thus suggesting that ^{15}N labelling primarily affects the amide-II modes. The higher frequency band of **1**** is red-shifted by ~ 4 cm^{-1} from that of **1***. The difference spectrum between **1**** and **1*** reveals clearly the additional effect of ^{15}N labelling, with major spectral changes occurring in the high frequency band. This finding indicates that the N-H group of the third peptide linkage is involved in hydrogen bonding. For a 3_{10}-helix, its bonding partner is the C=O group of the first peptide linkage (**Fig. 2.15**).

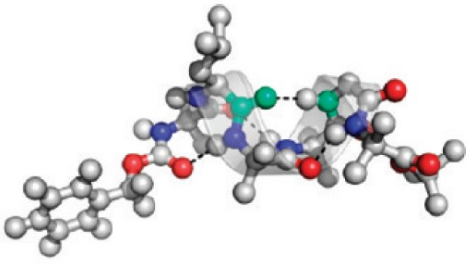

Fig. 2.15 Molecular structure of **1** adopting an ideal 3_{10}-helical conformation with the dihedral angles (φ, ψ) = (-57°, -30°).[6] The atoms labelled with ^{13}C, ^{18}O, and ^{15}N for **1*** and **1**** are colored green.

The 2D IR measurements of the hexapeptides in $CDCl_3$ were conducted using a home-built (at Irvine) IR spectral interferometry setup. The details of the setup and the data processing procedure have already been described.[76-78] The center frequency of IR pulses was tuned to ~ 1600 cm^{-1} to excite all of the unlabelled and labelled amide-I and -II modes and observe their cross peaks. We also performed 2D IR measurements with the IR frequency centered at ~ 1550 cm^{-1} to more clearly investigate cross peaks between the labelled $^{13}C=^{18}O$ amide-I mode and the amide-II modes. To collect rephasing (R) and nonrephasing (NR) spectra, the delay time τ between the first and second incident pulses was scanned from 0 to ~ 2.9 ps and 0 to ~ 2.5 ps, respectively, with a step of 9 fs. Nonresonant solvent response was utilized to find the time zero between the three pulses, and its effects were minimized by setting the waiting time T between the second and third pulses to 200 fs during the data collection of the 2D IR spectra. Spectral interferograms were collected and processed to give data in the ω_t-dimension. All of spectral measurements were conducted at ambient temperature 20 ± 1 °C.

To characterize the conformation of hexapeptides in $CDCl_3$, we measured the amide-I cross-peak pattern of **1**, as shown in **Fig. 2.16**. The amide-I doublet pattern at (ω_t, ω_τ) ~ (1675, -1660) cm^{-1} and (1650, -1665) cm^{-1} indicates that the peptide takes a 3_{10}-helical conformation.[76-78] The weak peak in the upper right corner may originate from the C=O stretching modes of the fraying urethane and/or ester capping groups.

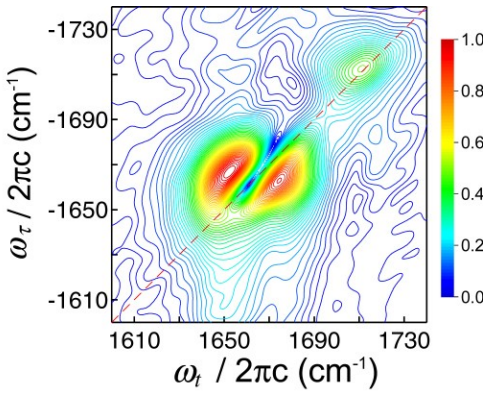

Fig. 2.16 2D IR R cross-peak pattern of **1** in $CDCl_3$.

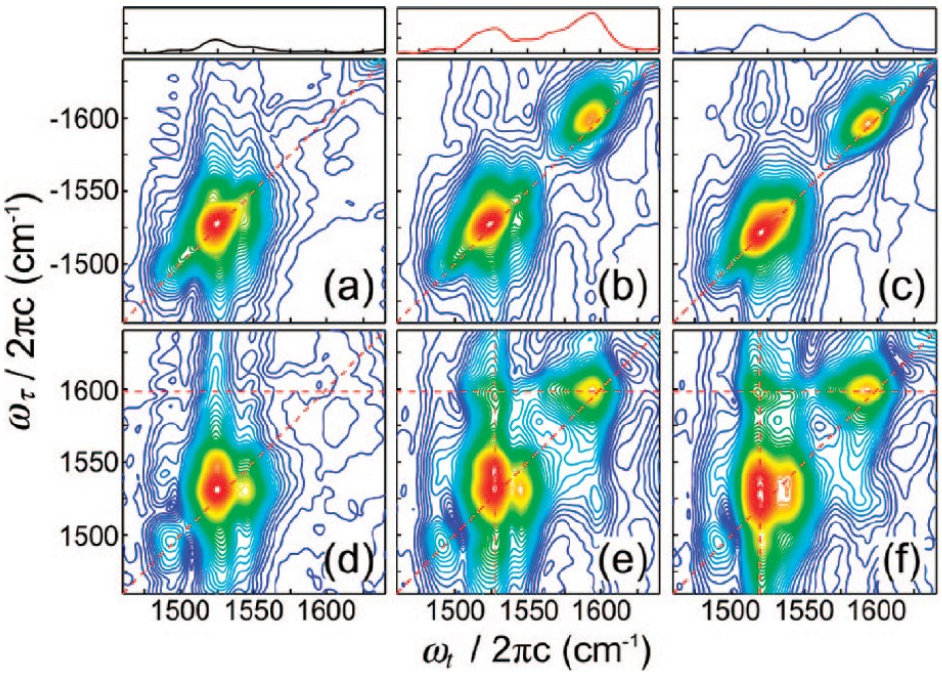

Fig. 2.17 Normalized absolute magnitude 2D IR rephasing (R, a-c) and nonrephasing (NR, d-f) spectra of **1**, **1***, and **1**** (from left to right) in $CDCl_3$. Horizontal slices of the NR spectra along the dashed line at ω_τ = 1598 cm^{-1} are shown in the top panels.

Fig. 2.17 presents 2D IR rephasing (R) and nonrephasing (NR) spectra. Because of the finite bandwidth of the IR pulses, the peaks near the center frequency are strongly enhanced. Overall, we observed better resolved diagonal peaks and more distinct cross-peaks in the NR spectra than in the R spectra. The NR sequence has higher resolving power due to destructive interference effects.[102] The nonrephasing nature of this pulse sequence is particularly useful for line-narrowing cross peaks between anticorrelated vibrators,[103] such as hydrogen-bonded amide-I and -II modes. In the R spectra of **1*** and **1****, the $^{13}C=^{18}O$ amide-I mode at the second peptide linkage is observed at (ω_t, ω_τ) ≈ (1593, -1598) cm^{-1} and no peak appears here in the spectrum of **1**. For the amide-II region, the strongest diagonal peak at (1525, -1528) cm^{-1} in the R spectrum of **1** corresponds to the high frequency band in the linear spectrum. Upon isotope labelling, the amide-II band maximum maintains at about the same position for **1***, but shifts to (1520, -1521) cm^{-1} for **1****. The free amide-II band appears in the 2D IR spectrum of **1** as a diagonally elongated shoulder on the red side of the main peak, but it is clearly resolved as a separate peak in the NR spectrum at (1493, 1497) cm^{-1}. The complex couplings among the amide-II modes manifest as many cross-peaks in the NR spectra.

The most interesting features in the 2D spectra are the cross peaks between the $^{13}C=^{18}O$ amide-I mode and the amide-II modes. They are weak in the R spectrum, but much stronger in the NR spectrum. For **1***, the cross peaks are located at (1527, 1598) cm^{-1} and (1596, 1524) cm^{-1}. These cross-peaks reveal the presence of couplings between the labelled amide-I mode and some modes within the high-frequency amide-II band. The couplings can involve anharmonic interactions between amide-I/II modes within the second peptide linkage and/or between the second amide-I and amide-II on other linkages. Whether the fourth linkage contributes to the latter interactions can be revealed by observing the changes of these cross peaks upon ^{15}N labelling. The top panels in **Fig. 2.17** show the slices through 2D NR spectra at ω_τ = 1598 cm^{-1}. The cross-peak maximum of **1**** is at 1518 cm^{-1}, significantly red-shifted from that of **1*** by 9 cm^{-1}. This finding is a clear evidence that the amide-II local mode on the fourth peptide linkage is coupled to the amide-I local mode on the second peptide unit. ^{15}N labelling changes the fourth amide-II local mode frequency and results in corresponding shifts in the cross-peak frequencies. Such coupling information is not obtainable from linear IR. The cross-peak line shapes observed here are quite complex because there are many amide-II exciton states that the $^{13}C=^{18}O$ labelled amide-I mode can couple to. Although detailed analysis is still underway, it may be worthwhile to estimate how this coupling depends on the existence of 3_{10}-helix based on the transition charge coupling model.[104] Using partial charges and charge derivatives along the amide-I and -II modes of NMA from a DFT calculation, the estimated coupling between the two modes separated by two peptide units was found to be -12 cm^{-1} in the ideal 3_{10}-helix [(φ, ψ) = (-57°, -30°)][6] and -0.1 cm^{-1} in the *semi*-extended structure [(-78°, 146°)]. Such a difference in the coupling strength suggests that these cross peaks would be useful for detecting helix formation. In a recent experiment the couplings between labelled amide-I modes separated by 1-3 residues have been measured in an Ala- rich α-helix.[105] Measuring the amide-I/II couplings with labels at several different sites will enable further refinement of the peptide local structure. Also, it would be interesting to theoretically investigate the amide-I/II coupling mechanism, including through-(hydrogen)-bond and through-space interactions. Although our new observation for the coupled amide-I and amide-II modes was made in a 3_{10}-helix, this technique is generally applicable to systems involving couplings between C=O stretching and N-H bending modes.

It is fascinating to investigate how sensitively the cross peaks between the amide-I and -II modes can distinguish between a single 3_{10}-helical turn and a *semi*-extended structure. We discussed this sensitivity based on model calculations because it is difficult to devise experimental conditions that will allow us to measure 2D IR spectra of **1**** in two different conformations while using the same solvent. A simulation protocol[76,78] was applied to calculate the NR spectra of the hexapeptides that are in an ideal *semi*-extended structure with the average dihedral angles centered at (φ, ψ) = (-78°, 146°).[106] For the *semi*-extended structure, all peptide units are exposed to solvent without forming intramolecular C=O···H-N hydrogen bonds. The amide-I/II coupling between i, i + 2 peptide units is -0.1 cm^{-1}, much smaller than the -11.6 cm^{-1} coupling for the 3_{10}-helical conformation. Such a small coupling is expected to give negligible contributions to the cross peaks.

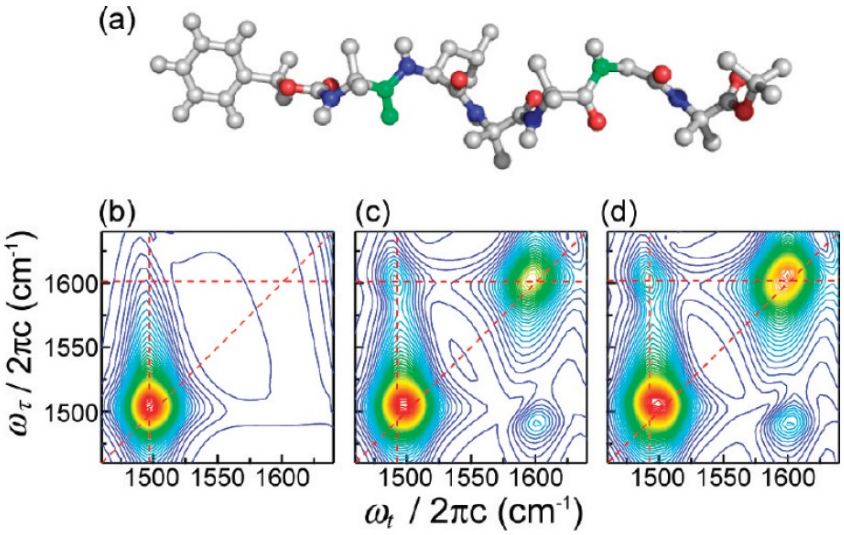

Fig. 2.18 (a) Model structure of the hexapeptide forming the ideal *semi*-extended conformation with (φ, ψ)) (-78°, 146°), in which the isotope labelled atoms are colored green. Absolute magnitude 2D NR spectra simulated for the unlabelled (b), monolabelled (c), and double-labelled (d) hexapeptides.

Fig. 2.18 shows the simulated 2D NR spectra with the convolution centered at 1550 cm^{-1}. The spectrum for the unlabelled peptide has only one diagonal amide-II peak at (1499, 1504) cm^{-1} because all amide-II modes are exposed to solvent, in contrast to the two amide-II bands in **Fig. 2.17 (d)**. For the mono-labelled peptide with $^{13}C=^{18}O$, the cross peaks between the labelled amide-I mode and unlabelled amide-II modes clearly appear at (1493, 1602) cm^{-1} and (1602, 1491) cm^{-1}. Comparing to the

monolabelled peptide, the double-labelled peptide exhibits changes in the diagonal peak pattern in the 2D spectrum because of the local mode frequency shift by 16 cm^{-1} upon ^{15}N substitution. However, the cross peaks between the amide-I and -II modes do not exhibit isotope shift, in sharp contrast to the strong isotope dependence simulated in the case of 3_{10}-helical conformation [**Fig. 2.17 (f)**] in which the $^{13}C=^{18}O$ amide-I and ^{15}N amide-II modes are strongly coupled. For the *semi*-extended structure, the major contribution to the cross peaks of the mono and double-labelled peptides comes from the coupling between the $^{13}C=^{18}O$-labelled amide-I and the amide-II modes within the same second peptide linkage. The amide-II mode on the fourth peptide unit does not couple to the labelled amide-I mode strongly, hence there is no noticeable ^{15}N isotope effect. These calculation results indicate that the isotope-dependence of amide-I/II cross peaks clearly reflects the local structure arrangement, for example, whether or not the two modes are brought into spatial proximity by the presence of intramolecular hydrogen bonding. Therefore, they can serve as a promising reporter for detecting whether a peptide undergoes a local structure transition from an *semi*-extended structure to the formation of a single helical turn.

2.1.3 Conclusions

In summary, our experimental results and simulations show that the combination of 2D IR and a novel isotope substitution scheme can open avenues for detecting unique vibrational couplings between specific residues, leading to new structural information which is hard to acquire from other spectroscopic methods. The new combination of $^{13}C=^{18}O$-labelled amide-I and ^{15}N-labelled amide-II modes on the first and third peptide linkages, respectively, in the 3_{10}-helical hexapeptides results in isotope-dependent cross peaks that are clearly detectable, especially in the NR spectra.

The simulated spectra of the *semi*-extended conformation exhibit no isotope shifts in the amide-I/II cross peaks because the C=O group on the first peptide group and the N-H group on the third peptide group are quite spatially separated without the existence of an intramolecular hydrogen bond. This conformational sensitivity originates from the dramatic difference in the amide-I/II coupling between the two structures: -0.1 cm^{-1} for the *semi*-extended structure and -12 cm^{-1} for the 3_{10}-helix.

We expect that the same strategy is also applicable for detecting the formation of a single α-helical turn in solution when the $^{13}C=^{18}O$ and ^{15}N labels are substituted on the *i*, *i* + 3 peptide linkages. The coupling is -6 cm^{-1} in this case, also much larger than that of the *semi*-extended structure. This strategy is thus promising for probing the nucleation step of nascent helix formation from an extended structure. Further experimental studies are needed to corroborate these theoretical predictions.

2.2 VCD

As the focus of developing research in the broad arena of Chemical Biology moves from genomics to proteomics, the ability to obtain structural information about protein systems on a relatively rapid time scale is an increasingly important factor in moving from sequence (or genetics) toward function (proteomics, which is intimately tied to the protein fold). Optical spectroscopy and circular dichroism of electronic transitions (ECD) in the UV spectral range have long been important tools for determination of secondary structure and monitoring of structural change.[107,108] However, the information content of UV absorption spectra is limited by the inherently low resolution, high overlap and conformational insensitivity of the few accessible electronic transitions. The differentially polarized absorption of ECD adds chiral sensitivity, and extension of such measurements to the vacuum UV region (e.g. with synchrotron radiation) significantly enhances information content.[109,110]

By contrast, in the vibrational region of the spectrum, characteristic transitions of the amide functionality are naturally well-resolved from most other transitions, such as side-chain modes. Spectral separation of structurally characteristic vibrational modes (or chromophores) underlies IR absorption and Raman spectroscopies, in which structure is correlated to frequencies, whereas in ECD it is to bandshapes enhanced by sign variation. The desire to access multiple localized transitions with conformationally sensitive bandshapes led to the development of vibrational CD (VCD) and its differential scattering analogue, Raman optical activity (ROA). VCD measures the difference between absorption of left and right circularly polarized light by chiral substances in the infrared spectral region. ROA, on the other hand, gives complete vibrational optical activity spectra of chiral molecules via circularly polarized Raman spectroscopy.[111-113] Because of its sensitivity to chirality, ROA is a powerful new probe of the aqueous solution structure and behaviour of biomolecules including peptides, proteins, carbohydrates, nucleic acids and viruses.[114,115]

VCD originally centered on small molecule conformational analysis and theory, and still has important roles there, particularly for chiral drug enantiomeric

determination studies.[116,117] Applicability of VCD (and ROA) to studies of biopolymers (peptides, nucleic acids, carbohydrates) developed later.[111,113,118-121]

The local character of vibrational excitations gives VCD some important properties. Overlap with aromatic modes (a major problem for ECD) is basically resolved in the IR and becomes even less of an interference for VCD because side chains are locally achiral and do not couple strongly to the amides. Furthermore, vibrational coupling tends to be short range, primarily to the next residue (or to a hydrogen bonded one), and the dipole moments are relatively weak, so VCD samples structure more locally than does ECD.[119,120,122] Secondary structure information can be derived from amide VCD bandshapes, which reflect the helicity of the backbone, much like ECD. Frequencies are also useful (especially relative to the IR) but are perturbed by solvent and environment, whereas the bandshape is less affected. Analyses of this structural information content from VCD spectra for biological systems have ranged from totally empirical correlation to fully theoretical predictions. For proteins, a statistically based, empirical VCD secondary structure prediction model has been developed, paralleling ECD and IR[123] methods. While for peptides, *ab initio* quantum mechanical VCD simulations are possible.[120,124]

Most VCD measurements have been made with instruments constructed by modifying either a dispersive or Fourier transform IR (FTIR)-based absorption spectrometer. Commercial FTIR-based VCD instruments are now available[125-129] and provide high quality spectra for small molecules in non-aqueous solutions. Aqueous biopolymer VCD imposes high demands, particularly with regard to baseline artifacts.

Proteins with different folds give characteristic VCD shapes, which vary most for the amide I mode, but are also easily detectable for the broader amide II/III (very weak) modes. Examples are shown in **Fig. 2.19**. Surveys of protein (and even nucleic acid) spectra show that secondary structure determines the dominant contributions to the VCD shape.[119,120]

Analyses of amide I′, plus amide II, III, and amide I+II VCD and combinations of VCD and ECD or FT-IR data all yield secondary structure at some level.[111,118,123,130] The important aspects were that VCD sensed sheet and other structural elements (including turns) differently than did ECD, which in turn was superior for helix determination. Combining them gave better determination of all components, especially minimizing the impact of outliers on the prediction scheme.[118,119,123]

Empirical correlations of peptide VCD bandshapes with secondary structure were developed in the 1980s, particularly for polypeptides in non-aqueous environments.[120,131,132] The key element was determination that the amide VCD depended on the conformation of the peptide chain, and was independent of other functional groups.

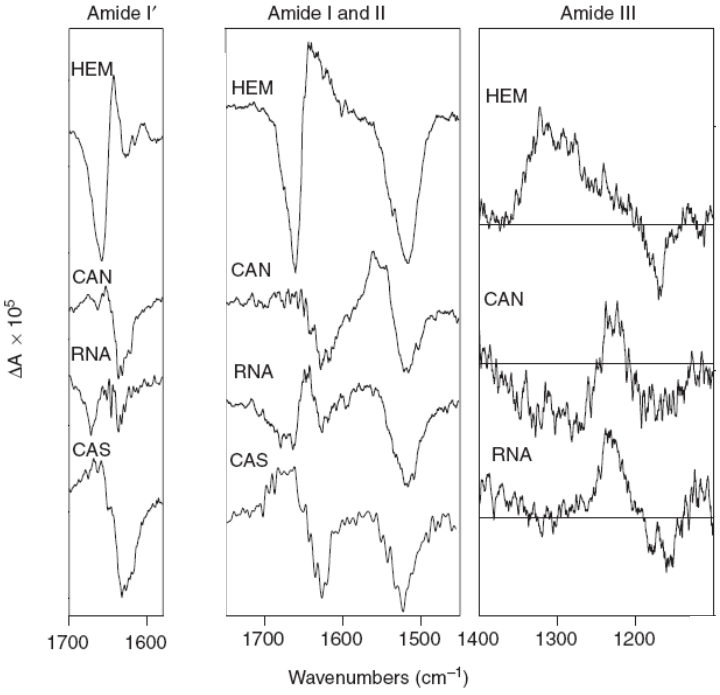

Fig. 2.19 Comparison of typical amide I′ (N-deuterated, left), amide I and II (middle) and amide III (right) VCD spectra for proteins in solution that have different dominant secondary structures. Spectra are for hemoglobin (HEM, top, highly helical); concanavalin A (CAN, highly β-sheet, no helix); ribonuclease A (RNA, second from bottom, sheet and helix mixed); and casein (CAS, bottom, a 'random coil' protein with no extensive secondary structure).

The helical chirality was the major bandshape criterion, a point demonstrated by VCD of poly-γ-(α-phenethyl)-L-glutamates having side chains of different chirality (*R* and *S*) but developing the same sign amide I and II VCD.[133] Another significant contribution of peptide VCD to conformational studies was confirmation of an old proposal[134] that the random coil conformation, such as seen in poly-L-lysine (PLL) or poly-L-glutamic acid at neutral pH contained a significant component of 'extended helix' with a left-handed twist. Length-dependent studies of PLL and proline oligomers showed that all gave rise to a characteristic poly-L-proline II (PLP II) VCD spectrum that broadened

and weakened for short or higher temperature PLL samples.[122,132,134] VCD and ROA, in summary, can complement IR absorption, Raman, and ECD analyses of complex biological systems and their structural changes. Also, these all can sense biopolymer structure in solution on a rapid time scale appropriate to biological activity. Although all have limitations, together they support and correct interpretations derived from each independently.

Determination of peptide and protein secondary structure relies on frequency shifts for characteristic vibrational transitions (i.e. FT-IR absorption or Raman spectroscopy) or on band shapes and intensity patterns (ECD). In each case, the resultant spectral parameters are the consequences of coupling between sequential amide groups in the oligo- (or poly-)peptide chains. Since the transitions arising from different sites in the sequence overlap, these spectrally determined structural components are necessarily averages for the entire molecule and are not spatially or sequentially distinct. However, as reported in the previous section, it is possible to gain site specificity with vibrational spectra through isotopic labelling. In particular, ^{13}C substitution on the amide C=O leads to a shift to lower frequency of its related stretching mode by ~ 40 cm^{-1}, which usually generates a resolution of the contribution of those labelled residues to the amide I band from that of the unlabelled ^{12}C=O groups. If two or more sites are labelled, the position of the observed ^{13}C=O band is dependent on their mutual coupling as well as the basic shifts caused by isotopic substitution. This coupling is the fundamental interaction between amides that gives vibrational spectroscopy its sensitivity to secondary structure, and thus it has an intrinsic value that has been evaluated both empirically for structure prediction as well as theoretically for model evaluation.

In general, the observed position of the coupled ^{13}C=O band differed if two labels were placed adjacent or separated by one or more residues in the sequences. Separating the labels reduces their coupling, but can also change the sign of the coupling constant so that the more intense coupled component might be either higher or lower in frequency from the isotope shifted position of an isolated amide ^{13}C=O.[135,136] The latter can be determined empirically by preparation of the same peptide sequence with just one labelled residue. For β-sheet structure the behavior is more complex, yet still can be modeled with DFT-based theoretical methods.[137-142]

Despite being resolved from the $^{12}C=O$ component, the $^{13}C=O$ contributions from two or more labelled residues to the amide I overlap each other in IR absorption or Raman spectra. Thus, their splitting, and hence the coupling constant cannot be directly measured. However, due to the complimentarity of IR absorption and Raman techniques, the resultant $^{13}C=O$ amide I contributions can have different intensity distributions, i.e. the in-phase coupling can be weaker or stronger than the out-of-phase coupling, for a given structure and technique. These differences can enable determination of at least a lower bound to the coupling constant, depending on the relative IR absorption and Raman intensities of the coupled components. However, in some cases, since the intensity patterns for the oppositely phased components are similar for IR absorption and Raman, an empirical measure of the coupling constant cannot be obtained with just this information as the observed band in both spectra has the same frequency position.

For coupling modes such as the case of two labelled $^{13}C=O$ groups, the vibrational CD (VCD) will obviously correspond to a coupled mode with the same splitting, but in this case the two components will normally have oppositely signed intensity contributions. When the frequencies of these VCD components are compared with the IR band position, the combined IR absorption and VCD spectra can provide a measure of an upper bound to the coupling constant. Alternatively, IR absorption, Raman and VCD spectra can be simulated using DFT methods and the resultant spectral patterns can be compared to those observed experimentally. Achieving agreement between simulated and experimental spectral patterns thus validates the sign and order of magnitude obtained for the computed coupling constant.

Previously, vibrational coupling for conformationally stable peptide sequences have been studied in α-helical[121,135] and β-sheet[137,139] conformations by use of isotopic labelling and DFT modeling, followed by related studies of β-hairpins[138,140,141] and poly-$(Pro)_n$ type-II (PPII) (3_1-) helices.[136]

In the present study, conducted in collaboration with the group of Prof. T. A. Keiderling (University of Illinois at Chicago), we report experimental and theoretical investigations on coupling constants between ^{13}C-labelled amide groups in a synthetic 3_{10}-folded peptide chain through a combination of FT-IR absorption, VCD and Raman optical activity.

2.2.1 Peptide synthesis and characterization

The following sequences were designed and synthesized:

Notation	Peptide Sequence
UH	*i*PrCO-Aib-Ala-Aib-Ala-Ala-Aib-NH*i*Pr
A4H	*i*PrCO-Aib-Ala-Aib-Ala*-Ala-Aib-NH*i*Pr
A5H	*i*PrCO-Aib-Ala-Aib-Ala-Ala*-Aib-NH*i*Pr
A4A5H	*i*PrCO-Aib-Ala-Aib-Ala*-Ala*-Aib-NH*i*Pr
A2A4H	*i*PrCO-Aib-Ala*-Aib-Ala*-Ala-Aib-NH*i*Pr
A2A5H	*i*PrCO-Aib-Ala*-Aib-Ala-Ala*-Aib-NH*i*Pr
A4A5O	Ac-Aib-Ala-Aib-Ala*-Ala*-Aib-Aib-Aib-OMe

(Ala* is (1-^{13}C)-alanine)

IR absorption, VCD, and Raman spectra were performed on the peptides which all have the same basic sequence -Aib-Ala-Aib-Ala-Ala-Aib-, and compared to DFT simulations of the spectra. The double labelled hexapeptides varied only in sequential position of the isotopic label (^{13}C=O) on two of the Ala residues resulting in three different compounds, hence designated as **A4A5H**, **A2A4H**, and **A2A5H**. In addition, a double labelled octapeptide, **A4A5O**, was synthesized to address probable end effects on the Ala5 labelled position in the shorter hexapeptides. Finally, the unlabelled **UH** and the single labelled **A4H** and **A5H** hexapeptides were prepared as spectral references.

Peptide synthesis was performed step-by-step by solution methods, using the EDC/HOBt,[85] or, more efficiently, the EDC/HOAt,[86] C-activation procedure. Coupling reactions were conducted in anhydrous CH_2Cl_2 in the presence of diisopropylethylamine. For labelling purpose, the commercial (Cambridge Isotopes, Andover, MA) α-amino acid H-(1-^{13}C)-Ala-OH was used. The N-terminus of each hexapeptide was blocked with *i*PrCO and the C-terminus with NH*i*Pr. The octapeptide was blocked in a different manner at the N-terminus, with Ac, and protected at the C-

terminus with OMe. All purified peptides were characterized by melting point (where appropriate) and polarimetric determinations, solid-state IR absorption, and ^{1}H NMR. The final hexa- and octapeptides were additionally checked by HPLC and mass spectrometry.

A preliminary conformational study in solution was performed by FT-IR absorption and ECD. The IR absorption spectra of the unlabelled hexapeptide and the labelled octapeptide in $CDCl_3$ at two different concentrations ($1x10^{-2}$ and $1x10^{-3}$ M) in the amide A region are shown in **Fig. 2.20** and **Fig. 2.21**.

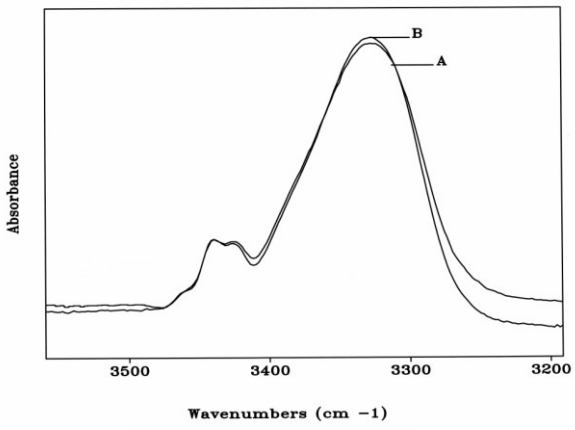

Fig. 2.20 FT-IR absorption spectra of *i*PrCO-Aib-Ala-Aib-Ala-Ala-Aib-NH*i*Pr in the amide A region in $CDCl_3$ solution. Peptide concentrations: 10 mM (A), 1 mM (B).

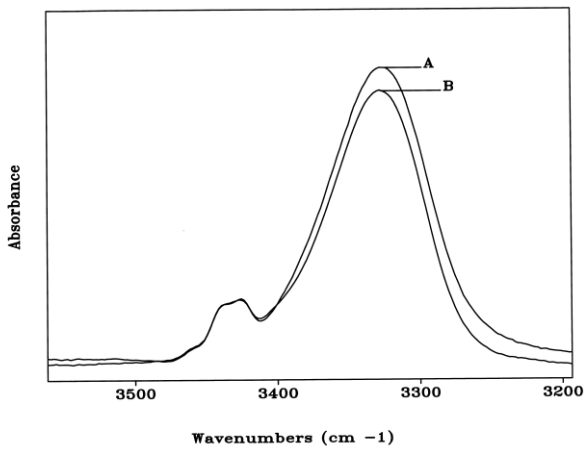

Fig. 2.21 FT-IR absorption spectra of Ac-Aib-Ala-Aib-Ala*-Ala*-Aib-Aib-Aib-OMe in the amide A region in $CDCl_3$ solution. Peptide concentrations: 10 mM (A) and 1 mM (B).

The presence of two bands in the 3300-3500 cm^{-1} is due to H-bonded and free NH stretching absorptions,[17,91-93] respectively. The peptides are predominantly intramolecularly H-bonded in solution, as the effect observed upon dilution is modest. The development of a rigid, helical structure can be seen (**Fig. 2.22** and **2.23**) by correlating the elongation of the peptide chain with the number of the hydrogen-bonded NHs (~ 3330 cm^{-1}) and the gradual red-shift for the absorption maxima. This latter behaviour indicates that the peptide growth induces an increased structural rigidity.

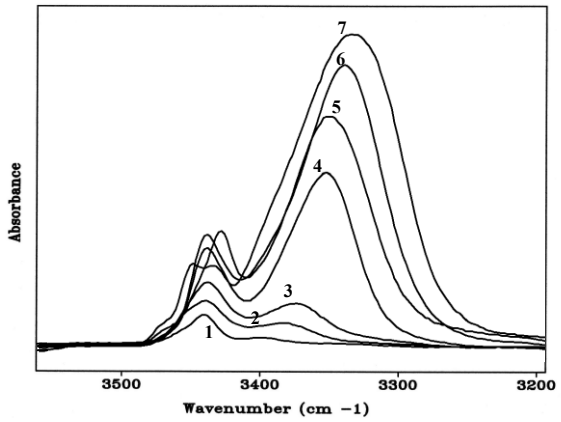

Fig. 2.22 FT-IR absorption spectra of *i*PrCO-Aib-Ala-Aib-Ala-Ala-Aib-NH*i*Pr and its shorter sequences in the 3200-3550 cm^{-1} region. Spectra (1-6): Z-protected peptides; spectrum (7): **UH**. Peptide concentrations: 1 mM in $CDCl_3$.

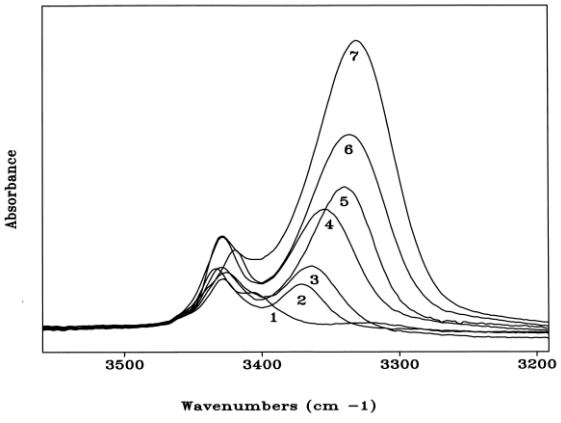

Fig. 2.23 FT-IR absorption spectra of Ac-Aib-Ala-Aib-Ala*-Ala*-Aib-Aib-Aib-OMe and its shorter sequences in the 3200-3550 cm^{-1} region. Spectra (1-6): Z-protected peptides, starting from Z-Aib_2-OMe; spectrum (7): **A4A5O**. Peptide concentrations: 1 mM in $CDCl_3$.

Further structural information was obtained on **A4H**, **A2A4H** and **A4A5O** by ECD[143] (**Fig. 2.24**).

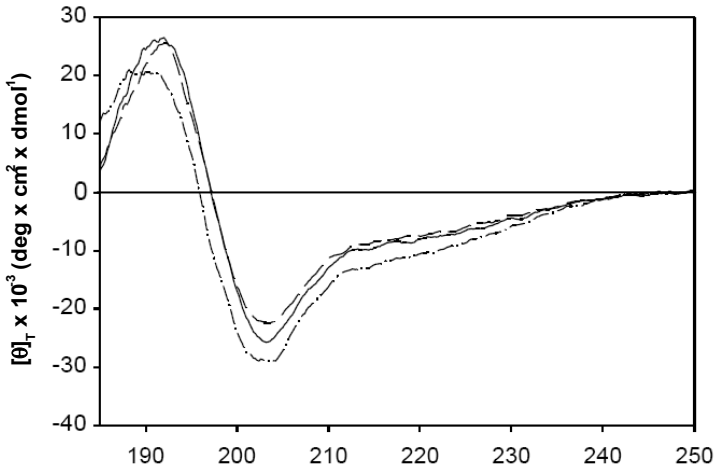

Fig. 2.24 Experimental far-UV ECD spectra of **A4H** (solid line), **A2A4H** (dashed line) and **A4A5O** (dotted-dashed line). The spectra were measured in TFE from 185 to 250 nm.

The ratio between the intensities of the negative Cotton effects at 222 and 205 nm in the ECD spectrum, recently designated as the *R* value, was used to distinguish 3_{10}- and α-helices.[21,26,65,66,70,144] Values between 0.3 and 0.4 favor a 3_{10}-helix structure, while values ~ 1.0 are typically found for α-helices. All three spectra exhibit a significant negative band at 204 nm and a weak negative shoulder at ~222 nm, with an *R* value of 0.35-0.40, consistent with a largely predominant 3_{10}-helix conformation. Similar *R* values were obtained for the other hexapeptides (data not shown).

2.2.2 VCD analysis

The VCD spectrum of a 3_{10}-helix conformation gives rise to a weak positive couplet (positive to lower energy) for the amide I band, and a strong, relatively sharp negative amide II band, while for an α-helix the same sign patterns are observed, but its amide I VCD is there dominant and amide II is broad and weak.[66,70,135,145,146] Again, these patterns are somewhat sensitive to the degree of C^{α}-alkylation and have small frequency shifts in different solvents. The relative intensity between the amide I and II features is the main determinant for distinguishing 3_{10}- and α-helices and the relative band shapes offer secondary confirmation (**Fig. 2.25**).

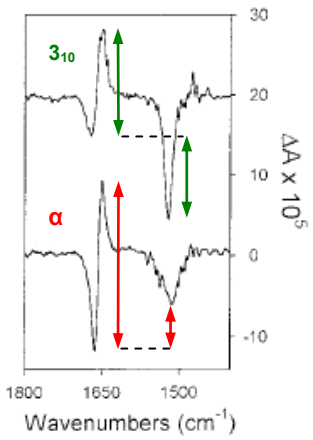

Fig. 2.25 Comparison between the different 3_{10}- and α-helical bandshapes revealed by VCD.[147]

The VCD spectra for the unlabelled (**UH**), and the labelled **A4A5H** and **A4A5O** peptides were measured in a TFE/$CHCl_3$ mixture and normalized to the area of the amide I band, as shown in **Fig. 2.26**. Due to normalization, the intensities should be independent of length to first order, which is approximately seen. The relative bandshapes for these peptides are consistent with that of a 3_{10}-helix, although the hexapeptide amide II appears weaker than expected, perhaps due to its higher relative contribution of Ala residues.[71] It is stronger for the octapeptide (**A4A5O**), fitting the 3_{10}-helical VCD pattern, but these differences are small.[66,146,148] The spectrum in the amide I region is more complex for the **A4A5H** and **A4A5O** peptides due to labelling, as discussed below, but the dominant 3_{10}-helical patterns are quite evident. The

comparison of the **A4A5H** and **A4A5O** indicates that adding two Aib residues increases the stability of the 3_{10}-helix conformation, shows no sign of an α-helical component, and fits results previously found for an octapeptide having an even higher fraction of Aib residues.[146,148] Similar relative amide I and II VCD lineshapes were observed for all other peptides investigated in this work.

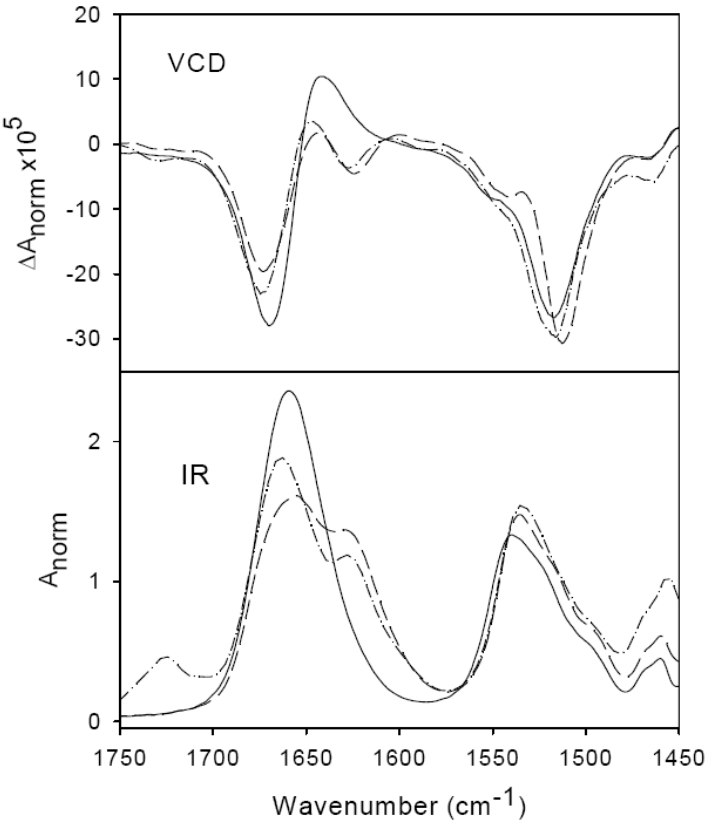

Fig. 2.26 Amide I-normalized VCD and FT-IR absorption spectra in the amide I and amide II band regions of peptides **UH** (solid line), **A4A5H** (dashed line), and **A4A5O** (dotted-dashed line) measured in TFE/$CHCl_3$ (1:3 v/v).

Unlabelled and single labelled peptides

The IR absorption spectrum of the unlabelled (**UH**) peptide in the amide I region (**Fig. 2.27**, *central panel*) consists of a single band with slightly asymmetrical lineshape to the lower energy side. This band can be fit to two Gaussian components, a main one at ~ 1660 cm^{-1} and a small feature at ~ 1630 cm^{-1} which both probably result from the dispersion of the exciton coupled $^{12}C{=}O$ local stretching modes that make up the amide

I band. The observed unlabelled hexapeptide amide I VCD spectra (**Figure 2.27**, *upper panel*) has a positive (lower frequency) then negative couplet, indicative of right-handed helical formation. This couplet could be fit to three Gaussian components, but details of the VCD fits have proven less reliable than for the IR absorption and Raman fits, and will not be discussed further.

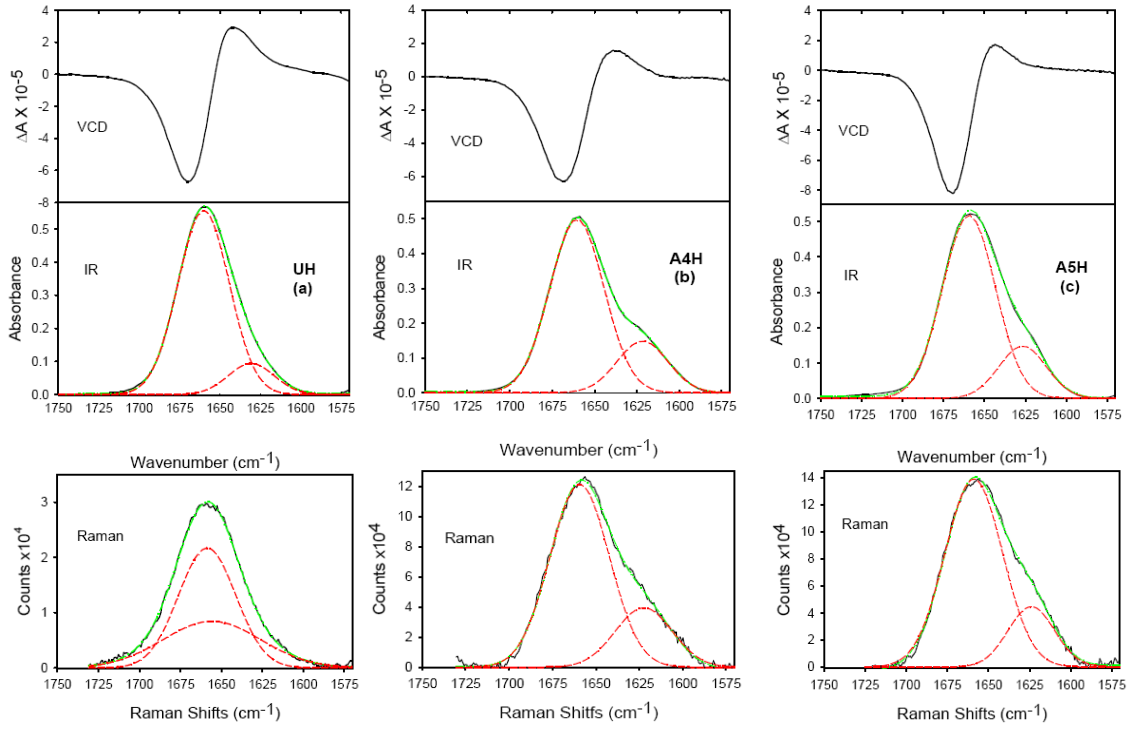

Fig. 2.27 Experimental VCD (upper panel), IR absorption (middle panel), and Raman (bottom panel) spectra of **UH** (a), **A4** (b), and **A5** (c)**.** The spectra, measured in TFE/$CHCl_3$ (1:3 v/v), only show the amide I region. The fitted Gaussian peaks in the IR absorption and Raman spectra are indicated with a dashed line.

For the single labelled **A4H** and **A5H** peptides an additional $^{13}C{=}O$ band appears in the IR absorption spectrum (**Fig. 2.27**), as a shoulder on the lower energy side of the amide I band. The **A5H** $^{13}C{=}O$ mode was fit to a band component at higher energy (~ 1626 cm^{-1}) than that for **A4H** (~ 1621 cm^{-1}). The difference arises because the Ala5 C=O group does not have a H-bond to another amide group, which results in that local mode having a higher energy than if it were intramolecularly H-bonded, as for Ala4. The significance of missing a H-bond (end effect) at Ala5 will be addressed further with variations in hexa- and octapeptides.

The measured **A4H** and **A5H** VCD bandshapes, shown in **Fig. 2.27** (upper panel), resemble that of the unlabelled (**UH**) peptide, since no identifiable VCD features are seen due to the single $^{13}C=O$ label. This lack of $^{13}C=O$ VCD is a consequence of its reduced coupling with other ($^{12}C=O$) vibrations and offers graphic evidence of the importance of coupling in providing structural sensitivity to the spectral response. For **A4H** and **A5H**, the VCD is weaker than for the unlabelled hexapeptide, due to its having one less coupled $^{12}C=O$ oscillator, and the spectra are somewhat broader, probably due to the break in the exciton coupling which disperses the intensity over more modes instead of concentrating it in one or two coupled modes.

The Raman spectra (lower panels in **Fig. 2.27)** reflect the IR absorption result, showing just a weak shoulder to low frequency on the main Raman amide I band. In each case the IR absorption band ($^{12}C=O$) maximum is at ~ 1660 cm^{-1}, while that of the Raman band is at ~ 1658 cm^{-1}. This shift is due to the relative distribution of intensity among the exciton split amide I modes.

The calculated IR absorption and VCD spectra for the idealized 3_{10}-helix geometry qualitatively agree with the **A4H** experimental spectra as shown in **Fig. 2.28**. The main differences are that the DFT calculated amide I frequency is too high (40 – 45 cm^{-1}) and the $^{12}C=O$ – $^{13}C=O$ separation is too large for **A4H** in comparison to the experimentally observed patterns. By contrast, for **A5H** (**Fig. 2.28**) the computed $^{13}C=O$ mode is not resolved from the $^{12}C=O$ amide I band. This difference between the Ala4 and Ala5 C=O frequencies has two sources, being due to the FF overestimating the end effect for Ala5 and overestimating the FF positional dependence for Ala4. Nonetheless, these effects (mostly H-bond formation differences) clearly lead to a non-degeneracy in the two local oscillators (Ala4 and Ala5) which can be seen experimentally (but much smaller) and must be taken into account in order to analyze the coupling between pairs of C=O groups on different sites. This phenomenon provided a continuing challenge in interpreting the theoretical simulation analyses of the experimental spectra. As a partial fix, the octapeptide (**A4A5O**) sample was prepared so that the Ala4 and Ala5 positions were well-contained in the 3_{10}-helical fold and were internally H-bonded to amides further in the sequence.

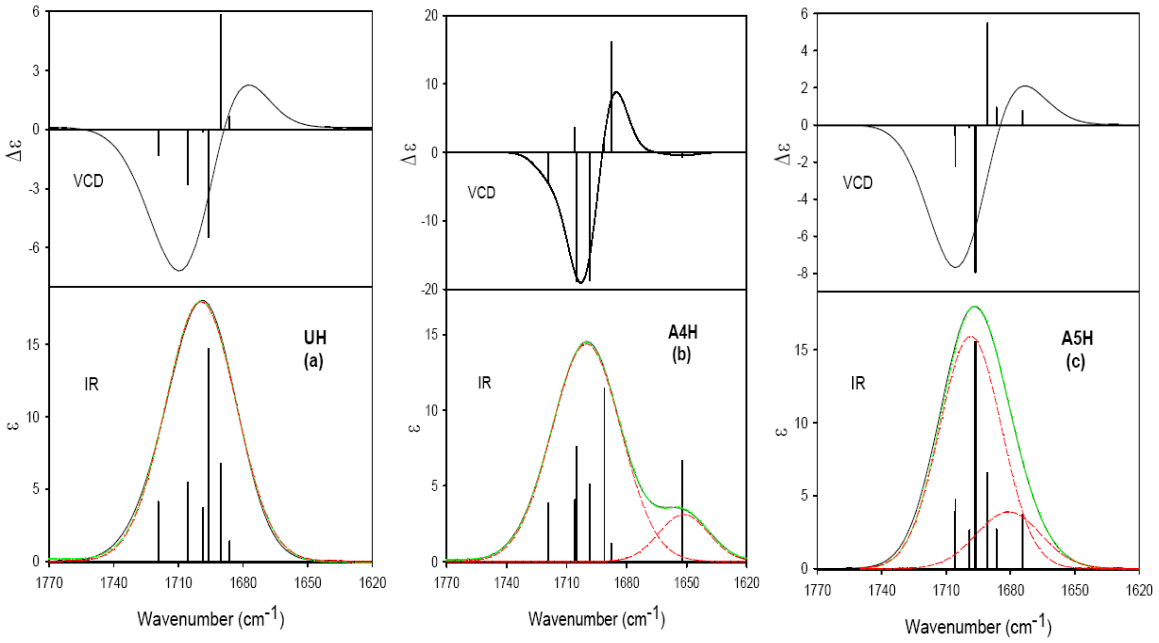

Fig. 2.28 Simulated IR absorption (*bottom panel*) and VCD (*upper panel*) spectra of **UH** (a), **A4H** (b) and **A5H** (c), are indicated with normal modes. Simulated IR absorption of **UH** is fitted with one Gaussian peak, whereas those of **A4H** and **A5H**, fitted with two Gaussian peaks, are indicated with a dashed line.

Double labelled hexa- and octapeptides

The experimental amide I IR absorption, VCD, and Raman spectra for the double isotope labelled **A4A5H** hexapeptide and **A4A5O** octapeptide are shown in **Fig. 2.28**. The ^{13}C=O mode in the IR absorption spectra appears as a pronounced shoulder on the ^{12}C=O amide I band. The sideband has reduced relative intensity for **A4A5O** compared to that of **A4A5H**, due to there being proportionately fewer ^{13}C=O oscillators in the double labelled octapeptide. This band is also shifted to lower frequency in **A2A5O**, presumably due to its two coupled modes having more comparable H-bond formation (Ala5 is not H-bonded in the hexapeptide), which makes the overlap of ^{12}C=O and ^{13}C=O bands less for **A4A5O**.

The corresponding VCD spectra for both **A4A5H** and **A4A5O** have a positive couplet shape in both the ^{13}C=O and ^{12}C=O amide I bands, with positive lobe to the lower frequency side of the corresponding IR absorption band, but, due to overlap and to the negative bias of the dominant ^{12}C=O couplet, the positive contributions are diminished. The isotope shifted **A4A5H** VCD appears to be relatively more intense.

However, that result is partly due to the enhanced fraction of ^{12}C=O and increased VCD intensity in **A4A5O**, plus some effects of the non-degeneracy of the Ala4 and Ala5 ^{13}C=O oscillators in the hexapeptide. The ratio of ΔA/A for the ^{13}C=O bands in each peptide is comparable. The Raman spectra for **A4A5H** and **A4A5O** are again like the IR absorption results, but appear to be broader, especially for the ^{13}C=O contribution in **A4A5O**.

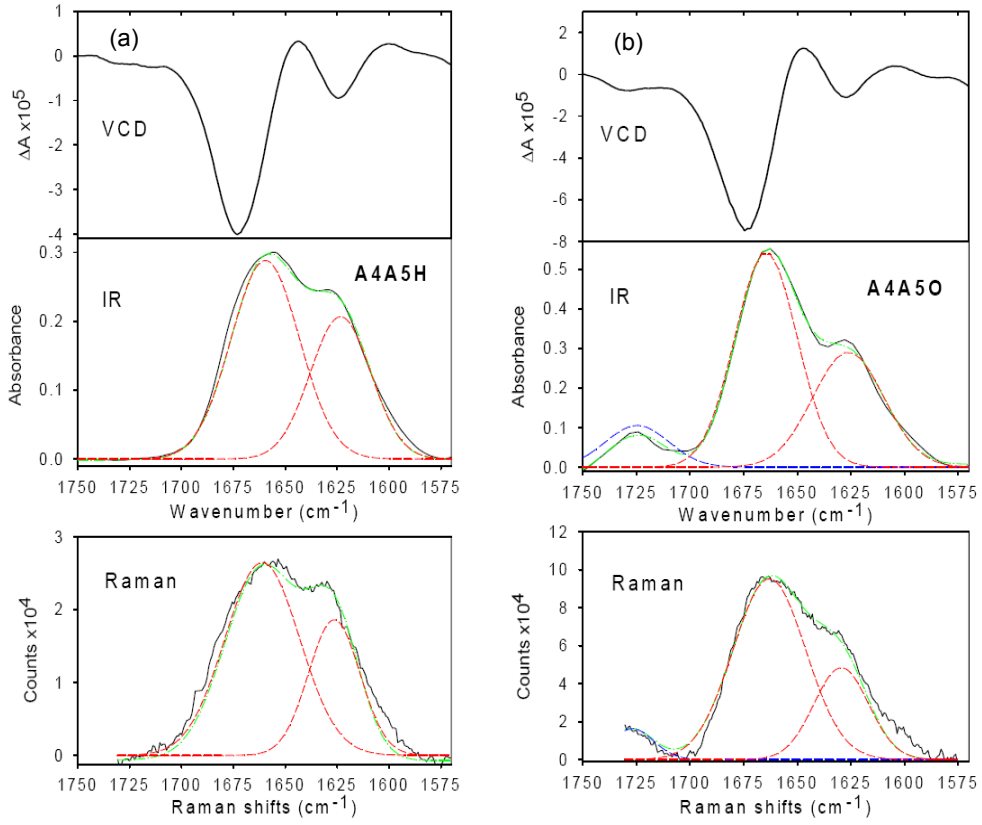

Fig. 2.29 Experimental VCD (*upper panel*), IR absorption (*middle panel*), and Raman (*bottom panel*) spectra of **A4A5H** and **A4A5O**. The spectra were measured in TFE/$CHCl_3$ (1:3 v/v) and only illustrated in the amide I region. For **A4A5O**, the C-terminal (OMe) cap band is seen near 1725 cm^{-1}. Experimental IR absorption and Raman spectra are also fitted to two Gaussian peaks in the ^{12}C/^{13}C region.

When the labelled residues are further separated in the sequence, as in **A2A4H** and **A2A5H**, the coupling is reduced. Experimentally, this result has a relatively minor impact on the IR absorption and Raman spectra but has much greater effect on the VCD band shape, as seen in **Fig. 2.30** (*upper panels*). In the IR absorption spectra, a ^{13}C=O band resolved from the ^{12}C=O band is evident in **A2A4H** and **A2A5H**, but is weaker in

intensity than that seen above for **A4A5H**. In the VCD the two separated labels for these 3_{10}-helical peptides give very different patterns. The **A2A4H** peptide has a quite broad negative component and a weak positive one that appears on the high frequency side of the $^{13}C=O$ IR absorption band. Moreover, the **A2A5H** VCD has resolved positive $^{13}C=O$, on the low frequency side of the IR absorption band, and negative $^{12}C=O$ bands with a weak negative shoulder lying between them. Raman spectra of the amide I modes for the **A2A5H** and **A2A4H** peptides are also shown in **Fig. 29 (***lower panel*). Again, these curves strongly resemble the IR absorption patterns, but are somewhat broader and less resolved, which may be due to the higher concentration needed to obtain good Raman spectra.

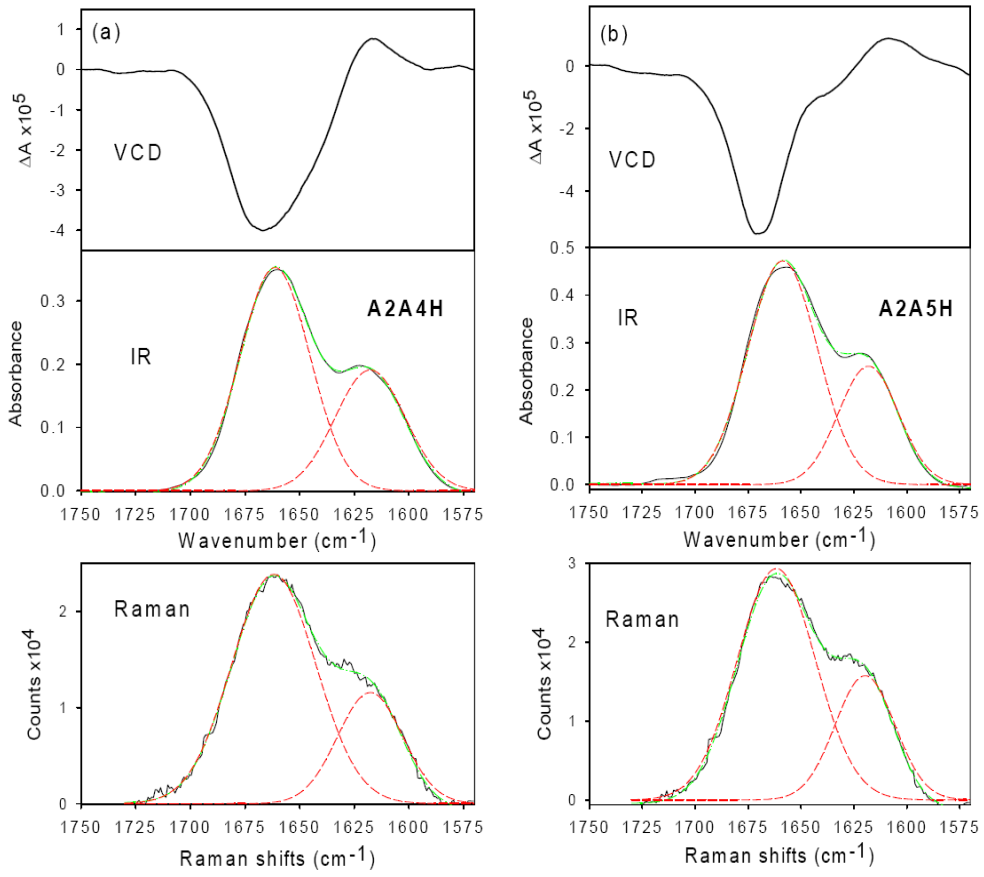

Fig. 2.30 Experimental VCD (*upper panel*), IR absorption (*middle panel*) and Raman (*bottom panel*) spectra of **A2A4H** and **A2A5H**. The spectra, measured in TFE/$CHCl_3$ (1:3 v/v), only shows the amide I region. IR absorption and Raman spectra are fitted to few Gaussian peaks.

Due to the anomalous behavior of the Ala5 position $^{13}C=O$ in the hexapeptide, for which the single mode frequencies were not well represented in modeling **A5H**, the computed splittings for the double labelled **A4A5H** and **A2A5H** were expected to have difficulty reproducing the experimental results, so that the simulated bandshapes are only qualitatively useful (**Fig. 2.31**).

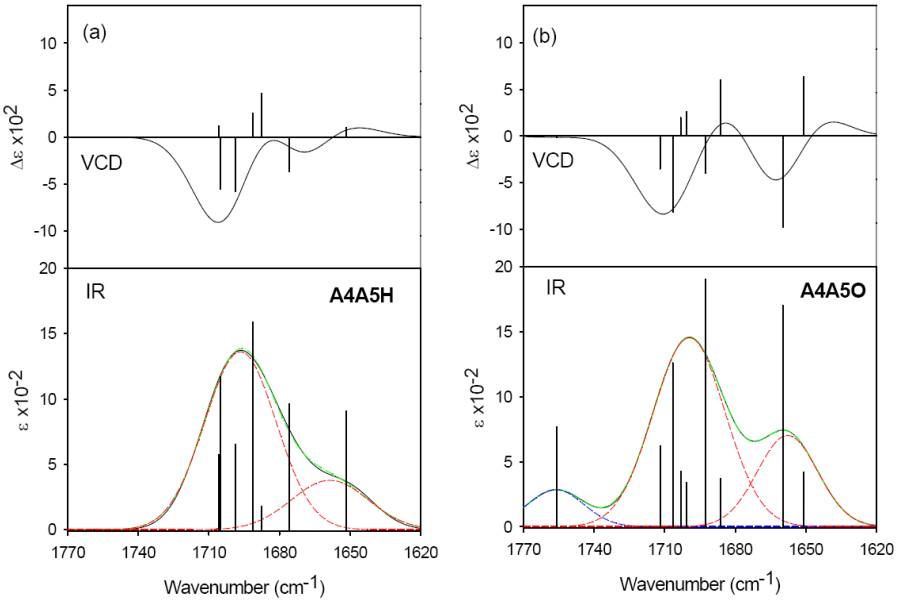

Fig. 2.31 Simulated IR absorption (*bottom panel*) and VCD (*upper panel*) spectra of **A4A5H** and **A4A5O** are indicated with normal modes. Simulated IR absorption of **A4A5** is fitted with two Gaussians peaks (indicated with a red dashed line), whereas **A4A5O** is fitted with two Gaussian peaks. An additional peak, added between 1770 and 1740 cm^{-1} to compensate for the band of the C-terminal (OMe) group, is indicated as a blue dashed line.

The IR absorption for all the double labelled peptides are predicted to have a $^{13}C=O$ side band, but for the hexapeptides only those for **A2A4H** have relative intensities that match the experiment. This result is because only one mode (computed at ~ 1652 cm^{-1}) contributes to the simulated $^{13}C=O$ band for **A4A5H** and **A2A5H**, while the other $^{13}C=O$ mode (~ 1674 cm^{-1}) basically appears as the lowest frequency component of the apparent exciton broadened $^{12}C=O$ band (the center of which fits to a broadened Gaussian at ~ 1698 cm^{-1}). The frequencies for the computed $^{13}C=O$ modes and Gaussian fits to the lineshape broadened patterns are listed in **Table 2.2**. Computed frequencies are all high by ~ 50 cm^{-1} due to lack of correction for solvent effects and to

normal DFT errors. As determined from these simulations, the IR absorption and Raman amide I spectra are predicted to have very similar intensity patterns, making their measurement confirmatory for 3_{10}-helices, in contrast to the complementary isotope shifts found for other structures such as the PPII helices[15].

Notation	^{13}C Peak position (cm^{-1})		Gaussian fit
A4H	1652		1652
A5H	1674		1681
A4O	1657		1655
A5O	1652		1652
A4A5H	1675	1652	1659
A4A5O	1659^{S}	1651^{A}	1658
A2A4H	1654^{A}	1648^{S}	1650
A2A5H	1674	1651	1656

^{A}Asymmetric mode; ^{S}symmetric mode.

Table 2.2 Theoretical frequency values (normal modes) for the peptides investigated

Reducing the spectral complications due to the end effects was addressed by preparing the **A4A5O** octapeptide which again has distinct ^{13}C=O and ^{12}C=O bands but with different relative experimental intensities, as shown in **Fig. 2.29**. For **A4A5O** an additional band is observed ~ 1725 cm^{-1}, due to the ester (OMe) protecting group at the C-terminus. In the experimental IR absorption, the **A4A5O** ^{12}C=O band is sharper than that for **A4A5H** and better overlaps the **A2A4H** result. Both **A2A4H** and **A4A5O** have both ^{13}C=O modes intramolecularly H-bonded, thereby eliminating distortion and high overlap with the ^{12}C=O modes, which is a problem for **A4A5H** (and for **A2A5H**). The **A4A5O** VCD spectrum has a clear, but weak negative-positive couplet ^{12}C=O amide I, followed by a negative-positive ^{13}C=O couplet due to ^{13}C modes (**Fig. 2.29**, upper panel), in good qualitative agreement with the **A4A5H** results. Attempts to measure the spectrum with higher resolution (not shown) gave essentially the same spectral result. The simulated IR absorption and VCD spectra for **A4A5O** again qualitatively agree with the experiment ones, now having the correct relative IR absorption intensity for the ^{13}C=O contribution.

Coupling analysis

To better analyze and compare these overlapping contributions between different labelling patterns, all the IR absorption spectra were fit to a minimal number of Gaussian band components to give the same type of fit pattern to each spectrum, experimental and simulated, even if more components might have reduced the overall fitting error. From this point of view, a more systematic variation develops with isotope substitution pattern and the fits are quite acceptable (**Figs. 2.27-2.32**). The fit bands for the computed $^{13}C=O$ IR absorption components in **A4A5H** and **A2A5H** are ~ 6-8 cm^{-1} higher in frequency than for **A2A4H.** This finding is in qualitative agreement with the **A2A5H** fitted experimental $^{13}C=O$ band being ~ 6 cm^{-1} higher than that for **A2A4H** (however, the **A2A5H** was about the same) as summarized in **Table 2.2**. Similarly, the **A4A5O** and **A4A5H** experimental and theoretical fit band positions are about the same, but the details are a bit more complex in that the high-frequency Ala5 mode does not seem to have the same sort of effect it apparently has for **A2A5H**.

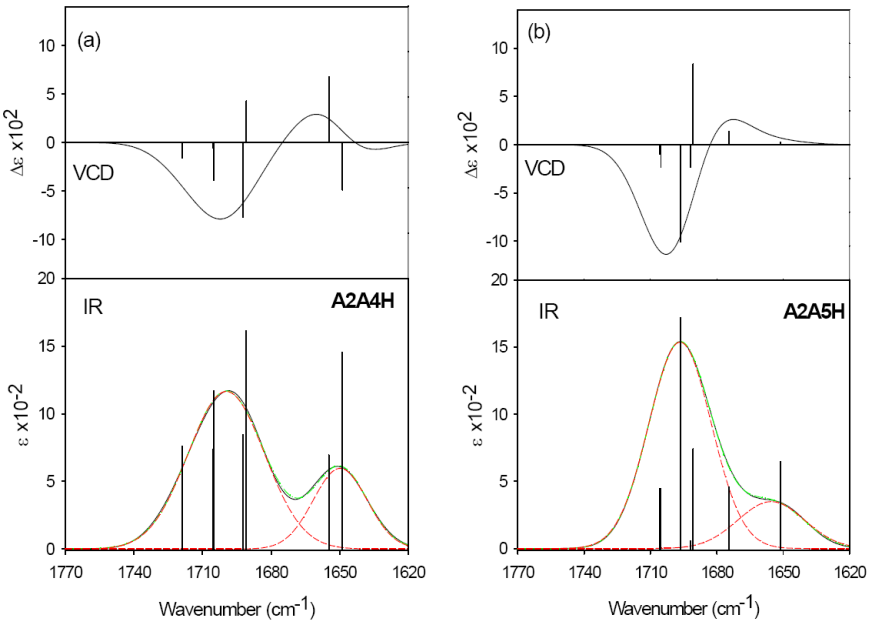

Fig. 2.32. Simulated IR absorption (*bottom panel*) and VCD (*upper panel*) spectra of **A2A4H** and **A2A5H**.

The quality of the simulated VCD patterns in both **A4A5H** and **A4A5O**, as shown in **Fig. 2.31** (*upper panel*), may be surprisingly good given the impact of end effects on the mode mixing for **A4A5H**, but the primary criterion determining the VCD sign pattern is the sign of the coupling between the two labelled residues. This sign is correctly predicted and is the same in both, although the splitting is larger for **A4A5H** due to the end effect. Thus, the experimental IR absorption frequency is higher and the relative VCD contribution appears to be larger for **A4A5H** as well, due to the local Ala5 and Ala4 mode (diagonal force constant) differences. The simulations have overestimated the contributions from both these diagonal FF differences for the 3_{10}-helical pattern, as seen in the mode positions in **Table 2.2** which directly reflect the difference between **A4H** and **A5H**. However, the impact of this overestimation on the position of the fitted Gaussian components is small, which appears to be a coincidence due to multiple overlapping broadened components. The computed ^{13}C=O VCD for the octapeptide is actually larger than for the hexapeptide, due to the complex mode mixing affecting the overlap of positive and negative ^{12}C=O VCD contributions in the middle of the amide I band. The root cause of the problem for the simulations is the overestimation of the difference of the diagonal FF for Ala4 and Ala5, as was brought out in the **A4H** and **A5H** comparison. This overestimation makes the analysis of the coupling more complex than for **A2A4H**, for example.

For the simulated **A2A4H** peptide spectra, as shown in **Fig. 2.32**, the more intense, in-phase, mode is computed at a lower frequency (1648 cm^{-1}), while the out-of-phase mode is at a higher frequency (1654 cm^{-1}), with a mode splitting of 6 cm^{-1} (**Table 2.2**). If we assume that the uncoupled, Ala2 and Ala4 amide I local modes were degenerate, then the coupling constant would be ~ 3 cm^{-1}. This assumption is supported by the relatively large difference in Raman intensities computed for the two bands (not shown), implying strong mixing, and by the near degenerate computed frequencies for the Ala4 (1652 cm^{-1}) and Ala2 (1651 cm^{-1}) ^{13}C=O modes. The virtue of this model is in its fit to the experimental spectra, which, compared to the computed amide I IR absorption spectra, shows a reasonable agreement (**Fig.s 2.30** and **2.32**; **Table 2.3**). The VCD can also be seen to be in agreement, in that the positive ^{13}C=O component is higher in frequency than the IR absorption band and a weak negative VCD is seen to lower frequency, in agreement with the computed spectrum. Higher resolution might better define the ^{13}C=O contributions to VCD, but the signals are predicted to be small

(and our preliminary tests with higher resolution did not yield more bandshape variation). Thus, this comparison to the experimental spectra supports the validity of the computed -3 cm^{-1} coupling constant, which is quite comparable in sign and magnitude to the 1→3 coupling constant we derived for α-helices.[135]

	$^{12}C/^{13}C$ Peak positions (cm^{-1})					
	Experimental				Theoretical	
	IR		Raman		IR	
Notation	^{12}C	^{13}C	^{12}C	^{13}C	^{12}C	^{13}C
UH	1660	1631	1659	1656	1700	
A4H	1660	1622	1659	1622	1700	1652
A5H	1659	1627	1659	1624	1699	1681
A4A5H	1660	1623	1661	1626	1697	1659
A2A4H	1661	1618	1662	1618	1700	1650
A2A5H	1659	1618	1662	1620	1697	1656
A4A5O	1665	1626	1663	1629	1699	1658

Table 2.3 Experimental and theoretical band fitted values for the peptides investigated

Such a simple approximation of directly using the mode splitting to determine the coupling constant for **A4A5H** does not work due to the end effects on the Ala5 $^{13}C=O$ group. The simulated **A4A5H** spectra have the in-phase mode of $^{13}C=O$ at a high frequency, close to the $^{12}C=O$ mode, while the out-of-phase mode is at lower frequency, which immediately demonstrates that the **A4A5H** coupling is opposite in sign (positive) as compared to that of **A2A4H**. This finding parallels the result found for α-helices in that adjacent *vs.* separated labels had opposite signed coupling constants, and both had the same sign as seen here for the 3_{10}-helices. Again, in both α- and 3_{10}-helical cases, the coupling sign is the reason that the VCD flips sign as well.[135] The computed splitting between these $^{13}C=O$ modes is ~ 24 cm^{-1} in **A4A5H** (**Table 2.2**) and their intensities are similar indicating that there is only a weak coupling between them. However, the sign change is confirmed by the relative sign pattern of the two components in the simulated VCD spectrum and its match to experiment, being positive to low frequency for **A4A5H** (and **A4A5O**), but negative (albeit weak) for **A2A4H**.

The simulated VCD spectrum of **A4A5H** (**Fig. 2.31**, *upper panel*) resembles the experimental result, *i.e.* the ^{12}C and ^{13}C amide I components both have positive couplet VCD band shapes [**Fig.s 2.29 (a)** and **2.31 (a)**]. This agreement of predicted IR absorption and VCD spectra with experimental results for the **A4A5H** supports the validity of the computations and encourages us to use the theoretical spectra to derive a coupling constant by correcting for the end-effect difference in the two oscillators. As opposed to the simple degenerate coupling model used above for **A2A4H,** with **A4A5H** we need a non-degenerate model. The **A4H** and **A5H** simulations suggest that the computed components will have a distinct non-degeneracy of 22 cm^{-1} (Ala4, 1652 cm^{-1} and Ala5, 1674 cm^{-1}). However, the comparison of experimental and simulated spectra show these two computational estimates are too severe to fit the oserved isotope shift. Use of the simulated single label values in a non-degenerate coupling analysis will provide a basis for estimating the coupling constant derived from the **A4A5H** simulation, without knowing the absolute values, for comparison to experiment. With a non-degenerate frequency difference of 22 cm^{-1}, a coupling constant of 5 cm^{-1} would yield a resultant 24 cm^{-1} splitting of the coupled modes, which can be viewed to be a lower bound for coupling of adjacent C=O groups in a 3_{10}-helix.

Alternatively, we can analyze the **A4A5O** data to determine the adjacent coupling. If we again use the degenerate coupled oscillator assumption (as done for **A2A4H**) for **A4A5O**, we would assume that the computed splitting of ~ 8 cm^{-1} (**Table 2.2**) was twice the coupling or that the coupling constant was ~ 4 cm^{-1}, in excellent agreement with the result derived from the **A4A5H** computation above. This value, substantially smaller than that found for α-helices (~ 7 cm^{-1}),[135] probably accounts for the smaller relative impact the ^{13}C=O bands have on the 3_{10}-helical spectra, particularly the difference in the IR absorption frequencies with **A2A4H** and their VCD intensities in comparison to the ^{12}C=O components.

2.2.3 Conclusions

We have evaluated the coupling between amide C=O groups on adjacent and separated residues in a series of 3_{10}-helical model peptides. Values determined are smaller than those found for α-helices for adjacent residues and about the same for separated ones. The sign patterns are the same for α- and 3_{10}-helices. The adjacent C=O

groups have a positive coupling, yielding the same VCD sign pattern and a more intense IR component to higher energy (closer to the ^{12}C=O band). The C=O groups separated by one residue have the opposite sign pattern. The computations qualitatively supported the observed isotopic shifts and splittings of coupled modes, but the details seemed dependent on minor changes in the FF or on solvation effects which were not included in the modeling. VCD for 3_{10}-helices is weaker than for the corresponding α-helices due to this weaker coupling, leading to less dispersion in the exciton coupled band, both in the labelled residues and in the overall amide I bandshape. This reduced coupling appears to result form the different angle of the H-bonded C=O groups with respect to the helix axis in the 3_{10}-helices as compared to the α-helix H-bonding pattern.

3. C^{α}-methyl proline: a unique example of split personality

3.1 Introduction

Nature vividly teaches that copolymer sequence is a powerful way to meet diverse chemical challenges. The breadth of structure and function displayed by the molecules of biology is remarkable and comprises catalysis, tight and specific binding, directed flow of electrons or information storage. The large molecules entrusted with these crucial and fascinating tasks, mostly proteins but sometimes nucleic acids are unique relative to other biological and synthetic polymers in that they adopt specific compact conformations that are thermodynamically and kinetically stable, exerting a masterful control over the non-covalent forces that govern folding and self-assembly processes.

Systematic studies on alternative monomers closely related to the constituents of the three major biopolymer backbones found in nature (proteins, ribonucleic acids, and polysaccharides) have provided clues about the fitness of α-amino acids, ribofuranosyl (5′→3′) nucleic acids, and phosphodiester linkages. Yet "why nature is such, and not otherwise"[149] is a question that continues to be asked. Looking beyond the range of chemical capabilities that evolution has elicited from biopolymers and their related derivatives however, it is possible to design analogous capabilities into unnatural polymers or chain molecules that fold into compact and specific conformations and display similar functions. This prediction has only recently begun to be tested, raising questions of great fundamental interest. On a more practical level, the discovery of new functional polymers clearly has widespread potential for both chemistry and biology.

Since biological evolution has operated under many constraints, the functional properties of biopolymers should be viewed as merely exemplifying the potential of compactly folded polymers. The chemist's domain includes all possible combinations of the elements, and the biological realm, vast and complex though it may be, is only a small part of that domain. Therefore, realization of the potential of folding polymers may be limited more by the human imagination than by physical barriers.

A *foldamer* is any oligomer that folds into a conformationally ordered state in solution, the structures of which are stabilized by a collection of noncovalent interactions between nonadjacent monomer units.[150,151] There are two major classes of foldamers: single-stranded foldamers that only fold (peptidomimetics and their abiotic analogues) and multiple-stranded foldamers that both associate and fold (nucleotidomimetics and their abiotic analogues). Furthermore, foldamers can be roughly classified into three categories with regard to their monomer types: peptidomimetic foldamers, nucleotidomimetic foldamers, and abiotic foldamers. The former two are inspired by the structures of proteins and nucleic acids, and are mainly based on the modification of the chemical structure of the monomer (amino acids and nucleotides), while the latter one utilizes aromatic interactions, charge-transfer interactions, and others, that are not general in the Nature. Examples of the three groups of foldamers are illustrated in **Figs. 3.1-3.3**.

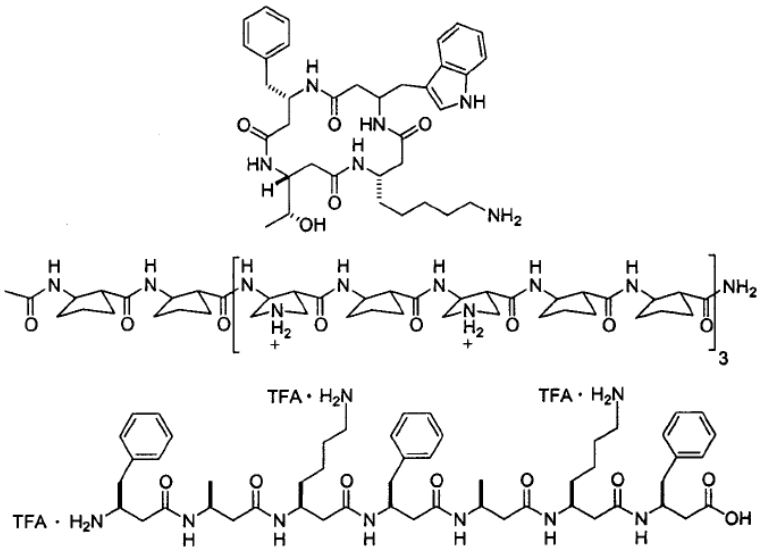

Fig. 3.1 β-Peptide oligomers studied for their biological activity.[152-154]

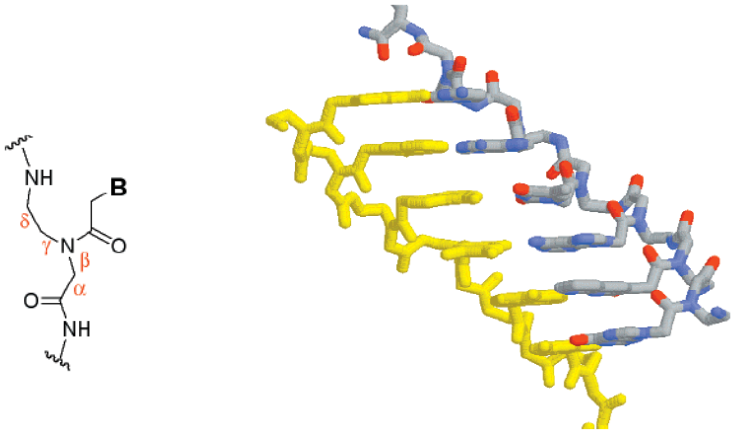

Fig. 3.2 Left: structure of peptide nucleic acids (PNAs; **B** is a nucleobase) labeled with dihedral angles; right: crystal structure of a peptide nucleic acid duplex.[155]

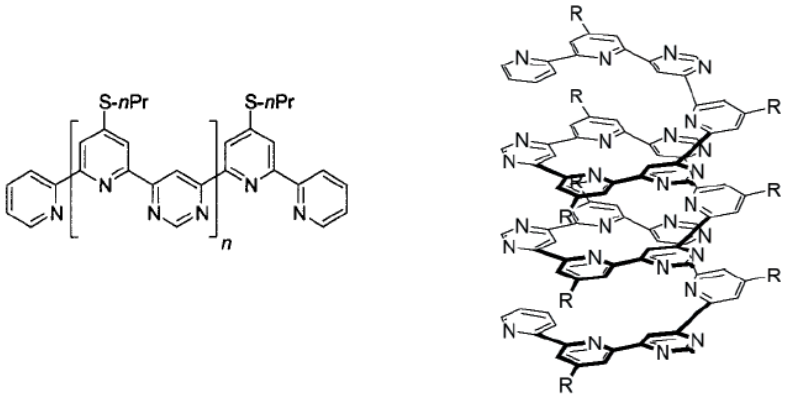

Fig. 3.3 Drawing (right) of the proposed helical conformation of the oligomer on the left (n = 8).[156,157]

The path to creating useful foldamers involves several daunting steps, like (*i*) identifying new polymeric backbones with suitable folding propensities (*i.e.* developing a predictively useful understanding of the relationship between the repetitive features of monomer structure and conformational properties at the polymer level), (*ii*) endowing the resulting foldamers with interesting chemical functions, by design, by randomization and screening ("evolution"), or by some combination of these two approaches and (*iii*) being able to produce a foldamer efficiently.

The general first step in foldamer design consists of identifying new backbones with well-defined secondary structural preferences. Within the past twenty years, an increasing number of research groups have described unnatural oligomers with

interesting conformational propensities. The motivations behind such efforts are varied, but these studies suggest a collective, emerging realization that control over oligomer and polymer folding could lead to new types of molecules with useful properties.

Among the three categories previously reported, the peptidomimetic foldamers have been most actively investigated so far. Since this research field has been motivated by (and takes inpiration from) the well-known, highly-ordered structures of biopolymers, it is obvious that foldamers ability in mimicking the attributes of proteins, nucleic acids, and polysaccharides can be interpreted with their folding into well-defined conformations, such as helices, sheets, turns, as seen in biological macromolecules. The major advantage in peptidomimetic foldamers is that the amide groups, that combine monomers into the chain, also act as cross-linking points via hydrogen bonding between the NH proton and the carbonyl oxygen to fold the chain into a regular structure. Therefore, these structures are able to easily form secondary structures (various helix-types, strand-like conformations, and turns) and are capable of forming higher-order self-assemblies too. That's why they belong among the most intriguing models of unnatural polymers.

Obtaining structural information on well-defined local structures (secondary structure elements) is the key to an effective and rational designing of new and useful tertiary structure in Nature-inspired, foldameric systems, as conformational analysis of both proteins[158] and RNA[159-161] is hierarchical. The characteristics shown by these biopolymers seem to teach us, however, that we will not be able to generate new tertiary structures until we know how to identify unnatural backbones that are predisposed to adopt specific secondary structures. The types of secondary structure most crucial for foldamer development are those that display long-range order, *i.e.* helices and sheets. Chan and Dill have predicted that these two long-range secondary structures will be characteristic of all compactly folded polymers.[162]

Approaches to mimicking structural features found in proteins[163-166] have based, for example, on strategies to control local chain folding *via* short- and medium-range interactions[167-169] like patterning of hydrophobic and hydrophilic residues along the sequence to drive folding in a predetermined direction.[170] In general, this quest has been achieved using lessons gained from inspection of the large body of available protein three-dimensional structures,[171] like the use of Asn-Gly to nucleate β-hairpin

formation[172-178] and the cross-strand Trp-Trp interactions to stabilize antiparallel strands.[179]

As previously seen (Chapter 1), the peptide foldamers synthesized and studied in this Thesis exploited another strategy to such mimicks, based on the use of non-proteinogenic amino acids to impose local backbone folding constraints, specifically the use of Aib and related $C^{\alpha,\alpha}$-dialkyl α-amino acids. Their introduction in a peptide sequence directs the course of chain folding, by biasing the choice of local conformations; helix nucleation and stabilization may be readily achieved by strategic incorporation of these conformationally constrained amino acids. An alternate approach towards nucleating helical folding is the use of diproline templates. Developed by Kemp and co-workers[180-182] and subsequently extended by the group of Hanessian,[183] this approach is based on early observation that the diproline-containing sequences can form incipient 3_{10}-helical structures in organic solvents, where consecutive type-III β-turn formation is driven by successive H-bond formation.[184]

L-Proline is conformationally unique among coded amino acids in that its φ torsion angle is severely restricted (-65 ± 10°) by its characteristic five-membered pyrrolidine ring structure and the preceding ω torsion angle can undergo a *cis* (0°) ⇌ *trans* (180°) equilibrium, thus generating a significant population of *cis* isomers for tertiary amides when compared with the negligible populations for the secondary amides of the usual peptide bonds. In addition, its ψ torsion angle is commonly found either in the right-handed 3_{10}-/α-helical region (-30 to -50°, or *cis*' conformation) or in the left-handed, *semi*-extended, region [-150 ± 10°, or *trans*', or poly-$(L\text{-}Pro)_n$ conformation]. Poly-$(L\text{-}Pro)_n$ is known to exhibit dimorphism (**Fig. 3.4**). This phenomenon is related to the ω *cis* ⇌ *trans* isomerism: in the poly-$(L\text{-}Pro)_n$ I conformation all ω torsion angles are *cis*, but in the more stable type-II conformation they are all *trans*. Furthermore, Pro is an amino acid with a marked preference for the *i* + 1 corner position of either type-I or type-II β-turn.[17,92] A Pro residue internal to a peptide sequence cannot offer the classical H-bonding donor N-H group for helix stabilization. It is for this reason that Pro residues are normally found near the N-terminus of peptide helices. However, if a Pro residue is internal to a helical sequence, it usually generates a kink, thereby interrupting the regular continuation of the helix (in that segment the peptide backbone is often solvated). Interestingly, if combined with a strongly helicogenic residue such as Aib, Pro can still be part of an intramolecular H-

bonded helical structure. Indeed, the -(Aib-L-Pro)$_n$- sequence was shown to fold into a variant of the right-handed 3_{10}-helix, known as the β-bend ribbon.[185,186] This helix is stabilized by 50% of the intramolecular H-bonds occurring in a regular 3_{10}-helix. An additional property of Pro is that it occurs extensively in the collagen triple helix (**Fig. 3.4**). The typical -(Pro-Xxx-Gly)$_n$- triplet of this fibrous protein forms a left-handed, type-II poly-(L-Pro)$_n$ conformation. In this structure the intrachain N···O distances are definitely too long for N-H···O=C H-bond formation. Indeed, the collagen superhelical arrangement is stabilized by a set of interchain H-bonds, in which the Pro residues behave as H-bonding acceptors. The relevance of this helical structure resides in that it is specifically bound by SH3 domains; this binding is important for many protein-protein interactions and even for interactions between the domains of a single protein.[187-189]

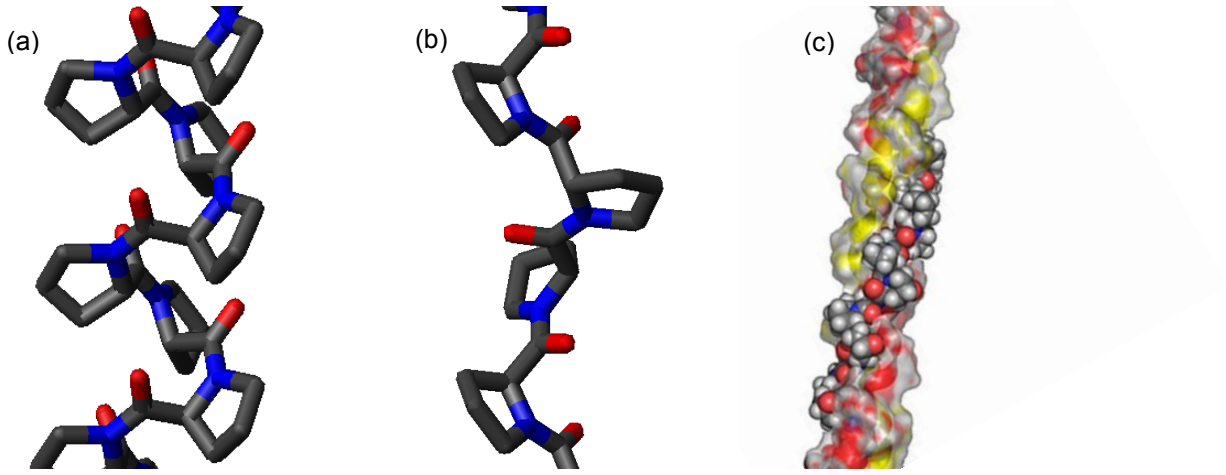

Fig. 3.4 Poly-(L-Pro)$_n$ type I (a), poly-(L-Pro)$_n$ type II (b) and collagen triple helix (c).

To extend and combine the two chacteristics of C^{α}-tetrasubstitution and the constraints exhibited by the unique Pro ring we decided to carry on a conformational analysis on the C^{α}-methylated derivative of Pro, (αMe)Pro. Despite its great potential interest, however, only few, scattered, and nonsystematic studies have been so far reported on the conformational preferences of (αMe)Pro. Indeed, among the C^{α}-methylated derivatives of the coded amino acids, (αMe)Pro is by far the most conformationally restricted (φ is blocked; in linear peptides the preceding tertiary amide

torsion angle ω is expected to adopt only the *trans* conformation; the side-chain χ^n torsion angles are also rigidified).

In 1974, in their theoretical study on the effect of C^{α}-methylation on the energetically preferred conformations of L-Pro derivatives, Leach and co-workers predicted that this backbone substitution, producing C^{α}-methyl L-proline (L-(αMe)Pro), would generate a φ,ψ energy surface uniquely restricted to a single region, namely, that of the righthanded helical conformation.[190] A decade later, Flippen-Anderson et al.,[191] by use of X-ray diffraction, showed that the simple, racemic "monopeptide" Ac-D,L-(αMe)Pro-NHMe (Ac = acetyl; NHMe = methylamino) is indeed helical in the crystalline state (without any stabilization arising from a C=O···H-N intramolecular hydrogen bond) and its L-enantiomer adopts right-handedness. On the contrary, by use of conformational energy calculations, Delaney and Madison[192] demonstrated that the total energy for the L-enantiomer has a deep well at the right-handed C_7' (inverse γ turn) conformation.[193,194] For this compound both the *semi*-extended [also termed poly $(L\text{-}Pro)_n$ II] and right-handed helical regions are less stable. However, the barrier separating the C_7' and helical regions is rather low and the population of the C_7' conformation tends to be overestimated in compounds too short to form β-turns[17,91,92] or 3_{10}/α-helices.[6,72] From a combined ^{13}C NMR, IR absorption, and CD analysis these authors[195] confirmed the preference of Ac-L-(αMe)Pro-NHMe for the C_7' conformation, irrespective of the solvent used. Conformational potential-energy calculations suggested that poly-$(L\text{-}(\alpha Me)Pro)_n$ is locked in the type-II poly $(L\text{-}Pro)_n$ conformation.[196] The CD spectrum of a solution of poly-$(L\text{-}(\alpha Me)Pro)_n$ of low molecular weight in alcohol, synthesized by means of N-carboxyanhydride polymerization, is reminiscent of that of type-II poly $(L\text{-}Pro)_n$.[196] The preferred conformations of the heterochiral dipeptides Z-L-Pro-D-(αMe)Pro-NHMe and Z-D-(αMe)Pro-L-Pro-NHMe were examined by IR absorption and ^1H and ^{13}C NMR spectroscopic techniques.[197] The former adopts a type-II β-turn conformation [in which D-(aMe)Pro is a left-handed helix], whereas in the latter the coexistence of at least four conformers was reported.

L-(αMe)Pro, inserted into a peptide antigen,[198,199] or at position 3 or 7 of the nonapeptide hormone bradykinin,[200-202] or in the NPNA-repeat motif of the *Plasmodium falciparium* protein,[203,204] was demonstrated by 2D NMR experiments to strongly stabilize β-turn conformations. Analogous results [β-turn formation and *trans*

L-Xxx-L(αMe)Pro peptide bonds] were reported for L-(αMe)Pro-containing analogues of an antigen mimotope peptide[205] and the antimicrobial peptide buforin 2.[206] Interestingly, as opposed to the results from molecular mechanics simulations, it was experimentally shown that the sequence L-(αMe)Pro-L-Pro is not tightly folded.[207] A combined molecular modelling, and solution and crystal-state conformational study of acyl-L-Val-L-Xxx-NHR peptides [where Xxx is 4-methylene-L-(αMe)Pro] suggests the absence of any C=O···H-N intramolecular H-bond in this sequence.[208,209] According to the X-ray diffraction data, the 4-substituted L-(αMe)Pro residue is right-handed helical.

Recently, the X-ray diffraction structure of *c*-[L-(αMe)Pro]$_2$ was obtained.[210] Using unnatural amino acid mutagenesis, an L-(αMe)Pro and other modified Pro residues were incorporated in a member of the Cys-loop receptor protein superfamily.[211] L-Pro analogues, as L-(αMe)Pro, that strongly favor the *ω trans* conformer, were found to produce non-functional ion channels. Finally, in a DFT calculation study on Ac-L-(αMe)Pro-NHMe, in addition to non-unexpected conclusions, such as replacement of the C^{α}-hydrogen with a methyl in Pro destabilizes the *ω cis* conformation, a surprising structural finding associated with L-Pro C^{α}-methylation was reported, namely the stabilization of the type-II poly-(L-Pro)$_n$ II conformation, which was identified as an energy minimum for the L-(αMe)Pro "mono-peptide", but not for those of the corresponding, unmethylated protein amino acid.[212]

Because of the published partially contradictory results mentioned above on the preferred conformation(s) of (αMe)Pro peptides, in this experimental work we decided to synthesize and investigate a large set of N^{α}-acylated, homo- and heterochiral dipeptide monoalkylamide systems of the type RCO-L (or D)-(αMe)Pro-Xxx-NHR′ and RCO-Xxx-L(or D)-(αMe)Pro-NHR′ [where Xxx is L (or D)-Ala, Aib, or L (or D)-(αMe)Pro] long enough to fold into C=O···H-N intramolecularly H-bonded γ- or β-turns. The results are systematically compared with those obtained for the corresponding dipeptides based on the prototypical Pro, a well known turn-forming residue.[185,187,213-221] We have chosen -NH*i*Pr (*iso*propylamino) as the C-terminal, potential H-bonding donor, blocking group because it best mimicks the continuation of the peptide main chain The (αMe)Pro homo-dipeptides and the (αMe)Pro dipeptides containing the helicogenic Aib[19,222-224] are unusual in that they combine two amino acids with a quaternary C^{α}-atom. For the crystal-state 3D-structural analysis we

exploited X-ray diffraction, while for our solution conformational study we heavily relied on the FT-IR absorption, NMR, and CD techniques.

3.1.1 Synthesis and characterization

D-(αMe)Pro and L-(αMe)Pro amide were obtained by amidase-catalyzed enzymatic resolution (**Fig. 3.5**).[225] Using the amidase from *Mycobacterium neoaurum* ATCC 25795, a conversion of 45% was obtained after 70 h (E ratio 240), whereas with the amidase from *Ochrobacterium anthropi* NCIMB 40321 (overexpressed in *E. coli*)[226] 48% conversion was reached after 26 h (E ratio 317). Interestingly, whereas both amidases are in general L-selective for acyclic α-amino amides, for the (αMe)Pro amide the stereoselectivity is reversed.

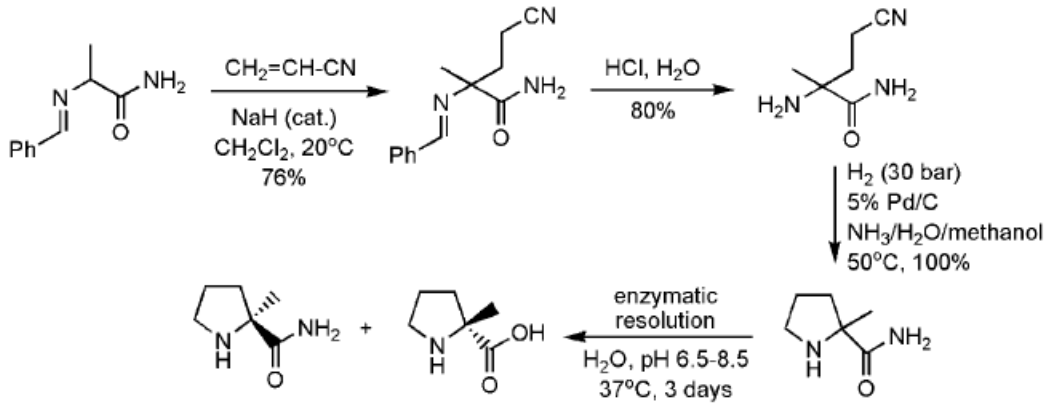

enzyme	conversion%	*ee* (amide)%	*ee* (acid)%
M. neoaurum	45	79	98
GMO *O. anthropi*	48	91	98

Fig. 3.5 Chemoenzymatic synthesis of D-(αMe)Pro and L-(αMe)Pro amide with the conversion and enantiomeric excess (*ee*) values.

The H-D,L-(αMe)Pro-NH_2 racemic substrate was obtained in 61% overall yield by base-catalyzed cyanoethylation of N-benzylidene-Ala amide, followed by acidic hydrolysis and ring-closing hydrogenation over palladium on charcoal.[227]

In the (αMe)Pro-based compounds, peptide and isopropylamide bond formations were achieved by the EDC/HOBt[85] or HOAt[86] C-activation method in CH_2Cl_2 solution in the presence of NMM or DIPEA; for the highly hindered (αMe)Pro-(αMe)Pro coupling $SOCl_2$ C-activation was used. Despite the occurrence of the severely

sterically demanding (αMe)Pro residue, coupling yields were from good to excellent (65-96%) with the single exception of that of the Aib-D-(αMe)Pro bond (24%). The *t*Boc and Z urethane groups were removed by acidic treatment (HCl/TFA) and by catalytic hydrogenation, respectively. N^{α}-Acetylation, *iso*butanoylation, and *para*-bromo-benzoylation were performed on the N^{α}-deprotected (αMe)Pro *iso*propylamide or (αMe)Pro-containing dipeptide *iso*propylamides using the corresponding symmetrical anhydrides. All newly synthesized compounds were fully characterized, including by ^{1}H NMR spectrometry.

3.1.2 Crystal-state conformational analysis

The 3D-structures of the synthesized oligopeptides were solved by X-ray diffraction by Dr. M. Crisma (ICB, Padova unit, CNR). The structures of three novel, N^{α}-blocked, (αMe)Pro-containing dipeptide alkylamides, namely *t*Boc-L-Ala-L-(αMe)Pro-NH*i*Pr, Z-Aib-D-(αMe)Pro-NH*i*Pr, and Z-D-(αMe)Pro-D-(αMe)Pro-NH*i*Pr have been solved. These crystal structures, combined with the five recently published,[228] Ac-L-Ala-L-(αMe)Pro-NH*i*Pr, Ac-D-(αMe)Pro-D-Ala-NH*i*Pr, Ac-D-(αMe)Pro-L-Ala-NH*i*Pr, *i*Bu-L-Ala-D-(αMe)Pro-NH*i*Pr, and Ac-D-(αMe)Pro-Aib-NHiPr, offer an almost exhaustive overview of the conformations preferred by this sterically demanding amino acid. The only missing, non-crystalline, dipeptide sequence in this list of X-ray diffraction structures is D-(αMe)Pro-L-(αMe)Pro or its L-D enantiomer. We have also solved the crystal structures of two N^{α}-blocked dipeptide alkylamides based on the related, coded amino acid Pro: Ac-Aib-L-Pro-NH*i*Pr and Z-L-Pro-D-Pro-NH*i*Pr. The molecular structures of the five new structures are illustrated in **Fig. 3.6**. **Table 3.1** summarizes the ϕ,ψ torsion angles for all published (αMe)Pro-containing peptides and their related Pro analogues.

Table 3.1 3D-Structural parameters in the crystal state for the known Ala/Aib/Pro/(αMe)Pro N^{α}-blocked and C-amidated dipeptide sequences.

Dipeptide sequence	Backbone torsion angles				Type of turn
	ϕ_{i+1}	ψ_{i+1}	ϕ_{i+2}	ψ_{i+2}	
Ac-L-Ala-L-(αMe)Pro-NH*i*Pr[228]	-135	77	-58	-37	—
*t*Boc-L-Ala-L-(αMe)Pro-NH*i*Pr	-76	130	-59	-36	—
*i*Bu-L-Ala-L-Pro-NH*i*Pr[229]	-129	76	-67	-22	—
Piv-D-Ala-D-Pro-NH*i*Pr[230]	74	-150	57	-142	—
	64	-152	83	-156	—
Ac-D-(αMe)Pro-D-Ala-NH*i*Pr[228]	53	32	66	25	β-III′
Ac-L-Pro-L-Ala-NH*t*Bu[231]	-66	166	-71	154	—
*i*Bu-L-Pro-L-Ala-NH*i*Pr[232,233]	-59	136	66	14	β-II
Ac-D-(αMe)Pro-L-Ala-NH*i*Pr[228]	53	-129	-77	-12	β-II′
Z-D-Pro-L-Ala-NH*t*Bu[231]	58	-137	-76	-14	β-II′
*i*Bu-L-Pro-D-Ala-NH*i*Pr[232,233]	-62	137	96	3	β-II
*i*Bu-L-Pro-D-Ala-NH*t*Bu[234]	-60	133	82	15	β-II
*i*Bu-L-Ala-D-(αMe)Pro-NH*i*Pr[228]	-55	133	78	0	β-II
Piv-D-Ala-L-Pro-NH*i*Pr[235]	60	-140	-89	9	β-II′
Ac-D-(αMe)Pro-Aib-NH*i*Pr[228]	53	37	61	28	β-III′
Piv-L-Pro-Aib-NHMe[236]	-58	139	61	25	β-II
Z-Aib-D-(αMe)Pro-NH*i*Pr	54	32	55	31	β-III′
	51	39	67	22	β-III′
Ac-Aib-L-Pro-NH*i*Pr	-50	-43	-80	-4	β-I
Z-Aib-L-Pro-NHMe[237]	-51	-40	-65	-25	β-III
Z-D-(αMe)Pro-D-(αMe)Pro-NH*i*Pr	50	34	57	28	β-III′
Piv-L-Pro-L-Pro-NHMe[238]	-60	138	-95	-7	—
Piv-L-Pro-D-Pro-NHMe[238]	-58	134	83	-7	β-II
	-56	139	84	-14	β-II
Z-L-Pro-D-Pro-NHiPr	-58	141	82	-3	β-II

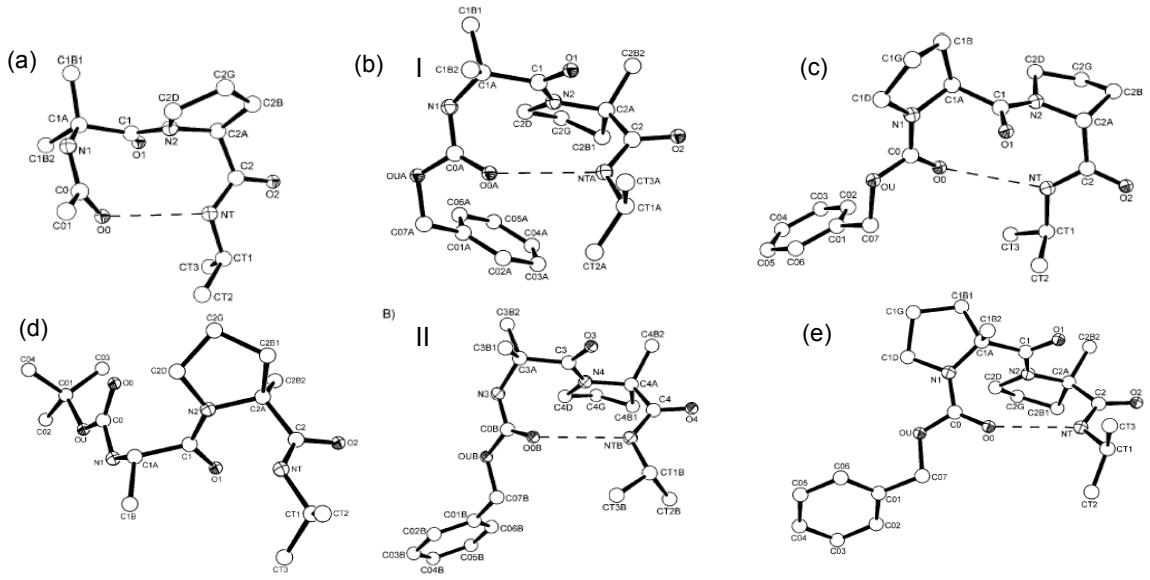

Fig. 3.6 X-ray diffraction structures of Ac-Aib-L-Pro-NH*i*Pr (a) [the second occupancy site of the Pro C^{γ} atom is omitted for clarity], Z-Aib-D-(αMe)Pro-NH*i*Pr (b) [two independent molecules (I and II) in the asymmetric unit], Z-L-Pro-D-Pro-NH*i*Pr (c), Boc-L-Ala-L-(αMe)Pro-NH*i*Pr (d) and Z-[D-(αMe)Pro]$_2$-NH*i*Pr (e). In each structure the C=O···H-N intramolecular hydrogen bond is represented by a dashed line.

Fig. 3.7 shows the average bond lengths and bond angles for the (αMe)Pro residue in comparison with those already reported for Pro.[213,239]

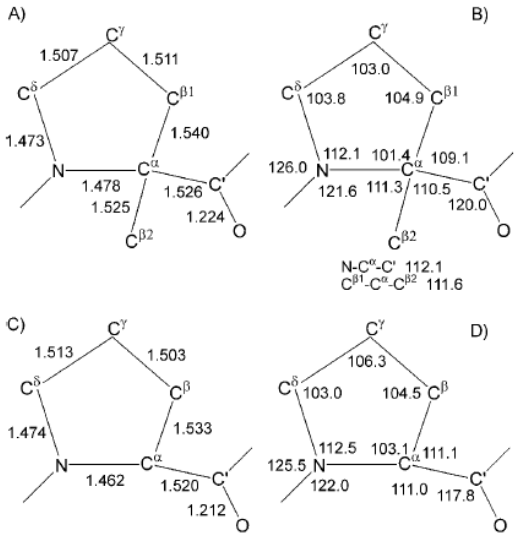

Fig. 3.7 Average bond lengths in Å (A and C) and bond angles in degrees (B and D) for the (αMe)Pro and Pro[213,239] residues, respectively.

All bond distances and most of the bond angles closely match each other. Differences between 1.0° and 2.0° are found for the corresponding bond angles around the C^{α} atom, which is trisubstituted for Pro and tetrasubstituted for (αMe)Pro. The steric effects of C^{α}-tetrasubstitution may also account for the widening of the C^{α}-C′-O bond angle for (αMe)Pro as compared to Pro. The sum of the average endocyclic bond angles is 525.2° for (αMe)Pro, while 529.4° for Pro. For comparison, in a planar, regular pentagon the sum of the internal angles is 540°.

In the five (αMe)Pro-/Pro-containing structures reported in this paper, all (secondary and tertiary) urethane, amide and peptide bonds (ω torsion angles) are in the usual *trans* conformation with modest deviations from the (180°) planarity ($|\Delta\omega| \leq 7.4°$), except for the amide ω_2 torsion angle of molecule **B** in the asymmetric unit of Z-Aib-D-(αMe)Pro-NH*i*Pr, 163.1(4)°. Four structures are folded in a β-turn conformation, which is stabilized by an $i \leftarrow (i + 3)$ [(urethane or amide) C0=O0···H-NT (amide)] H-bond. The only open structure is that of *t*Boc-L-Ala-L-(αMe)Pro-NH*i*Pr. The β-turns formed by the homochiral -D-(αMe)Pro-D-(αMe)Pro- and the heterochiral -L-Pro-D-Pro- dipeptides are of type-III′ and type-II, respectively, as expected from their sequence chirality.[238] In both -Aib-D-(αMe)Pro- and -Aib-L-Pro- sequences the achiral, helical Aib adopts the same screw sense as that of the following chiral residue, thus generating a type-III′ β-turn or a slightly distorted type-I β-turn, respectively. The difference, albeit small, between these two types of β-turn points to a higher propensity for a regular helical conformation assignable to (αMe)Pro as compared to Pro. All (αMe)Pro residues in these structures, included that of the open *t*Boc-L-Ala-L-(αMe)Pro-NH*i*Pr, are helical, with average ϕ,ψ torsion angles ($|57.6°|, |30.2°|$) remarkably close to those found experimentally for 3_{10}-helix peptides (57°, 30°), but less near those of α-helix peptides (63°, 42°).[6] It is worth pointing out that -D-(αMe)Pro-D-(αMe)Pro- is *the first linear (αMe)Pro homo-peptide sequence ever solved by X-ray diffraction*. The Ala residue in *t*Boc-L-Ala-L-(αMe)Pro-NH*i*Pr and the N-terminal Pro residue in Z-L-Pro-D-Pro-NH*i*Pr adopt the *semi*-extended conformation, while a conformation in the "bridge" region of the ϕ,ψ space[240] is seen for the C-terminal Pro residues of Ac-Aib-L-Pro-NH*i*Pr and Z-L-Pro-D-Pro-NH*i*Pr.

3.1.3 Solution conformational analysis

We performed an extensive conformational analysis of the N^{α}-blocked dipeptide alkylamides based on (αMe)Pro and/or Pro residues in solution by use of FT-IR absorption, NMR, and CD techniques.

The effects of replacing Pro with (αMe)Pro, sequence chirality, (αMe)Pro/Pro incorporation at position (*i* + 1) or (*i* + 2) in the sequence, presence of the weakly turn former Ala or the much stronger turn former Aib on the preferred conformation of model dipeptides are evident from the FT-IR absorption spectra in $CDCl_3$ in the informative N-H stretching region, reported in **Figs. 3.8** and **3.9**.

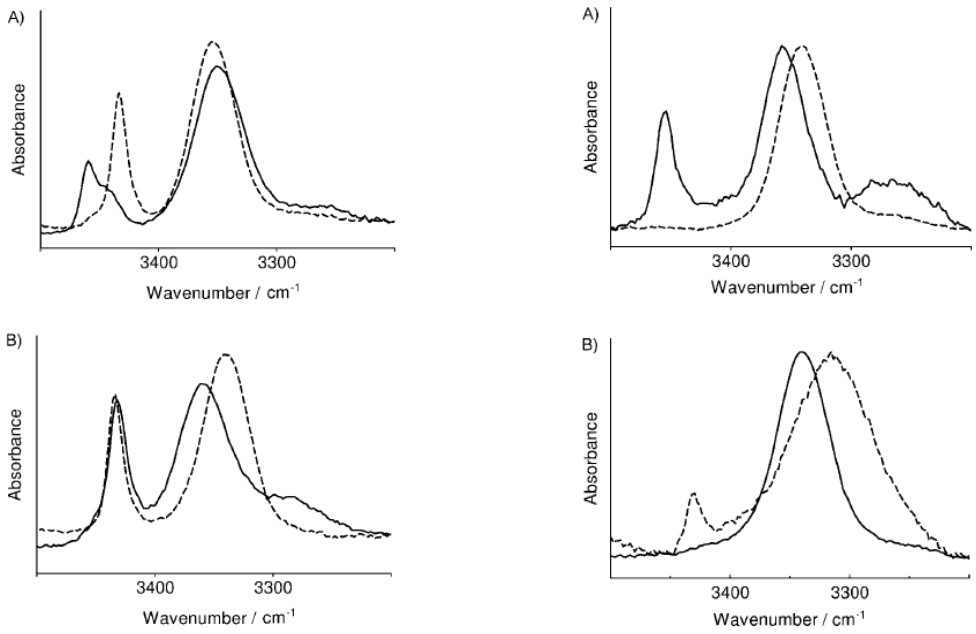

Figure 3.8 *(left)* FT-IR absorption spectra (3500-3200 cm^{-1} region) of A) Ac-D-(αMe)Pro-Aib-NHiPr (—) and Ac-Aib-D-(αMe)Pro-NHiPr (---); B) Ac-L-Pro-Aib-NHiPr (—) and Ac-Aib-L-Pro-NHiPr (---) in $CDCl_3$ solution ([peptide]: 1 mM). *(right)* FT-IR absorption spectra (3500-3200 cm^{-1} region) of A) Ac-L-(αMe)Pro-D-(αMe)Pro-NHiPr (—) and Ac-$[D\text{-}(\alpha Me)Pro]_2$-NHiPr (---); B) Ac-L-Pro-D-Pro-NHiPr (—) and Ac-$[D\text{-}Pro]_2$-NHiPr (---) in $CDCl_3$ solution ([peptide]: 1 mM).

The results obtained by checking the concentration dependence of all peptides investigated (between 10 and 0.1 mM) indicate that at 1 mM concentration there is no evidence for significant self-association *via* intermolecular H-bonding, *i.e.* that all NH groups are either free (solvated by $CDCl_3$) or intramolecularly H-bonded.

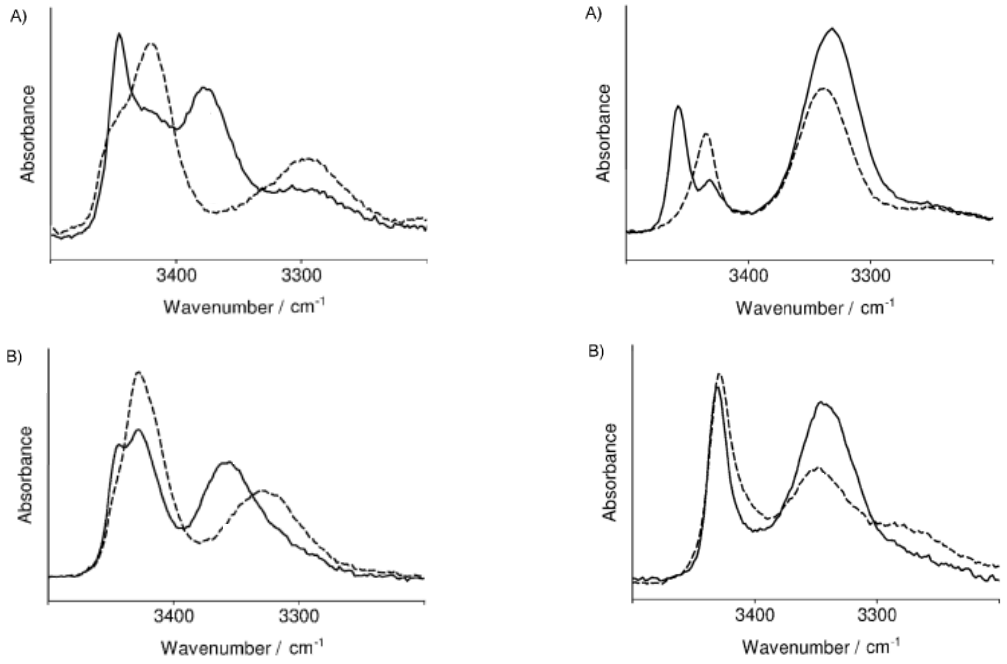

Figure 3.9 *(left)* FT-IR absorption spectra (3500-3200 cm^{-1} region) of: A) Ac-L-Ala-D-(αMe)Pro-NH*i*Pr (—) and Ac-L-Ala-L-(αMe)Pro-NH*i*Pr (---); B) Ac-L-Ala-D-Pro-NH*i*Pr (—) and Ac-L-Ala-L-Pro-NH*i*Pr (---) in $CDCl_3$ solution ([peptide]: 1 mM). *(right)* FT-IR absorption spectra (3500-3200 cm^{-1} region) of A) Ac-D-(αMe)Pro-L-Ala-NH*i*Pr (—) and Ac-D-(αMe)Pro-D-Ala-NH*i*Pr (---); and B) Ac-D-Pro-L-Ala-NH*i*Pr (—) and Ac-L-Pro-L-Ala-NH*i*Pr (---) in $CDCl_3$ solution ([peptide]: 1 mM).

The curves are characterized by two more or less intense bands, one located above 3400 cm^{-1} (free NHs) and the other below 3400 cm^{-1} (H-bonded NHs), respectively. The following considerations can be drawn from our analysis: (*i*) As opposed to the homochiral sequences, the heterochiral sequences exhibit a higher tendency to fold. However, this conclusion does not apply to the two -(αMe)Pro-(αMe)Pro- dipeptides, where the opposite trend is found. (*ii*) Turn formation is enhanced when (αMe)Pro replaces Pro in the sequence. (*iii*) Positioning (αMe)Pro or Pro as residue (*i* + 1) is more favorable for folding than as residue (*i* + 2), particularly for (αMe)Pro. (*iv*) The Aib/(αMe)Pro or Pro combination is more efficient to induce a turn than the Ala/(αMe)Pro or Pro combination. (*v*) In the homo-dipeptides, the (αMe)Pro D-D and the Pro L-D stereoisomers appear to be folded to the highest extent observed in the present study (100%). This latter finding resembles that already reported for Z-L-Pro-D-(αMe)Pro-NHMe.[197]

Our conformational study in $CDCl_3$ solution was extended to NMR. Not surprisingly, the NH chemical shift perturbation trends observed in the titrations of the compounds studied in this work with the strong H-bond acceptor DMSO[88,89] are often difficult to interpret, because in general the slopes are significantly reduced if the peptide main chain is short (as in our dipeptides)[101] and if the NH groups to be solvated by the perturbing agent are significantly shielded, *e.g.* close to a sterically demanding α-amino acid, such as Aib and (αMe)Pro.

The NMR spectra of both Ac-D-Pro-D-Pro-NH*i*Pr and Ac-L-(αMe)Pro-D-(αMe)Pro-NH*i*Pr are complicated by *trans* - *cis* isomerism that generates multiple resonances, with observed chemical shifts differences for each conformer of ~ 0.8 ppm for the *iso*propylamido NH proton. In addition, the ratios of the conformers are 1 : 0.86 and 1:0.21, respectively. Conversely, their diastereomers Ac-D-(αMe)Pro-D-(αMe)Pro-NH*i*Pr and Ac-L-Pro-D-Pro-NH*i*Pr exhibit much simpler NMR spectra, thus paralleling their FT-IR absorption curves (**Fig. 3.8**, *right*), indicative of a 100% population of C=O···HN H-bonded folded conformers. For these diastereomers the chemical shifts of the *iso*propylamido NH proton single peak are seen at 7.11 and 7.06 ppm, respectively.

Complete assignments of the NMR signals were achieved by COSY, TOCSY, and HMBC experiments at 400 MHz. **Figs. 3.11-3.13** show the most conformationally informative sections of the ROESY spectra[241] of the homochiral (αMe)Pro homo-dipeptide, the heterochiral Pro homo-dipeptide, and the homo- and heterochiral -(αMe)Pro-Ala- dipeptides, respectively.

A molecular model [**Fig. 3.14** and **Fig. 3.6 (e)**] indicates that for the homochiral Ac-D-(αMe)Pro-D-(αMe)Pro-NH*i*Pr in a type-III′ β-turn conformation a strong sequential connectivity is expected between a δCH_2 proton of (αMe)Pro1 and a δCH_2 proton of (αMe)Pro2. This strong cross-peak is indeed observed (**Fig. 3.10**, *inset*), accompanied by additional, weaker (sequential and medium-range) cross-peaks involving the secondary amide NH proton. The chemical shift difference between the C^{β} and C^{γ} atoms ($\Delta\delta_{\beta\gamma}$) in Pro peptides has been shown to be correlated with the ψ torsion angle.[191,192,242,243] In this (αMe)Pro homo-dipeptide we observed $\Delta\delta_{\beta\gamma}$ values of 12.3 and 14.1 ppm for (αMe)Pro1 and (αMe)Pro2, respectively. However, for (αMe)Pro-containing peptides this parameter is less conformationally indicative, as it is much larger than that of Pro-containing peptides ($8.0 < \Delta\delta_{\beta\gamma} < -7.0$), in particular due to a

significant downfield variation in the chemical shift for the C^{β} carbon associated with the presence of the βCH_3 substituent.[195]

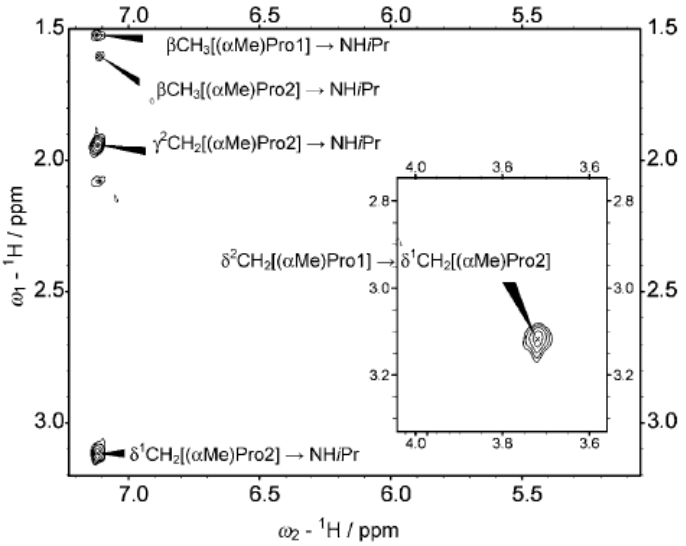

Fig. 3.11 Sections of the ROESY spectrum of Ac-D-(αMe)Pro-D-(aMe)Pro-NH*i*Pr in $CDCl_3$. The sequential connectivities βCH_3[(αMe)Pro2]→NH*i*Pr, γ^2CH_2[(αMe)Pro2]→NH*i*Pr, δ^1CH_2[(αMe)Pro2]→NH*i*Pr and δ^2[(αMe)Pro1]→ δ^1[(αMe)Pro2] (*inset*) are indicated as well as the medium-range connectivity βCH_3-[(αMe)Pro1]-NH*i*Pr ([peptide]: 5 mM).

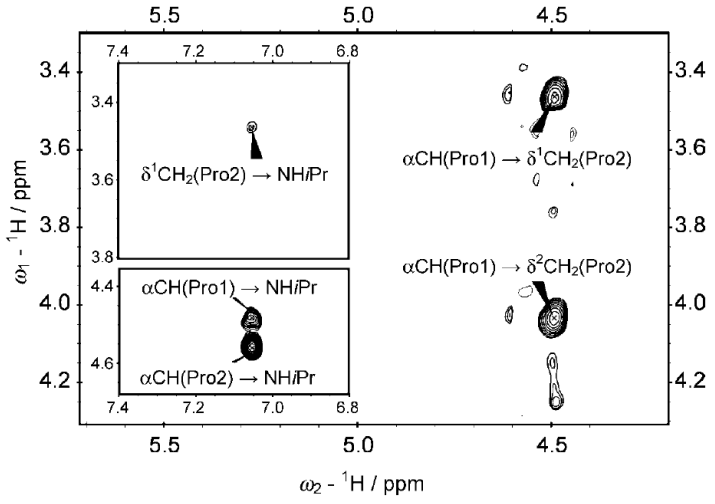

Fig. 3.12 Sections of the ROESY spectrum of Ac-L-Pro-D-Pro-NH*i*Pr in $CDCl_3$ solution. The sequential connectivities αCH(Pro1)→$\delta^{1,2}CH_2$(Pro2), αCH(Pro2)→NH*i*Pr (*inset, bottom*), and δ^1CH(Pro2)→NH*i*Pr (*inset, top*) are indicated as well as the medium-range connectivity αCH(Pro1)→NH*i*Pr (*inset, bottom*) ([peptide]: 5 mM)

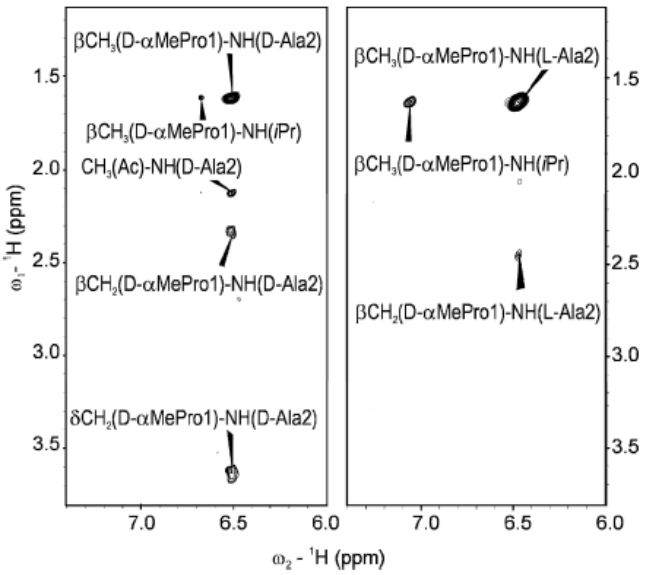

Fig. 3.13 Sections of the ROESY spectra of Ac-D-(αMe)Pro-D-Ala-NH*i*Pr (left) and Ac-D-(αMe)Pro-L-Ala-NH*i*Pr (right) in $CDCl_3$ solution. The sequential connectivities βCH_3[D-(αMe)Pro1]→NH(D- or L-Ala2) and βCH2[D-(αMe)Pro1]→NH(D- or L-Ala2), as well as the medium-range connectivity βCH3[D-(αMe)Pro1]→NH*i*Pr, are indicated for both peptides. For Ac-D-(αMe)Pro-D-Ala-NH*i*Pr, the sequential δCH_2[D-(αMe)Pro1]→NH(D-Ala2) and the medium-range CH_3(Ac)→NH(D-Ala2) connectivities are also observed ([peptide]: 5 mM).

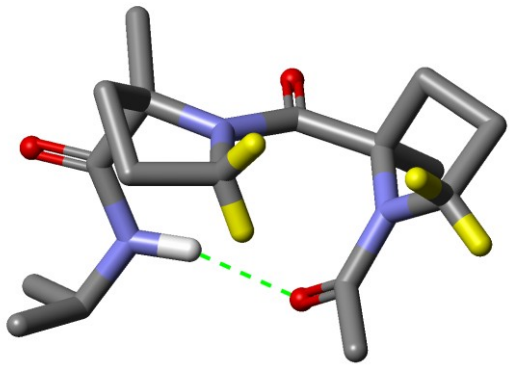

Fig. 3.14 Molecular model of Ac-D-(αMe)Pro-D-(αMe)Pro-NH*i*Pr in a type-III′ β-turn conformation. The δ^2[(αMe)Pro1] and δ^1[(αMe)Pro2] protons are shown yellow. The C=O···H-N intramolecular hydrogen bond is represented by a green, dashed line.

A molecular model [**Fig. 3.15** and **Fig. 3.6 (c)**] shows that for the heterochiral Ac-L-Pro-D-Pro-NH*i*Pr in a type-II β-turn conformation two strong sequential connectivities are expected between the αCH(Pro1) and the $\delta^{1,2}CH_2$(Pro2) protons and between the αCH(Pro1) and NH(*i*Pr) protons. A weak sequential connectivity between a δCH_2(Pro2) proton and the NH(*i*Pr) proton should be also seen. In this conformation the

minimization of the strain between the L-Pro1 αCH proton and the D-Pro2 δ-carbon restricts the rotation of the Pro1 torsion angle ψ to ~ 140° (*semi*-extended conformation;[244] see also **Table 3.1**). All of the above mentioned cross-peaks are clearly apparent in **Fig. 3.12**.

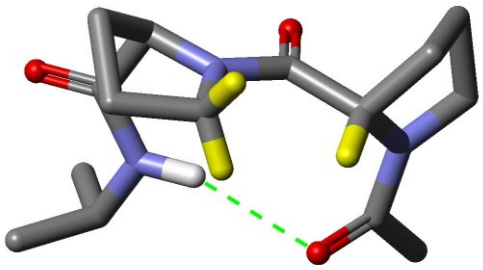

Fig. 3.15 Molecular model of Ac-L-Pro-D-Pro-NH*i*Pr in a type-II β-turn conformation. The αCH(Pro1) and the $\delta^{1,2}CH_2$(Pro2) protons are shown yellow. The C=O···H-N intramolecular H-bond is represented by a green, dashed line.

In this dipeptide $\Delta\delta_{\beta\gamma}$ values of 3.1 and 5.5 ppm were seen for Pro1 and Pro2, respectively.[191,192,242,243,245,246] A molecular model (**Fig. 3.16**) of Ac-L-(αMe)Pro-D-(αMe)Pro-NH*i*Pr indicates why this heterochiral dipeptide is not locked in the type-II β-turn conformation, typical of the -L-Pro-D-Pro- sequence. The model shows a very short distance between the βCH_3 substituent of residue 1 and the δ-carbon of residue 2. Rotation of the (αMe)Pro1 ψ torsion angle out of the region of the *semi*-extended conformation, required by the type-II β-turn for the (i + 1) position, can relieve this interaction. This finding is also consistent with the propensity of (αMe)Pro for the helical region of the conformational space.

All connectivities involving the ring protons of the (αMe)Pro2 residue seen in the ROESY spectrum of the type-III′ β-turn-forming Ac-D-(αMe)Pro-D-(αMe)Pro-NH*i*Pr (**Fig. 3.11**) are obviously missing in the corresponding spectrum of Ac-D-(αMe)Pro-D-Ala-NH*i*Pr (**Fig. 3.13**, *left*). However, both spectra do exhibit the only possible common connectivity, namely that between a βCH_3 proton of D-(αMe)Pro1 and the NH*i*Pr proton.

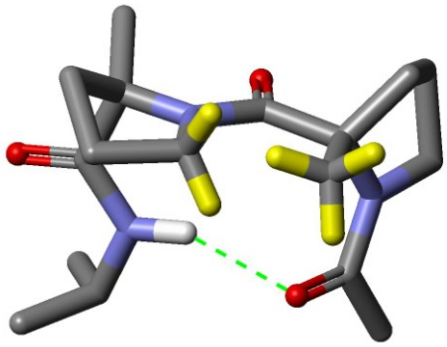

Fig. 3.16 Molecular model of Ac-L-Pro-D-Pro-NH*i*Pr in the unfavorable type-II β-turn conformation. The αCH_3[(αMe)Pro1] and the $\delta^{1,2}CH_2$[(αMe)Pro2] protons are shown yellow. The C=O···H-N intramolecular H-bond is represented by a green, dashed line.

Quite interestingly, if the structural restrictions imposed by the presence of the δCH_2 ring group of the (αMe)Pro2 residue are removed, as in Ac-D-(αMe)Pro-L-Ala-NH*i*Pr, then D-(αMe)Pro1 can accomodate in the unusual *semi*-extended conformation and the related -D-(αMe)Pro-L-Ala- sequence can fold in the type-II′ β-turn conformation, typical of a -D-L- heterochiral sequence. **Fig. 3.13** (*right*) shows that the cross-peak between a βCH_3 proton of D-(αMe)Pro1 and the NH*i*Pr proton is even more intense than the corresponding one in the homochiral sequence (**Fig. 3.13**, *left*). This observation is indeed expected on the basis of the related distances seen in the X-ray diffraction structures of these two -(αMe)Pro-Ala- dipeptides.[228] The $\Delta\delta_{\beta\gamma}$ values for the D-(αMe)Pro1 residue are 15.6 and 14.7 ppm for the homochiral -D-(αMe)Pro-D-Ala- and the heterochiral -D-(αMe)Pro-L-Ala- dipeptide sequences, respectively.

In summary, from our NMR data it turns out that the 3D-structures adopted by the (αMe)Pro-containing dipeptides in the crystalline state are highly (or exclusively) populated in $CDCl_3$ solution as well.

From our combined X-ray diffraction, FT-IR absorption, and NMR work on Ac-D-(αMe)Pro-D-(αMe)Pro-NH*i*Pr discussed above, it turns out clearly that this simple dipeptide is unique in that its Z-protected analogue is rigidly folded in a single, left-handed type-III′ β-turn in the crystal state and it is fully folded in the same conformation in $CDCl_3$ solution. Since the far-UV ECD spectrum of a single type-II β-turn is well established,[247-249] but the spectra of type-III and the closely related, non-helical, type-I β-turns have been the matter of controversy for a long time, in part due to

the fact that not completely appropriate (long linear or cyclic) model peptides were utilized in those studies, we decided to take advantage from our short linear dipeptide to conclusively offer the correct ECD spectrum for a type-III/I β-turn. To avoid any ambiguity, we used MeCN, a solvent of low polarity (in this sense similar to $CDCl_3$), but (in contrast to $CDCl_3$) compatible with an ECD measurement in the far-UV region.

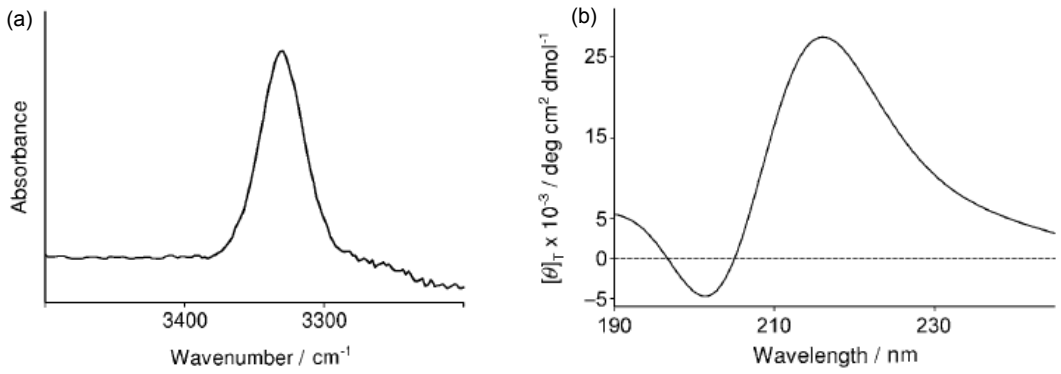

Fig. 17. FT-IR absorption spectrum (3500-3200 cm^{-1} region) (a) and far-UV ECD spectrum (b) of Ac-D-(αMe)Pro-D-(αMe)Pro-NH*i*Pr in MeCN ([peptide]: 1 mM).

Fig. 3.17 (a) shows that the band of free NH groups is absent in the FT-IR absorption spectrum in MeCN (only an intense band near 3330 cm^{-1} is seen), corroborating our data that this homochiral homo-dipeptide is 100% folded in an intramolecularly H-bonded β-turn conformation in a solvent of low polarity. The corresponding far-UV ECD spectrum in MeCN [**Fig. 3.17 (b)**] exhibits a very weak, positive shoulder at 225-230 nm followed by a remarkably strong positive Cotton effect centered at 216 nm and a weak Cotton effect of opposite sign at 202 nm. The cross-over point between the two latter bands is seen at 205 nm. Obviously, in the ECD spectrum of this D-D configurated dipeptide the signs of all Cotton effects are opposite to those observed for the more common all-L peptides. Not surprisingly, the overall shape of the ECD spectrum in **Fig. 3.17 (b)** closely resembles that of a 3_{10}-helix.[26,65,143] Indeed, a type-III/III′ β-turn is the basic unit of the 3_{10}-helix.[6] However, the positions of the Cotton effects and cross-over point in the spectrum of our model dipeptide are significantly shifted (by about 8 nm) to longer wavelengths. This latter effect is not

associated with the nature of the solvent, as the ECD spectrum of this same dipeptide in MeOH solution (not shown) exhibits a very similar general shape.

3.1.4 Conclusions

An analysis of the obtained experimental data allows us to extract the following major conclusions:

(*i*) Although the region of the (ϕ, ψ) conformational map overwhelmingly preferred by L-(αMe)Pro would indeed be that typical of *right*-handed 3_{10}-/α-helices, (with $\psi \approx$ -30° or *cis*′) as suggested in 1974 by Leach and coworkers,[190] the *semi*-extended, type-II poly-(L-Pro)$_n$ region (with $\psi \sim 150°$ or *trans*′) can also be explored (although rarely) by this extremely sterically hindered C^{α}-tetrasubstituted α-amino acid. Conversely, the ϕ, ψ region ($\psi \sim 60°$), exactly half-way between the two regions discussed above and corresponding to the C_7' (inverse γ-turn) conformation, does not seem to be accessible to L-(αMe)Pro.

(*ii*) In addition to the dramatic restriction of the ϕ torsion angle (to ~ -60°) by its five-membered pyrrolidine ring structure, L-(αMe)Pro undergoes rigidification of the preceding tertiary peptide bond (*trans*, or 180°, ω torsion angle) as well, as shown by all C^{α}-methylated L-α-amino acids investigated to date.

(*iii*) The known high propensity of the L-Pro residue for β-turn formation is even enhanced in peptides based on its C^{α}-methylated derivative when it is located at the (i + 1) corner position. Despite this characteristics, L-(αMe)Pro seems to be unable to nucleate a β-turn when it is located at the (i + 2) corner position of a homo-chiral dipeptide sequence [with a coded amino acid at position (i + 1)].

(*iv*) When incorporated at the (i + 1) corner position of the dipeptide sequence, L-(αMe)Pro tends to bias the β-turn to its helical type (III), as opposed to the non-helical type (II) typically induced by L-Pro.

(*v*) Based on the data obtained both from solution and solid-state structural analysis, the non ambiguous ECD signature of a peptide type III' β-turn conformation is also proposed.

4. Macrocyclizations on helical peptides

Biological activity of peptides is a well-known property that makes these molecules suitable for various biomedical applications. Peptide-based drugs are playing an increasing role in the development of new clinical methods targeted against several diseases. Also, their use in therapeutic treatments of cancer, diabetes, auto-immune diseases, more effective diagnostics and as chemical messengers and neurotransmitters is acquiring more and more interest.[250-252] According to a recent review by Danho *et al.*,[253] the peptide market is growing nearly twice as fast as the overall pharmaceutical market. There are 67 therapeutic peptides on the market, 150 in clinical phases and 400 in advance pre-clinical phases. In contrast to common small molecule-based drugs, peptides are target-specific, have the least lethal index (*i.e.* less side effects) and maximum therapeutic index (*i.e.* highest effectiveness).

On the other hand, the lack of resistance to enzymatic degradation and low bioavailability are the two major drawbacks encountered in generating therapeutics and biological probes using peptides because of their high conformational flexibility. In order to bind to (and to activate/inhibit) its biological target, a peptide must attain a specific conformation, strongly influenced by the nature of constituent amino acids and the biophysical environment.

Therefore, the pre-organization of peptide shape *via* the introduction of a structural motif that imparts conformational restriction, can enhance binding and hence therapeutic potential.[254] Structural modification of peptide structures can also extend the time they remain biologically active in the peripheral system.[250]

Recent developments in the domain of drug-discovery have focused attention on the synthesis of small-constrained mimics of bioactive conformations of potent therapeutic molecules.[255,256] It is very important for a peptide molecule to hold its conformational features *in vivo* in order to bind strongly to the target. The elements of local or global constraint in a molecule can lock it into a particular conformation, which may mimic the exact bioactive conformation[257-259]. Local constraints in terms of side-

chain modifications in the amino acids, incorporation of protein secondary structures like turns, helices, etc., into the molecule and cyclization[260] as part of global constraints are commonly practiced.

Cyclic peptides and their derivatives[261] attract much attention of synthetic chemists and biologists.[262] Apart from the occurrence of a variety of naturally occurring bioactive molecules, cyclic peptides are often more stable *in vivo* than their linear counterparts and therefore often represent promising drug candidates. Another feature that contributes to the appeal of cyclic peptides is their reduced conformational mobility which allows them to be used in the study and mimicry of protein folding and to present diverse functionality in a defined and predictable orientation.[263]

In view of the importance of constrained conformations, there have been many attempts to lock peptides into turn and helical structures and to synthesize molecules that might mimic normal peptides.[264] Reduction of the flexibility by intramolecular bridges, such as salt bridges[265] metal ligation between natural[266] and unnatural amino acids,[267] disulfide bridges,[268,269] or more complicated acetylenic or oxyethylenic bridges[270] which act as a "molecular staplers" are the well-known way to control the three-dimensional structure. Cyclic alkenes resulting from ring-closing metathesis reaction can be considered as a stable alternative of such bonds.

The ring-closing metathesis (RCM) reaction, catalyzed by transition metal carbenes, currently recognized as a popular, mild method for the formation of the new C-C bonds is utilized in many organic transformations. RCM is a part of a vast class of reactions which is known as olefin metathesis,[271] a unique carbon skeleton redistribution in which unsaturated carbon-carbon bonds are rearranged (with loss of ethylene). With the discovery of very efficient catalysts, this reaction has emerged as a powerful tool for a clean and fast formation of C-C bonds in chemistry. The number of applications of this reaction has dramatically increased in the past few years.

Olefin metathesis can be utilized in several closely related types of reactions[272][142] as summarized in **Fig. 4.1**.

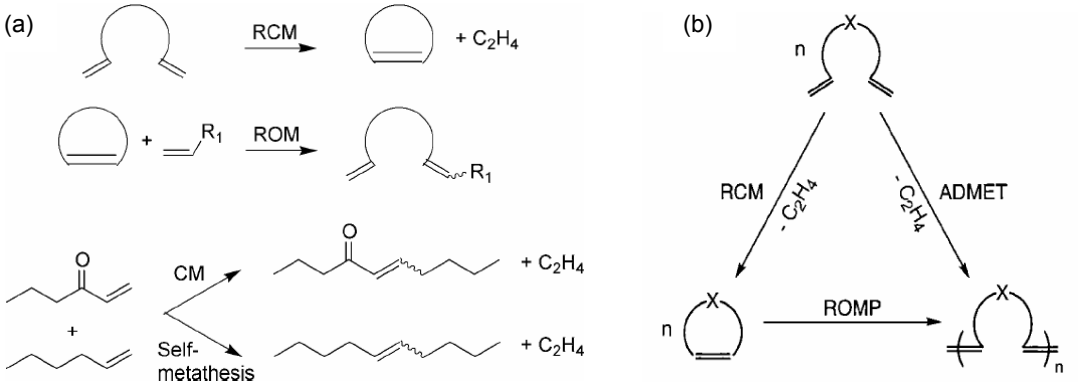

Fig. 4.1 Applications of olefin metathesis reactions: for synthetic organic chemistry (a) and for polymerizations (b).

Ring-closing metathesis (RCM) is the unimolecular condensation reaction of a diene to form a cyclic olefin and a small condensate olefin as a byproduct, and is being used extensively in critical ring-closure steps in the synthesis of complex organic molecules.[273,274] Acyclic dienes may also be polymerized, and whether a polymer or a cyclic compound is formed from any given diene is most often determined by thermodynamic rather than kinetic factors.

Ring-opening metathesis (ROM) is the reverse reaction of RCM, in which a cyclic olefin is reacted with an acyclic olefin to produce a new acyclic diene. ROM polymerization (ROMP) is thermodynamically favoured for strained ring systems such as 3- and 4-membered compounds. In many cases, ROMP of strained cyclic olefins initiated by metal carbene complexes shows the characteristic features of a living polymerization and therefore block copolymers can be prepared by sequential addition of different monomers.

Cross metathesis (CM) is the reaction of two acyclic olefins to form two new olefins.[275] Of critical importance to CM is the selectivity of the reaction, because it can happen the preference of the products of self metathesis, which is the metathesis of two identical molecules, over the forming so-called cross-product. ADMET (acyclic diene metathesis) is a “condensation” polymerization, and is essentially the self metathesis of a diene, usually a terminal diene, which forms a high polymer.

The number of catalyst systems devised to initiate olefin metathesis is very large, but only in recent years well-defined single component metal carbene complexes

have been prepared and utilized. Although a number of titanium[276] and tungsten[277] organometallic catalysts have been developed for metathesis and related reactions, molybdenum and ruthenium compounds have found the most numerous applications[278] (**Fig. 4.2**). Complexes of other metals (such as rhenium and osmium) appear to promote olefin metathesis, but these exhibit lower stability and/or reactivity, and have not been as extensively investigated. Critical drawbacks of the Mo-based highly active Schrock's catalyst (a) are its moderate to poor functional group tolerance, high sensitivity to air, moisture or even to trace impurities present in solvents, thermal instability on storage and expense of preparation. On the contrary, Ru-carbene systems, discovered by R. H. Grubbs, exhibit high reactivity in a variety of ROMP, RCM and CM reactions under mild conditions, but also have remarkable tolerance toward many different organic functional groups.

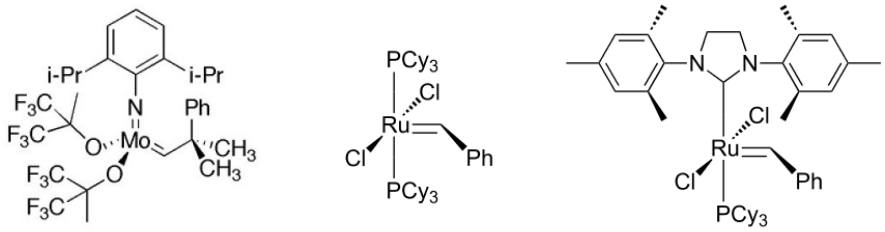

(a) (b) (c)

Fig. 4.2 Most commonly used olefin metathesis catalysts: Schrock's catalyst (a), Grubbs' First Generation (b) and Second Generation catalyst (c) (Cy = cyclohexyl).

Catalytic activity of such compounds is not reduced significantly in the presence of air and moisture and they can be stored even in the air atmosphere without severe decomposition for several weeks.[272] These reagents turned out to be very efficient catalysts for all kinds of metathesis reactions and have therefore found a vast number of applications in the synthesis of complex molecules and the preparation of different polymers.[279,280]

The Mo=C or Ru=C double bonds serve as points of contact between the catalyst and olefins. The metal centers are crucial to the properties of these catalysts. It is now generally accepted that the mechanism of both cyclic and acyclic olefin metatheses proceeds through a *metallacyclobutane* active complex. Although the

relative stability of carbenes and metallacyclobutanes can change with reaction conditions, catalyst composition and alkene substitutions, the mechanism of olefin metathesis appears to be the same for all catalysts.

Overall, the catalytic cycle (**Fig. 4.3**) consists of an initiation phase (generation of the active complex) and a propagation phase (the active complex promotes additional cycles).[281] Catalysis commences by a cross metathesis between an active carbene or alkylidene (M=C) and one of the two olefins of the substrate (**i**) to generate a metallacyclobutane (**ii**). The metallacyclobutane might revert to (**i**) and M=C [pathway (a)] or the other two bonds of the ring might be ruptured, furnishing (**iii**), where the metal (M) is within the substrate [pathway (b)].

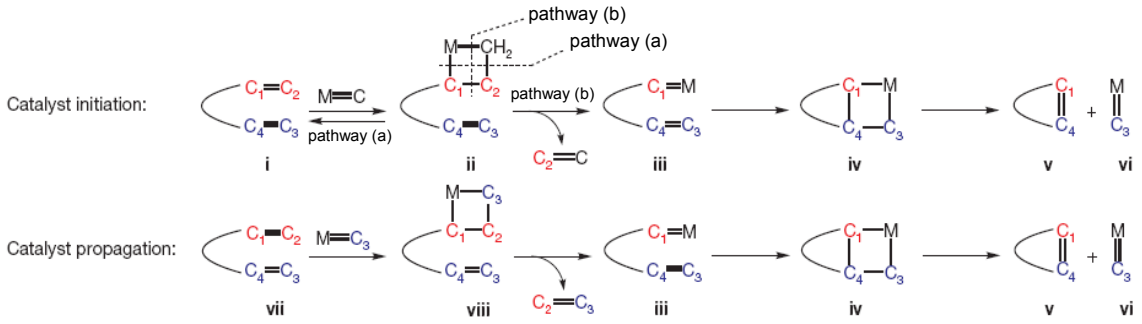

Fig. 4.3 The accepted general mechanism for ring-closing olefin metathesis.[281]

Formation of another metallacyclobutane (**iv**) and its disintegration furnishes cyclic product **v** and $M=C_3$ (**vi**), which is the metal-bearing agent serving as the catalyst. What typically drives reactions is that the cyclic product (**v**) does not easily react with the active catalyst ($M=C_3$) to cause ring-opening metathesis. The identity of the intermediates in the catalytic cycle is well understood;[282] it is, however, often unclear whether it is catalyst–substrate association [(**i**) and (**vii**) first chelate with the metal centre of M=C before conversion to (**ii**) or (**viii**)], formation of the metallacyclobutane or its cleavage that is the irreversible, product- or rate-determining step.

Efficient synthesis of the large ring depends on striking a balance among cross metathesis, a process that delivers the undesired coupling of two substrate molecules, ring-closing metathesis, a reaction that affords the desired product, and a ring-opening metathesis pathway that would destroy the desired cyclic compound.

Ring closing metathesis has emerged as a powerful tool for the synthesis of different ring systems from five-membered rings to macrocycles. However, the product distribution of monomer and oligomers is often a problem in the formation of medium to large rings. It was found that the product distribution is affected not only by the reaction concentration, but can also be improved by adjustment of the reaction temperature. Typically, metathesis reactions are carried out in degassed solvents (dichloromethane or benzene) in the presence of 5–10% ruthenium catalyst at concentrations ranging from 0.001 to 0.01 M. High dilution concentrations are employed to minimize the formation of dimers or polymers, resulting from cross-metathesis when the reaction rates are slow. The yields of monomer can be significantly enhanced relative to runs at lower temperature. This observation could be explained by the difference of entropy in activation energy leading to each product. If the formation of the monomer is entropically favored over that of the dimer, the kinetic ratio of the two products should shifts toward the monomer at higher temperature.[283] Anyway, since the metathesis is a catalyzed reaction, the monomer can eventually revert to the thermodynamically favored dimers or oligomers at longer reaction times.

It was also reported a noticeable improvement of ring-closing metathesis reaction under solvent-free conditions and by microwave activation under green chemistry conditions.[284]

Designing stable peptide β-turn and helix mimics with the aid of RCM appeared extremely useful. The synthesis of sterically hindered rigid α-amino acids which could considerably enhance conformational stability of peptides plays an important role in the design of new drugs. The most efficient approach to conformationally rigid peptides is based on introduction of medium-size, cyclic α-amino acids (usually, 5-7-membered) into strategic positions of peptide chains.[285] As a rule, this approach leads to significant improvement of pharmacological parameters of potential peptide drugs. Such cyclic amino acids and their derivatives and analogs can be easily made by intramolecular ring-closing metathesis of dienes and enynes.[286-288]

Though cyclizations to large rings are performed usually in diluted solutions to suppress competing ADMET, RCM is also applicable to polymer-supported substrates. Experiments were reported on the dimerization of peptides on solid-phase using a ruthenium catalyst after N-terminal acylation with different ω-alkenoic acids.[289] It was shown that the size of the peptide (up to four amino acid residues) did not influence the

reaction, meaning that the required length allowing cross linking is already reached with the smallest peptide and pentenoic acid. On the other hand, two or more methylene groups are required between the double bond and the carbonyl group for metathesis to proceed smoothly. The complete failure to obtain the dimeric product with 3-butenoic acid derived peptoids is not due to the inability to reach a second alkene on solid support, since the longer peptides should compensate for the shortness of the butenoic acid.

The cyclization/cleavage from solid support has also proven to be very effective for the synthesis of macrocycles.[290] According to the concept of Pernerstorfer *et al.*[291] (**Fig. 4.4**), the catalyst is expected to selectively attack a terminal double bond for steric reasons.

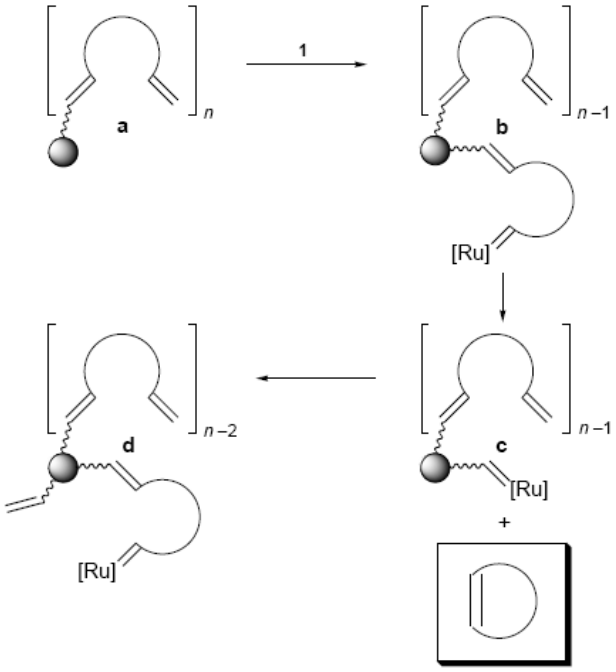

Fig. 4.4 Scheme of the solid-phase synthesis of peptide macrocycles.[291]

This initial step (**a** → **b**) is followed by a RCM resulting in the liberation of one equivalent of the macrocycle and in the formation of the polymer-bound metal-carbene complex (**c**). Assuming sufficient flexibility, a transfer of the metal complex on the polymer surface (**c** → **d**) should take place, thus enabling further catalytic cleavage cycles. By-products resulting from quasi-intermolecular crossed metatheses of terminal

double bonds remain bound to the resin during the entire process. Using such a strategy a series of the cyclic tetrapeptides was successfully synthesized. The extent of cyclization/cleavage was shown to depend strongly on the length of spacer, which separates the peptide chain from the polymer surface, and, thus, on the mobility of the polymer-supported intermediates. It appeared also that the relative cyclization/cleavage rates of different precursor dienes correlated with their probability to form β-turn-like structures and, therefore, depended on the proximity of double bonds. Polymer-bound substrates cyclized rapidly when exhibiting favourable conformations.

The replacement of a H-bond between the *i* and (*i* + 4) residues at the N-terminus of a short peptide with a carbon-carbon bond results in a highly stable, constrained α-helix, as it was shown by Chapman *et al.*[292] (**Fig. 4.5**). The advantage of this strategy is that it allows access to short α-helices with strict preservation of solvent-exposed molecular recognition surfaces required for biomolecular interactions and it does not remove the important side-chain functionalities. It also can nucleate the helical structure, as it was shown that the energetically demanding organization of three consecutive amino acids into this structure is a slow step in helix formation.[293]

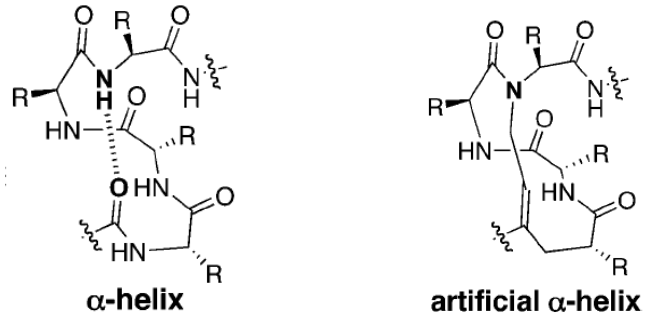

Fig. 4.5 Strategy of stabilization of an α-helix by replacement of a C=O···H-N moiety by covalent bonds.

The metabolic stability of C–C bonds makes olefin RCM a particularly attractive method for the synthesis of constrained cyclic peptide structures.[294] The Grubbs' group have reported a facile procedure wherein RCM is used to introduce a link between the *i* and *i* + 4 amino acid side chains.[295] Using the same strategy, Verdine and coworkers[296] succeeded in stabilizing the α-helical BH3 peptide, known to activate

apoptosis *in vivo*. The RCM-stabilized BH3 peptides not only proved to be helical, but they were also protease resistant, cell-permeable and, relative to the control peptide, they exhibited almost a ten times increase in their half-life *in vivo*. Another example comes from the Debnath's group,[297] who used stapling technology to induce a peptide of interest (NYAD-1) to enter cells. Interestingly, such RCM-stabilized α-helical peptide proved to block HIV infection in cell cultures (**Fig. 4.6**).

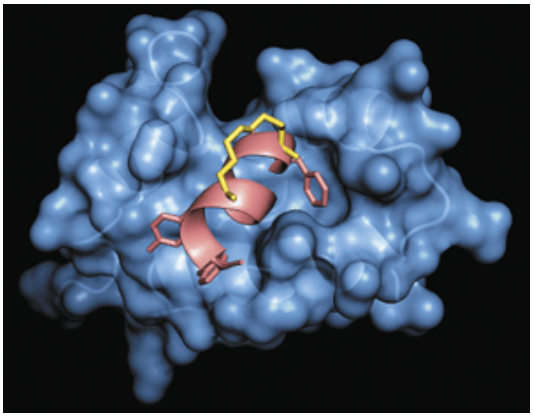

Fig. 4.6 Three-dimensional model of peptide NYAD-1 (*pink*), bound to the C-terminal capsid domain of the human immunodeficiency virus type 1. The tertiary structure shows that the hydrocarbon-stapled linkage of NYAD-1 (*yellow*) is located in a non-interfering site, distant from the hydrophobic pocket.[297]

Earlier work from our group, in collaboration with prof. D. J. O'Leary (Pomona College, Claremont, California) and was a former member of prof. Grubbs' group, showed that it is feasible to synthesize 3_{10}-helical peptides containing a stabilizing RCM crosslink between amino acids separated by two residues (*i* and *i* + 3).[298] Linkers bridging such positions deliver substantial stabilization of helical motifs by placing the tethered side chains on the same side of the helix.

In order to exploit the use and the applications of RCM in the peptide chemistry field and to continue such a profitable collaboration, I had the possibility to spend a research period of six months as a Visiting Student in the groups of prof. D.J. O'Leary and prof. R.H. Grubbs (California Institute of Technology, Pasadena, California) during the second year of my Ph.D. work.

The work described in the following paragraphs started in USA and was carried out in the laboratories of Caltech/Pomona College. It was then continued in Italy during the course of the third year.

4.1 Ladder peptides

After having investigated the effect of cross-linking ("stapling") *via* RCM the side-chains of *i* and (*i* + 3) α-amino acids in short 3_{10}-helical peptide sequences,[298] it was decided to exploit this joint research opportunity in order to use the metathesis reaction as a tool to create a small peptide bundle (also called *ladder peptide*) constituted by two Aib-rich helices held together by two or more carbon-based linkers (**Fig. 4.7**).

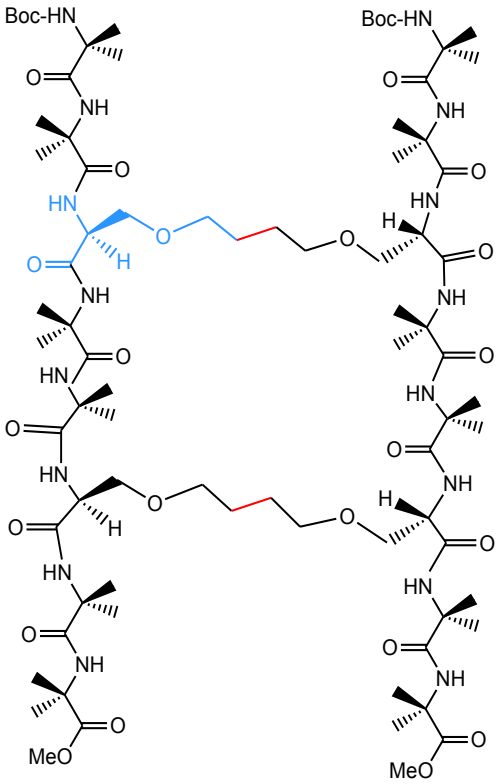

Fig. 4.7 First approach to an Aib-rich peptide bundle, or *ladder peptide*. Blue: linking the α-amino acid (L-Ser(Al)); red: new C-C bond obtained *via* metathesis.

Interest in these protein-like structures has increased during the last years, due to their high relevance in many fundamental biochemical processes. It is now clear that protein-protein interactions are at the center of almost every cellular process from cell motility to DNA replication. Among other things, protein-protein interactions allow a cell to see the surrounding milieu, talk to the neighboring cells, and respond to extracellular signals. Transient protein-protein interactions are involved in the regulation of fundamental cellular processes, like secondary structure favourable/ unfavourable interactions, tertiary structure stabilization, protein-protein interactions, receptor binding and signal transduction pathways.[299,300] Understanding protein-protein interactions provides with clues to help elucidate the function of a known or novel protein and the role it plays in a known pathway. Alterations in protein-protein interactions perturb the normal sequence of events in the cell and contribute to diseases, such as cancer. Thus, keeping track of the normal protein-protein interactions patterns can lead to the development of drugs to fight the underlying cause of the diseases.[296,299,300]

In an era of small-molecule targeted therapies for cancer, there is increasing interest in defining and understanding signal transduction networks. For instance, growth factor pathways have been known for a while but are not fully understood. The number of clinically available drugs affecting the function of specific proteins (by inhibition or activation) is huge; furthermore, this research topic has received much of the attention in designing new pharmacologically active compounds in the past. On the contrary, little is known about the intimate mechanisms which control interactions between large biomolecules, even if these are the actual biochemical regulatory processes at the cellular level.

The potential ability offered by metathesis in holding peptide helices close together suggested, in view of the previous discussion, the possibility to study the role of packing (and the interactions) between 3_{10}-helical structures in solution. This process regulates protein folding and the propension in maintaining their native structure.[301] Indeed, the relative spatial arrangement of peptide helices in the protein matrix is controlled by their strong dipole moments, other than hydrogen bonding, van der Waals and ionic-ionic contact interactions (**Fig. 4.8**).

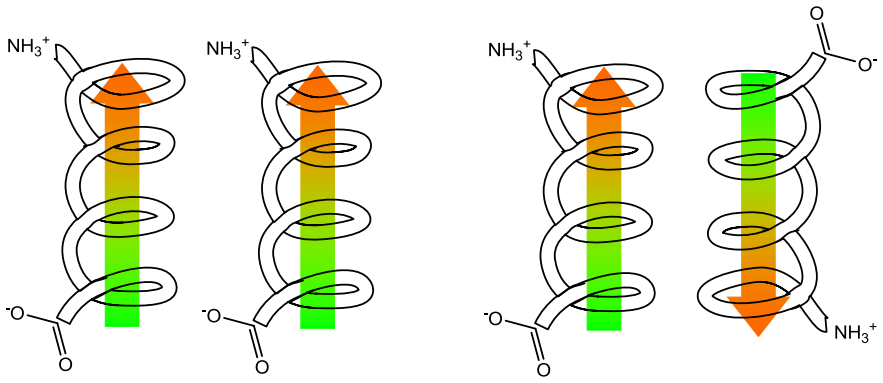

Fig. 4.8 Different electrostatic interactions between peptide helices: parallel (*left*) and unparallel (*right*).

Preliminar electrostatics considerations suggest that antiparallel packing between helices is the most energetically favoured.[302] However, parallel arrangement is possible only for α-helices having a high number of hydrophobic residues on their contact surfaces, balancing the electrostatic repulsion.[303] On the other hand, little is known about 3_{10}-helices mutual interactions and relative disposition.[304]

In light of what have been shown up to this point, the synthesis of a *bis*-peptide bundle like the one shown in **Fig. 4.7** was proposed to study whether it would be possible to "pack" two 3_{10}-helical peptides in a parallel fashion while retaining 3_{10}-helicity. Because we are particularly interested in studying 3_{10}-helices, we expect to make use of synthtetic RCM strategies to attempt to induce a 3_{10}-structure. Synthesis and 3D-structural characterization of these peptide bundles may offer insight into the packing patterns of helical peptides and can increase the range of spatial conditions available for investigating physico-chemical interactions between probes and host-guest functionalities.

We commenced evaluating the synthetic aspects of building such a *ladder peptide* by using side-chain allylated α-amino acids. The need of *terminal* double bond is essential in order to make use of the metathesis reaction. In their previous work, prof. O'Leary and his group used O-allylated Ser [Ser(Al)] as the source of olefinic ether linkage included at the *i* and (*i* + 3) positions (**Fig. 4.7**). However, the side-chain modification of Ser turned out to be a major issue, owing to the extensive C^{α} racemization exhibited during the allylation reaction. The strongly basic reaction conditions (Williamson ether synthesis protocol) employed during functionalization,

combined with the electron-withdrawing properties of the β-oxygen (supposed to increase the acidity of the chiral C^{α}-hydrogen), substantially discouraged us from using Ser residues (**Fig. 4.9**).

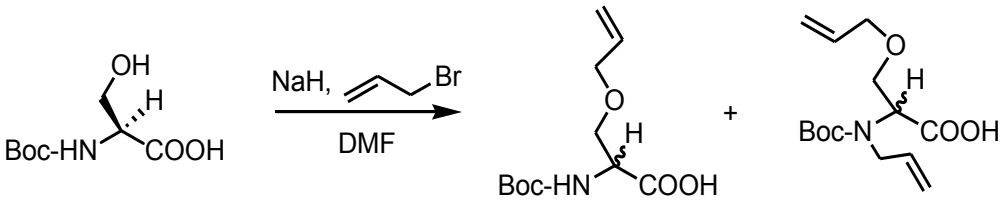

Fig. 4.9 Protected L-Ser racemization and formation of a N,O-diallylated by-product during allylation.

On the other hand, in order to avoid tedious purification steps, the necessity to have an enantiomerically pure O-allylated α-amino acid was requested by our Aib-rich peptides.

Trying to overcome this problem, we devised an allylation strategy involving the use of the Ser higher homolog, namely homoserine (Hse, **Fig. 4.10**). This non-proteinogenic (but still found in nature[305]) α-aminoacid was thought to be less prone to racemization, due to the increased distance between the oxygen and the C^{α}-hydrogen.

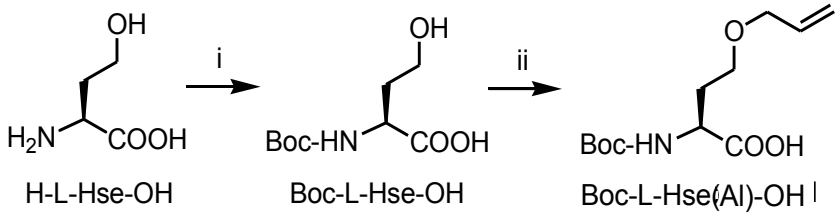

Fig. 4.10 Proposed reaction scheme leading to Boc-L-Hse(Al)-OH.
(i) N^{α}-Boc protection; (ii) O-allylation.

The proposed synthetic plan to access Boc-L-Hse(OAl)-OH from Hse followed the same approach used for Ser. However, an unexpected and fast lactonization occurred during the first N^{α}-protection step. Though Boc introduction is generally considered a straightforward reaction, that is not the case for Hse. The unexpected behaviour exhibited by Hse dramatically reduced the possibilities to submit such α-amino acid to side-chain allylation.

Anyway, several attempts to obtain Boc-protected Hse were carried on according to different literature methods (**Fig. 4.11**). Despite the different reaction conditions, none of them proved to afford sufficiently pure, non-cyclized product, as clearly shown by NMR (**Fig. 4.12**) and TLC analysis. Furthermore, separation of the cyclized/open Boc-Hse mixture was not feasible *via* flash chromatography, as only traces of open product could be recovered.

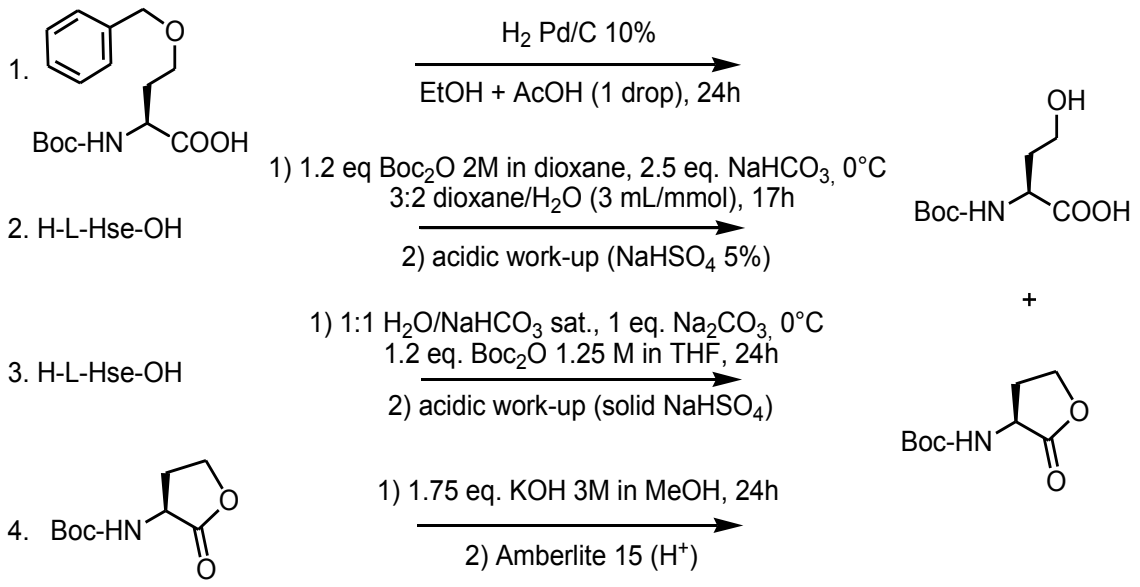

Fig. 4.11 Different literature methods explored to obtain Boc-L-Hse-OH. 1) debenzylation of Boc-L-(Bzl)Hse-OH, purchased from Iris Biotech GmbH; 2) see ref. [306]; 3) see ref. [307]; 4) see ref. [308].

According to Ozinskas,[309] this fast intramolecular lactonization is catalyzed by traces of acid in solution. Boc-Hse-OH half-life ($t_{1/2}$) corresponds to four days in common organic solvents at room temperature. For example, the solvent ($CDCl_3$) used for recording the NMR spectrum of acyclic Boc-L-Hse-OH [**Fig. 4.12**, (**1**)] had to be previously treated with solid K_2CO_3 to slow down lactonization in solution. The fact that this material is tough to get pure is witnessed by its high price, compared to other commercial, Boc-protected α-amino acids. As a matter of fact, Boc-L-Hse-OH is commercially available from Aldrich at 240$/gram. At this point, an alternative, clean procedure was needed.

Eventually, the last, different approach was found to be efficient, giving Boc-L-Hse-OH in 70% yield. The reaction conditions are described in **Fig. 4.13**.

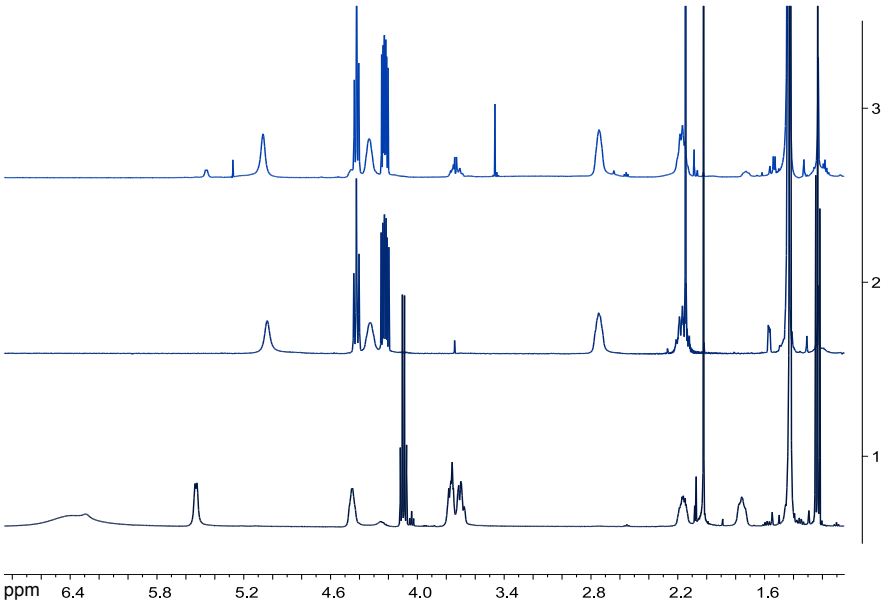

Fig. 4.12 Comparison between NMR spectra of Boc-L-Hse-OH (1); Boc-L-Hse lactone (2) and of a mixture of the two compounds as obtained from reactions reported in **Fig. 4. 11**. Signals at 1.26, 2.05 and 4.12 ppm in spectrum (1) are due to residual EtOAc.

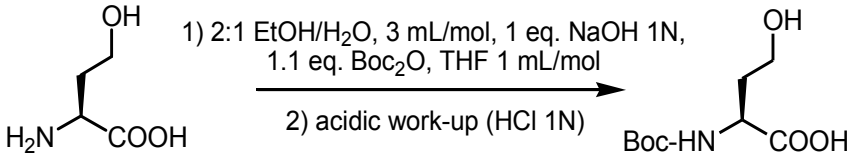

Fig. 4.13 Reaction protocol used to efficiently synthesize Boc-L-Hse-OH.[309]

Having in hands the N^{α}-Boc-protected L-Hse, we proceeded to side-chain functionalization, using a similar procedure to that used for Ser.[310] In order to minimize the cyclization reaction, the Boc-Hse-OH solution was quickly dissolved in cold, anhydrous DMF and added dropwise to the sodium hydride/DMF mixture under Ar. After reaction completion, the allylated product was obtained as an oil after acidic work-up and a flash chromatography purification step.

As in the case of Ser, racemization (although to a more limited extent) was expected to occur for Hse too. Unfortunately, such Boc-protected, allylated amino acid does not have any strong chromophore and is too polar for a reliable chiral-phase GC analysis. To overcome these difficulties, we derivatized it with a UV-active optically

pure amine [α-(*S*)-naphtylethylamine, **Fig. 4.14**] and checked the possible presence of diasteromers *via* NMR.

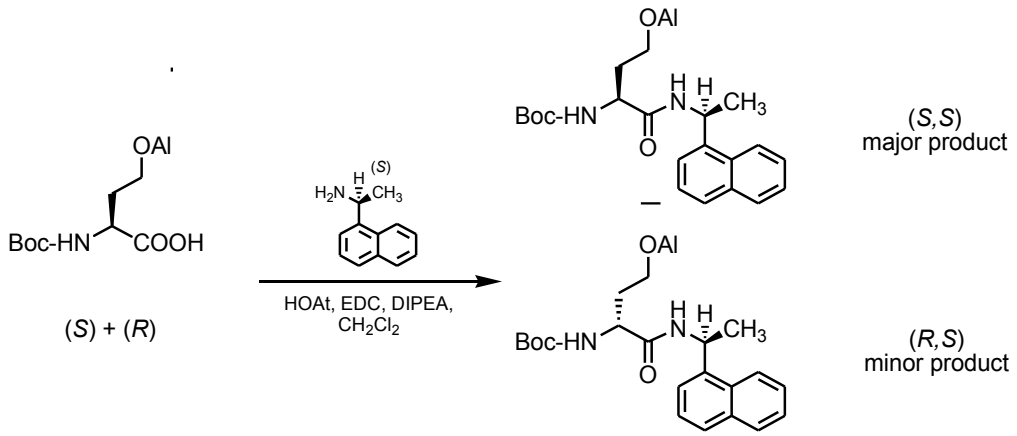

Fig. 4.14 Coupling between Boc-Hse(Al)-OH and α-(*S*)-naphtylethylamine *via* EDC/HOAt C-activation.[86]

Fig. 4.15 shows the most informative portions of two NMR spectra (recorded in two different solvents, CD_3CN and CD_3OD) of the coupling product diastereomeric mixture reported previously. The presence of side peaks for the same proton resonances proves that the allylation reaction cause racemization. Unfortunately, NMR peaks are not sufficiently resolved to evaluate correctly the *S*/*R* ratio of the products.

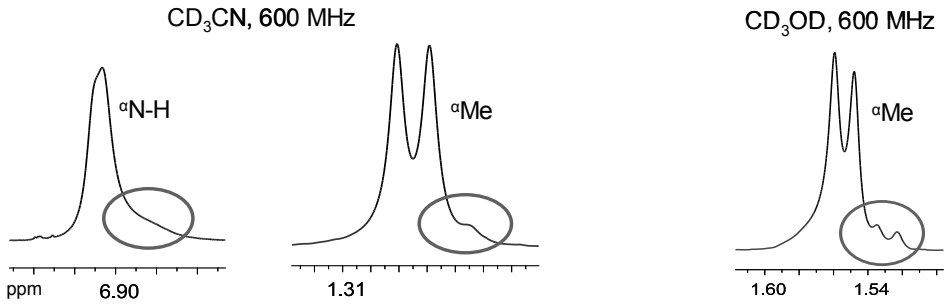

Fig. 4.15 NMR spectra of Boc-Hse(Al)-α-(*S*)-naphtylethylamide in CD_3CN (*left*) and CD_3OD (*right*), 600 MHz, in the αN-H and the α-CH_3 regions.

At this point, chiral stationary phase HPLC analysis was used on the diasteromeric mixture to monitor the relative amount of the two diastereomers, as seen in **Fig. 4.16**.

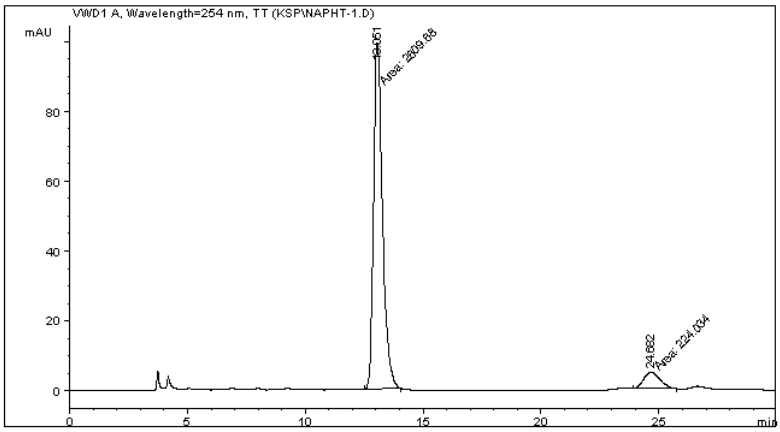

Peak #	RetTime [min]	Type	Width [min]	Area mAU *s	Height [mAU]	Area %
1	13.051	MM	0.4377	2609.67554	99.36920	92.0940
2	24.682	MM	0.8137	224.03392	4.58896	7.9060

Fig. 4.16 HPLC profile of the Boc-Hse(Al)-α-(*S*)-naphtylethylamide diastereomeric mixture. Retention times and relative areas are reported.

Taking the assumption that an enantiomerically pure starting material (*i.e.* H-L-Hse-OH) was used, we can put forward the hypothesis that the higher peak is due to the (*S,S*) diastereomer. Therefore, it is reasonable to say that the allylation reaction proceeds with a partial racemization at the level of the Hse C^{α}-proton with a L/D ratio of 92:8 and a *e.e.* = 84%. This hypothesis was also proved by HPLC/MS analysis [**Fig. 17 (a)**]. Despite the separation between the two diastereomers would not be excellent, the major peak at 11.42 min. has a shoulder that can be assigned to its diastereomer. To support this assignment, Boc-Hse(Al)-OH was coupled to *racemic* α-naphtylethylamide and the obtained reaction mixture, containing the four possible diastereomers, was subjected to HLPC/MS analysis with the same elution parameters in order to have a retention time reference [**Fig. 17 (b)**]. The chromatogram indeed showed two peaks, strongly supporting the presence of the two diastereomers (in addition to their unseparable enantiomeric dyad) in the former HPLC/MS spectrum. In this way, it was unambiguosly proved that the optical activity loss during Hse allylation is about 8%.

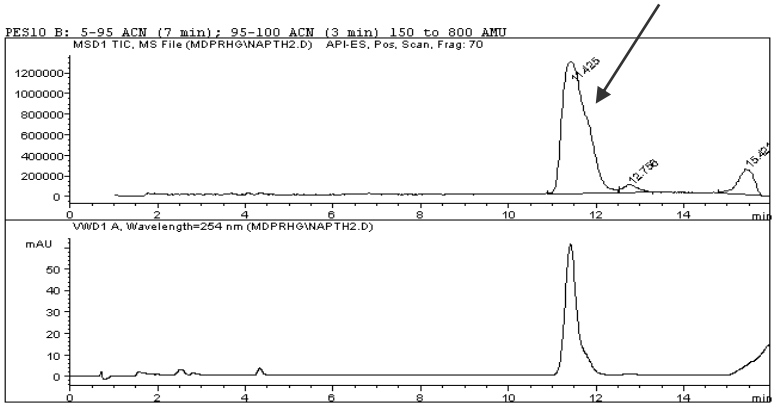

Fig. 17 (a) HPLC/MS chromatogram of the Boc-Hse(Al)-α-(*S*)-naphtylethylamide diastereomeric mixture. MS spectrum (*top*); HPLC profile (*bottom*).
Arrow indicates the shoulder due to the (*R,S*) diastereomer.

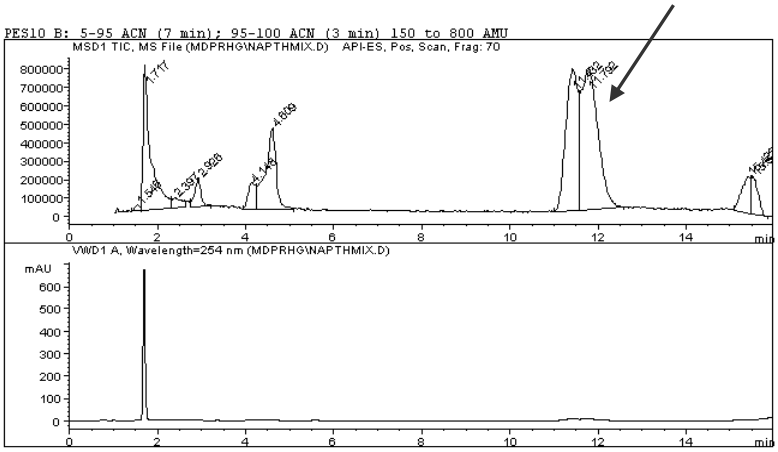

Fig. 17 (b) HPLC/MS chromatogram of the Boc-Hse(Al)-α-(*S,R*)-naphtylethylamide diastereomeric mixture. MS spectrum (*top*); HPLC profile (*bottom*).
Arrow indicates the peak due to the (*R,S*) + (*S,R*) enantiomeric dyad.

At this point it is safe to conclude that even in the case of Hse, allylation gives rise to racemization, in a reduced, but similar manner as with Ser. Consequently, the reaction procedure was slightly modified to favour retention of configuration during allylation. First of all, the reaction was conducted in a dry-box and anydrous NaH was used. This procedure actually removed moisture contamination and related weighting errors. Then, allyl bromide was introduced in a single portion soon after the addition of Boc-Hse-OH to the DMF/NaH mixture, to suppress the acid-base equilibrium between the Hse side-chain alkoxide ion ($R\text{-}O^-$) and the C^{α}-proton, which was thought to be

responsible for the racemization. Finally, excess NaH was quenched with a saturated solution of NaH_2PO_4, to keep the reaction medium at a neutral pH.

The racemization extent of the recovered allylated product was checked by ^{19}F-NMR analysis. To this purpose, Hse(Al) was derivatized with the Mosher's acid [(*R*)-α-trifluoro-α-methoxyphenylacetic acid[311], **Fig. 4.18**], preventing any possible, further racemization occurring during activation of the carboxyl function *via* EDC/HOAt and increasing the accuracy of the *e.e.* determination as well.

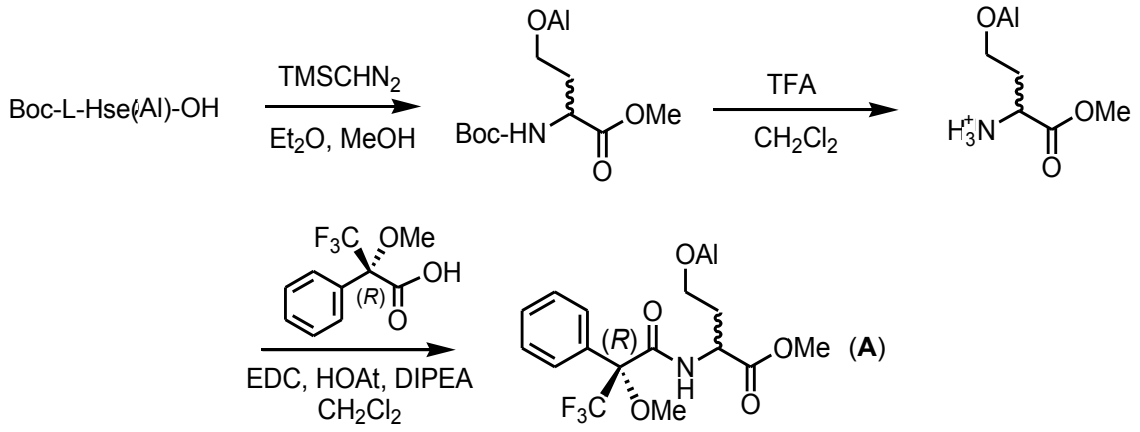

Fig. 4.18 Synthetic scheme describing the derivatization of Hse(Al) with the Mosher's acid for the ^{19}F-NMR *e.e.* analysis.

According to **Fig. 4.18**, Boc-Hse(Al)-OH was treated with trimethylsilyl-diazomethane to give the corresponding methyl ester,[312] then Boc-deprotected with TFA and coupled with the Mosher's acid to give compound (**A**), suitable for the ^{19}F-NMR analysis. In this way, the enantiomeric eccess was determined by integrating the two ^{19}F signals at 68.9 and 69.3 ppm, assigned to the (*R,R*) and (*R,S*) diastereomers, respectively.

Despite the use of different reaction conditions, the observed L/D ratio is again at about 92:8, as showed in **Fig. 4.19**. At this point, it is evident that the Williamson allylation protocol is too harsh for Hse to completely retain configuration.

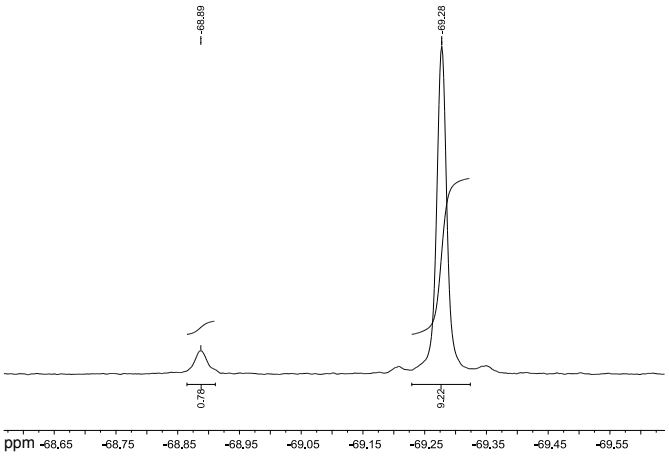

Fig. 4.19 ^{19}F NMR spectrum ($CDCl_3$, 400 MHz) of the Mosher's acid derivative (**A**), showing the two different ^{19}F signals.

For the sake of completeness, an *e.e.* analysis was also accomplished on the starting H-L-Hse-OH (98%, Acros Organics). In this case, the aminoacid was N^{α}-protected with benzyloxycarbonyl to be detectable *via* chiral-phase HPLC. Z-Hse-OH was then subjected to esterification with $TMSCHN_2$[312] and the lactone-containing mixture was purified to get pure Z-Hse-OMe, although in low yields (**Fig. 4.20**).

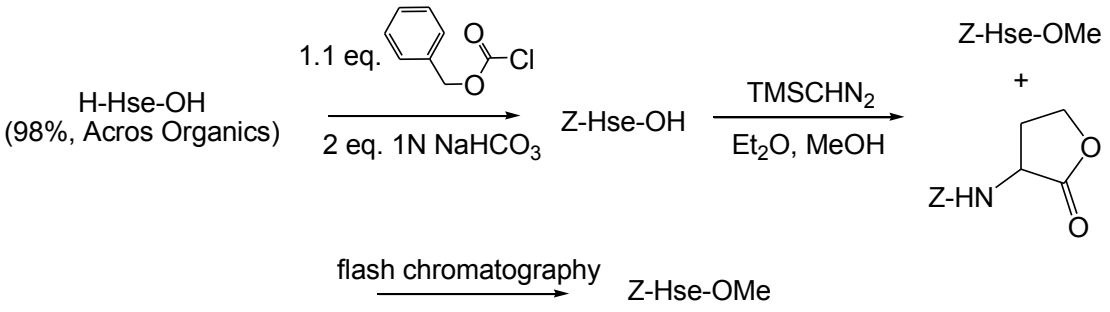

Fig. 4.20 Synthesis of Z-Hse-OMe.[309]

The HPLC profile demonstrated the presence of two enantiomers of the derivatized Hse, with an *e.e.* of about 93% (**Fig. 4.21**).

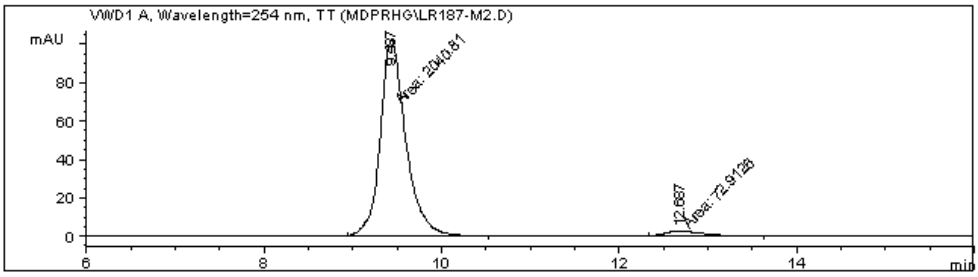

Peak #	RetTime [min]	Type	Width [min]	Area mAU *s	Height [mAU]	Area %
1	9.437	MM	0.3324	2040.80566	102.34142	96.5505
2	12.687	MM	0.4370	72.91255	2.78054	3.4495

Fig. 4.21 Chiral phase HPLC of Z-Hse-OMe.

Combining this latter result with the previously determined optical activity loss, the racemization extent of Hse allylation can be considered to be not less than 4.5%. As unfortunately this value appeared too high for the goal of our work, a different approach was followed to achieve Hse side-chain allylation.

To avoid basic conditions, we tried to use two different allylation strategies.

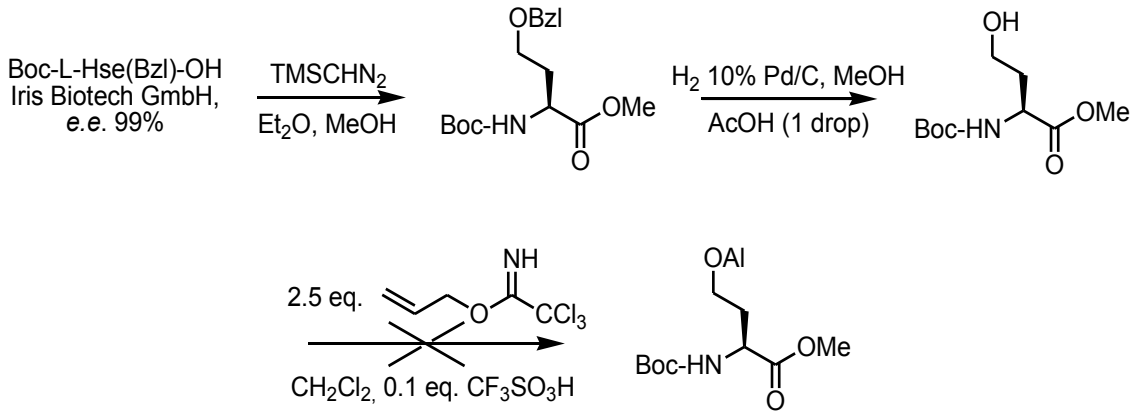

Fig. 4.22 Synthetic scheme for side-chain allylation using O-allyltrichloroacetimidate.

The first attempt (**Fig. 4.22**) employed O-allyltrichloroacetimidate as an electrophilic allyl donor. After the usual esterification of Boc-L-Hse(Bzl)-OH (99% *e.e.*, Iris Biotech GmbH) and catalytic O-debenzylation, the alcohol was treated with O-allyltrichloroacetimidate in an acidic environment. However, Boc protection did not appear to tolerate these conditions, even if the literature protocol stated just the

opposite.[313,314] Considering also the very high price of this allylation reagent, this method was discarded.

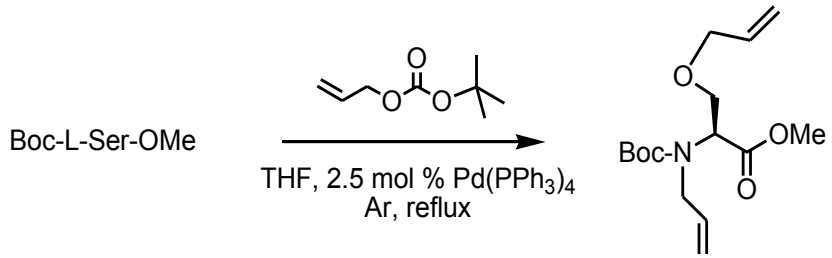

Fig. 4.23 Pd-mediated catalytic allylation of Boc-L-Ser-OMe.

A second approach[315,316] is illustrated in **Fig. 4.23**. A Pd-mediated, catalytic allylation with *tert*-butylallylcarbonate[317] was employed. This latter compound is not commercial and had to be specifically prepared. The reaction mechanism proceeds through the initial formation of a Pd (II) π-allyl complex. This intermediate then undergoes decarboxylation and subsequent nucleophile addition of alcoholic oxygen on the allylic ligand. Since no basic species are formed in the progress of the reaction, protected L-Ser was used because it was already available. Anyway, the reaction exhibited no selectivity towards the two different nucleophiles (*i.e.* alcoholic OH and urethane NH), as the double-allylated amino acid was the only product recovered.

In view of the previously discussed results, we can draw some conclusions on the Ser/Hse side-chain allyl insertion. Our goal was to prepare an enantiomerically pure (>98-99%) allylated amino acid relatively quickly, but none of the previous methods proved to be eligible to that purpose, because of racemization issues or tedious synthetic procedures. This results actually do not make Hse or Ser suitable candidates for building up an Aib-rich, 3_{10}-helical ladder peptide.

In order to definitely remove the racemization problems during side-chain allylation, we tried to use a C^{α}-tetrasubstituted α-amino acid. Boc-C^{α}-methyl-L-serine (99%, Anaspec, Fremont, USA) was chosen and then allylated to give Boc-L-(αMe)Ser(Al)-OH. This extremely hindered (and expensive!) amino acid derivative exhibited a very low reactivity in solution-phase peptide couplings with the Aib-NH nucleophile, so this strategy (**Fig. 4.24**) was abandoned.

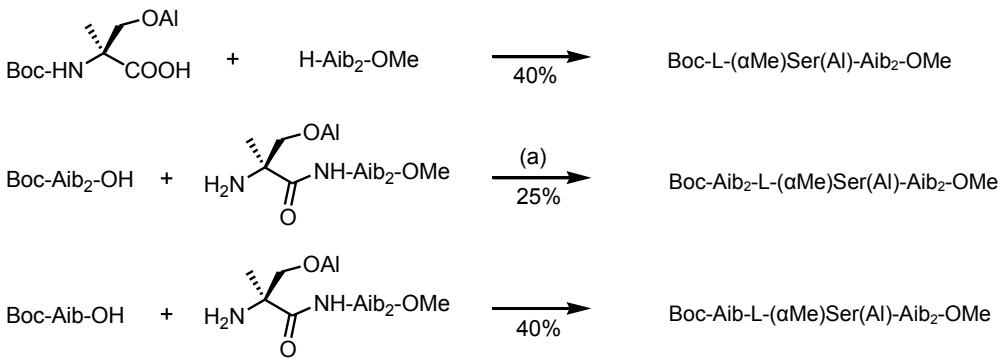

Fig. 4.24 Explored coupling reactions with Boc-L-(αMe)Ser(Al)-OH with EDC/HOAt C-activation.[86] (a): *via* the 5-(4*H*)-oxazolone intermediate.

At this point, a radical change of our plan was required. Ser, Hse and (αMe)Ser request harsh conditions for allyl incorporation, giving rise to problems that were considered beyond the scope of this thesis to be solved. A valid alternative was found by carefully examining the broad proteinogenic α-amino acid list.

Aspartic acid seemed to give the solution, because it is commercially available as Z-L-Asp(O*t*Bu)-OH. Indeed, this relatively inexpensive compound possesses a Z-orthogonal side-chain *tert*-butyl ester protection that can be easily functionalized into an allyl ester *after* the insertion in the peptide chain. Even if this derivative does not have the same side-chain flexibility characteristics of the corresponding allyl ether (as in the case of Hse or Ser), this alternative represented a good compromise.

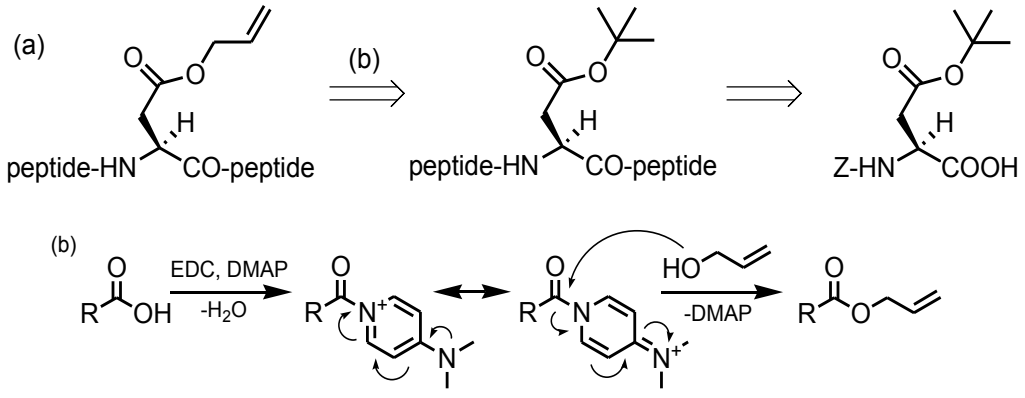

Fig. 4.25 Retrosynthetic analysis for Asp(Al) incorporation into a peptide sequence (a) and mechanism of DMAP-mediated Asp side-chain esterification (b).

The actual retrosynthetic scheme, applied to build the target peptide bundle, is illustrated in **Fig. 4.25**. The esterification on Asp side-chain was accomplished *via* the method introduced by Steglich[318], using EDC for C^{γ}-activation and DMAP as catalyst. This approach allowed the fast incorporation of the allyl moiety inside the peptide, as shown in **Fig. 4.26**.

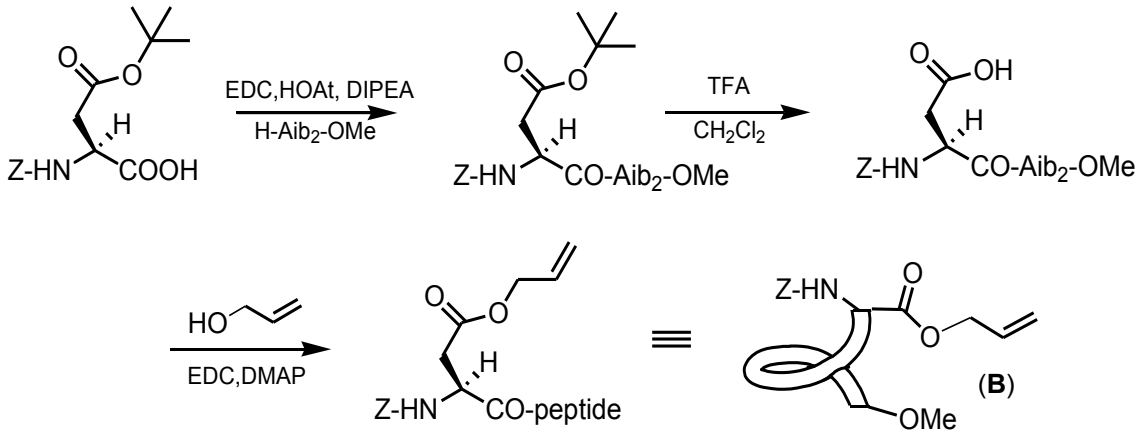

Fig. 4.26 Synthesis of ladder fragment (1) from Z-Asp(O*t*Bu)-OH.

Then, the allylated ladder fragment (**B**) was subjected to *self*-metathesis with Second Generation Grubbs' catalyst [**Fig. 2 (c)**] which gave high yields of compound (**C**), shown in **Fig. 4.27**. The use of First Generation catalyst [**Fig. 2 (b)**] for the synthesis of (**C**) was also explored, but the final reaction yield was not good. Since high quantities of this material were needed to proceed up to the final step, we also devised another route to synthetize (**C**) employing a pre-formed diester linker (1,4-butanediol), as reported in **Fig. 4.28**.

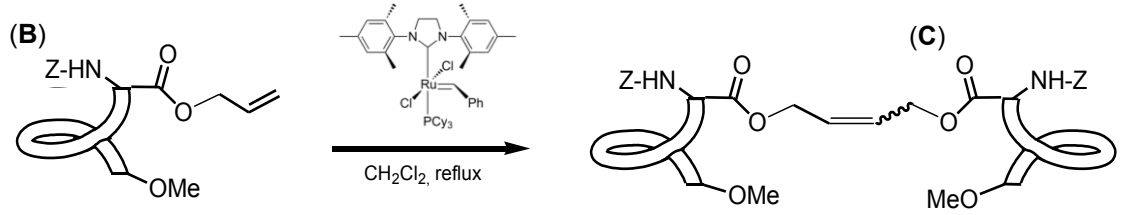

Fig. 4.27 Synthesis of the ladder peptide's first "step" (**C**) *via* self-metathesis.

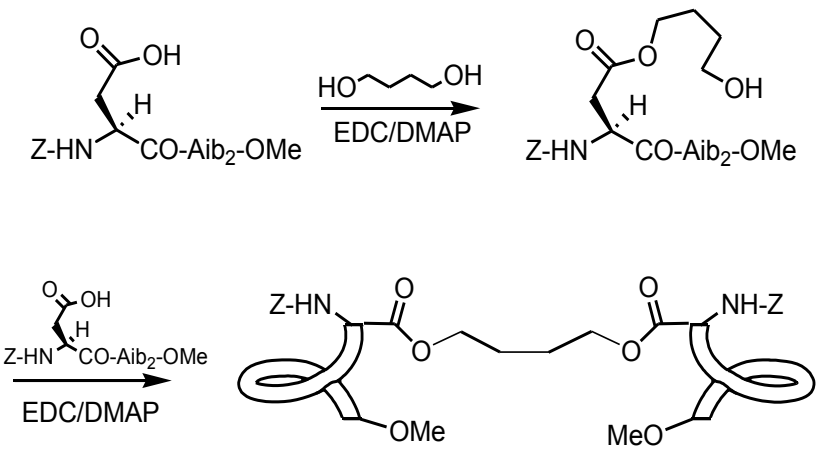

Fig. 4.28 Synthesis of the saturated ladder peptide's first "step" *via* double esterification with 1,4-butanediol.

Couplings *via* EDC/HOAt[86] C-activation were run on both ends of the peptide obtained in the first "step" of the ladder. Despite the overall low yield (because of two concurrent couplings in the same reaction) along with several tedious purification and optimization steps, the synthesis of the diallylated, open *bis*-peptide bundle (**D**) was accomplished.

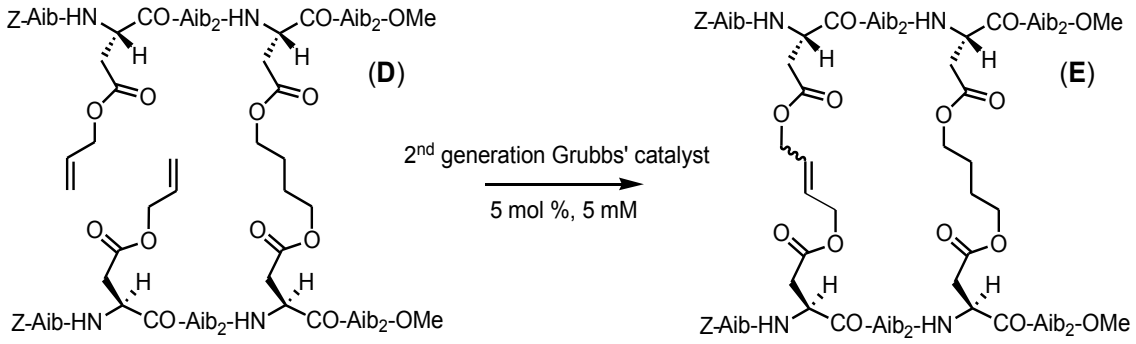

Fig. 4.29 RCM macrocyclization of (**D**) with Second Generation Grubbs' catalyst.

When treated with Second Generation Grubbs' catalyst, diene (**D**) underwent rapid macrocyclization to afford (**E**) in high yields, as confirmed by MS (**Fig. 4.29**). The newly formed olefin was mainly in the *E*-configuration (*cis*/*trans* ratio ~ 1:15), as

deduced by its NMR spectrum. This result is consistent with the picture of a very big macrocycle being assembled during RCM and with a general preference for an *E* over *Z* stereoselectivity exhibited in such a catalyzed reaction. Moreover, the origin of the higher *E*-form propensity in such Aib-rich peptides may be due to φ/ψ conformational restrictions imposed by the C^{α}-tetrasubstituted α-amino acid residues.

4.2 Ladder peptides: conformational characterization

A preliminary conformational investigation was possible by combining data from different solution-phase physico-chemical techniques. For clarity, the peptides studied, their shorter sequences and their amino acid sequences will be renamed according to **Table 4.1** from now on.

Table 4.1 Sequences of peptides studied and corresponding numbering.

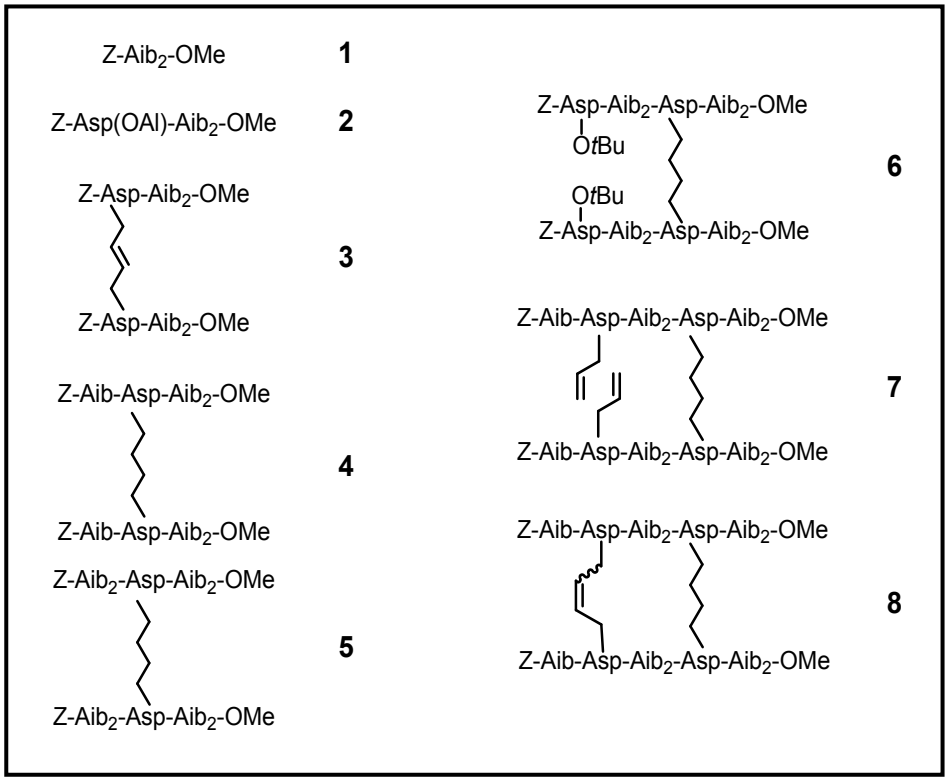

FT-IR absorption analysis in $CDCl_3$ solution was conducted in the informative region of free (solvated) and H-bonded N-H stretching modes (3200-3500 cm^{-1}). **Fig. 4.30 (a)** shows that for the open diester [(**7**) in **Table 4.1**] the effects observed upon dilution are negligible, thus indicating that this peptide is predominantly intramolecularly H-bonded in solution.

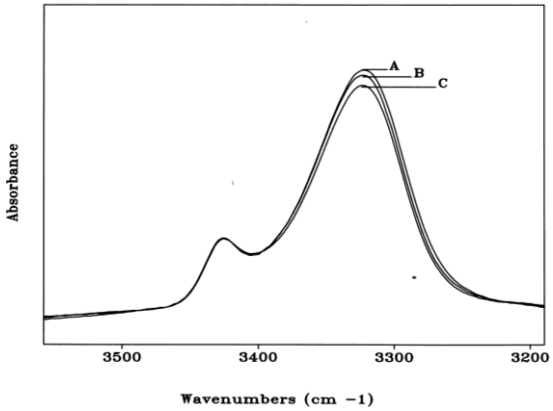

Fig. 4.30 (a) FT-IR absorption spectra of the open ladder peptide [(**7**) in **Table 4.1**] in the 3200-3500 cm^{-1} region in $CDCl_3$ solution. Peptide concentrations: 10 mM (A), 1 mM (B) and 0.1 mM (C).

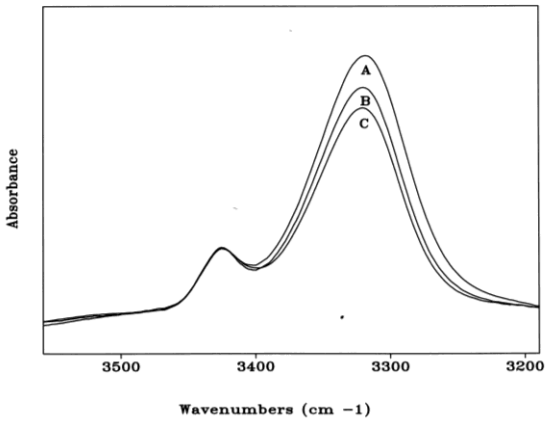

Fig. 4.30 (b) FT-IR absorption spectra of the RCM ladder peptide [(**8**) in **Table 4.1**] in the 3200-3500 cm^{-1} region in $CDCl_3$ solution. Peptide concentrations: 10 mM (A), 1 mM (B) and 0.1 mM (C).

As for the RCM ladder peptide [(**8**) in **Table 4.1**], on the other hand, the effects observed upon dilution are slightly more evident, indicating a relatively stronger tendency to aggregation [**Fig. 4.30 (b)**]. This finding is consistent with a more ordered secondary structure, with two peptide helices locked in a parallel fashion. The development of a secondary structure in the ladder peptide is supported by correlation of the elongation of the two peptide chains with the number of H-bonded NHs (~ 3330 cm^{-1}) and the gradual red-shift of the absorption maxima (**Fig. 4.31**). This latter behaviour indicates that the peptide main chain length increase induces a more substantial structural rigidity. Notably, comparing the spectra of peptides (**3**) and (**4**) [**Table 4.1**], a dramatic increase of the absorption band due to the H-bonded NHs is observed. This result is consistent with the presence of an additional Aib residue at N-terminus of peptide (**4**). The same effect is observed when a further Aib unit is added, as seen on going from (**4**) to (**5**).

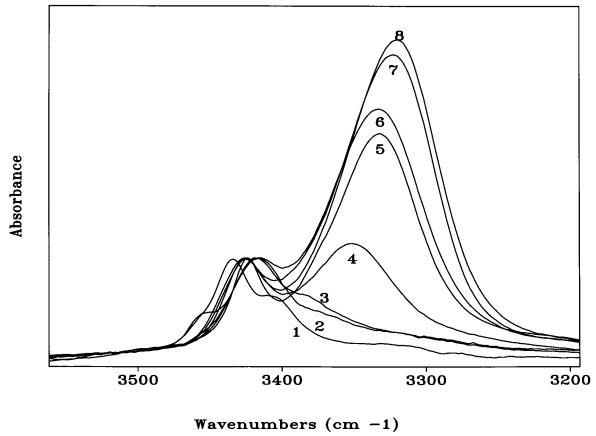

Fig. 4.31 FT-IR absorption spectra of peptides [(**1-8**) in **Table 4.1**] in the 3200-3550 cm^{-1} region. Peptide concentrations: 1 mM in $CDCl_3$.

The structural analyses of open (**7**) and RCM-cyclized (**8**) peptides were performed also using NMR. By combining the information extracted from the two-dimensional TOCSY spectrum[94-96] with the through-space connectivities of the $C^{\alpha}H(i)\rightarrow NH(i + n)$ and $NH(i)\rightarrow NH(i + 1)$ types, as obtained from the ROESY and NOESY experiments,[95] we were able to assign all of the proton resonances in CD_3OH or DMSO-d_6 solution (**Figs. 4.32-4.35**). Unfortunately, the high content of C^{α}-

tetrasubstituted Aib residues in these peptides complicated the conformational analysis by reducing the number of C^{α}-protons available.

Indeed, typical helical cross-peaks were detected in CD_3OH solution for both the "open" and the RCM ladder peptides [(**7**) and (**8**), respectively, in **Table 4.1**], like *intramolecular* $d_{\alpha N}$ (i, $i + 2$) [distance between C^{α}_i-proton and N_{i+2} proton, typical of a 3_{10} helix], and *intramolecular* d_{NN} (i, $i + 1$) [distance between NH_i proton and NH_{i+2} proton]. These connectivities account for the presence of a helical structure,[241] although an accurate and detailed conformational analysis is not straightforward.

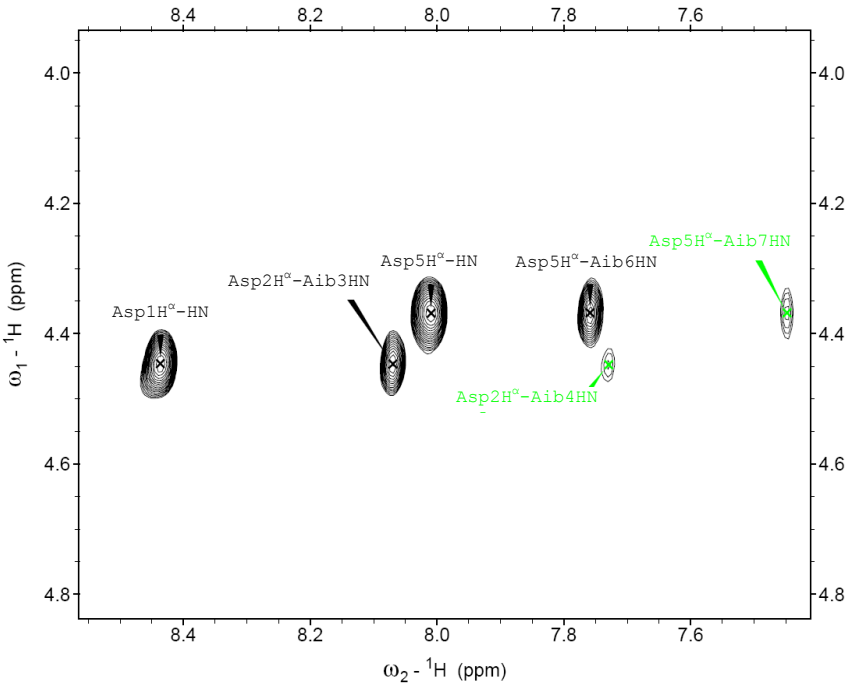

Fig. 4.32 Portion of the 2D ROESY spectrum of the diallylated ladder peptide ["open", (**7**) in **Table 4.1**] in CD_3OH solution. Green: $d_{\alpha N}$ (i, $i + 2$) 3_{10}-helical connectivities; black: other connectivities.

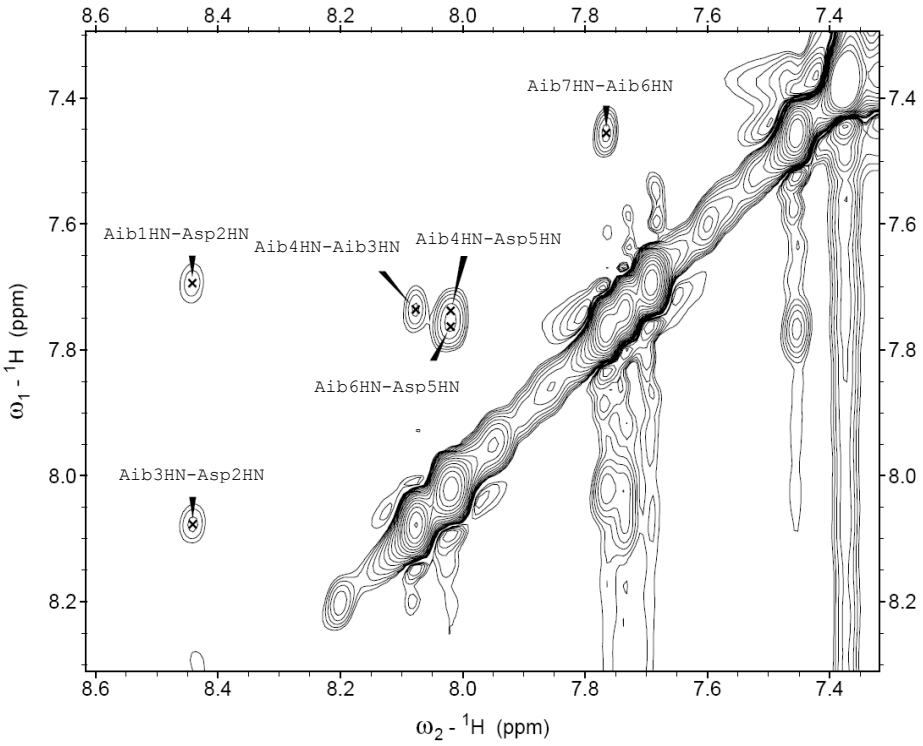

Fig. 4.33 Portion of the 2D ROESY spectrum of the diallylated ladder peptide ["open", (**7**) in **Table 4.1**] in CD_3OH solution: d_{NN} (i, i + 1) connectivities are shown.

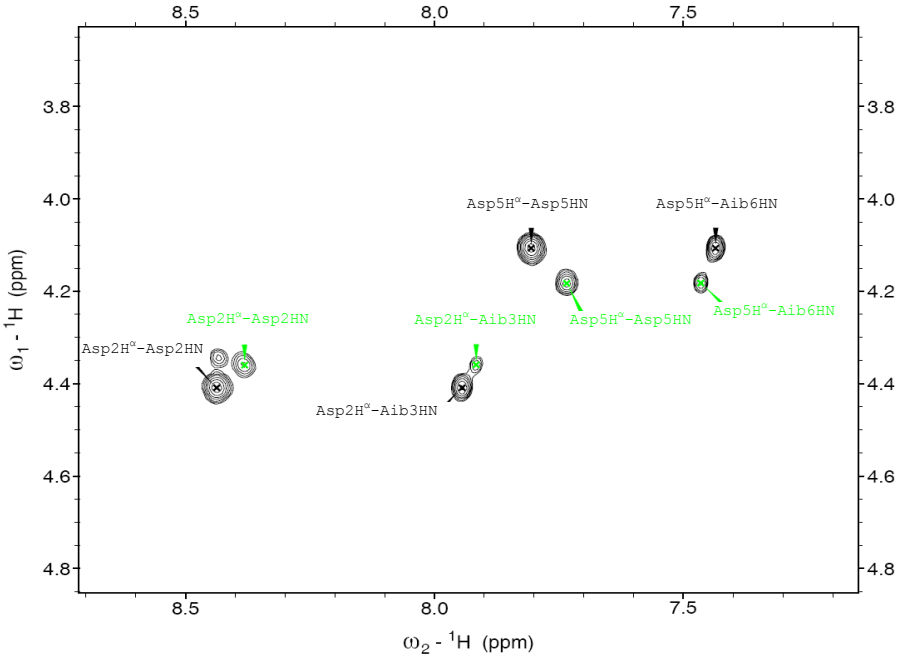

Fig. 4.34 Portion of the 2D NOESY spectrum of the RCM ladder peptide [(**8**) in **Table 4.1**] in DMSO-d_6 solution: $d_{\alpha N}$ (i, i + 1) connectivities are shown.

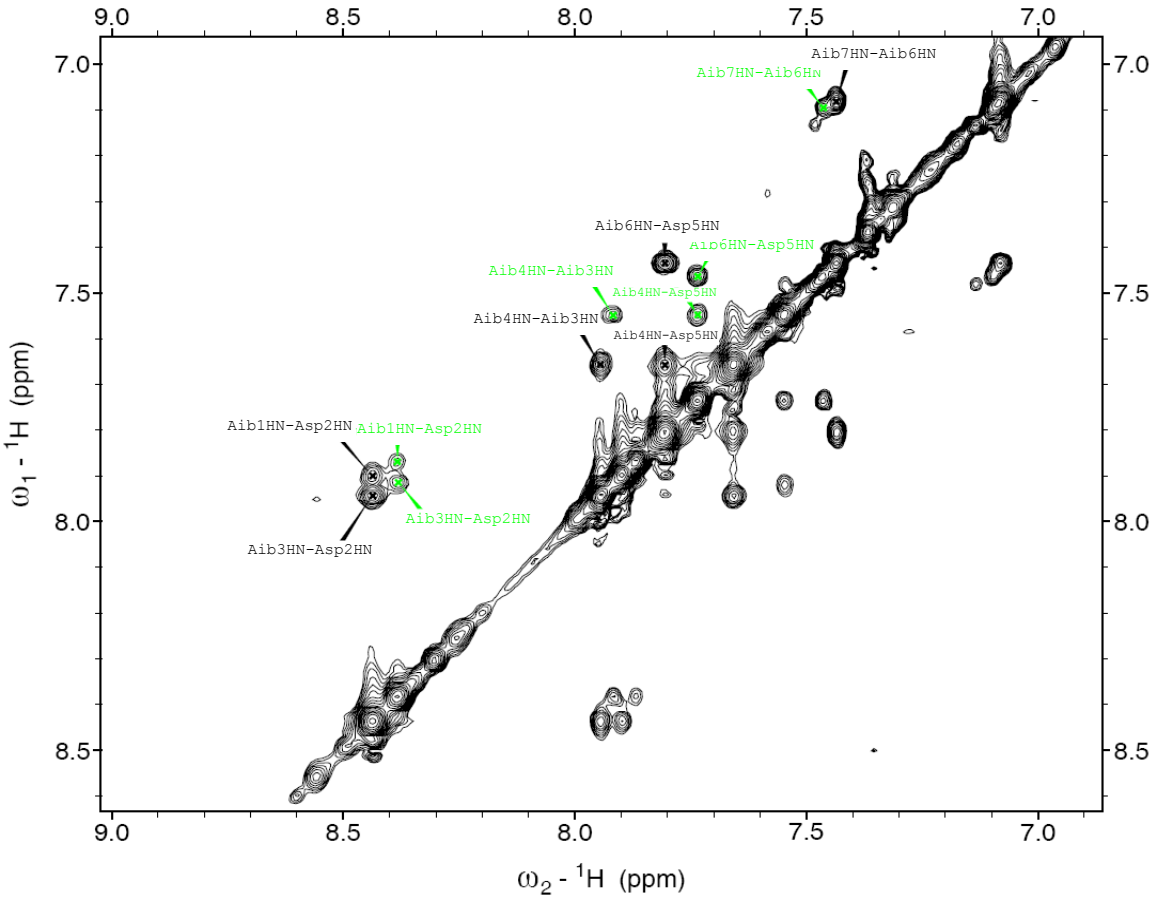

Fig. 4.35 Portion of the 2D NOESY spectrum of the RCM ladder peptide [(**8**) in **Table 4.1**] in DMSO-d_6 solution: d_{NN} (i, i +1) connectivities are shown.

Considering the ECD spectra of the two peptides studied (**Fig. 4.36**), they exhibit a significant negative band at 202 nm and a weak negative shoulder at 224 nm, with an R value $([\Theta_T]_{224}/[\Theta_T]_{202})$[21,26,65,66,70,144] of ~ 0.15, consistent with a largely predominant 3_{10}-helix conformation in CH_3OH solution.

The helical conformation hypothesis suggested by NMR and FT-IR absorption for both the open and RCM ladder peptides is strongly supported also by their ECD spectra. However, in order to obtain a definitive picture, the solution-phase results should be compared with crystal-state data. Unfortunately, so far we were not able to grow any single crystal suitable for X-ray diffraction analysis.

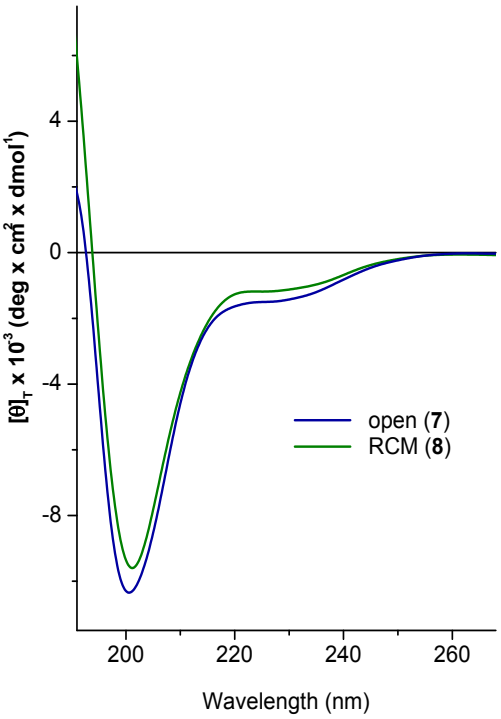

Fig. 4.36 Far-UV ECD spectra of the ladder peptide "open" [(**7**) in **Table 4.1**, blue] and RCM [(**8**) in **Table 4.1**, green]. Peptide concentration: 0.5 mM in CH_3OH.

At a first glance, it is reasonable to conclude that RCM constraints do not seem to induce any detectable impairment to the overall 3_{10}-helical secondary structure adopted by the tethered *bis*-peptide bundle [(**8**) in **Table 4.1**]. Anyway, it is worth noting that the ECD intensity of the cyclized peptide is slightly lower than that of its open counterpart (**Fig. 4.36**). This phenomenon might be explained, in principle, as the outcome of a weak interaction between the dipole moments of the two helices packed in an unfavourable, parallel fashion, giving rise to a modest nonconservative hypochromic effect. Although this hypothesis needs to be checked further, it is in accordance with a spatial proximity of the two tied helices, as already pointed out in the introductory paragraphs (**Fig. 4.8**).

Interestingly, a closer inspection of the NOESY spectrum of the RCM ladder peptide [(**8**) in **Table 4.1**] provides evidence for two mutually independent cross-peak systems (**Figs. 4.34** and **4.35**, black and green connectivities) which could be consistent with the presence of an equilibrium between at least two major conformations in

DMSO-d_6 solution. Incidentally, such an effect was not observed in a comparably more polar solvent like MeOH.

Based on the amount of structural information obtained from previous conformational analysis, we tried to rationalize this unexpected behaviour by noting that the diester constraints could allow a reciprocal, slight rotation of the two helices relatively to each other in solution. In a viscous solvent like DMSO, this tilting motion is probably slowed down enough to be sensed, according to the NMR time-scale. Thus, two different sets of signals appear, accounting for the two major conformers, represented graphically in **Fig. 4.37**, which are each other in a diastereomeric relationship.

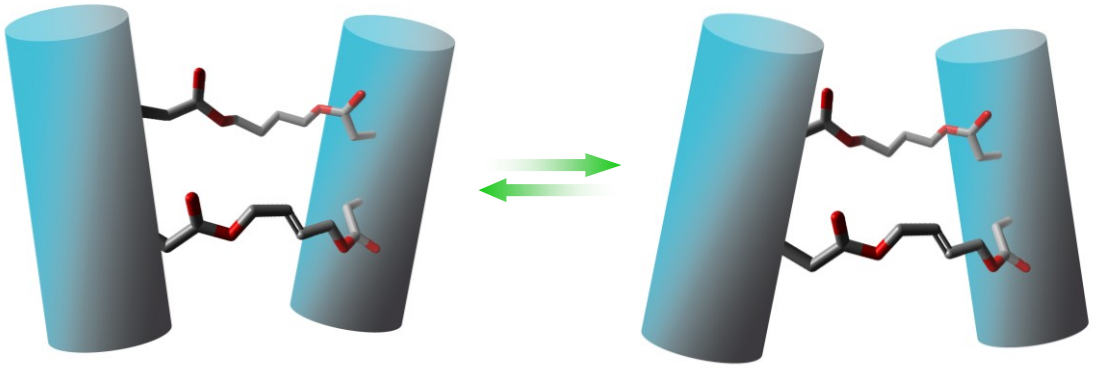

Fig. 4.37 Graphical models of the two proposed conformations in DMSO-d_6 solution for the RCM ladder peptide [(**8**) in **Table 4.1**]. The blue cylinders represent the two peptide helices.

To corroborate this possible mechanism, a more detailed NMR analysis, for example, could show coalescence of the two sets of signals with increasing temperature. Also, adding a third tether could improve the bundle rigidity, suppressing any tilting motion by locking the two helices in a strictly parallel disposition. Detailed investigation is underway to shed light into the validity of the proposed model.

4.3 Conclusions

In this chapter we have reported the synthesis and preliminary conformational characterizations of the *first 3_{10}-helical bis-peptide bundle* (*ladder peptide*). Our approach relied on the use of the ring-closing olefin metathesis reaction as a powerful tool to connect and cyclize a large peptide macrocycle rich in C^{α}-tetrasubstituted α-amino acids (Aib).

The first part of this work was carried out in the laboratories of prof. R.H. Grubbs and D.J. O'Leary. We evaluated the possibility of incorporating an allyl moiety into an α-amino acid side chain without loss of optical activity. A such compound would have been used as a linker in the preparation of the ladder peptide, so the extent of racemization had to be the lowest possible. To this purpose, a large number of attempts was explored, but eventually the use of Asp as a practical alternative was proposed.

After several steps, we accomplished the synthesis of the target *bis*-peptide bundle. Preliminary results from our conformational analyses in solution (FT-IR absorption, 2D NMR and ECD) suggested this cyclic peptide to be largely 3_{10}-helical, confirming the known, high structural propensity exhibited by Aib-containing peptides.

Interestingly, such RCM-tethered helices appeared to show a conformational equilibrium, as evidenced by the presence of two major conformers detected *via* NMR. Although further investigations are needed to confirm this hypothesis, a model involving a tilting motion between the two helices was tentatively proposed to explain the latter result.

5. EXPERIMENTAL PART

5.1 Reagents and solvents

Acros-Janssen (Geel, Belgium):
α-amino isobutyric acid, glicine, deuterated dimethylsulphoxyde, N-benzyloxycarbonyloxysuccinimide, 1,4-butanediol, deuterochloroform, leucine, proline, alanine, allyl alcohol, allyl bromide, thionyl chloride, N-ethyl-N'-(3-dimethylamino)propyl-carbodiimide hydrochloride, sodium chloride, N,N-dimethylformamide, acetic anhydride, ethyl vinyl ether, glacial acetic acid, N,N-diisopropylethylamine, *iso*propylamine, 4-dimethylaminopyridine, homo-serine, benzylchloroformate, *p*-bromobenzoyl bromide.

Carlo Erba (Milan, Italy):
ethyl acetate, acetone, sodium bicarbonate, potassium bisulphate, 1-butanol, chloroform, dichloromethane, acetonitrile, ethanol, methanol, diethyl ether, dioxane, petroleum ether, isobutene, sodium hydroxyde, sodium hypochlorite, methanol, triethylamine, anhydrous sodium sulphate.

Sigma Aldrich (St. Louis, MO USA):
[1,3-*bis*(2,4,6-trimethylphenyl)-2-imidazolidinylidene](dichloro)(phenylmethylene)(tricyclohexylphosphine)ruthenium (Grubbs' IInd generation catalyst), benzylidene-*bis*(tricyclohexylphosphine)dichlororuthenium (Grubbs' Ist generation catalyst), O-allyltrichloroacetimidate, sodium hydride, trfluoro methanesulphonic acid, (*R*)-α-trifluoro-α-methoxyphenylacetic acid (Mosher's acid), trimethylsilyldiazomethane, (*S*)- and (*R*)-α-naphtylethylamine, amberlite 15 (H^+), Boc-L-Hse-OH.

Fluka (Buchs, Switzerland):
trifluoroacetic acid, 10% Pd/C catalist, N-methylmorpholine, ninhydrin, 1-hydroxy-7-azabenzotriazol.

Strem Chemical (Newburyport, MA USA):
Tetrakis(triphenylphosphine)palladium.

Anaspec (Fremont, CA USA):
Boc-L-(αMe)Ser-OH.

Merck (Darmstadt, Germany):
silica gel for *flash* chromatography.

Alphagaz (Liscate, Milano):
*iso*butene, anhydrous hydrochloric acid.

DSM Research (Geleen, The Netherlands):
C^{α}-methylproline.

Cambridge Isotope Laboratories (Andover, MA, USA)
$H_2{}^{18}O$ 97%, H-(1-^{13}C)-Ala-OH, H-(1-^{13}C)-Leu-OH, H-(^{15}N)-Gly-OH, D_2O, CD_3OD, CD_3OH, CD_3CN.

Iris Biotech GmbH (Marktredwitz, Germany)
N^{α}-Boc-(O-Benzyl)-Hse-OH.

Bachem (Bubendorf, Switzerland)
Z-Asp(O*t*Bu)-OH.

5.2 Instruments and methods

Thin layer chromatography

The reactions were followed by thin layer chromatography using plates of silica gel 60 F_{254} (Merck). The retention coefficients were measured using the following solvent mixtures:

$CHCl_3$/EtOH 9:1	Rf_1
1-butanol/AcOH/H_2O 3:1:1	Rf_2
toluene/EtOH 7:1	Rf_3

For the determination of the products on the plates, a UV lamp, iodine vapours, $KMnO_4$, the reagent TDM for amide groups, and a ninhydrin reagent[319] for the primary amino groups were used.

Melting points determination

Melting points were measured on the Leitz apparatus model Laborlux 12.

Electronic Circular dichroism

ECD spectra were recorded on dichrographs Jasco model J-715 or model J-810 using quartz cells (Hellma, 0.01-0.05 cm).

Vibrational Circular Dichroism

All VCD spectra were measured using a home-made dispersive instrument separately described in detail.[320] Briefly, it consists of a 0.3 m monochromator (Acton Research Corporation, SpectraPro 2300i), C-Rod source, 57 KHz CaF_2 modulator (Hinds International) and narrow band liquid-nitrogen-cooled MCT detector (Infrared Assoc.). Data are processed with independent digitization of transmission and modulation intensity and ratioing in a control computer programmed in LabView.

Raman Optical Activity

Raman measurements were obtained using a home-made Raman spectrometer with a 785 nm (380 mW) excitation laser (Innovative Photonic Solutions), passing through a laser-line filter (Semrock) and focused with 5-cm focal length lens into a quartz sample cell. The 90o collection geometry includes an edge filter (Semrock) to block the laser lines before focusing the scattered light on the entrance slit of a 0.64 m, f/5.4 monochromator (Jobin-Yvon) equipped with a back-illuminated CCD detector (Andor Technology).

Flash chromatography

For the *flash* chromatography silica gel 60 Merck (40-63 μm) was used. In various purifications the product dissolved in a selected eluant was directly loaded on top of the column.

HPLC

HPLC analyses and purifications were carried out with a chromatograph Agilent 1200 series. UV detection was set at 226 nm. *Semi*-preparative (250 × 10 mm, flowrate 1 ml/min) and analytical (250 × 4.6 mm, flowrate 5 ml/min) reverse phase columns C_{18} Vydac were used. As an eluant, the following solvent mixtures were used:

A: H_2O/CH_3CN 9:1 + TFA 0.05%

B: CH_3CN/H_2O 9:1 + TFA 0.05%

Preparative purifications were carried out using a Shimadzu (Kyoto, Japan) series LC-6A chromatographic apparatus, equipped with two independent pump units, an UV–Vis detector, and a Vydac C_{18} column (250 x 22 mm, 10 μm, flow rate at 15 mL/min). As an eluant, the following solvent mixtures were used:

A: H_2O + TFA 0.1%

B: CH_3CN/H_2O 9:1 + TFA 0.1%

Analytical chiral HPLC was performed with an Agilent 1100 Series HPLC utilizing a Chiralpak AD column (250 x 4.6 mm, flowrate 1 ml/min) obtained from Daicel Chemical Industries, Ltd., with UV visualization at 254 nm.

Polarimetric measurements

Polarimetric measurements were carried out on a Perkin-Elmer model 241 polarimeter with an Haake model D8 thermostat, using a cell with an optical pathlength of 10 cm.

Mass spectrometry

Mass spectra were recorded on mass spectrometer Mariner model ESI-TOF (Perseptive Biosystems). The positive and negative ions were accelerated at 10, 15, 20 or 30 keV.

FT-IR absorption spectroscopy

IR absorption measurements in solution were performed on a Perkin Elmer model 1720 X FT-IR spectrophotometer, nitrogen flushed, equipped with a sample-shuttle device, at 2 cm^{-1} nominal resolution, averaging 100 scans. Solvent (baseline) spectra were obtained under the same conditions. Cells with pathlengths of 0.1, 1 and 10 mm (with CaF_2 windows) were used.

2D-IR absorption spectroscopy[102]

Measurements of 2D IR spectra were carried out using IR pulses generated by a home-built optical parametric amplifier and a difference frequency generator (1 μJ/pulse, a bandwidth of about 160 cm^{-1} with a central frequency of 1660 cm^{-1} and pulse duration of 100 fs at a repetition rate of 1 kHz). A collimated IR pulse is split into three parts with equal pulse energy and focused onto a sample cell with CaF2 windows. Third-order nonlinear signals were induced and detected at the phase-matching direction of $-k_a + k_b + k_c$ determined by the wavevectors of three incident IR pulses ka, kb and kc. The delay time between the first and second incoming pulses is denoted as τ and the second and third pulses as T. Absolute magnitude 2D IR spectra were obtained by 2D Fourier transform of the collected data matrix along τ and t whose conjugated frequency was ω_τ and ω_t, respectively.

UV-Vis absorption spectroscopy

UV-*Vis* absorption experiments were carried out at room temperature on solutions contained in quartz cells (Hellma, 0.01-0.05 cm) with a Cary 100 scan and UV- 250 1 PC Shimadzu spectrophotometers.

NMR spectroscopy

1D and 2D-NMR spectra were recorded on Bruker AM 200, AM 400, AM 600 and Varian Inova 500 spectrometers. As a reference tetramethylsilane was used. For the elaboration of the spectra the programs, Sparky, XwinNMR and MestRe-C 2.3 were applied. ^{19}F NMR spectra were recorded on a Varian Mercury 300 instrument (at 282 MHz) and are reported relative to external F_3CCO_2H standard (δ –76.53).

5.3 Peptide Syntheses

5.3.1 New spectroscopic techniques and helical peptides

2D-IR

Unlabeled aminoacid derivatives and peptides

Z-Gly-OH

To a solution of H-Gly-OH (25 g, 0.33 mol) in 180 ml H_2O, Et_3N was added (46.48 ml, 0.33 mol). To this solution was added dropwise Z-OSu (83 g, 0.33 mol) in 180 ml CH_3CN under stirring. The mixture was left stirring overnight, then the CH_3CN is removed and pH is brought to 8 with the addition of Et_3N. Unreacted Z-OSu was extracted with Et_2O. Then a solution of 10% $KHSO_4$ was added to pH 2. The aqueous phase was extracted with 3x100 mL EtOAc. The organic phase was washed with H_2O, brine, dried over Na_2SO_4 and evaporated to dryness. Yield: 92%.

mp: 120°-121°C.

Rf_1: 0.18, Rf_2: 0.75, Rf_3: 0.12.

IR (KBr): 3335, 1727, 1710, 1693, 1679, 1537 cm^{-1}.

^1H NMR ($CDCl_3$, 200 MHz): δ 7.35 (m, 5H, Z phenyl-CH), 5.26 (m, 1H, N-H Gly), 5.14 (s, 2H, Z-CH_2), 4.05 (m, 2H, α-CH Gly).

Z-Gly-O*t*Bu:

Z-Gly-OH (10.148 g, 48.5 mmol) was suspended in anhydrous CH_2Cl_2 (270 ml) in a pressure-proof bottle and the temperature was brought to -60°C with an external dry ice/acetone bath. Isobutene (70 ml) was carefully bubbled and 0.5 mL H_2SO_4 was added. The reaction mixture was allowed to warm to room temperature and left reacting for 8 days. The clear solution was then cooled to -40°C and unreacted isobutene was evaporated by allowing the reaction mixture to warm to room temperature again. Then the solution was poured in 50 mL $NaHCO_3$ 5%. Phases were separated and the aqueous phase is extracted with CH_2Cl_2. The combined organic solvent was removed under vacuum, the residue was dissolved in EtOAc, washed with $NaHCO_3$ 5%, H_2O, citric acid 0.5 M, H_2O, dried over Na_2SO_4 and the solvent removed under vacuum. Oil. Yield: 84%.

Rf_1: 0.95, Rf_2: 0.90, Rf_3: 0.85.

IR (KBr): 3380, 3359, 1724, 1523 cm^{-1}.

^1H NMR (200 MHz, $CDCl_3$): δ 7.36 (m, 5H, Z phenyl-CH), 5.32 (t, 1H, N-H Gly), 5.11 (s, 2H, Z-CH_2), 3.86 (d, 2H, α-CH Gly), 1.46 (s, 9H, CH_3-*t*Bu).

_i_PrCO-Gly-O_t_Bu

To a solution of *i*PrCOOH (238 mg, 2.7 mmol) in anhydrous CH_2Cl_2, cooled to 0°C, HOAt (367 mg, 2.7 mmol) and EDC (517 mg, 2.7 mmol) were added. After 2 min this solution was added to a solution of H-Gly-O*t*Bu (obtained by Pd-catalyzed hydrogenolysis of 480 mg, 2.1 mmol, of the corresponding Z-protected derivative) in CH_2Cl_2. To the resulting mixture DIPEA (470 µl, 2.7 mmol) was added. The mixture was stirred at room temperature for 30 hs while keeping the pH at 8 by addition of DIPEA. Then, the solvent was removed and the residue was purified by flash chromatography (eluant, EtOAc/PE 1:1). Oil.

Yield 40%.

Rf_1: 0.95, Rf_2: 0.90, Rf_3: 0.85.

IR (KBr): 3381, 1726, 1525 cm^{-1}.

^1H NMR (200 MHz, $CDCl_3$): δ 6.06 (s, 1H, N-H), 3.90 (d, 2H, α-CH Gly), 2.39 (m, 1H, *i*Pr-CH), 1.43 (s, 9H, CH_3-*t*Bu), 1.15 (d, 6H, *i*Pr-CH_3).

Z-L-Ala-OH:

To a solution of H-Ala-OH (25 g, 0.28 mol) in 180 ml H_2O, Et_3N was added (39.11 ml, 0.28 mol). To this solution was added dropwise Z-OSu (50 g, 0.25 mol) in 180 ml CH_3CN under stirring. The mixture was left stirring overnight, then the CH_3CN is removed and pH was brought to 8 with the addition of Et_3N. Unreacted Z-OSu was extracted with Et_2O. Then a solution of 10% $KHSO_4$ was added to pH 2. The aqueous phase was extracted with 3x100 mL EtOAc. The organic phase was washed with H_2O, brine, dried over Na_2SO_4 and evaporated to dryness. Yield: 89%.

mp: 84-85 °C.

Rf_1: 0.65, Rf_2: 0.95, Rf_3: 0.40.

$[\alpha]_D^{20}$ = -15.3 (c = 0.5, MeOH)

IR (KBr): 3335, 1694, 1535 cm^{-1}.

^{1}H NMR (200MHz, $CDCl_3$): 7.35 (m, 5H, Z phenyl-CH), 6.93-5.36 (2d, 1H, N-H *cis/trans*), 5.10 (m, 2H, Z-CH_2), 4.42 (m, 1H, α-CH *cis/trans*), 1.45 (d, 3H, β-CH_3).

Z-Aib-OH:

To a solution of H-Aib-OH (15 g, 0.145 mol) in 75 ml H_2O, Et_3N was added (20 ml, 0.15 mol). To this solution was added dropwise Z-OSu (36.13 g, 0.145 mol) in 40 mL CH_3CN under stirring. After 3 hs pH is adjusted at 8.5-9 with the addition of sufficient TEA. The mixture was left stirring for 3 days, then the CH_3CN was removed and pH was brought to 8 with the addition of Et_3N. Unreacted Z-OSu was extracted with Et_2O. Then a solution of 10% $KHSO_4$ was added to pH 2. The aqueous phase was extracted with 3x100 mL EtOAc. The organic phase was washed with H_2O, brine, dried over Na_2SO_4 and evaporated to dryness. Yield: 60%.

mp: 84°-85°C

Rf_1: 0.65, Rf_2: 0.90, Rf_3: 0.40.

IR (KBr): 3320, 1718, 1672, 1550 cm^{-1}.

^{1}H NMR (200 MHz, $CDCl_3$): δ 11.38 (s, 1H, COOH), 7.34 (m, 5H, Z phenyl-CH), 5.41 (s, 1H, N-H), 5.10 (s, 2H, Z-CH_2), 1.58 (s, 6H, β-CH_3 Aib).

Z-Aib-O*t*Bu

Z-Aib-OH (10.06 g, 42 mmol) was suspended in anhydrous CH_2Cl_2 (100 ml) in a pressure-proof bottle and the temperature was brought to -60°C with an external dry ice/acetone bath. Isobutene (50 ml) was carefully bubbled and 0.42 ml H_2SO_4 was added. The reaction mixture was allowed to warm to room temperature and left reacting for 8 days. The clear solution was then cooled to -40°C and unreacted isobutene was evaporated by allowing the reaction mixture to warm to room temperature again. Then the solution was poured in 50 mL $NaHCO_3$ 5%. Phases were separated and the aqueous phase was extracted with CH_2Cl_2. The combined organic solvent was removed under vacuum, the residue was dissolved in EtOAc and washed with $NaHCO_3$ 5%, H_2O, $KHSO_4$ 10%, H_2O, dried over Na_2SO_4 and the solvent removed under vacuum. Yield: 79%

mp: 63°-64°C

Rf_1: 0.95, Rf_2: 0.95, Rf_3: 0.80.

IR (KBr): 3372, 1711, 1563 cm^{-1}.

^{1}H NMR (200 MHz, $CDCl_3$): δ 7.33 (m, 5H, Z phenyl-CH), 5.42 (s, 1H, N-H uretanico), 5.06 (s, 2H, Z-CH_2), 1.50 (s, 6H, β-CH_3 Aib), 1.42 (s, 9H, CH_3-*t*Bu).

Z-L-Leu-OH:

To a solution of H-Leu-OH (25.16 g, 0.19 mol) in 200 ml NaOH/dioxane (1:1) Z-OSu (48.85 g, 0.196 mol) was slowly added. pH is regulated at ~ 8 with some drops of NaOH 1N and the reaction mixture was left strirring overnight. Dioxane was then removed under vacuum and the solution was diluted with water. Unreacted Z-OSu was extracted with Et_2O and the aqueous phase was acidified to pH ~ 2 with the addition of $KHSO_4$. The product was extracted with EtOAc, the organic phase was washed several times with water, dried over Na_2SO_4 and the solvent removed under vacuum. Oil. Yield: 96%.

Rf_1: 0.80, Rf_2: 0.95. Rf_3:0.20.

$[\alpha]_D^{20}$: -14.7 (c=0.5, MeOH).

IR (film): 3325, 1714, 1532 cm^{-1}

^{1}H NMR (200 MHz, $CDCl_3$): δ 7.34 (m, 5H, Z phenyl-CH), 6.08-5.23 (2d, 1H, *cis/trans* N-H Leu), 5.13 (s, 2H, Z-CH_2), 4.46-4.19 (m, 1H, *cis/trans* α-CH Leu), 1.83-1.47 (m, 3H, β-CH_2,γ-CH Leu), 1.00-0.80 (m, 6H, δ-CH_3 Leu).

Synthesis of Z-L-Leu-Aib-L-Ala-Gly-OtBu (unlabeled tetrapeptide)

Z-L-Ala-Gly-O*t*Bu

To a solution of Z-Ala-OH (1.62 g, 7.25 mmol) in anhydrous CH_2Cl_2, cooled to 0°C, HOBt (1.11 g, 8.7 mmol) and EDC (1.57 g, 8.7 mmol) were added. After 2 min this solution was added to a solution of H-Gly-O*t*Bu (obtained by Pd-catalyzed hydrogenolysis of 4.13 g, 31 mmol, of the corresponding Z-protected derivative) in CH_2Cl_2. To the resulting mixture DIPEA (1.14 ml, 8.7 mmoli) was added. The mixture was stirred at room temperature for 24 hs while keeping the pH at 8 by addition of DIPEA. Then, the solvent was removed and the residue dissolved in EtOAc. The solution was washed with 10% $KHSO_4$, H_2O, 5% $NaHCO_3$ and H_2O, dried over Na_2SO_4, and evaporated to dryness. Yield 88%.

mp: 47°-48°C

Rf_1: 0.78, Rf_2: 0.95, Rf_3: 0.30.

$[\alpha]_D^{20}$ = -24.8 (c = 0.5, MeOH).

IR (KBr): 3319, 1727, 1666, 1529 cm^{-1}.

^1H NMR (200 MHz, $CDCl_3$): δ 7.35 (m, 5H, Z phenyl-CH), 6.53 (s, 1H, N-H Gly), 5.37 (d, 1H, N-H Ala), 5.11 (d, 2H, Z-CH_2), 4.29 (q, 1H, α-CH Ala), 3.92 (d, 2H, α-CH Gly), 1.47 (s, 9H, CH_3-tBu), 1.40 (d, 3H, β-CH_3 Ala).

Z-Aib-L-Ala-Gly-O*t*Bu

To a solution of Z-Aib-OH (3.57 g, 15 mmol) in anhydrous CH_2Cl_2, cooled to 0°C, HOBt (2.1 g, 15 mmol) and EDC (3.61 g, 18 mmol) were added. After 2 min this solution was added to a solution of H-L-Ala-Gly-O*t*Bu (obtained by Pd-catalyzed hydrogenolysis of 2 g, 5.9 mmol, of the corresponding Z-protected derivative) in CH_2Cl_2. To the resulting mixture DIPEA (2.60 ml, 18 mmol) was added. The mixture was stirred at room temperature for 72 hs while keeping the pH at 8 by addition of DIPEA. Then, the solvent was removed and the residue dissolved in EtOAc. The solution was washed with 10% $KHSO_4$, H_2O, 5% $NaHCO_3$ and H_2O, dried over Na_2SO_4, and evaporated to dryness. The product was purified by flash chromatography (eluant, 3:1 PE/AcOEt). Yield 63%.

mp: 81°-83°C

Rf_1: 0.60, Rf_2: 0.90, Rf_3: 0.31.

$[\alpha]_D^{20}$ = -9.5, $[\alpha]_{578}^{20}$ = -10.6 (c = 0.5, MeOH).

IR (KBr): 3318, 1740, 1656, 1526 cm^{-1}.

^1H NMR (200 MHz, $CDCl_3$): δ 7.35 (m, 5H, Z phenyl-CH), 7.09 (s, 1H, N-H Gly), 6.63 (d, 1H, N-H Ala), 5.27 (s, 1H, N-H Aib), 5.08 (s, 2H, Z-CH_2), 4.53 (q, 1H, α-CH Ala), 3.79 (dd, 2H, α-CH Gly), 1.52 (2, 6H, β-CH_3 Aib), 1.45 (s, 9H, CH_3-O*t*Bu), 1.40 (d, 3H, β-CH_3 Ala).

Z-L-Leu-Aib-L-Ala-Gly-O*t*Bu

To a solution of Z-Leu-OH (1.51 g, 5.7 mmol) in anhydrous CH_2Cl_2, cooled to 0°C, HOBt (0.84 g, 6.2 mmol) and EDC (1.31 g, 6.8 mmol) were added. After 2 min this solution was added to a solution of H-Aib-L-Ala-Gly-O*t*Bu (obtained by Pd-catalyzed hydrogenolysis of 1.15 g, 4.0 mmol, of the corresponding Z-protected derivative) in CH_2Cl_2. To the resulting mixture DIPEA (0.94 ml, 6.8 mmol) was added. The mixture

was stirred at room temperature for 48 hs while keeping the pH at 8 by addition of DIPEA. Then, the solvent was removed and the residue dissolved in EtOAc. The solution was washed with 10% $KHSO_4$, H_2O, 5% $NaHCO_3$ and H_2O, dried over Na_2SO_4, and evaporated to dryness. The product was purified by flash chromatography (eluant, 1:3 PE/AcOEt). Yield 26%.

mp: 72°-74°C

Rf_1: 0.58, Rf_2: 0.95, Rf_3: 0.33.

HPLC: t_r = 20.05 min; Conditions: analytical Vydac C_{18} column (particle size: 5 μm; pore size: 300 Å); gradient system, 40→70%B in 30 min; flow rate, 1 ml/min (eluant A: H2O/acetonitrile 9/1 + 0.05% TFA; eluant B: acetonitrile/H2O 9/1 + 0.05% TFA); room temperature; absorbance detector at 226 nm.

$[\alpha]_D^{20}$ = -8.9, $[\alpha]_{578}^{20}$ = -9.0 (c = 0.5, MeOH).

IR (KBr): 3321, 1700, 1659, 1529 cm^{-1}.

^{1}H NMR (200 MHz, $CDCl_3$): δ 7.35 (m, 5H, Z phenyl-CH), 7.22 (m, 1H, N-H Gly), 7.03 (d, 1H, N-H Ala), 6.52 (s, 1H, N-H Aib), 5.28 (s, 1H, N-H Leu), 5.12 (dd, 2H, Z-CH_2), 4.45 (q, 1H, α-CH Ala), 4.01 (d, 2H, α-CH Gly), 3.74 (dd, 1H, α-CH Leu), 1.8-1.6 (m, 3H, γ-CH, β-CH_2 Leu), 1.51 (s, 6H, β-CH_3 Aib), 1.44 (s, 9H, CH_3-O*t*Bu), 1.40 (s, 3H, β-CH_3 Ala), 0.94 (m, 3H, δ-CH_3 Leu).

Synthesis of Z-Aib-L-Leu-Aib-Aib-Gly-Aib-OtBu (unlabeled hexapeptide)

Z-Gly-Aib-O*t*Bu

To a solution of Z-Gly-OH (2.45 g, 11.7 mmol) in anhydrous CH_2Cl_2, cooled to 0°C, HOBt (1.89 g, 14 mmol) and EDC (2.69 g, 14 mmol) were added. After 2 min this solution was added to a solution of H-Aib-O*t*Bu (obtained by Pd-catalyzed hydrogenolysis of 9.58 g, 33 mmol, of the corresponding Z-protected derivative) in CH_2Cl_2. To the resulting mixture DIPEA (1.94 ml, 14 mmol) was added. The mixture was stirred at room temperature for 24 hs while keeping the pH at 8 by addition of DIPEA. Then, the solvent was removed and the residue dissolved in EtOAc. The solution was washed with 10% $KHSO_4$, H_2O, 5% $NaHCO_3$ and H_2O, dried over Na_2SO_4, and evaporated to dryness. The product was crystallized from AcOEt/PE. Yield 54%.

mp: 90°-92°C

Rf_1: 0.72, Rf_2: 0.95, Rf_3: 0.40.

IR (KBr): 3354, 3344, 3280, 1732, 1710, 1667, 1535 cm^{-1}.

^1H NMR (200 MHz, $CDCl_3$): δ 7.36 (m, 5H, Z phenyl-CH), 6.61 (s, 1H, N-H Aib), 5.35 (s, 1H, N-H Gly), 5.14 (s, 2H, Z-CH_2), 3.83 (d, 2H, α-CH Gly), 1.54 (s, 6H, β-CH_3 Aib), 1.46 (s, 9H, CH_3-*t*Bu).

Z-Aib-Aib-O*t*Bu

To a solution of Z-Aib-OH (5.22 g, 22 mmol) in anhydrous CH_2Cl_2, cooled to 0°C, HOBt (3.59, 26 mmol) and EDC (5.06 g, 26 mmol) were added. After 2 min this solution was added to a solution of H-Aib-O*t*Bu (obtained previously from 5.43 g, 22 mmol of the corresponding Z-protected derivative) in CH_2Cl_2. To the resulting mixture DIPEA (3.67 ml, 26 mmol) was added. The mixture was stirred at room temperature for 96 hs while keeping the pH at 8 by addition of DIPEA. Then, the solvent was removed and the residue dissolved in EtOAc. The solution was washed with 10% $KHSO_4$, H_2O, 5% $NaHCO_3$ and H_2O, dried over Na_2SO_4, and evaporated to dryness. The product was crystallized from AcOEt/PE. Yield 46%.

mp: 136°-137°C

Rf_1: 0.81, Rf_2: 0.95, Rf_3: 0.44.

IR (KBr): 3293, 1719, 1657, 1536, 1516 cm^{-1}.

^1H NMR (200 MHz, $CDCl_3$): δ 7.35 (m, 5H, Z phenyl-CH), 6.91 (s, 1H, N-H Aib), 5.36 (s, 1H, N-H Aib), 5.09 (s, 2H, Z-CH_2), 1.53 (s, 6H, β-CH_3 Aib), 1.51 (s, 6H, β-CH_3 Aib), 1.43 (s, 9H, CH_3-*t*Bu).

Z-Aib-Aib-OH

Previously synthesized Z-Aib-Aib-O*t*Bu (1.7 g, 4.5 mmol) was dissolved in anhydrous CH_2Cl_2 (10 ml) and TFA (5 ml) was added. After stirring for 2 hs, the volatiles were removed under vacuum. To the residue Et_2O (10 ml) was added and removed under vacuum. This operation was repeated until a white solid was obtained. Yield: 99%

mp: 161°-162°C

Rf_1: 0.25.

IR (KBr): 3297, 1726, 1705, 1679, 1660, 1527 cm^{-1}.

^{1}H NMR (200 MHz, $CDCl_3$): δ 7.37 (m, 5H, Z phenyl-CH), 7.10 (s, 1H, N-H Aib), 5.56 (s, 1H, N-H Aib), 5.15 (s, 2H, Z-CH_2), 1.59 (s, 6H, β-CH_3 Aib), 1.57 (s, 6H, β-CH_3 Aib).

Z-Aib-Aib-Gly-Aib-O*t*Bu

To a solution of Z-Aib-Aib-OH (1 g, 3.1 mmol) in CH_2Cl_2, cooled at 0 °C, EDC (0.65 g, 3.4) was added. After 3 h the corresponding 5(4*H*)-oxazolone was formed. Then, the solvent was removed and the residue dissolved in EtOAc. The organic solution was quickly washed with 10% $KHSO_4$, H_2O, 5% $NaHCO_3$ and H_2O, dried over Na_2SO_4, and evaporated to dryness. The residue was dissolved in anhydrous CH_3CN and H-Gly-Aib-O*t*Bu (obtained by Pd-catalyzed hydrogenolysis of 1.66 g, 4.7 mmol, of the corresponding Z-protected derivative) in CH_3CN was added and the mixture stirred at 70°C for 24 hs. Then, the solvent was removed and the residue dissolved in EtOAc. The solution was washed with 10% $KHSO_4$, H_2O, 5% $NaHCO_3$ and H_2O, dried over Na_2SO_4, and evaporated to dryness. The product was crystallized from AcOEt/PE. Yield: 74%.

mp: 148°-151°C

Rf_1: 0.48, Rf_2: 0.90, Rf_3: 0.23.

IR (KBr): 3323, 1734, 1700, 1660, 1530 cm^{-1}.

^{1}H NMR (200 MHz, $CDCl_3$): δ 7.57 (m, 1H, N-H Gly), 7.34 (m, 5H, Z phenyl-CH), 7.17 (s, 1H, N-H Aib), 6.31 (s, 1H, N-H Aib), 5.21 (s, 1H, N-H Aib), 5.08 (s, 2H, Z-CH_2), 3.86 (d, 2H, α-CH Gly), 1.49 (s, 6H, β-CH_3 Aib), 1.48 (s, 6H, β-CH_3 Aib), 1.44 (s, 9H, CH_3-*t*Bu), 1.22 (s, 6H, β-CH_3 Aib).

Z-L-Leu-Aib-Aib-Gly-Aib-O*t*Bu

To a solution of Z-Leu-OH (147 mg, 0.55 mmol) in anhydrous CH_2Cl_2, cooled to 0°C, HOAt (89 mg, 6.5 mmol) and EDC (84 mg, 6.5 mmol) were added. After 2 min this solution was added to a solution of H-Aib-Aib-Gly-Aib-O*t*Bu (obtained by Pd-catalyzed hydrogenolysis of 150 mg, 0.3 mmol, of the corresponding Z-protected derivative) in CH_2Cl_2. To the resulting mixture DIPEA (60 µl, 0.6 mmol) was added. The mixture was stirred at room temperature for 72 hs while keeping the pH at 8 by addition of DIPEA. Then, the solvent was removed and the residue dissolved in EtOAc. The solution was washed with 10% $KHSO_4$, H_2O, 5% $NaHCO_3$ and H_2O, dried over

Na_2SO_4, and evaporated to dryness. The product was crystallized from AcOEt/PE. Yield 59%.

mp: 170°-175°C

Rf_1: 0.50, Rf_2: 0.95, Rf_3: 0.27.

HPLC: t_r = 25.13 min; Conditions: analytical Vydac C_{18} column (particle size: 5 μm; pore size: 300 Å); gradient system, 50→70%B in 30 min; flow rate, 1 ml/min (eluant A: H2O/acetonitrile 9/1 + 0.05% TFA; eluant B: acetonitrile/H2O 9/1 + 0.05% TFA); room temperature; absorbance detector at 226 nm.

$[\alpha]_D^{20}$ = -36.5, $[\alpha]_{578}^{20}$ = -36.5 (c = 0.5, MeOH).

IR (KBr): 3331, 1733, 1706, 1653, 1533 cm^{-1}.

^1H NMR (200 MHz, $CDCl_3$): δ 7.66 (m, 1H, N-H Gly), 7.33 (m, 5H, Z phenyl-CH), 7.23 (s, 1H, N-H Aib), 6.80 (s, 1H, N-H Aib), 6.58 (s, 1H, N-H Aib), 5.61 (m, 1H, N-H Leu), 5.09 (s, 2H, Z-CH_2), 3.89 (m, 2H, α-CH Leu), 3.78 (m, 1H, α-CH Gly), 1.65 (m, 2H, β-CH_3 Leu), 1.47-1.38 (m, 19H, β-CH_3 Aib + γ-CH Leu), 1.42 (s, 9H, CH_3-*t*Bu), 1.22 (m, 6H, δ-CH_3 Leu).

Z-Aib-L-Leu-Aib-Aib-Gly-Aib-O*t*Bu

To a solution of Z-Aib-OH (36 mg, 0.15 mmol) in anhydrous CH_2Cl_2, cooled to 0°C, HOAt (24 mg, 0.18 mmol) and EDC (34 mg, 0.18 mmol) were added. After 2 min this solution was added to a solution of H-L-Leu-Aib-Aib-Gly-Aib-O*t*Bu (obtained by Pd-catalyzed hydrogenolysis of 70 mg, 0.11 mmol, of the corresponding Z-protected derivative) in CH_2Cl_2. To the resulting mixture DIPEA (25 μl, 0.18 mmol) was added. The mixture was stirred at room temperature for 72 hs while keeping the pH at 8 by addition of DIPEA. Then, the solvent was removed and the residue dissolved in EtOAc. The solution was washed with 10% $KHSO_4$, H_2O, 5% $NaHCO_3$ and H_2O, dried over Na_2SO_4, and evaporated to dryness. The product was purified by flash chromatography (eluant, $CHCl_3$/EtOH 98:2→95:5). Yield 43%.

mp: 210°-212°C

Rf_1: 0.60, Rf_2: 0.95, Rf_3: 0.27.

$[\alpha]_D^{20}$ = -13.2, $[\alpha]_{578}^{20}$ = - 14.3 (c = 0.5, MeOH).

IR (KBr): 3315, 1703, 1664, 1527 cm^{-1}.

^{1}H NMR (200 MHz, $CDCl_3$): δ 7.78 (t, 1H, N-H Gly), 7.57 (s, 1H, N-H Aib), 7.47 (s, 1H, N-H Aib), 7.37 (m, 5H, Z phenyl-CH), 7.13 (s, 1H, N-H Aib), 6.45 (m, 1H, N-H Aib), 5.27 (d, 1H, N-H Leu), 5.12 (q, 2H, Z-CH_2), 3.92 (m, 2H, α-CH Leu), 3.89 (m, 1H, α-CH Gly), 1.55 (m, 2H, β-CH_3 Leu), 1.52-1.30 (m, 34H, β-CH_3 Aib + γ-CH Leu + CH_3-*t*Bu), 0.88 (m, 6H, δ-CH_3 Leu).

Synthesis of Z-L-Leu-Aib-Aib-Gly-Aib-Aib-Aib-Aib-Otbu (unlabeled octapeptide)

Z-Aib-Aib-Aib-O*t*Bu

To a solution of Z-Aib-OH (863 mg, 3.1 mmol) in anhydrous CH_2Cl_2, cooled to 0°C, HOAt (505 mg, 3.7 mmol) and EDC (713 mg, 3.7 mmol) were added. After 2 min this solution was added to a solution of H-Aib-Aib-O*t*Bu (obtained by Pd-catalyzed hydrogenolysis of 650 mg, 2.6 mmol, of the corresponding Z-protected derivative) in CH_2Cl_2. To the resulting mixture TEA (0.52 ml, 3.7 mmol) was added. The mixture was stirred at room temperature for 96 hs while keeping the pH at 8 by addition of TEA. Then, the solvent was removed and the residue dissolved in EtOAc. The solution was washed with 10% $KHSO_4$, H_2O, 5% $NaHCO_3$ and H_2O, dried over Na_2SO_4, and evaporated to dryness. The product was crystallized from AcOEt/PE. Yield 89%.

mp: 163°-165°C

Rf_1: 0.68, Rf_2: 0.90, Rf_3: 0.31.

IR (KBr): 3329, 1724, 1697, 1668, 1653, 1532 cm^{-1}.

^{1}H NMR (200 MHz, $CDCl_3$): δ 7.36 (m, 5H, Z phenyl-CH), 7.07 (s, 1H, N-H Aib), 6.51 (s, 1H, N-H Aib), 5.18 (s, 1H, N-H Aib), 5.10 (s, 2H, Z-CH_2), 1.49-1.45 (s, 18H, β-CH_3 Aib), 1.46 (s, 9H, CH_3-*t*Bu).

Z-Aib-Aib-Gly-Aib-Aib-Aib-Aib-O*t*Bu

Z-Aib-Aib-Gly-Aib-O*t*Bu (700 mg, 1.3 mmol) was dissolved in anhydrous CH_2Cl_2 (10 ml) and TFA (1 ml) was added. After stirring for 2 hs, the volatiles were removed under vacuum. To the residue Et_2O (10 ml) was added and removed under vacuum. This operation was repeated until a white solid was obtained. The residue (600 mg, 1.3 mmol) was dissolved in CH_2Cl_2, cooled at 0 °C and EDC (0.65 g, 3.4) was added. After 3 h the corresponding 5(4*H*)-oxazolone was formed. Then, the solvent was removed and the residue dissolved in EtOAc. The organic solution was quickly washed with 10%

$KHSO_4$, H_2O, 5% $NaHCO_3$ and H_2O, dried over Na_2SO_4, and evaporated to dryness. The residue was dissolved in anhydrous CH_3CN and H-Aib-Aib-Aib-O*t*Bu (360 mg, 1.1) in CH_3CN was added and the mixture stirred at 90°C for 48 hs. Then, the solvent was removed and the residue dissolved in EtOAc. The solution was washed with 10% $KHSO_4$, H_2O, 5% $NaHCO_3$ and H_2O, dried over Na_2SO_4, and evaporated to dryness. The product was purified by flash chromatography (eluant, AcOEt→AcOEt/PE 19:1). Yield: 24%.

punto di fusione: 99°-103°C

Rf_1: 0.45, Rf_2: 0.90, Rf_3: 0.15.

IR (KBr): 3328, 1732, 1664, 1531 cm^{-1}.

^1H NMR (200 MHz, $CDCl_3$): δ 7.78 (t, 1H, N-H Gly), 7.52, 7.40, 7.18, 7.13, 6.37, 5.51 (s, 6H, N-H Aib), 7.35 (m, 5H, Z phenyl-CH), 5.10 (s, 2H, Z-CH_2), 3.73 (d, 2H, α-CH Gly), 1.51-1.37 (s-m, 45H, β-CH_3 Aib + CH_3-*t*Bu).

Z-L-Leu-Aib-Aib-Gly-Aib-Aib-Aib-Aib-O*t*Bu

To a solution of Z-Leu-OH (0.12 g, 0.44 mmol) in anhydrous CH_2Cl_2, cooled to 0°C, HOAt (0.065 g, 0.48 mmol) and EDC (0.093 g, 0.48 mmol) were added. After 2 min this solution was added to a solution of H-Aib-Aib-Gly-Aib-Aib-Aib-Aib-O*t*Bu (obtained by Pd-catalyzed hydrogenolysis of 190 mg, 0.22 mmol, of the corresponding Z-protected derivative) in CH_2Cl_2. To the resulting mixture DIPEA (67 µl, 0.48 mmol) was added. The mixture was stirred at room temperature for 24 hs while keeping the pH at 8 by addition of DIPEA. Then, the solvent was removed and the residue dissolved in EtOAc. The solution was washed with 10% $KHSO_4$, H_2O, 5% $NaHCO_3$ and H_2O, dried over Na_2SO_4, and evaporated to dryness. The product was crystallized from AcOEt/PE. Yield 56%.

mp: 197°-202°C

Rf_1: 0.52, Rf_2: 0.90, Rf_3: 0.21.

HPLC: t_r = 27.74 min; Conditions: analytical Vydac C_{18} column (particle size: 5 µm; pore size: 300 Å); gradient system, 50→70%B in 30 min; flow rate, 1 ml/min (eluant A: H2O/acetonitrile 9/1 + 0.05% TFA; eluant B: acetonitrile/H2O 9/1 + 0.05% TFA); room temperature; absorbance detector at 226 nm.

$[\alpha]_D^{20}$ = -17.3, $[\alpha]_{578}^{20}$ = - 17.7 (c = 0.5, MeOH).

IR (KBr): 3328, 1732, 1664, 1531 cm^{-1}.

^{1}H NMR (200 MHz, DMSO-d_6): δ 8.67 (s, 1H, N-H Aib), 7.98, 7.92, 7.58, 7.57, 7.55, 7.41, 7.33, 7.26 (s, 8H, N-H Aib + Leu + Gly), 7.34 (m, 1H, Z phenyl-CH), 5.02 (d, 2H, Z-CH_2), 4.04 (m, 2H, α-CH Gly), 3.60 (m, 1H, α-CH Leu), 1.44-1.31 (m, 47H, β-CH_3 Aib + β-CH_3 Leu + γ-CH Leu + CH_3-*t*Bu), 0.86 (d, 6H, δ-CH_3 Leu).

Labeled aminoacid derivatives and peptides

Z-(^{15}N)Gly-OH

The same procedure reported for the synthesis of Z-Gly-OH was followed for the synthesis of this compound.

Yield: 96%

punto di fusione: 119°-120°C

Rf_1: 0.18, Rf_2: 0.75, Rf_3: 0.12.

IR (KBr): 3322, 3030, 2938, 2648, 1727, 1710, 1691, 1677, 1520 cm^{-1}.

^{1}H NMR (200 MHz, $CDCl_3$): δ 7.35 (m, 5H, Z phenyl-CH), 5.27 (dt, 1H, ^{15}N-^{1}H), 5.14 (s, 2H, Z-CH_2), 4.04 (d, 2H, α-CH Gly).

Z-(^{15}N)Gly-O*t*Bu

To a solution of Z-(^{15}N)-Gly-OH (1 g, 4.7 mmol), DMAP (0.64 g, 5.2 mmol), anhydrous *t*BuOH (0.89 ml, 9.4 mmoli) and EDC (1.08 g, 5.6 mmoli) were added. The solution is left stirring for 24 hs, then the solvent is removed under vacuum. AcOEt is added to the residue, then the organic phase is washed with $KHSO_4$ 10%, $NaHCO_3$ 5%, brine, dried over Na_2SO_4 and the solvent evaporated. The product was purified by flash chromatography (eluant, $CHCl_3$/EtOH 9:1). Oil.

Yield: 32%.

Rf_1: 0.95, Rf_2: 0.90, Rf_3: 0.85.

IR (KBr): 3347, 1724, 1498, 1454 cm^{-1}.

^{1}H NMR (200 MHz, $CDCl_3$): δ 7.35 (m, 5H, Z phenyl-CH), 5.35 (dt, 1H, ^{15}N-^{1}H), 5.11 (s, 2H, Z-CH_2), 3.85 (d, 2H, α-CH Gly), 1.45 (s, 9H, CH_3-tBu).

***i*PrCO-(^{15}N)Gly-O*t*Bu**

To a solution of *i*PrCOOH (238 mg, 2.7 mmol) in anhydrous CH_2Cl_2, cooled to 0°C, HOAt (367 mg, 2.7 mmol) and EDC (517 mg, 2.7 mmol) were added. After 2 min this

solution was added to a solution of H-(^{15}N)Gly-O*t*Bu (obtained by Pd-catalyzed hydrogenolysis of 480 mg, 2.1 mmol, of the corresponding Z-protected derivative) in CH_2Cl_2. To the resulting mixture DIPEA (470 µl, 2.7 mmol) was added. The mixture was stirred at room temperature for 30 hs while keeping the pH at 8 by addition of DIPEA. Then, the solvent was removed and the residue was pruified by flash chromatography (eluant, AcOEt/PE 1:1). Oil.

Yield 40%.

Rf_1: 0.95, Rf_2: 0.90, Rf_3: 0.85.

IR (KBr): 3345, 1727, 1499, 1455 cm^{-1}.

^{1}H NMR (200 MHz, $CDCl_3$): δ 6.06 (dt, 1H, ^{15}N-^{1}H), 3.90 (d, 2H, α-CH Gly), 2.39 (m, 1H, *i*Pr-CH), 1.43 (s, 9H, CH_3-*t*Bu), 1.15 (d, 6H, *i*Pr-CH_3).

H-L-(1-^{13}C,^{18}O)Leu-^{18}OH

H-(1-^{13}C)-L-Leu-OH (500 mg, 3.8 mmol) was added to a large excess of 97% $H_2{}^{18}O$ (8 g, 400 mmol) at 0 °C under N_2 flux. Anhydrous HCl was bubbled slowly into the suspension to achieve solubilization of the amino acid. The temperature of the solution was kept at 60 °C for 4 days. The solution was brought to room temperature, the excess $H_2{}^{18}O$ was recovered by distillation, and the remaining wet solid was dried over P_2O_5 in vacuo.

Mass spectrometry (ESI) shows that 85% of the 1-^{13}C L-Leu molecules are doubly ^{18}O labeled (M_1), while 15% of them are singly labeled (M_2): $[M_1+H]^+_{calc}$ = 137.1; $[M_1+H]^+_{exp}$ = 137.0; $[M_2+H]^+_{calc}$ = 135.1; $[M_2+H]^+_{exp}$ = 135.1.

4) **Z-L-(1-^{13}C,^{18}O)Leu-^{18}OH**

The same procedure reported for the synthesis of Z-Leu-OH was followed for the synthesis of this compound. Oil.

Yield: 95%

Rf_1: 0.80, Rf_2: 0.95. Rf_3:0.20.

ESI-MS: calcd: 271.23; found: 271.19 $[M+H]^+$.

$[\alpha]_D^{20}$: -14.7 (c=0.5, MeOH).

IR (KBr): 3318, 1696, 1529 cm^{-1}.

^{1}H NMR (250 MHz, $CDCl_3$): δ 8.04 (s, 1H, $C^{18}O_2H$), 7.35 (m, 5H, Z phenyl-CH), 5.16 (s, 1H, N-H), 5.12 (s, 2H, Z-CH_2), 4.41 (m, 1H, α-CH Leu), 1.72-1.58 (m, 3H, β-CH_2 Leu + γ-CH Leu), 0.96 (m, 6H, δ-CH_3 Leu).

Synthesis of Z-L-(^{13}C,^{18}O)Leu-Aib-L-Ala-(^{15}N)Gly-OtBu (double-labeled tetrapeptide)

Z-L-Ala-(^{15}N)Gly-O*t*Bu

To a solution of Z-L-Ala-OH (0.58 g, 2.6 mmol) in anhydrous CH_2Cl_2, cooled to 0°C, HOAt (0.389 g, 2.8 mmol) and EDC (0.548 g, 2.8 mmol) were added. After 2 min this solution was added to a solution of H-(^{15}N)Gly-O*t*Bu (obtained by Pd-catalyzed hydrogenolysis of 0.39 g, 1.8 mmol, of the corresponding Z-protected derivative) in CH_2Cl_2. To the resulting mixture DIPEA (0.400 mL, 2.8 mmol) was added. The mixture was stirred at room temperature for 24 hs while keeping the pH at 8 by addition of DIPEA. Then, the solvent was removed and the residue dissolved in EtOAc. The solution was washed with 10% $KHSO_4$, H_2O, 5% $NaHCO_3$ and H_2O, dried over Na_2SO_4, and evaporated to dryness. Yield 68%.

mp: 46°-47°C

Rf_1: 0.78, Rf_2: 0.95, Rf_3: 0.30.

$[\alpha]_D^{20}$ = -24.8 (c = 0.5, MeOH).

IR (KBr): 3318, 1725, 1671, 1523, 1454 cm^{-1}.

^{1}H NMR (400 MHz, $CDCl_3$): δ 7.35 (m, 5H, Z phenyl-CH), 6.52 (dt, 1H, ^{15}N-^{1}H), 5.36 (s, 1H, N-H Aib), 5.11 (d, 2H, Z-CH_2), 4.29 (quint., 1H, α-CH Ala), 3.91 (d, 2H, α-CH Gly), 1.46 (s, 9H, CH_3-tBu), 1.40 (d, 3H, β-CH_3 Ala).

Z-Aib-L-Ala-(^{15}N)Gly-O*t*Bu

To a solution of Z-Aib-OH (0.355 g, 1.5 mmol) in anhydrous CH_2Cl_2, cooled to 0°C, HOAt (0.204, 1.5 mmol) and EDC (0.287 g, 1.5 mmol) were added. After 2 min this solution was added to a solution of H-L-Ala-(^{15}N)Gly-O*t*Bu (obtained by Pd-catalyzed hydrogenolysis of 0.250 g, 0.7 mmol, of the corresponding Z-protected derivative) in CH_2Cl_2. To the resulting mixture DIPEA (208 μL, 1.5 mmol) was added. The mixture was stirred at room temperature for 48 hs while keeping the pH at 8 by addition of DIPEA. Then, the solvent was removed and the residue dissolved in EtOAc. The solution was washed with 10% $KHSO_4$, H_2O, 5% $NaHCO_3$ and H_2O, dried over

Na_2SO_4, and evaporated to dryness. The product was purified by flash chromatography (eluant, AcOEt/PE 2:1). Oil. Yield 85%

Rf_1: 0.60, Rf_2: 0.90, Rf_3: 0.31.

mp: 81°-83°C

$[\alpha]_D^{20}$= -9.5, $[\alpha]_{578}^{20}$= -10.6 (c = 0.5, MeOH).

IR (KBr): 3310, 1740, 1702, 1656, 1528 cm^{-1}.

^1H NMR (250 MHz, $CDCl_3$): δ 7.36 (m, 5H, Z phenyl-CH), 7.08 (dt, 1H, ^{15}N-^1H), 6.61 (d, 1H, N-H Ala), 5.19 (s, 1H, N-H Aib), 5.08 (s, 2H, Z-CH_2), 4.51 (m, 1H, α-CH Ala), 3.73 (dd, 2H, α-CH Gly), 1.52 (d, 6H, β-CH_3 Aib), 1.45 (s, 9H, CH_3-tBu), 1.40 (d, 3H, β-CH_3 Ala).

Z-L -(1-^{13}C,^{18}O)Leu-Aib-L-Ala-(^{15}N)Gly-O*t*Bu

To a solution of Z-L-(1-^{13}C,^{18}O)Leu-^{18}OH (84 mg, 0.31 mmol) in anhydrous CH_2Cl_2, cooled to 0°C, HOAt (42 mg, 0.31 mmol) and EDC (59 mg, 0.31 mmol) were added. After 2 min this solution was added to a solution of H-Aib-L-Ala-(^{15}N)Gly-O*t*Bu (obtained by Pd-catalyzed hydrogenolysis of 0.250 g, 0.7 mmol, of the corresponding Z-protected derivative) in CH_2Cl_2. To the resulting mixture DIPEA (43 μL, 0.31 mmol) was added. The mixture was stirred at room temperature for 72 hs while keeping the pH at 8 by addition of DIPEA. Then, the solvent was removed and the residue dissolved in EtOAc. The solution was washed with 10% $KHSO_4$, H_2O, 5% $NaHCO_3$ and H_2O, dried over Na_2SO_4, and evaporated to dryness. The product was purified by flash chromatography (eluant, $CHCl_3$/EtOH 9:1).

Yield: 46%

mp: 72°-74°C

Rf_1: 0.58, Rf_2: 0.95, Rf_3: 0.33.

ESI-MS: calcd: 539.66; found: 539.6046 $[M+H]^+$

$[\alpha]_D^{20}$= -8.9, $[\alpha]_{578}^{20}$= -9.0 (c = 0.5, MeOH).

IR (KBr): 3416, 3324, 3229, 1736, 1706, 1680, 1644, 1543, 1531 cm^{-1}.

^1H NMR (200 MHz, $CDCl_3$): δ 7.35 (m, 5H, Z phenyl-CH), 7.21 (dt, 1H, ^{15}N-^1H Gly), 7.03 (d, 1H, N-H Ala), 6.52 (s, 1H, N-H Aib), 5.28 (s, 1H, N-H Leu), 5.12 (dd, 2H, Z-CH_2), 4.45 (q, 1H, α-CH Ala), 4.01 (d, 2H, α-CH Gly), 3.74 (m, 1H, α-CH Leu), 1.8-

1.6 (m, 3H, γ-CH, β-CH_2 Leu), 1.51 (s, 6H, β-CH_3 Aib), 1.44 (s, 9H, CH_3-O*t*Bu), 1.40 (s, 3H, β-CH_3 Ala), 0.94 (m, 3H, δ-CH_3 Leu).

Synthesis of Z-Aib-L-(1-^{13}C,^{18}O)Leu-Aib-Aib-Gly-Aib-OtBu (labeled hexapeptide)

Z-L-(1-^{13}C,^{18}O)Leu-Aib-Aib-Gly-Aib-O*t*Bu

To a solution of Z-L-(1-^{13}C,^{18}O)Leu-^{18}OH (116 mg, 0.43 mmol) in anhydrous CH_2Cl_2, cooled to 0°C, HOAt (58 mg, 0.43 mmol) and EDC (83 mg, 0.43 mmol) were added. After 2 min this solution was added to a solution of H-Aib-Aib-Gly-Aib-O*t*Bu (obtained by Pd-catalyzed hydrogenolysis of 0.250 g, 0.7 mmol, of the corresponding Z-protected derivative) in CH_2Cl_2. To the resulting mixture DIPEA (59 μL, 0.43 mmol) was added. The mixture was stirred at room temperature for 72 hs while keeping the pH at 8 by addition of DIPEA. Then, the solvent was removed and the residue dissolved in EtOAc. The solution was washed with 10% $KHSO_4$, H_2O, 5% $NaHCO_3$ and H_2O, dried over Na_2SO_4, and evaporated to dryness. The product was purified by flash chromatography (eluant, $CHCl_3$/EtOH 9:1).

Yield: 32%.

Rf_1: 0.50, Rf_2: 0.90, Rf_3: 0.27.

mp: 170°-175°C

$[\alpha]_D^{20}$ = -36.5, $[\alpha]_{578}^{20}$ = -36.5 (c = 0.5, MeOH).

IR (KBr): 3416, 3333, 1704, 1679, 1645, 1533 cm^{-1}.

^{1}H NMR (200 MHz, $CDCl_3$): δ 7.67 (m, 1H, N-H Gly), 7.33 (m, 5H, Z phenyl-CH), 7.23 (s, 1H, N-H Aib), 6.80 (s, 1H, N-H Aib), 6.58 (s, 1H, N-H Aib), 5.61 (m, 1H, N-H Leu), 5.09 (d, 2H, Z-CH_2), 3.90 (m, 1H, α-CH Leu), 3.81 (m, 2H, α-CH Gly), 1.65 (m, 2H, β-CH_2 Leu), 1.48-1.39 (m, 19H, β-CH_3 Aib + γ-CH Leu), 1.42 (s, 9H, CH_3-*t*Bu), 1.22 (m, 6H, δ-CH_3 Leu).

Z-Aib-L-(1-^{13}C,^{18}O)Leu-Aib-Aib-Gly-Aib-O*t*Bu

To a solution of Z-Aib-OH (28 mg, 0.12 mmol) in anhydrous CH_2Cl_2, cooled to 0°C, HOAt (16 mg, 0.012 mmol) and EDC (23 mg, 0.012 mmol) were added. After 2 min this solution was added to a solution of H-L-(1-^{13}C,^{18}O)Leu-Aib-Aib-Gly-Aib-O*t*Bu (obtained by Pd-catalyzed hydrogenolysis of 65 mg, 0.010 mmol, of the corresponding Z-protected derivative) in CH_2Cl_2. To the resulting mixture DIPEA (16 μL, 0.012

mmol) was added. The mixture was stirred at room temperature for 72 hs while keeping the pH at 8 by addition of DIPEA. Then, the solvent was removed and the residue dissolved in EtOAc. The solution was washed with 10% $KHSO_4$, H_2O, 5% $NaHCO_3$ and H_2O, dried over Na_2SO_4, and evaporated to dryness.

Yield: 35%

mp: 72°-74°C

Rf_1: 0.58, Rf_2: 0.95, Rf_3: 0.33.

ESI-MS: calcd: 722.91; found: 722.8153 $[M+H]^+$

$[\alpha]_D^{20}$ = -13.2, $[\alpha]_{578}^{20}$ = - 14.3 (c = 0.5, MeOH).

IR (KBr): 3317, 1733, 1704, 1662, 1528 cm^{-1}.

^1H NMR (200 MHz, $CDCl_3$): δ 7.79 (t, 1H, N-H Gly), 7.51 (s, 1H, N-H Aib), 7.42 (s, 1H, N-H Aib), 7.36 (m, 5H, Z phenyl-CH), 7.16 (s, 1H, N-H Aib), 6.64 (s, 1H, N-H Aib), 5.85 (dd, 1H, N-H Leu), 5.10 (q, 2H, Z-CH_2), 3.92 (m, 1H, α-CH Leu), 3.89 (dq, 2H, α-CH Gly), 1.55 (m, 2H, β-CH_2 Leu), 1.52-1.30 (m, 34H, β-CH_3 Aib + γ-CH Leu + CH_3-*t*Bu), 0.89 (m, 6H, δ-CH_3 Leu).

Synthesis of Z-Aib-L-(1-^{13}C,^{18}O)Leu-Aib-Aib-(^{15}N)Gly-Aib-OtBu (double-labeled hexa-peptide)

Z-(^{15}N)Gly-Aib-O*t*Bu

To a solution of Z-(^{15}N)Gly-OH (0.115 g, 0.55 mmol) in anhydrous CH_2Cl_2, cooled to 0°C, HOAt (75 mg, 0.55 mmol) and EDC (105 mg, 0.55 mmol) were added. After 2 min this solution was added to a solution of H-Aib-O*t*Bu (obtained by Pd-catalyzed hydrogenolysis of 140 mg, 0.48 mmol, of the corresponding Z-protected derivative) in CH_2Cl_2. To the resulting mixture DIPEA (76 µL, 0.55 mmol) was added. The mixture was stirred at room temperature for 24 hs while keeping the pH at 8 by addition of DIPEA. Then, the solvent was removed and the residue dissolved in EtOAc. The solution was washed with 10% $KHSO_4$, H_2O, 5% $NaHCO_3$ and H_2O, dried over Na_2SO_4, and evaporated to dryness. The product was crystallized from AcOEt/PE.

Yield: 80%

mp: 96°-99°C

Rf_1: 0.72, Rf_2: 0.95, Rf_3: 0.40.

IR (KBr): 3416, 3354, 3344, 3271, 1731, 1709, 1667, 1533 cm^{-1}.

^{1}H NMR (400 MHz, $CDCl_3$): δ 7.36 (m, 5H, Z phenyl-CH), 6.59 (s, 1H, N-H Aib), 5.36 (dt, 1H, ^{15}N-^{1}H Gly), 5.14 (s, 2H, Z-CH_2), 3.83 (d, 2H, α-CH Gly), 1.54 (s, 6H, β-CG_3 Aib), 1.46 (s, 9H, CH_3-*t*Bu).

Z-Aib-Aib-(^{15}N)Gly-Aib-O*t*Bu

To a solution of Z-Aib-Aib-OH (66 mg, 0.205 mmol) in anhydrous CH_2Cl_2, cooled to 0°C, HOAt (28 mg, 0.205 mmol) and EDC (39 mg, 0.205 mmol) were added. After 2 min this solution was added to a solution of H-(^{15}N)Gly-Aib-O*t*Bu (obtained by Pd-catalyzed hydrogenolysis of 60 mg, 0.17 mmol, of the corresponding Z-protected derivative) in CH_2Cl_2. To the resulting mixture DIPEA (28 μL, 0.205 mmol) was added. The mixture was stirred at room temperature for 24 hs while keeping the pH at 8 by addition of DIPEA. Then, the solvent was removed and the residue dissolved in EtOAc. The solution was washed with 10% $KHSO_4$, H_2O, 5% $NaHCO_3$ and H_2O, dried over Na_2SO_4, and evaporated to dryness. The product was crystallized from AcOEt/PE.

Yield: 55%

mp: 145°-148°C

Rf_1: 0.48, Rf_2: 0.90, Rf_3: 0.23.

IR (KBr): 3320, 1735, 1699, 1659, 1538, 1527 cm^{-1}.

^{1}H NMR (400 MHz, $CDCl_3$): δ 7.51 (dt, 1H, ^{15}N-^{1}H Gly), 7.34 (m, 5H, Z phenyl-CH), 7.14 (s, 1H, N-H Aib), 6.30 (s, 1H, N-H Aib), 5.13 (s, 1H, N-H Aib), 5.09 (s, 2H, Z-CH_2), 3.85 (d, 2H, α-CH Gly), 1.49 (s, 6H, β-CH_3 Aib), 1.47 (s, 6H, β-CH_3 Aib), 1.45 (s, 9H, CH_3-*t*Bu), 1.40 (s, 6H, β-CH_3 Aib).

Z-L-(1-^{13}C,^{18}O)Leu-Aib-Aib-(^{15}N)Gly-Aib-O*t*Bu

To a solution of Z-L-(1-^{13}C,^{18}O)Leu-^{18}OH (28 mg, 0.11 mmol) in anhydrous CH_2Cl_2, cooled to 0°C, HOAt (14 mg, 0.11 mmol) and EDC (20 mg, 0.11 mmol) were added. After 2 min this solution was added to a solution of H-Aib-Aib-(^{15}N)Gly-Aib-O*t*Bu (obtained by Pd-catalyzed hydrogenolysis of 46 mg, 0.09 mmol, of the corresponding Z-protected derivative) in CH_2Cl_2. To the resulting mixture DIPEA (15 μL, 0.11 mmol) was added. The mixture was stirred at room temperature for 72 hs while keeping the pH at 8 by addition of DIPEA. Then, the solvent was removed and the residue dissolved in EtOAc. The solution was washed with 10% $KHSO_4$, H_2O, 5% $NaHCO_3$ and H_2O, dried over Na_2SO_4, and evaporated to dryness.

Yield: 83%

mp: 170°-175°C

Rf_1: 0.50, Rf_2: 0.95, Rf_3: 0.27.

ESI-MS: calcd: 638.80; found: 638.7970 $[M+H]^+$

$[\alpha]_D^{20}$ = -36.5, $[\alpha]_{578}^{20}$ = -36.5 (c = 0.5, MeOH).

IR (KBr): 3416, 3333, 1704, 1679, 1645, 1533 cm^{-1}.

^1H NMR (200 MHz, $CDCl_3$): δ 7.66 (dt, 1H, ^{15}N-^1H Gly), 7.33 (m, 5H, Z phenyl-CH), 7.23 (s, 1H, N-H Aib), 6.80 (s, 1H, N-H Aib), 6.58 (s, 1H, N-H Aib), 5.61 (m, 1H, N-H Leu), 5.09 (d, 2H, Z-CH_2), 3.92 (m, 2H, α-CH Leu), 3.86 (m, 1H, α-CH Gly), 1.65 (m, 2H, β-CH_2 Leu), 1.48-1.39 (m, 19H, β-CH_3 Aib + γ-CH Leu), 1.42 (s, 9H, CH_3-*t*Bu), 1.22 (m, 6H, δ-CH_3 Leu).

Synthesis of Z-L-(1-^{13}C,^{18}O)Leu-Aib-Aib-Gly-Aib-Aib-Aib-Aib-OtBu (labeled octapeptide)

Z-L-(1-^{13}C,^{18}O)Leu-Aib-Aib-Gly-Aib-Aib-Aib-Aib-O*t*Bu

To a solution of Z-L-(1-^{13}C,^{18}O)Leu-^{18}OH (77 mg, 0.28 mmol) in anhydrous CH_2Cl_2, cooled to 0°C, HOAt (38 mg, 0.28 mmol) and EDC (54 mg, 0.31 mmol) were added. After 2 min this solution was added to a solution of H-Aib-Aib-Gly-Aib-Aib-Aib-Aib-O*t*Bu (obtained by Pd-catalyzed hydrogenolysis of 200 mg, 0.26 mmol, of the corresponding Z-protected derivative) in CH_2Cl_2. To the resulting mixture DIPEA (39 µL, 0.28 mmol) was added. The mixture was stirred at room temperature for 72 hs while keeping the pH at 8 by addition of DIPEA. Then, the solvent was removed and the residue dissolved in EtOAc. The solution was washed with 10% $KHSO_4$, H_2O, 5% $NaHCO_3$ and H_2O, dried over Na_2SO_4, and evaporated to dryness. The product was crystallized from $CHCl_3$/eptane/PE.

Yield: 55%

mp: 198°-200°C

Rf_1: 0.52, Rf_2: 0.95, Rf_3: 0.21.

ESI-MS: calcd: 892.13; found: 892.1439 $[M+H]^+$; 914.5183 $[M+Na]^+$

$[\alpha]_D^{20}$ = -17.3, $[\alpha]_{578}^{20}$ = - 17.7 (c = 0.5, MeOH).

IR (KBr): 3314, 1662, 1532 cm^{-1}.

^{1}H NMR (400 MHz, $CDCl_3$): δ 7.89 (dt, 1H, N-H Gly), 7.36, 7.41, 7.19, 7.07, 6.44, (s, 6H, N-H Aib), 7.58 (m, 5H, Z phenyl-CH), 5.35 (m, 1H, N-H (1-^{13}C,^{18}O)Leu), 5.11 (s, 2H, Z-CH_2), 3.89 (m, 1H, α-CH Leu), 3.76 (d, 2H, α-CH Gly), 1.51-1.43 (s, 48H, β-CH_3 Aib + β-CH_2 Leu + γ-CH Leu + CH_3-*t*Bu), 1.01 (t, 6H, δ-CH_3 Leu).

Synthesis of Z-L-(1-^{13}C,^{18}O)Leu-Aib-Aib-(^{15}N)Gly-Aib-Aib-Aib-Aib-OtBu (double-labeled octapeptide)

Z-(^{15}N)Gly-Aib-Aib-Aib-Aib-O*t*Bu

To a solution of Z-(^{15}N)Gly-OH (281 mg, 1.3 mmol) in anhydrous CH_2Cl_2, cooled to 0°C, HOAt (182 mg, 1.3 mmol) and EDC (257 mg, 1.3 mmol) were added. After 2 min this solution was added to a solution of H-Aib-Aib-Aib-Aib-O*t*Bu (obtained by Pd-catalyzed hydrogenolysis of 604 mg, 1.1 mmol, of the corresponding Z-protected derivative) in CH_2Cl_2. To the resulting mixture DIPEA (186 µL, 1.3 mmol) was added. During the following 2 hours, a white precipitate was formed. TLC and NMR analysis show that to be a first crop of the product. The reaction was left stirring for other 24 hs, while keeping the pH at 8 by addition of DIPEA. The solvent was removed and the residue dissolved in EtOAc. The solution was washed with 10% $KHSO_4$, H_2O, 5% $NaHCO_3$ and H_2O, dried over Na_2SO_4, and evaporated to dryness.

Yield: 88%

mp: 208°-213°C

Rf_1: 0.45, Rf_2: 0.90, Rf_3: 0.15.

IR (KBr): 3330, 1721, 1706, 1672, 1653, 1524, 1455 cm^{-1}.

^{1}H NMR (400 MHz, $CDCl_3$): δ 7.36 (m, 5H, Z phenyl-CH), 7.35 (s, 1H, N-H Aib), 7.02 (s, 1H, N-H Aib), 6.81 (s, 1H, N-H Aib), 6.36 (s, 1H, N-H Aib), 5.68 (dt, 1H, ^{15}N-^{1}H Aib), 5.14 (s, 2H, Z-CH_2), 3.74 (d, 2H, α-CH Gly), 1.49 (s, 6H, β-CH_3 Aib), 1.46 (s, 6H, β-CH_3 Aib), 1.44 (s, 6H, β-CH_3 Aib), 1.42 (s, 15H, CH_3-*t*Bu + β-CH_3 Aib).

Z-Aib-(^{15}N)Gly-Aib-Aib-Aib-Aib-O*t*Bu

To a solution of Z-Aib-OH (196 mg, 0.83 mmol) in anhydrous CH_2Cl_2, cooled to 0°C, HOAt (112 mg, 0.83 mmol) and EDC (159 mg, 0.83 mmol) were added. After 2 min this solution was added to a solution of H-(^{15}N)Gly-Aib-Aib-Aib-Aib-O*t*Bu (obtained by Pd-catalyzed hydrogenolysis of 60 mg, 0.17 mmol, of the corresponding Z-protected

derivative) in CH_2Cl_2. To the resulting mixture DIPEA (115 µL, 0.83 mmol) was added. The mixture was stirred at room temperature for 48 hs while keeping the pH at 8 by addition of DIPEA. Then, the solvent was removed and the residue dissolved in EtOAc. The solution was washed with 10% $KHSO_4$, H_2O, 5% $NaHCO_3$ and H_2O, dried over Na_2SO_4, and evaporated to dryness. The product was crystallized from AcOEt/PE.

Yield: 91%

mp: 222°-225°C

Rf_1: 0.35, Rf_2: 0.95, Rf_3: 0.14.

IR (KBr): 3333, 1727, 1701, 1662, 1523 cm^{-1}.

^1H NMR (400 MHz, $CDCl_3$): δ 7.53 (s, 1H, N-H Aib), 7.40 (s, 1H, N-H Aib), 7.37 (m, 5H, Z phenyl-CH), 7.16 (s, 1H, N-H Aib), 7.13 (s, 1H, N-H Aib), 7.05 (dt, 1H, ^{15}N-^1H Gly), 5.46 (s, 1H, N-H Aib), 5.11 (s, 2H, Z-CH_2), 3.78 (d, 2H, α-CH Gly), 1.62 (s, 6H, β-CH_3 Aib), 1.51 (s, 6H, β-CH_3 Aib), 1.50 (s, 6H, β-CH_3 Aib), 1.49 (s, 6H, β-CH_3 Aib), 1.48 (s, 6H, β-CH_3 Aib), 1.43 (s, 9H, CH_3-*t*Bu).

Z-Aib-Aib-(^{15}N)Gly-Aib-Aib-Aib-Aib-O*t*Bu

To a solution of Z-Aib-OH (156 mg, 0.66 mmol) in anhydrous CH_2Cl_2, cooled to 0°C, HOAt (90 mg, 0.66 mmol) and EDC (126 mg, 0.66 mmol) were added. After 2 min this solution was added to a solution of H-Aib-(^{15}N)Gly-Aib-Aib-Aib-Aib-O*t*Bu (obtained by Pd-catalyzed hydrogenolysis of 395 mg, 0.57 mmol, of the corresponding Z-protected derivative) in CH_2Cl_2. To the resulting mixture DIPEA (91 µL, 0.66 mmol) was added. The mixture was stirred at room temperature for 48 hs while keeping the pH at 8 by addition of DIPEA. Then, the solvent was removed and the residue dissolved in EtOAc. The solution was washed with 10% $KHSO_4$, H_2O, 5% $NaHCO_3$ and H_2O, dried over Na_2SO_4, and evaporated to dryness. The product was purified by flash chromatography (eluant, $CHCl_3$/EtOH 9:1).

Yield: 88%

mp: 99°-102°C

Rf_1: 0.45, Rf_2: 0.90, Rf_3: 0.15.

IR (KBr): 3411, 3323, 1730, 1694, 1666, 1531, cm^{-1}.

^1H NMR (400 MHz, $CDCl_3$): δ 7.78 (dt, 1H, ^{15}N-^1H Gly), 7.52 (s, 1H, N-H Aib), 7.39 (s, 1H, N-H Aib), 7.35 (m, 5H, Z phenyl-CH), 7.17 (s, 1H, N-H Aib), 7.13 (s, 1H, N-H

Aib), 6.35 (dt, 1H, ^{15}N-^{1}H Aib), 5.44 (s, 1H, N-H Aib), 5.11 (s, 2H, Z-CH_2), 3.72 (d, 2H, α-CH Gly), 1.51-1.37 (m, 45H, β-CH_3 Aib + CH_3-*t*Bu).

Z-(1-^{13}C,^{18}O)L-Leu-Aib-Aib-(^{15}N)Gly-Aib-Aib-Aib-Aib-O*t*Bu

To a solution of Z-L-(1-^{13}C,^{18}O)Leu-^{18}OH (77 mg, 0.28 mmol) in anhydrous CH_2Cl_2, cooled to 0°C, HOAt (38 mg, 0.28 mmol) and EDC (54 mg, 0.28 mmol) were added. After 2 min this solution was added to a solution of H-Aib-Aib-(^{15}N)Gly-Aib-Aib-Aib-Aib-O*t*Bu (obtained by Pd-catalyzed hydrogenolysis of 200 mg, 0.26 mmol, of the corresponding Z-protected derivative) in CH_2Cl_2. To the resulting mixture DIPEA (39 µL, 0.28 mmol) was added. The mixture was stirred at room temperature for 72 hs while keeping the pH at 8 by addition of DIPEA. Then, the solvent was removed and the residue dissolved in EtOAc. The solution was washed with 10% $KHSO_4$, H_2O, 5% $NaHCO_3$ and H_2O, dried over Na_2SO_4, and evaporated to dryness. The product was crystallized from CH_2Cl_2/PE.

Yield: 60%

mp: 198°-200°C

Rf_1: 0.52, Rf_2: 0.95, Rf_3: 0.21.

ESI-MS: calcd: 893.13; found: 893.1213 $[M+H]^+$; 915.5183 $[M+Na]^+$

$[\alpha]_D^{20}$ = -17.3, $[\alpha]_{578}^{20}$ = - 17.7 (c = 0.5, MeOH).

IR (KBr): 3311, 1662, 1531 cm^{-1}.

^{1}H NMR (400 MHz, $CDCl_3$): δ 7.89 (dt, 1H, ^{15}N-^{1}H Gly), 7.36, 7.41, 7.19, 7.07, 6.44, (s, 6H, N-H Aib), 7.58 (m, 5H, Z phenyl-CH), 5.35 (m, 1H, N-H (1-^{13}C,^{18}O)Leu), 5.11 (s, 2H, Z-CH_2), 3.89 (m, 1H, α-CH Leu), 3.76 (d, 2H, α-CH Gly), 1.51-1.43 (m, 48H, β-CH_3 Aib + β-CH_3 Leu + γ-CH Leu + CH_3-*t*Bu), 1.01 (t, 6H, δ-CH_3 Leu).

2.2 VCD

Synthesis of iPrCO-Aib-Ala-Aib-Ala-Ala-Aib-NHiPr (unlabeled hexapeptide)

Z-Aib-NH*i*Pr

To a solution of Z-L-Aib-OH (5 g, 2.1 mmol) in anhydrous CH_2Cl_2, cooled to 0°C HOAt (2.29 g, 21 mmol), EDC (3.55 g, 21 mmol), isopropylamine (2.1 mL, 25 mmol) and DIPEA (2.4 ml, 23 mmol) were added. The mixture was stirred at room temperature for 48 hs while keeping the pH at 8 by addition of DIPEA. Then, the solvent was removed and the residue dissolved in EtOAc. The solution was washed with 10% $KHSO_4$, H_2O, 5% $NaHCO_3$ and H_2O, dried over Na_2SO_4, and evaporated to dryness. Yield 88%.

m.p. 123°-125°C

Rf_1 0.85, Rf_2 0.90, Rf_3 0.35.

IR (KBr) 3308, 1688, 1648, 1532 cm^{-1}.

^1H NMR (200 MHz, $CDCl_3$): δ 7.35 (m, 5H, Z-phenyl CH), 6.05 (m, 1H, *i*Pr N-H), 5.37 (s, 1H, N-H Aib), 5.10 (s, 2H, Z-CH_2), 4.03 (m, 1H, *i*Pr-CH), 1.51 (s, 6H, β-CH_3 Aib), 1.10 (dd, 6H, *i*Pr-CH_3).

Z-Ala-Aib-NH*i*Pr

To a solution of Z-L-Ala-OH (820 mg, 3.6 mmol) in anhydrous CH_2Cl_2, cooled to 0°C, HOAt (503 mg, 3.6 mmol) and EDC (730 mg, 3.6 mmol) were added. After 2 min this solution was added to a solution of H-Aib-NH*i*Pr (obtained by Pd-catalyzed hydrogenolysis of 1.12 g, 3.1 mmol, of the corresponding Z-protected derivative) in CH_2Cl_2. To the resulting mixture DIPEA (660 µl, 0.0036 mmol) was added. The mixture was stirred at room temperature for 24 hs while keeping the pH at 8 by addition of DIPEA. Then, the solvent was removed and the residue dissolved in EtOAc. The solution was washed with 10% $KHSO_4$, H_2O, 5% $NaHCO_3$ and H_2O, dried over Na_2SO_4, and evaporated to dryness. Yield 98%.

m.p. 145°-148°C

Rf_1 0.75, Rf_2 0.85, Rf_3 0.30.

$[\alpha]_{589}$: -16.9 (c = 0.5, MeOH).

IR (KBr) 3292, 1707, 1681, 1636, 1539 cm^{-1}.

^{1}H NMR (200 MHz, $CDCl_3$): δ 7.35 (m, 5H, Z-phenyl CH), 6.43 (m, 1H, *i*Pr N-H), 6.29 (s, 1H, N-H Aib), 5.21 (d, 1H, N-H Ala), 5.12 (s, 2H, Z-CH_2), 4.05 (m, 2H, α-CH Ala and *i*Pr-CH), 1.50 (s, 6H, β-CH_3 Aib), 1.37 (d, 3H, β-CH_3 Ala), 1.14 (dd, 6H, *i*Pr-CH_3).

Z-Ala-Ala-Aib-NH*i*Pr

To a solution of Z-L-Ala-OH (320 mg, 1.4 mmol) in anhydrous CH_2Cl_2, cooled to 0°C, HOAt (194 mg, 1.4 mmol) and EDC (287 mg, 1.4 mmol) were added. After 2 min this solution was added to a solution of H-Ala-Aib-NH*i*Pr (obtained by Pd-catalyzed hydrogenolysis of 500 mg, 1.57 mmol, of the corresponding Z-protected derivative) in CH_2Cl_2. To the resulting mixture DIPEA (308 μl, 1.7 mmol) was added. The mixture was stirred at room temperature for 24 hs while keeping the pH at 8 by addition of DIPEA. Then, the solvent was removed and the residue dissolved in EtOAc. The solution was washed with 10% $KHSO_4$, H_2O, 5% $NaHCO_3$ and H_2O, dried over Na_2SO_4, and evaporated to dryness. The product was purified by flash chromatography (eluant, 95:5 $CHCl_3$/EtOH). Oil. Yield 74%.

Rf_1 0.75, Rf_2 0.80, Rf_3 0.30.

$[\alpha]_{589}$: -16 (c = 0.5, MeOH).

IR (KBr) 3311, 1650, 1532 cm^{-1}.

^{1}H NMR (200 MHz, $CDCl_3$): δ 7.36 (m, 5H, Z-phenyl CH), 6.70 (s, 1H, N-H Aib), 6.52 (d, 1H, N-H Ala), 6.34 (m, 1H, *i*Pr N-H), 5.29 (d, 1H, N-H Ala), 5.12 (s, 2H, Z-CH_2), 4.19 (q, 1H, α-CH Ala), 4.14 (q, 1H, α-CH Ala), 4.01 (m, 1H, *i*Pr-CH), 1.50 (d, 6H, β-CH_3 Aib), 1.40 (d, 3H, β-CH_3 Ala), 1.34 (d, 3H, β-CH_3 Ala), 1.15 (dd, 6H, *i*Pr-CH_3).

Z-Aib-Ala-Ala-Aib-NH*i*Pr

To a solution of Z-Aib-OH (677 mg, 2.8 mmol) in anhydrous CH_2Cl_2, cooled at 0°C, HOBt (386 mg, 2.8 mmol) and EDC (550 mg, 2.8 mmol) were added. After 2 min this solution was added to a solution of H-Ala-Ala-Aib-NH*i*Pr (obtained by Pd-catalyzed hydrogenolysis of 580 mg, 1.4 mmol, of the corresponding Z-protected derivative) in CH_2Cl_2. To the resulting mixture DIPEA (490 μl, 2.8 mmol) was added. The mixture was stirred at room temperature for 24 hs while keeping the pH at 8 by addition of DIPEA. Then, the solvent was removed and the residue dissolved in EtOAc. The solution was washed with 10% $KHSO_4$, H_2O, 5% $NaHCO_3$ and H_2O, dried over

Na_2SO_4, and evaporated to dryness. The product was purified by flash chromatography (eluant, 95:5 $CHCl_3$/EtOH). Yield 74%.

m.p. 90°-92°C

Rf_1 0.75, Rf_2 0.80, Rf_3 0.30.

$[\alpha]_{589}$: +30 (c = 0.5, MeOH).

IR (KBr) 3316, 1659, 1531 cm^{-1}.

^1H NMR (200 MHz, $CDCl_3$): δ 7.58 (s, 1H, N-H Aib) 7.30 (m, 5H, Z-phenyl CH), 7.10 (d, 1H, N-H Ala), 7.05 (d, 1H, N-H Ala), 6.77 (m, 1H, *i*Pr N-H), 5.54 (s, 1H, N-H Aib), 5.07 (s, 2H, Z-CH_2), 4.11 (q, 1H, α-CH Ala), 4.09 (q, 1H, α-CH Ala), 3.95 (m, 1H, *i*Pr-CH), 1.49 (s, 6H, β-CH_3 Aib), 1.45 (s, 6H, β-CH_3 Aib), 1.38 (d, 3H, β-CH_3 Ala), 1.26 (d, 3H, β-CH_3 Ala), 1.06 (dd, 6H, *i*Pr-CH_3).

Z-Ala-Aib-Ala-Ala-Aib-NH*i*Pr

To a solution of Z-Aib-OH (264 mg, 1.1 mmol) in anhydrous CH_2Cl_2, cooled to 0°C, HOBt (386 mg, 1.1 mmol) and EDC (550 mg, 1.1 mmol) were added. After 2 min this solution was added to a solution of H-Aib-Ala-Ala-Aib-NH*i*Pr (obtained by Pd-catalyzed hydrogenolysis of 300 mg, 0.6 mmol, of the corresponding Z-protected derivative) in CH_2Cl_2. To the resulting mixture DIPEA (195 µl, 1.1 mmol) was added. The mixture was stirred at room temperature for 12 hs while keeping the pH at 8 by addition of DIPEA. Then, the solvent was removed and the residue dissolved in EtOAc. The solution was washed with 10% $KHSO_4$, H_2O, 5% $NaHCO_3$ and H_2O, dried over Na_2SO_4, and evaporated to dryness. The product was purified by flash chromatography (eluant, 9:1 $CHCl_3$/EtOH). Yield 55%.

m.p. 119°-122°C

Rf_1 0.55, Rf_2 0.55, Rf_3 0.20.

$[\alpha]_{589}$: -29.2 (c = 0.5, MeOH).

IR (KBr) 3311, 1660, 1532 cm^{-1}.

^1H NMR (200 MHz, $CDCl_3$): δ 7.53 (d, 1H, N-H Ala), 7.35 (m, 5H, Z-phenyl CH), 7.11 (d, 1H, N-H Ala), 6.95 (s, 1H, N-H Aib), 6.82 (s, 1H, N-H Aib), 6.57 (m, 1H, *i*Pr N-H), 5.97 (d, 1H, N-H Ala), 5.15 (q, 2H, Z-CH_2), 4.23 (q, 1H, α-CH Ala), 4.12 (q, 1H, α-CH Ala), 3.98 (q, 1H, α-CH Ala), 3.95 (m, 1H, *i*Pr-CH), 1.34 (d, 3H, β-CH_3 Ala), 1.52 (s, 6H, β-CH_3 Aib), 1.50 (s, 6H, β-CH_3 Aib), 1.44 (d, 3H, β-CH_3 Ala), 1.39 (d, 3H, β-CH_3 Ala), 1.11 (dd, 6H, *i*Pr-CH_3).

Z-Aib-Ala-Aib-Ala-Ala-Aib-NH*i*Pr

To a solution of Z-Aib-OH (188 mg, 0.9 mmol) in anhydrous CH_2Cl_2, cooled at 0°C, HOBt (106 mg, 0.9 mmol) and EDC (151 mg, 0.9 mmol) were added. After 2 min this solution was added to a solution of H-Ala-Aib-Ala-Ala-Aib-NH*i*Pr (obtained by Pd-catalyzed hydrogenolysis of 230 mg, 0.46 mmol, of the corresponding Z-protected derivative) in CH_2Cl_2. To the resulting mixture DIPEA (136 µl, 0.9 mmol) was added. The mixture was stirred at room temperature for 36 hs while keeping the pH at 8 by addition of DIPEA. Then, the solvent was removed and the residue dissolved in EtOAc. The solution was washed with 10% $KHSO_4$, H_2O, 5% $NaHCO_3$ and H_2O, dried over Na_2SO_4, and evaporated to dryness. The product was purified by flash chromatography (eluant, 95:5 $CHCl_3$/EtOH). Yield 60%.

m.p. 160°-162°C

Rf_1 0.60, Rf_2 0.65, Rf_3 0.25.

$[\alpha]_{589}$: +15 (c = 0.5, MeOH).

IR (KBr) 3313, 1657, 1531 cm^{-1}.

^1H NMR (200 MHz, $CDCl_3$): δ 7.55 (d, 1H, N-H Ala), 7.53 (d, 1H, N-H Ala), 7.35 (m, 5H, Z-phenyl CH), 7.31 (s, 1H, N-H Aib), 7.02 (s, 1H, NH Aib), 6.81 (d, 1H, N-H Ala), 6.59 (d, 1H, *i*Pr N-H), 6.10 (s, 1H, NH Aib), 5.06 (q, 2H, Z-CH_2), 4.21 (q, 1H, α-CH Ala), 4.05 (q, 1H, α-CH Ala), 3.93 (q, 1H, α-CH Ala), 3.84 (m, 1H, *i*Pr-CH), 1.45 (s, 6H, β-CH_3 Aib), 1.43 (s, 6H, β-CH_3 Aib), 1.40 (d, 3H, β-CH_3 Ala), 1.38 (d, 3H, β-CH_3 Ala), 1.34 (s, 6H, β-CH_3 Aib), 1.25 (d, 3H, β-CH_3 Ala), 1.03 (dd, 6H, *i*Pr-CH_3).

***i*PrCO-Aib-Ala-Aib-Ala-Ala-Aib-NH*i*Pr**

To a solution of isobutyric acid (*i*Pr-COOH, 51 µl, 0.6 mmol) in anhydrous CH_2Cl_2, cooled to 0°C, HOAt (80 mg, 0.6 mmol) and EDC (112 mg, 0.6 mmol) were added. After 2 min this solution was added to a solution of H-Aib-Ala-Aib-Ala-Ala-Aib-NH*i*Pr (obtained by Pd-catalyzed hydrogenolysis of 130 mg, 0.2 mmol, of the corresponding Z-protected derivative) in CH_2Cl_2. To the resulting mixture DIPEA (100 µl, 0.6 mmol) was added. The mixture was stirred at room temperature for 24 hs while keeping the pH at 8 by addition of DIPEA. Then, the solvent was removed and the residue dissolved in EtOAc. The solution was washed with 10% $KHSO_4$, H_2O, 5% $NaHCO_3$ and H_2O, dried over Na_2SO_4, and evaporated to dryness. The product was purified by flash chromatography (eluant, 95:5 $CHCl_3$/EtOH). Yield 40%.

m.p. 249°-251°C

Rf_1 0.60, Rf_2 0.60, Rf_3 0.20.

ESI-MS: calcd: 598.57; found: 598.38 $[M+H]^+$.

HPLC: t_r = 9.6 min; Conditions: analytical Vydac C_{18} column (particle size: 5 μm; pore size: 300 Å); gradient system, 5→35%B in 20 min; flow rate, 1 ml/min (eluant A: H2O/acetonitrile 9/1 + 0.05% TFA; eluant B: acetonitrile/H2O 9/1 + 0.05% TFA); room temperature; absorbance detector at 226 nm.

$[\alpha]_{589}$: +8.3 (c = 0.5, MeOH).

IR (KBr) 3310, 1654, 1534 cm^{-1}.

^1H NMR (200 MHz, $CDCl_3$): δ 7.79 (d, 1H, N-H Ala), 7.59 (d, 1H, N-H Ala), 7.27 (m, 5H, Z-phenyl CH), 7.21 (d, 1H, N-H Ala), 6.98 (s, 1H, N-H Aib), 6.86 (s, 1H, N-H Aib), 6.53 (m, 1H, *i*Pr N-H), 6.11 (d, 1H, N-H Aib), 4.21-3.97 (m, 4H, 3 α-CH_3 Ala and *i*Pr-CH), 2.53 (m, 1H, *i*Pr-CH), 1.54 (s, 12H, β-CH_3 Aib), 1.49 (s, 6H, β-CH_3 Aib), 1.48 (d, 6H, β-CH_3 Ala), 1.40 (s, 3H, β-CH_3 Ala), 1.03 (m, 12H, *i*Pr-CH_3).

Synthesis of Ac-Aib-Ala-Aib-Ala-Ala*-Aib-Aib-Aib-OMe (double-labeled octapeptide)*

Z-Ala*-Aib-Aib-Aib-OMe

To a solution of Z-L-Ala*-OH (1.33 g, 6 mmol, prepared as reported previously for Z-Ala-OH) in anhydrous CH_2Cl_2, cooled to 0°C, HOAt (810 mg, 6 mmol) and EDC (1.14 g, 6 mmol) were added. After 2 min this solution was added to a solution of H-Aib_3-OMe (obtained by Pd-catalyzed hydrogenolysis of 3 g, 6 mmol, of the corresponding Z-protected derivative) in CH_2Cl_2. To the resulting mixture DIPEA (2.05 ml, 6 mmol) was added. The mixture was stirred at room temperature for 72 hs while keeping the pH at 8 by addition of DIPEA. Then, the solvent was removed and the residue was purified by flash chromatography (eluant 95:5 $CHCl_3$/EtOH). Oil. Yield 60%.

Rf_1 0.80, Rf_2 0.65, Rf_3 0.30.

$[\alpha]_{589}$: -18.9 (c = 0.5, MeOH).

IR (KBr) 3318, 1705, 1668, 1528 cm^{-1}.

^1H NMR (200 MHz, $CDCl_3$): δ 7.34 (m, 5H, Z-phenyl CH), 7.26 (s, 1H, N-H Aib), 6.65 (s, 1H, N-H Aib), 6.63 (s, 1H, NH Aib), 5.75 (d, 1H, N-H Ala), 5.12 (s, 2H, Z-CH_2), 4.10 (q, 1H, α-CH Ala), 3.65 (s, 3H, CH_3 OMe), 1.49 (s, 6H, β-CH_3 Aib), 1.48 (s, 6H, β-CH_3 Aib), 1.46 (s, 6H, β-CH_3 Aib), 1.38 (d, 3H, β-CH_3 Ala).

Z-Ala*-Ala*-Aib-Aib-Aib-OMe

To a solution of Z-L-Ala*-OH (500 mg, 2.3 mmol) in anhydrous CH_2Cl_2, cooled at 0°C, HOAt (300 mg, 2.3 mmol) and EDC (420 mg, 2.3 mmol) were added. After 2 min this solution was added to a solution of H-Ala*-Aib-Aib-Aib-OMe (obtained by Pd-catalyzed hydrogenolysis of 1.3 g, 2.3 mmol, of the corresponding Z-protected derivative) in CH_2Cl_2. To the resulting mixture DIPEA (0.76 ml, 4.6 mmol) was added. The mixture was stirred at room temperature for 48 hours while keeping the pH at 8 by addition of DIPEA. Then, the solvent was removed and the residue dissolved in EtOAc. The solution was washed with 10% $KHSO_4$, H_2O, 5% $NaHCO_3$ and H_2O, dried over Na_2SO_4, and evaporated to dryness. The product crystallizes from EtOAc.Yield 70%.

m.p. 190°-193°C

Rf_1 0.70, Rf_2 0.60, Rf_3 0.25.

$[\alpha]_{589}$: -49 (c = 0.5, MeOH).

IR (KBr) 3318, 1728, 1670, 1632, 1527 cm^{-1}.

^1H NMR (200 MHz, $CDCl_3$): δ 7.35 (m, 5H, Z-phenyl CH), 7.02 (s, 1H, N-H Aib), 6.85 (s, 1H, N-H Aib), 6.80 (s, 1H, N-H Aib), 6.73 (d, 1H, NH Ala), 5.65 (d, 1H, N-H Ala), 5.10 (s, 2H, Z-CH_2), 3.98 (m, 2H, 2 α-CH Ala), 3.64 (s, 3H, CH_3 OMe), 1.49 (s, 6H, β-CH_3 Aib), 1.48 (s, 6H, β-CH_3 Aib), 1.45 (s, 6H, β-CH_3 Aib), 1.42 (d, 3H, β-CH_3 Ala), 1.35 (d, 3H, β-CH_3 Ala).

Z-Aib-Ala*-Ala*-Aib-Aib-Aib-OMe

To a solution of Z-Aib-OH (664 mg, 2.8 mmol) in anhydrous CH_2Cl_2, cooled at 0°C, HOAt (380 mg, 2.8 mmol) and EDC (536 mg, 2.8 mmol) were added. After 2 min this solution was added to a solution of H-Ala*-Ala*-Aib-Aib-Aib-OMe (obtained by Pd-catalyzed hydrogenolysis of 800 mg, 1.4 mmol, of the corresponding Z-protected derivative) in CH_2Cl_2. To the resulting mixture DIPEA (484 µl, 2.8 mmol) was added. The mixture was stirred at room temperature for 96 hs while keeping the pH at 8 by addition of DIPEA. Then, the solvent was removed and the residue dissolved in EtOAc. The solution was washed with 10% $KHSO_4$, H_2O, 5% $NaHCO_3$ and H_2O, dried over Na_2SO_4, and evaporated to dryness and the residue was purified by flash chromatography (eluant 95:5 $CHCl_3$/EtOH).Yield 88%.

m.p. 209°-211°C

Rf_1 0.80, Rf_2 0.75, Rf_3 0.30.

$[\alpha]_{589}$: +14.1 (c = 0.5, MeOH).

IR (KBr) 3319, 1663, 1624, 1525 cm^{-1}.

^1H NMR (200 MHz, $CDCl_3$): δ 7.59 (d, 1H, NH Ala), 7.39 (s, 1H, NH Aib), 7.37 (s, 1H, NH Aib), 7.34 (m, 5H, Z-phenyl CH), 7.22 (d, 1H, NH Ala), 6.69 (s, 1H, NH Aib), 6.55 (s, 1H, N-H Aib), 5.06 (s, 2H, Z-CH_2), 4.16 (q, 1H, α-CH_3 Ala), 4.12 (q, 1H, α-CH_3 Ala), 3.66 (s, 3H, CH_3 OMe), 1.53 (s, 6H, β-CH_3 Aib), 1.51 (s, 6H, β-CH_3 Aib), 1.50 (s, 6H, β-CH_3 Aib), 1.49 (d, 3H, β-CH_3 Ala), 1.47 (d, 3H, β-CH_3 Ala), 1.41 (s, 6H, β-CH_3 Aib).

Z-Ala-Aib-Ala*-Ala*-Aib-Aib-Aib-OMe

To a solution of Z-Ala-OH (385 mg, 1.7 mmol) in anhydrous CH_2Cl_2, cooled to 0°C, HOAt (229 mg, 1.7 mmol) and EDC (325 mg, 1.7 mmol) were added. After 2 min this solution was added to a solution of H-Aib-Ala*-Ala*-Aib-Aib-Aib-OMe (obtained by Pd-catalyzed hydrogenolysis of 750 mg, 1.1 mmol, of the corresponding Z-protected derivative) in CH_2Cl_2. To the resulting mixture DIPEA (294 µl, 1.7 mmol) was added. The mixture was stirred at room temperature for 72 hs while keeping the pH at 8 by addition of DIPEA. Then, the solvent was removed and the residue dissolved in EtOAc. The solution was washed with 10% $KHSO_4$, H_2O, 5% $NaHCO_3$ and H_2O, dried over Na_2SO_4, and evaporated to dryness and the residue was purified by flash chromatography (eluant 9:1 $CHCl_3$/EtOH). Yield 72%.

m.p. 220°-223°C

Rf_1 0.60, Rf_2 0.55, Rf_3 0.20.

$[\alpha]_{589}$: -10.2 (c = 0.5, MeOH).

IR (KBr) 3316, 1666, 1527 cm^{-1}.

^1H NMR (200 MHz, $CDCl_3$): δ 7.58 (d, 1H, N-H Ala), 7.43 (s, 1H, N-H Aib), 7.34 (m, 5H, Z-phenyl CH), 7.23 (s, 1H, N-H Aib), 7.19 (s, 1H, N-H Aib), 6.82 (d, 1H, N-H Ala), 6.75 (s, 1H, N-H Aib), 6.26 (d, 1H, N-H Ala), 5.10 (s, 2H, Z-CH_2), 4.16 (q, 1H, α-CH Ala), 4.10 (q, 1H, α-CH Ala), 3.93 (q, 1H, α-CH Ala), 3.64 (s, 3H, CH_3 OMe), 1.50 (s, 6H, β-CH_3 Aib), 1.48 (s, 6H, β-CH_3 Aib), 1.47 (s, 6H, β-CH_3 Aib), 1.45 (d, 3H, β-CH_3 Ala), 1.47 (d, 3H, β-CH_3 Ala), 1.41 (s, 6H, β-CH_3 Aib), 1.33 (d, 3H, β-CH_3 Ala).

Z-Aib-Ala-Aib-Ala*-Ala*-Aib-Aib-Aib-OMe

To a solution of Z-Aib-OH (394 mg, 1.6 mmol) in anhydrous CH_2Cl_2, cooled at 0°C, HOAt (225 mg, 1.6 mmol) and EDC (320 mg, 1.6 mmol) were added. After 2 min this solution was added to a solution of H-Ala-Aib-Ala*-Ala*-Aib_3-OMe (obtained by Pd-catalyzed hydrogenolysis of 600 mg, 0.8 mmol, of the corresponding Z-protected derivative) in CH_2Cl_2. To the resulting mixture DIPEA (289 µl, 1.6 mmol) was added. The mixture was stirred at room temperature for 48 hs while keeping the pH at 8 by addition of DIPEA. Then, the solvent was removed and the residue dissolved in AcOEt. The solution was washed with 10% $KHSO_4$, H_2O, 5% $NaHCO_3$ and H_2O, dried over Na_2SO_4, and evaporated to dryness. The residue was purified by flash chromatography (eluant 95:5 $CHCl_3$/EtOH). Yield 72%.

m.p. 198°-200°C

Rf_1 0.70, Rf_2 0.60, Rf_3 0.22.

$[\alpha]_{589}$: +5.4 (c = 0.5, MeOH).

IR (KBr) 3319, 1665, 1527 cm^{-1}.

^1H NMR (200 MHz, $CDCl_3$): δ 7.56 (m, 2H, 2 N-H Ala), 7.42 (s, 1H, N-H Aib), 7.38 (s, 1H, N-H Aib), 7.36 (m, 5H, Z-phenyl CH), 7.22 (s, 1H, N-H Aib), 6.82 (d, 1H, N-H Ala), 6.65 (d, 1H, N-H Ala), 5.96 (s, 1H, N-H Aib), 5.10 (s, 2H, Z-CH_2), 4.14 (q, 1H, α-CH Ala), 4.11 (q, 1H, α-CH Ala), 3.91 (q, 1H, α-CH Ala), 3.65 (s, 3H, CH_3 OMe), 1.52 (s, 6H, β-CH_3 Aib), 1.50 (s, 6H, β-CH_3 Aib), 1.47 (s, 6H, β-CH_3 Aib), 1.46 (s, 6H, β-CH_3 Aib), 1.44 (d, 3H, β-CH_3 Ala), 1.42 (d, 3H, β-CH_3 Ala), 1.41 (s, 6H, β-CH_3 Aib), 1.32 (d, 3H, β-CH_3 Ala).

Ac-Aib-Ala-Aib-Ala*-Ala*-Aib_3-OMe

To a solution of H-Aib-Ala-Aib-Ala*-Ala*-Aib_3-OMe (obtained by Pd-catalyzed hydrogenolysis of 470 mg, 0.6 mmol, of the corresponding Z-protected derivative) in CH_2Cl_2, cooled at 0°C, acetic anhydride (0.6 µl, 6 mmol) was added. The mixture was stirred at room temperature overnight. Then, the solvent was removed and the residue residue was purified by flash chromatography (eluant 9:1 $CHCl_3$/EtOH). Yield 63%.

m.p. 265°-268°C

Rf_1 0.60, Rf_2 0.55, Rf_3 0.20.

ESI-MS: calcd: 715.84; found: 715.37 $[M+H]^+$.

HPLC: t_r = 13.4 min; Conditions: analytical Vydac C_{18} column (particle size: 5 μm; pore size: 300 Å); gradient system, 30→70%B in 20 min; flow rate, 1 ml/min (eluant A: H2O/acetonitrile 9/1 + 0.05% TFA; eluant B: acetonitrile/H2O 9/1 + 0.05% TFA); room temperature; absorbance detector at 226 nm.

$[\alpha]_{589}$: -6.8 (c = 0.5, MeOH).

IR (KBr) 3325, 1660, 1528 cm^{-1}.

^{1}H NMR (200 MHz, DMSO-d_6): δ 8.40 (d, 2H, 2 N-H Ala), 8.20 (s, 1H, N-H Aib), 7.79 (s, 1H, N-H Aib), 7.71 (s, 1H, N-H Aib), 7.67 (s, 1H, N-H Aib), 7.28 (d, 1H, N-H Ala), 6.99 (s, 1H, N-H Aib), 3.98 (m, 3H, 3 α-CH Ala), 3.52 (s, 3H, CH_3 OMe), 1.90 (s, 3H, CH_3CO), 1.32 (m, 39H, β-CH_3 Aib and β-CH_3 Ala).

5.3.2 (αMe)Pro a unique example of split personality

Ala and Aib derivatives

Boc-L-Ala-NH*i*Pr

To a solution of Boc-L-Ala-OH (1.0 g, 5.28 mmol) in CH_2Cl_2 cooled to 0°C, EDC (1.0 g, 5.28 mmol) and HOBt (713 mg, 5.28 mmol) were added. After 20 min, isopropylamine (0.90 ml, 10.56 mmol) was added and the reaction was stirred at room temperature for 1 d. Then, the solvent was removed under reduced pressure and the residue dissolved in EtOAc. The solution was washed with 10% $KHSO_4$, H_2O, 5% $NaHCO_3$ and H_2O, dried over anhydrous Na_2SO_4, and evaporated to dryness. The product was crystallized from EtOAc/PE. Yield: 66 %.

mp:112-114 °C

$Rf_1 = 0.70$, $Rf_2 = 0.95$, $Rf_3 = 0.45$

$[\alpha]_{589}$: = -24 (c = 0.5, MeOH)

IR (KBr): 3315, 1681, 1648, 1531 cm^{-1}.

^1H NMR ($CDCl_3$): δ 5.91 (s, 1H, Ala NH), 4.96 (s, 1H, NH*i*Pr), 4.07 (m, 2H, Ala α-CH, iPr CH), 1.45 (s, 9H, Boc CH_3), 1.33 (d, 3H, Ala β-CH_3), 1.15 (dd, 6H, *i*Pr-CH_3).

Boc-Aib-NH*i*Pr

To a solution of Boc-Aib-OH (0.5 g, 2.4 mmol) in CH_2Cl_2 cooled to 0°C, EDC (470 mg, 2.4 mmol) and HOBt (324 mg, 2.4 mmol) were added. After 20 min, isopropylamine (1.0 ml, 12 mmol) was added and the reaction was stirred at room temperature for 1 d. Then, the solvent was removed under reduced pressure and the residue dissolved in EtOAc. The solution was washed with 10% $KHSO_4$, H_2O, 5% $NaHCO_3$ and H_2O, dried over anhydrous Na_2SO_4, and evaporated to dryness. The product was crystallized from EtOAc/PE. Yield: 79 %.

mp: 127-128 °C

$Rf_1 = 0.70$, $Rf_2 = 0.90$, $Rf_3 = 0.40$

IR (KBr): 3341, 3315, 1683, 1643, 1614, 1545 cm^{-1}.

^1H NMR ($CDCl_3$): δ 6.23 (s, 1H, Aib NH), 4.90 (s, 1H, NH*i*Pr), 4.02 (m, 1H, *i*Pr α-CH), 1.47 (s, 9H, Boc CH_3), 1.44 (s, 6H, Aib β-CH_3), 1.14 (dd, 6H, *i*Pr CH_3).

(αMe)Pro and derivatives

Boc-L-(αMe)Pro-OH

A solution of H-L-(αMe)Pro-OH (1 g, 9 mmol) and NaOH (0.36 g, 9 mmol) in dioxane/H_2O (1:1) (20 ml) was cooled to 0°C. Boc_2O (1.96 g, 9 mmol) in three portions and the reaction was stirred at room temperature for 5 d. Then, the dioxane was evaporated under reduced pressure. Unreacted Boc_2O was extracted with Et_2O. Then a solution of 10% $KHSO_4$ is added to pH 3. The aqueous phase is extracted with AcOEt. The organic phase is washed with H_2O, brine, dried over Na_2SO_4 and evaporated to dryness. Yield: 52%.

mp: 127-129 °C.

Rf_1: 0.70, Rf_2: 0.95, Rf_3: 0.40.

$[\alpha]_{589}$: = -6, $[\alpha]_{578}$= +7.5 (c = 0.5, MeOH)

IR (KBr): 3450, 1794, 1698, 1626 cm^{-1}.

^1H NMR (200 MHz, $CDCl_3$): δ 3.7-3.4 (m, 2H, δ-CH_2), 2.7-1.7 (m, 4H, β,γ-CH_2), 1.53 (s, 3H, α-CH_3), 1.48 (s, 9H, Boc CH_3).

Z-L-(αMe)Pro-OH

H-L-(αMe)Pro-OH (2 g, 15.2 mmol) was suspended in a H_2O (8 ml) and CH_3CN (8 ml) solution, then TEA (2.5 ml, 15.2 mmol) was added and the mixture was stirred at rt until a clear solution formed. Then, Z-OSu (4.0 g, 16.3 mmol), dissolved in CH_3CN (15 ml), was added and stirring was continued for 2 d, while keeping the pH at 8 by addition of TEA. Additional Z-OSu (0.5 equivalents) was added during the reaction. Then, CH_3CN was removed *in vacuo* and the excess of Z-OSu was extracted with Et_2O. The aqueous layer was acidified to pH 2-3 with $KHSO_4$ and the product extracted with EtOAc. The organic solution was washed with 10% $KHSO_4$ and H_2O, dried over Na_2SO_4, and evaporated to dryness. Yield: 65%.

mp: 99°-101°C.

Rf_1: 0.70; Rf_2: 0.95; Rf_3: 0.50.

$[\alpha]_{589}$: = -8, $[\alpha]_{578}$= +5 (c = 0.5, MeOH)

IR (film) : 1722, 1706 cm^{-1}.

^{1}H NMR (250 MHz, $CDCl_3$): δ 7.56 (brs,1H, COOH), 7.35 (m, 5H, Z phenyl CH), 5.15-5.10 (2s, 2H, *cis-trans* Z CH_2), 3.70-3.50 (m, 2H, δ-CH_2), 2.05-1.80 (4H, 1 β-CH_2, 1 γ-CH_2), 1.62-1.53 (2s, 3H, *cis-trans* α-CH_3).

Boc-D-(αMe)Pro-OH

A solution of H-D-(αMe)Pro-OH (1.0 g, 9 mmol) and NaOH (0.36 g, 9 mmol) in dioxane/H_2O (1:1) (20 ml) was cooled to 0 °C. Boc_2O (1.96 g, 9 mmol) was added in three portions and the reaction was stirred at room temperature for 5 d. Then, the dioxane was evaporated under reduced pressure. Excess of Boc_2O was extracted with Et_2O and the aqueous layer was acidified to pH 3 with 10% $KHSO_4$. The product was extracted with EtOAc and washed with 10% $KHSO_4$ and H_2O, and dried over Na_2SO_4. The solvent was evaporated under reduced pressure and the residue was crystallized from EtOAc/PE. Yield: 35%.

mp: 122-124°C

Rf_1 = 0.70, Rf_2 = 0.95, Rf_3 = 0.40

$[\alpha]_{589}$: = -7, $[\alpha]_{578}$= -8 (c = 0.5, MeOH)

IR (KBr): 3452, 1734, 1699, 1627 cm^{-1}

^{1}H NMR ($CDCl_3$): δ 3.7-3.4 (m, 2H, δCH_2), 2.7-1.7 (m, 4H, β and γ CH_2), 1.53 (s, 3H, αMe CH_3), 1.48 (s, 9H, Boc CH_3).

Boc-L-(αMe)Pro-NH*i*Pr

To a solution of Boc-L-(αMe)Pro-OH (600 mg, 2.8 mmol) in CH_2Cl_2 cooled to 0°C, EDC (535 mg, 2.8 mmol) and HOBt (378 mg, 2.8 mmol) were added. After 20 min, isopropylamine (0.95 ml, 11.2 mmol) was added and the reaction was stirred at room temperature for 1 d. Then, the solvent was removed under reduced pressure and the residue dissolved in EtOAc. The solution was washed with 10% $KHSO_4$, H_2O, 5% $NaHCO_3$ and H_2O, dried over anhydrous Na_2SO_4, and evaporated to dryness. The product was crystallized from EtOAc/PE. Yield: 79 %.

mp: 60-62 °C

Rf_1 = 0.70, Rf_2 = 0.90, Rf_3 = 0.45

$[\alpha]_{589}$: = +58 (c = 0.5, MeOH)

IR (KBr): 3340, 1699, 1644, 1525 cm^{-1}.

^{1}H NMR ($CDCl_3$): δ 5.76 (s, 1H, NH*i*Pr), 4.02 (m, 1H, iPr α-CH), 3.54 [s, 2H, (αMe)Pro δCH_2], 2.7-1.7 [m, 4H, (αMe)Pro β,γ-CH_2], 1.57 [s, 3H, (αMe)Pro β-CH_3], 1.46 (s, 9H, Boc CH_3), 1.14 (dd, 6H, *i*Pr CH_3).

Boc-D-(αMe)Pro-NH*i*Pr

To a solution of Boc-D-(αMe)Pro-OH (400 mg, 1.88 mmol) in CH_2Cl_2 cooled to 0°C, EDC (360 mg, 1.88 mmol) and HOBt (254 mg, 1.88 mmol) were added. After 20 min, isopropylamine (0.64 ml, 7.52 mmol) was added and the reaction was stirred at room temperature for 1 d. Then, the solvent was removed under reduced pressure and the residue dissolved in EtOAc. The solution was washed with 10% $KHSO_4$, H_2O, 5% $NaHCO_3$ and H_2O, dried over anhydrous Na_2SO_4, and evaporated to dryness. The product was crystallized from EtOAc/PE. Yield: 81 %.

mp: 64-66 °C

Rf_1 = 0.70, Rf_2 = 0.90, Rf_3 = 0.45

$[\alpha]_{589}$: = -63 (c 0.5, MeOH)

IR (KBr): 3340, 1700, 1644, 1525 cm^{-1}.

^{1}H NMR ($CDCl_3$): δ 5.76 (s, 1H, NHiPr), 4.03 (m, 1H, iPr α-CH), 3.54 [s, 2H, (αMe)Pro δ-CH_2], 2.7-1.7 [m, 4H, (αMe)Pro β,γ-CH_2], 1.57 [s, 3H, (αMe)Pro CH_3], 1.46 (s, 9H, Boc CH_3), 1.14 (dd, 6H, *i*Pr CH_3).

Boc-L-Ala-L-(αMe)Pro-NH*i*Pr

To a solution of Boc-L-Ala-OH (532 mg, 2.81 mmol) in CH_2Cl_2 cooled to 0°C, EDC (536 mg, 2.81 mmol) and HOAt (382 mg, 2.81 mmol) were added. After 30 min, H-L-(αMe)Pro-NHiPr (obtained by treatment of the corresponding Boc-protected aminoacid isopropylamide, 500 mg, 1.97 mmol) with a solution of TFA and CH_2Cl_2 1:1 for 1 hr] neutralized with NMM (0.6 ml, 5.63 mmol) was added. The reaction mixture was stirred for 3 d. Then, EtOAc was added and the solution was extracted with 10% $KHSO_4$, H_2O, 5% $NaHCO_3$, H_2O, and dried over anhydrous Na_2SO_4. The product was crystallized from EtOAc/PE. Yield: 50 %.

mp: 160-162 °C

Rf_1 = 0.70, Rf_2 = 0.95, Rf_3 = 0.40

$[\alpha]_{589}$: = +28 (c = 0.5, MeOH)

IR (KBr): 3379, 3344, 1684, 1657, 1526 cm^{-1}.

^1H NMR ($CDCl_3$): δ 6.68 (s, 1H, NH*i*Pr), 5.13 (d, 1H, Ala NH), 4.15-3.85 (m, 2H, Ala α-CH, iPr CH), 3.51 [m, 2H, (αMe)Pro δ-CH_2], 2.0-1.7 [m, 4H, (αMe)Pro β,γ-CH_2], 1.62 [s, 3H, (αMe)Pro β-CH_3], 1.44 (s, 9H, Boc CH_3), 1.26 (d, 3H, Ala β-CH_3), 1.12 (dd, 6H, iPr CH_3).

Boc-L-Ala-D-(αMe)Pro-NH*i*Pr

To a solution of Boc-L-Ala-OH (378 mg, 2 mmol) in CH_2Cl_2 (10 ml) cooled to 0°C, EDC (382 mg, 2 mmol) and HOAt (270 mg, 2 mmol) were added. After 30 min, H-D-(αMe)Pro-NH*i*Pr [obtained by treatment of the corresponding Boc-protected aminoacid isopropylamide (350 mg, 1.38 mmol) with a solution of TFA and CH_2Cl_2 1:1 for 1 hr] neutralized with NMM (0.45 ml, 4.14 mmol) was added. The reaction mixture was stirred for 4 d. Then, EtOAc was added and the solution was extracted with 10% $KHSO_4$, H_2O, 5% $NaHCO_3$, H_2O, and dried over anhydrous Na_2SO_4. The product was crystallized from EtOAc/PE. Yield: 56 %.

mp: 155-157 °C

Rf_1 = 0.70, Rf_2 = 0.95, Rf_3 = 0.40

$[\alpha]_{589}$: = -99 (c = 0.5, MeOH)

IR (KBr): 3466, 3364, 3333, 1701, 1670, 1633, 1542 cm^{-1}.

^1H NMR ($CDCl_3$): δ 6.74 (bs, 1H, NHiPr), 5.30 (bd, 1H, Ala NH), (m, 2H, Ala α-CH, iPr CH), [m, 2H, (αMe)Pro δ-CH_2], [m, 4H, (αMe)Pro β-CH_2 and γ-CH_2], 1.66 [s, 3H, (αMe)Pro β-CH_3], 1.43 (s, 9H, Boc CH_3), 1.31 (d, 3H, Ala β-CH_3), 1.11 (dd, 6H, iPr CH_3).

Boc-D-(αMe)Pro-L-Ala-NH*i*Pr

To a solution of Boc-D-(αMe)Pro-OH (250 mg, 1.17 mmol) in CH_2Cl_2 (10 ml) cooled to 0°C, HATU (444 mg, 1.17 mmol) and DIEA (0.2 ml, 1.17 mmol) were added. After 30 min, H-L-Ala-NHiPr [obtained by treatment of the corresponding Boc-protected aminoacid isopropylamide (400 mg, 1.75 mmol) with a solution of TFA and CH_2Cl_2 1:1 for 1 hr] neutralized with DIEA (0.2 ml, 1.17 mmol) was added. The reaction mixture was stirred for 4 d. Then, EtOAc was added and the solution was extracted with

10% $KHSO_4$, H_2O, 5% $NaHCO_3$, H_2O, and dried over anhydrous Na_2SO_4. The product was crystallized from EtOAc/petroleum ether. Yield: 62 %.

mp: 149-151 °C

Rf_1 = 0.70, Rf_2 = 0.85, Rf_3 = 0.40

$[\alpha]_{589}$: = -39 (c = 0.5, MeOH)

IR (KBr): 3353, 3277, 1680, 1657, 1538 cm^{-1}.

^1H NMR ($CDCl_3$): δ 7.04 (bs, 1H, NHiPr), 6.40 (bd, 1H, Ala NH), 4.35(m, 1H, Ala α-CH), 4.00 (m, 1H, iPr CH), 3.53 [m, 2H, (αMe)Pro δ-CH_2], 2.4-1.7 [m, 4H, (αMe)Pro β-CH_2 and γ-CH_2], 1.57 [s, 3H, (αMe)Pro β-CH_3], 1.47 (s, 9H, Boc CH_3), 1.37 (d, 3H, Ala β-CH_3), 14 (dd, 6H, iPr CH_3).

Boc-L-(αMe)Pro-Aib-NH*i*Pr

To a solution of Boc-L-(αMe)Pro-OH (300 mg, 1.4 mmol) in CH_2Cl_2 (10 ml) cooled to 0°C, HATU (537 mg, 1.4 mmol) and DIEA (0.23 ml, 1.4 mmol) were added. After 30 min, H-L-Ala-NHiPr [obtained by treatment of the corresponding Boc-protected aminoacid isopropylamide (512 mg, 2.1 mmol) with a solution of TFA and CH_2Cl_2 1:1 for 2 hr] neutralized with DIEA (0.34 ml, 2.1 mmol) was added. The reaction mixture was stirred for 2 d. Then, EtOAc was added and the solution was extracted with 10% $KHSO_4$, H_2O, 5% $NaHCO_3$, H_2O, and dried over anhydrous Na_2SO_4. The product was crystallized from EtOAc/petroleum ether. Yield: 65 %.

mp: 126-128 °C

Rf_1 = 0.80, Rf_2 = 0.85, Rf_3 = 0.35

$[\alpha]_{589}$: = +21.5 (c 0.5, MeOH)

IR (KBr): 3409, 3322, 1676, 1651, 1534 cm^{-1}.

^1H NMR ($CDCl_3$): δ 7.21 (s, 1H, NH*i*Pr), 6.28 (s, 1H, Ala NH), 4.04 (m, 1H, *i*Pr CH), 3.54 [m, 2H, (αMe)Pro δ-CH_2], 2.0-1.8 [m, 4H, (αMe)Pro β,γ-CH_2], 1.56 [s, 3H, (αMe)Pro β-CH_3], 1.53 (s, 6H, Aib CH_3), 1.48 (s, 9H, Boc CH_3), 1.14 (dd, 6H, *i*Pr CH_3).

Z-D-(αMe)Pro-NH*i*Pr

To a solution of Z-(αMe)Pro-OH (600 mg, 2.1 mmol) in anhydrous CH_2Cl_2, cooled to 0°C HOAt (283 mg, 2.1 mmol), EDC (450 mg, 2.1 mmol) and isopropylamine (0.53 ml, 6.3 mmol) were added. The mixture was stirred at room temperature for 48 hs.

Then, the solvent was removed and the residue dissolved in EtOAc. The solution was washed with 10% $KHSO_4$, H_2O, 5% $NaHCO_3$ and H_2O, dried over Na_2SO_4, and evaporated to dryness. Yield 95%.

mp: 123°-125°C

Rf_1 0.90, Rf_2 0.90, Rf_3 0.60.

$[\alpha]_{589}$: +50.8 (c = 0.5, MeOH).

IR (KBr) 3345, 1700, 1645, 1525 cm^{-1}.

^1H NMR (200 MHz, $CDCl_3$): δ 7.35 (m, 5H, Z-phenyl CH), 6.78-5.62 (s, 1H, NH *cis-trans*), 5.16 (m, 2H, Z-CH_2), 3.98 (m, 1H, *i*Pr-CH), 3.6 (m, 2H, δCH_2), 1.83-1.57 (m, 7H, β,γ-CH_2 and αCH_3), 1.04 (d, 6H, *i*Pr-CH_3).

Z-[D-(αMe)Pro]$_2$-NH*i*Pr

To a solution of Z-D-(αMe)Pro-OH (454 mg, 1.8 mmol) in anhydrous CH_2Cl_2, cooled to 0°C, $SOCl_2$ (1.306 ml, 18 mmol) and a drop of DMF was added. The mixture was warmed to a gentle reflux for 7 hs. When TLC analysis showed reaction completion, all the volatiles were removed under vacuum. The residue was dissolved in distilled CH_2Cl_2 and added to a cooled solution of H-D-(αMe)Pro-NH*i*Pr (obtained by Pd-catalyzed hydrogenolysis of 454 mg, 1.5 mmol, of the corresponding Z-protected derivative) and DIPEA (0.25 ml, 1.5 mmol) in CH_2Cl_2. The solution was stirred for 24 hs at room temperature. Then, the solvent was removed under vacuum and the residue purified by flash chromatography (eluant, $CHCl_3$ → $CHCl_3$/EtOH 9:1). Yield 45%.

mp: 127°-130°C

Rf_1 0.70, Rf_2 0.90, Rf_3 0.45.

$[\alpha]_{589}$: -22.6 (c = 0.6, MeOH).

IR (KBr) 3333, 1688, 1659, 1643, 1645, 1523 cm^{-1}.

^1H NMR (200 MHz, $CDCl_3$): δ 7.36 (m, 5H, Z-phenyl CH), 7.05 (d, 1H, NH), 5.26 (m, 1H, Z-CH_2), 4.95 (m, 1H, Z-CH_2), 4.06 (m, 1H, *i*Pr-CH), 3.74 (m, 2H, δCH_2 (αMe)Pro1), 3.36 (m, 2H, δCH_2 (αMe)Pro2), 2.03-1.70 (m, 8H, β,γ-CH_2), 1.55 (s, 3H, αCH_3 (αMe)Pro1), 1.51 (s, 3H, αCH_3 (αMe)Pro1), 1.18 (d, 6H, *i*Pr-CH_3).

Ac-[D-(αMe)Pro]$_2$-NH*i*Pr

To a solution of Z-[D-(αMe)Pro]$_2$-NH*i*Pr (170 mg, 0.33 mmol) in CH_2Cl_2, Pd/C (50 mg) and Ac_2O (0.3 ml, 3.3 mmol) were added. Then H_2 is bubbled for 7 hs, until TLC

analysis showed reaction completion. Then the volatiles were removed under vacuum and the residue dissolved in toluene and evaporated. This operation was repeated several times. The product was purified by flash chromatography (eluant, $CHCl_3$/EtOH 9:1). Yield: 65%.

mp: 179°-183°C

Rf_1 0.60, Rf_2 0.65, Rf_3 0.30.

$[\alpha]_{589}$: +5.0 (c = 0.7, MeOH).

IR (KBr) 3333, 1688, 1659, 1643, 1645, 1523 cm^{-1}.

^1H NMR (200 MHz, $CDCl_3$): δ 7.13 (d, 1H, NH), 4.03 (m, 1H, *i*Pr-CH), 3.71-3.08 (m, 4H, δCH_2), 2.20-1.85 (m, 8H, β,γ-CH_2), 1.57 (s, 3H, αCH_3 (αMe)Pro1), 1.50 (s, 3H, αCH_3 (αMe)Pro1), 1.15 (d, 6H, *i*Pr-CH_3).

_p_BrBz-L-(αMe)Pro-D-(αMe)Pro-NH*i*Pr

To a solution of *p*-bromobenzoic acid (700 mg, 3.5 mmol) in 15 ml CH_2Cl_2, cyanuric fluoride (0.7 ml, 3.7 mmol) and pyridine (0.28 ml, 3.7 mmol) were added. The reaction was left stirring at room temperature for 3 hs, then the mixture was washed with 2x15 ml of cold water, dired over Na_2SO_4 and evaporated. Then, the residue was added to a solution of H-[D-(αMe)Pro]$_2$-NH*i*Pr (obtained by Pd-catalyzed hydrogenolysis of 190 mg, 0.33 mmol, of the corresponding Z-protected derivative) and DIPEA (0.75 ml, 0.4 mmol) was added. The reaction was stirred at room temperature for 12 hs. Then the volatiles were removed under vacuum and the residue purified by flash chromatography (eluant, Et_2O/acetone 8:2). Yield: 56%.

mp: 185°-187°C

Rf_1 0.65, Rf_2 0.90, Rf_3 0.40.

$[\alpha]_{589}$: +38.3 (c = 0.7, MeOH).

IR (KBr) 3439, 1628, 1517 cm^{-1}.

^1H NMR (200 MHz, $CDCl_3$): δ 7.45 (dd, 4H, phenyl CH), 6.43 (d, 1H, NH), 3.98 (m, 1H, *i*Pr-CH), 3.42 (m, 4H, δ-CH_2), 2.35-1.87 (m, 8H, γ,β-CH_2), 1.76 (s, 3H, $\alpha CH_3$1), 1.64 (s, 3H, $\alpha CH_3$2), 1.07 (d, 6H, *i*Pr-CH_3).

Z-L-(αMe)Pro-D-(αMe)Pro-NH*i*Pr

For the synthesis of this compound, the same procedure used for Z-[D-(αMe)Pro]$_2$-NH*i*Pr was followed. Oil. Yield 53%.

Rf_1 0.65, Rf_2 0.45, Rf_3 0.95.

$[\alpha]_{589}$: +43 (c = 0.9, MeOH).

IR (KBr) 3364, 1700, 1642, 1517 cm^{-1}.

^1H NMR (200 MHz, $CDCl_3$): δ 7.31 (m, 5H, Z-phenyl CH), 6.20 (dd, 1H, NH), 6.14 5.12 (m, 1H, Z-CH_2), 4.94 (m, 1H, Z-CH_2), 3.98 (m, 1H, *i*Pr-CH), 3.76-2.98 (m, 8H, γ,δ-CH_2), 2.20-1.80 (m, 6H, β-CH_2), 1.57 (s, 3H, α$CH_3$1), 1.55 (s, 3H, α$CH_3$2), 1.10 (d, 6H, *i*Pr-CH_3).

Ac-L-(αMe)Pro-D-(αMe)Pro-NH*i*Pr

For the synthesis of this compound, the same procedure used for Ac-L-(αMe)Pro-D-(αMe)Pro-NH*i*Pr was followed. Oil. Yield 70%.

Rf_1 0.50, Rf_2 0.65, Rf_3 0.30.

$[\alpha]_{589}$: +7.5 (c = 0.9, MeOH).

IR (KBr) 3345, 1641, 1520 cm^{-1}.

^1H NMR (200 MHz, $CDCl_3$): δ 6.51 (d, 1H, NH), 3.98 (m, 1H, *i*Pr-CH), 3.82-3.31 (m, 4H, δ-CH_2), 2.26-1.82 (m, 8H, γ,β-CH_2), 1.58 (s, 3H, α$CH_3$1), 1.54 (s, 3H, α$CH_3$2), 1.05 (m, 6H, *i*Pr-CH_3).

Pro derivatives

Z-D-Pro-OH

To a solution of H-D-Pro-OH (1.6 g, 0.014 mol) in 7.5 ml H_2O, Et_3N was added (2.02 ml, 0.014 mol). To this solution was added dropwise Z-OSu (3.43 g, 0.014 mol) in 4 ml CH_3CN under stirring. The mixture was left stirring overnight, then the CH_3CN is removed and pH was brought to 8 with the addition of Et_3N. Unreacted Z-OSu was extracted with Et_2O. Then a solution of 10% $KHSO_4$ was added to pH 2. The aqueous phase was extracted with 3x20 mL EtOAc. The organic phase was washed with H_2O, brine, dried over Na_2SO_4 and evaporated to dryness. Yield: 89%.

mp: 75-77 °C.

Rf_1: 0.60, Rf_2: 0.90, Rf_3: 0.45.

$[\alpha]_D^{20}$ = +41 (c = 2, MeOH)

IR (KBr): 3295, 3085, 1697, 1683, 1547 cm^{-1}.

^{1}H NMR (200MHz, $CDCl_3$): δ 11.25 (s, 1H, COOH), 7.35 (m, 5H, Z phenyl-CH), 5.16 (m, 2H, Z-CH_2), 4.43 (m, 1H, α-CH), 3.60 (m, 2H, γ-CH_2), 2.16-1.93 (m, 4H, δ,β-CH_2).

Boc-L-Pro-NH*i*Pr

To a solution of Boc-L-Pro-OH (0.5 g, 2.3 mmol) in CH_2Cl_2) cooled to 0°C, EDC (440 mg, 2.3 mmol) and HOBt (310 mg, 2.3 mmol) were added. After 20 min, isopropylamine (0.4 ml, 4.6 mmol) was added and the reaction was stirred at room temperature for 2 d. Then, the solvent was removed under reduced pressure and the residue dissolved in EtOAc. The solution was washed with 10% $KHSO_4$, H_2O, 5% $NaHCO_3$ and H_2O, dried over anhydrous Na_2SO_4, and evaporated to dryness. The product was crystallized from EtOAc/PE. Yield: 68 %.

mp: 129-130 °C

Rf_1 = 0.70, Rf_2 = 0.90, Rf_3 = 0.40

$[\alpha]_{589}$: = -54 (c = 0.5, MeOH)

IR (KBr): 3296, 3084, 1697, 1681, 1651, 1550 cm^{-1}.

^{1}H NMR ($CDCl_3$): δ 6.75-5.81 (2bs, 1H, *cis-trans* NH*i*Pr), 4.12 (d, 1H, Pro α-CH), 3.43 (m, 2H, Pro δ-CH_2), 2.4-1.8 (m, 4H, Pro β,γ-CH_2), 1.46 (s, 9H, Boc CH_3), 1.13 (dd, 6H, *i*Pr CH_3).

Boc-D-Pro-NH*i*Pr

To a solution of Boc-D-Pro-OH (600 mg, 2.3 mmol) in CH_2Cl_2 cooled to 0°C, EDC (432 mg, 2.3 mmol) and HOBt (305 mg, 2.3 mmol) were added. After 20 min, isopropylamine (0.6 ml, 6.9 mmol) was added and the reaction was stirred at room temperature for 1 d. Then, the solvent was removed under reduced pressure and the residue dissolved in EtOAc. The solution was washed with 10% $KHSO_4$, H_2O, 5% $NaHCO_3$ and H_2O, dried over anhydrous Na_2SO_4, and evaporated to dryness. The product was crystallized from EtOAc/PE. Yield: 70 %.

mp: 123-124 °C

Rf_1 = 0.70, Rf_2 = 0.90, Rf_3 = 0.40

$[\alpha]_{589}$: = +56.5 (c = 0.5, MeOH)

IR (KBr): 3279, 3085, 1697, 1650, 1554 cm^{-1}.

^{1}H NMR ($CDCl_3$): δ 6.75-5.81 (2s, 1H, *cis-trans* NH*i*Pr), 4.12 (m, 1H, Pro α-CH), 3.42 (m, 2H, Pro δ-CH_2), 2.7-1.8 (m, 4H, Pro β,γ-CH_2), 1.46 (s, 9H, Boc CH_3), 1.13 (dd, 6H, *i*Pr CH_3).

Z-D-Pro-NH*i*Pr

To a solution of Z-D-Pro-OH (2.73 g, 11 mmol) in anhydrous CH_2Cl_2, cooled to 0°C, cooled to 0°C HOBt (1.48 g, 11 mmol), EDC (2.1 g, 11 mmol) and isopropylamine (2.78 ml, 33 mmol) were added. The mixture was stirred at room temperature for 8 hs. Then, the solvent was removed and the residue dissolved in EtOAc. The solution was washed with 10% $KHSO_4$, H_2O, 5% $NaHCO_3$ and H_2O, dried over Na_2SO_4, and evaporated to dryness. Yield 87%.

mp: 135-137 °C.

Rf_1: 0.70, Rf_2: 0.90, Rf_3: 0.50.

$[\alpha]_D^{20}$ = +45 (c = 2, MeOH)

IR (KBr): 3301, 3078, 1670, 1545 cm^{-1}.

^{1}H NMR (200MHz, $CDCl_3$): δ 7.32 (m, 5H, Z phenyl-CH), 5.16 (m, 2H, Z-CH_2), 4.43 (m, 1H, α-CH), 3.99 (m, 1H, *i*Pr-CH), 3.60 (m, 2H, γ-CH_2), 2.16-1.93 (m, 4H, δ,β-CH_2), 1.12 (m, 6H, *i*Pr-CH_3).

Boc-L-Pro-L-Ala-NH*i*Pr

To a solution of Boc-L-Pro-OH (160 mg, 0.8 mmol) in CH_2Cl_2 (5 ml) cooled to 0°C, HATU (304 mg, 0.8 mmol) and DIEA (0.04 ml, 0.8 mmol) were added. After 30 min, H-L-Ala-NHiPr [obtained by treatment of the corresponding Boc-protected aminoacid isopropylamide (200 mg, 0.8 mmol) with a solution of TFA and CH_2Cl_2 1:1 for 1 hr] neutralized with DIEA (0.08 ml, 1.6 mmol) was added. The reaction mixture was stirred for 2 d. Then, EtOAc was added and the solution was extracted with 10% $KHSO_4$, H_2O, 5% $NaHCO_3$, H_2O, and dried over anhydrous Na_2SO_4. The product was crystallized from EtOAc/PE. Yield: 60 %.

mp: 185-187 °C

Rf_1 = 0.60, Rf_2 = 0.85, Rf_3 = 0.40

$[\alpha]_{589}$: = -80 (c = 0.5, MeOH)

IR (KBr): 3296, 1699, 1645, 1543 cm^{-1}.

^{1}H NMR ($CDCl_3$): δ 6.60 (2s, 2H, NH*i*Pr and Ala NH), 4.39 (m, 1H, Ala α-CH), 4.24 (m, 1H, Pro α-CH), 4.04 (m, 1H, *i*Pr CH), 3.46 (m, 2H, Pro δ-CH_2), 2.2-1.7 (m, 4H, Pro β,γ-CH_2), 1.47 (s, 9H, Boc CH_3), 1.36 (d, 3H, Ala β-CH_3), 1.14 (dd, 6H, *i*Pr CH_3).

Z-[D-Pro]$_2$-NH*i*Pr

To a solution of Z-D-Pro-OH (1.19 g, 4.7 mmol) in anhydrous CH_2Cl_2, cooled to 0°C HOBt (635 mg, 4.7 mmol), EDC (902 mg, 4.7 mmol) and H-D-Pro-NH*i*Pr (obtained by Pd-catalyzed hydrogenolysis of 1.16 g, 4 mmol, of the corresponding Z-protected derivative) and DIPEA (0.87 ml, 5 mmol) was added. The reaction was stirred at room temperature for 12 hs. Then the volatiles were removed under vacuum and the residue dissolved in EtOAc. The solution was washed with 10% $KHSO_4$, H_2O, 5% $NaHCO_3$ and H_2O, dried over Na_2SO_4, evaporated to dryness and the residue purified by flash chromatography (eluant, $CHCl_3$/EtOH 95:5). Oil. Yield: 56%.

Rf_1: 0.75, Rf_2: 0.75, Rf_3: 0.45.

$[\alpha]_D^{20}$ = +83.1 (c = 0.9, MeOH)

IR (KBr): 3316, 1704, 1677, 1645, 1543 cm^{-1}.

^{1}H NMR (200MHz, $CDCl_3$): δ 7.33 (m, 5H, Z phenyl-CH), 6.99 (d, 1H, NH), 5.07 (m, 2H, Z-CH_2), 4.58 (m, 1H, α-CH Pro1), 4.35 (m, 1H, α-CH Pro2), 4.01 (m, 1H, *i*Pr-CH), 3.75-3.20 (m, 4H, γ-CH_2), 2.50-1.83 (m, 8H, δ,β-CH_2), 1.08 (m, 6H, *i*Pr-CH_3).

Ac-[D-Pro]$_2$-NH*i*Pr

To a solution of Z-[D-Pro]$_2$-NH*i*Pr (710 mg, 1.8 mmol) in CH_2Cl_2, Pd/C (150 mg) and Ac_2O (1.8 ml, 18 mmol) were added. Then H_2 is bubbled for 8 hs, until TLC analysis showed reaction completion. Then the volatiles were removed under vacuum and the residue dissolved in toluene and evaporated. This operation was repeated several times. The product was purified by flash chromatography (eluant, $CHCl_3$/EtOH 95:5). Oil. Yield: 55%.

Rf_1: 0.60, Rf_2: 0.65, Rf_3: 0.30.

$[\alpha]_D^{20}$ = +104.1 (c = 1, MeOH)

IR (KBr): 3300, 1640, 1543 cm^{-1}.

^{1}H NMR (200MHz, DMSO-d_6): δ 7.80 (d, 1H, NH), 4.71 (m, 1H, α-CH Pro1), 4.50 (m, 1H, α-CH Pro2), 4.20 (m, 1H, *i*Pr-CH), 3.80-3.34 (m, 4H, γ-CH_2), 2.12-1.65 (m, 8H, δ,β-CH_2), 1.01 (m, 6H, *i*Pr-CH_3).

Z-L-Pro-D-Pro-NH*i*Pr

For the synthesis of this compound, the same procedure used for Z-[D-Pro]-NH*i*Pr was followed. The product is recristallized from $CHCl_3$/PE.Yield: 60%.

mp: 118°-122°C.

Rf_1: 0.60, Rf_2: 0.90, Rf_3: 0.45.

$[\alpha]_D^{20}$ = +50.4 (c = 0.8, MeOH)

IR (KBr): 3363, 1653, 1520 cm^{-1}.

^{1}H NMR (200MHz, $CDCl_3$): δ 7.32 (m, 5H, Z phenyl-CH), 6.97 (d, 1H, NH), 5.09 (m, 2H, Z-CH_2), 4.60 (m, 1H, α-CH Pro1), 4.43 (m, 1H, α-CH Pro2), 4.04 (m, 1H, *i*Pr-CH), 3.98-3.42 (m, 4H, γ-CH_2), 2.36-1.86 (m, 8H, δ,β-CH_2), 1.10 (m, 6H, *i*Pr-CH_3).

Ac-L-Pro-D-Pro-NH*i*Pr

For the synthesis of this compound, the same procedure used for Ac-[D-Pro]-NH*i*Pr was followed.

mp: 143°-146°C.

Rf_1: 0.35, Rf_2: 0.65, Rf_3: 0.30.

$[\alpha]_D^{20}$ = +66.1 (c = 0.8, MeOH)

IR (KBr): 3333, 1666, 1621, 1525 cm^{-1}.

^{1}H NMR (200MHz, $CDCl_3$): δ 7.13 (d, 1H, NH), 4.58 (m, 1H, α-CH Pro1), 4.45 (m, 1H, α-CH Pro2), 4.04 (m, 1H, *i*Pr-CH), 3.73-3.39 (m, 4H, γ-CH_2), 2.31-1.78 (m, 8H, δ,β-CH_2), 1.15 (m, 6H, *i*Pr-CH_3).

5.3.3 Macrocyclization on helical peptides

Synthesis of ladder peptide: double-metathesis approach

Z-Asp(*t*Bu)-Aib$_2$-OMe

To a solution of Z-Asp(*t*Bu)-OH (2.88 g, 8.5 mmol) in anhydrous CH_2Cl_2, cooled to 0°C, HOAt (1.14, 8.5 mmol) and EDC (1.61 g, 8.5 mmol) were added. After 2 min this solution was added to a solution of H-Aib$_2$-O*t*Bu (obtained from Pd-catalyzed hydrogenolysis of 2.85 g, 8.5 mmol of the corresponding Z-protected derivative) in CH_2Cl_2. To the resulting mixture DIPEA (2.9 ml, 8.5 mmol) was added. The mixture was stirred at room temperature for 48 hs while keeping the pH at 8 by addition of DIPEA. Then, the solvent was removed and the residue dissolved in EtOAc. The solution was washed with 10% $KHSO_4$, H_2O, 5% $NaHCO_3$ and H_2O, dried over Na_2SO_4, and evaporated to dryness. The product was purified by flash chromatography (eluant, $CHCl_3$/EtOH, 98:2 → 9:1). Yield 65%.

mp: 153°-155°C

Rf_1: 0.80, Rf_2: 0.95, Rf_3: 0.40.

$[\alpha]_D^{20}$ = -24.5 (c = 0.5, MeOH).

IR (KBr): 3344, 1728, 1678, 1521, 1151 cm^{-1}.

^{1}H NMR (200 MHz, $CDCl_3$): δ 7.36 (m, 5H, Z phenyl-CH), 6.98 (s, 1H, N-H Aib), 6.74 (s, 1H, N-H Aib), 5.84 (d, 1H, N-H Asp), 5.14 (s, 2H, Z-CH_2), 4.42 (m, 1H, α-CH Asp), 3.70 (s, 3H, OMe), 2.94-2.67 (m, 2H, β-CH_2 Asp), 1.48 (s, 6H, β-CH_3 Aib), 1.47 (s, 6H, β-CH_3 Aib), 1.43 (s, 9H, CH_3-*t*Bu).

Z-Asp-Aib$_2$-OMe

To a solution of Z-Asp(*t*Bu)-Aib$_2$-OMe (1 g, 3 mmol) in anhydrous CH_2Cl_2, TFA (5 ml) was added. The mixture was stirred for 8 hs, then the volatiles were removed under vacuum. To the residue Et_2O (10 ml) was added and removed under vacuum. This operation was repeated until a white solid was obtained. Yield: 99%.

mp: 186°-187°C

Rf_1: 0.40, Rf_2: 0.70, Rf_3: 0.30.

$[\alpha]_D^{20}$ = -22.8 (c = 0.5, MeOH).

IR (KBr): 3362, 1729, 1652, 1527, 1160 cm^{-1}.

^{1}H NMR (200 MHz, $CDCl_3$): δ 7.35 (m, 5H, Z phenyl-CH), 7.04 (s, 1H, N-H Aib), 7.03 (s, 1H, N-H Aib), 6.08 (d, 1H, N-H Asp), 5.13 (s, 2H, Z-CH_2), 4.50 (m, 1H, α-CH Asp), 3.71 (s, 3H, OMe), 3.06-2.73 (m, 2H, β-CH_2 Asp), 1.48 (s, 6H, β-CH_3 Aib), 1.45 (s, 6H, β-CH_3 Aib).

Z-Asp(OAl)-Aib$_2$-OMe [(**2**) in **Table 4.1**]

To a solution of Z-Asp-Aib$_2$-OMe (273 mg, 0.6 mmol) in anhydrous CH_2Cl_2, cooled to 0°C, DMAP (81 mg, 0.66 mmol) and EDC (126 mg, 0.66 mmol) were added. After 5 min allyl alcohol (0.134 ml, 1.8 mmol) and DIPEA (0.114 ml, 0.66 mmol) were added. The mixture was stirred at room temperature for 24 hs, then the solvent was removed and the residue dissolved in EtOAc. The solution was washed with 10% $KHSO_4$, H_2O, 5% $NaHCO_3$ and H_2O, dried over Na_2SO_4, and evaporated to dryness. Yield 75%.

mp: 83°-85°C

Rf_1: 0.70, Rf_2: 0.80, Rf_3: 0.45.

$[\alpha]_D^{20}$ = -18.6 (c = 0.5, MeOH).

IR (KBr): 3348, 1719, 1670, 1662, 1524 cm^{-1}.

^{1}H NMR (200 MHz, $CDCl_3$): δ 7.35 (m, 5H, Z phenyl-CH), 6.89 (s, 1H, N-H Aib), 6.81 (s, 1H, N-H Aib), 6.73 (d, 1H, N-H Asp), 5.88 (m, 1H, C*H*=CH_2), 5.33 (m, 1H, CH=C*H*-H), 5.25 (m, 1H, CH=C*H*-H), 5.12 (s, 2H, Z-CH_2), 4.55 (d, 2H, CH_2-CH=CH_2), 4.47 (m, 1H, α-CH Asp), 3.68 (s, 3H, OMe), 2.95-2.79 (m, 2H, β-CH_2 Asp), 1.46 (s, 6H, β-CH_3 Aib), 1.45 (s, 6H, β-CH_3 Aib).

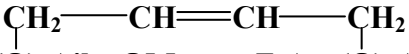

Z-Asp(O)-Aib$_2$-OMe **Z-Asp(O)-Aib$_2$-OMe** [(**3**) in **Table 4.1**]

Z-Asp(OAl)-Aib$_2$-OMe (50 mg, 0.1 mmol) was dissolved in $CHCl_3$ (1 ml) in a nitrogen-flushed flask. 1,3-*bis*(2,4,6-trimethylphenyl)-2-imidazolidinylidene)dichloro(phenylmethylene)(tricyclohexyl phosphine) ruthenium (second generation Grubbs' catalyst, 4.3 mg, 0.005 mmol, 5 mol%) was added in a single portion. After stirring at room temperature for 48 hs, the TLC revealed formation of a new lower-Rf product. Then the solvent was evaporated and the residue purified by flash chromatography (eluant, $CHCl_3$/EtOH 95:5). Yield: 65%.

mp: 126°-129°C

Rf_1: 0.60, Rf_2: 0.85, Rf_3: 0.40.

ESI-MS: calcd: 955.62; found: 955.46 $[M+H]^+$

$[\alpha]_D^{20}$ = -19.3 (c = 0.5, MeOH).

IR (KBr): 3352, 1719, 1698, 1680, 1527, 1154 cm^{-1}.

^1H NMR (200 MHz, $CDCl_3$): δ 7.35 (m, 10H, Z phenyl-CH), 6.89 (s, 2H, N-H Aib), 6.81 (s, 2H, N-H Aib), 6.72 (d, 2H, N-H Asp), 5.78-5.71 (m, 4H, C*H*=C*H cis*/*trans* ratio ~ 1:10), 5.12 (s, 4H, Z-CH_2), 4.55 (d, 4H, CH_2-CH=CH_2), 4.48 (m, 2H, α-CH Asp), 3.69 (s, 6H, OMe), 2.97-2.78 (m, 4H, β-CH_2 Asp), 1.49 (s, 12H, β-CH_3 Aib), 1.47 (s, 12H, β-CH_3 Aib).

Z-Aib-Asp(O-CH_2-CH_2-CH_2-CH_2-O)-Aib$_2$-OMe Z-Aib-Asp(O-CH_2-CH_2-CH_2-CH_2-O)-Aib$_2$-OMe [(**4**) in **Table 4.1**]

To a solution of Z-Aib-OH (1.45 g, 6 mmol) in anhydrous CH_2Cl_2, cooled to 0°C, HOAt (836 mg, 6 mmol) and EDC (1.25 g, 6 mmol) were added. After 2 min this solution was added to a solution of unprotected peptide [(**3**) in **Table 4.1**, obtained from Pd-catalyzed hydrogenolysis of 2.35 g, 2.5 mmol of the corresponding Z-protected, unsaturated derivative] in CH_2Cl_2. To the resulting mixture DIPEA (1.04 ml, 6 mmol) was added. The mixture was stirred at room temperature for 48 hs while keeping the pH at 8 by addition of DIPEA. Then, the solvent was removed and the residue dissolved in EtOAc. The solution was washed with 10% $KHSO_4$, H_2O, 5% $NaHCO_3$ and H_2O, dried over Na_2SO_4, and evaporated to dryness. The product was purified by flash chromatography (eluant, $CHCl_3$/EtOH, 95:5). Yield 52%.

mp: 180°-182°C

Rf_1: 0.65, Rf_2: 0.75, Rf_3: 0.45.

$[\alpha]_D^{20}$ = -13.5 (c = 0.5, MeOH).

IR (KBr): 3345, 1729, 1694, 1669, 1534, 1270, 1155 cm^{-1}.

^1H NMR (200 MHz, $CDCl_3$): δ 7.49 (d, 2H, NH Asp), 7.41 (s, 2H, N-H Aib), 7.36 (m, 10H, Z phenyl-CH), 6.94 (s, 2H, N-H Aib), 6.11 (s, 2H, N-H Aib), 5.07 (s, 4H, Z-CH_2), 4.45 (m, 2H, α-CH Asp), 4.06 (m, 4H, OC$H_2$$CH_2$), 3.60 (s, 6H, OMe), 2.85 (q, 4H, β-CH_2 Asp), 1.65 (m, 4H, OCH_2CH_2), 1.45-1.43 (m, 36H, β-CH_3 Aib).

Z-Aib$_2$-Asp(O-CH_2-CH_2-CH_2-CH_2-O)-Aib$_2$-OMe Z-Aib$_2$-Asp(O-CH_2-CH_2-CH_2-CH_2-O)-Aib$_2$-OMe [(**5**) in **Table 4.1**]

To a solution of Z-Aib-OH (981 mg, 4.1 mmol) in anhydrous CH_2Cl_2, cooled to 0°C, HOAt (558 mg, 4.1 mmol) and EDC (786 mg, 4.1 mmol) were added. After 2 min this

solution was added to a solution of unprotected peptide [(**4**) **Table 4.1**, obtained from Pd-catalyzed hydrogenolysis of 2.34 g, 2.1 mmol of the corresponding Z-protected derivative] in CH_2Cl_2. To the resulting mixture DIPEA (0.71 ml, 4.1 mmol) was added. The mixture was stirred at room temperature for 72 hs while keeping the pH at 8 by addition of DIPEA. Then, the solvent was removed and the residue dissolved in EtOAc. The solution was washed with 10% $KHSO_4$, H_2O, 5% $NaHCO_3$ and H_2O, dried over Na_2SO_4, and evaporated to dryness. The product was purified by flash chromatography (eluant, $CHCl_3$/EtOH 9:1). Yield 46%.

mp: 167°-169°C

Rf_1: 0.60, Rf_2: 0.70, Rf_3: 0.35.

ESI-MS: calcd: 1297.60; found: 1297.82 $[M+H]^+$; 649.36 $[M]^{2+}$

$[\alpha]_D^{20} = +8.1$ (c = 0.5, MeOH).

IR (KBr): 3365, 3316, 1739,1706, 1668, 1533, 1261, 1154 cm^{-1}.

^1H NMR (200 MHz, $CDCl_3$): δ 7.95 (d, 2H, NH Asp), 7.53 (s, 2H, N-H Aib), 7.35 (m, 10H, Z phenyl-CH), 7.02 (s, 2H, N-H Aib), 6.98 (s, 2H, N-H Aib), 6.30 (s, 2H, N-H Aib), 5.15 (s, 4H, Z-CH_2), 4.58 (m, 1H, α-CH Asp1), 4.13 (m, 1H, α-CH Asp2), 4.01 (m, 4H, OC$H_2$$CH_2$), 3.70 (s, 6H, OMe), 2.92 (m, 4H, β-CH_2 Asp), 1.70 (m, 4H, OCH_2CH_2), 1.57-1.39 (m, 48H, β-CH_3 Aib).

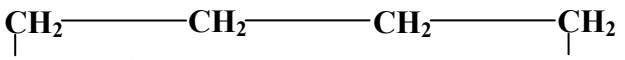

Z-Asp(*t*Bu)-Aib$_2$-Asp(O)-Aib$_2$-OMe **Z-Asp(*t*Bu)-Aib$_2$-Asp(O)-Aib$_2$-OMe**

[(**6**) in **Table 4.1**]

To a solution of Z-Asp(*t*Bu)-OH (975 mg, 2.7 mmol) in anhydrous CH_2Cl_2, cooled to 0°C, HOAt (390 mg, 2.7 mmol) and EDC (550 mg, 2.7 mmol) were added. After 2 min this solution was added to a solution of unprotected peptide [(**5**) in **Table 4.1**, obtained from Pd-catalyzed hydrogenolysis of 1.40 g, 0.9 mmol of the corresponding Z-protected derivative] in CH_2Cl_2. To the resulting mixture DIPEA (0.49 ml, 2.7 mmol) was added. The mixture was stirred at room temperature for 36 hs while keeping the pH at 8 by addition of DIPEA. Then, the solvent was removed and the residue dissolved in EtOAc. The solution was washed with 10% $KHSO_4$, H_2O, 5% $NaHCO_3$ and H_2O, dried over Na_2SO_4, and evaporated to dryness. The product was purified by flash chromatography (eluant, $CHCl_3$/EtOH 95:5 → 9:1). Yield 62%.

mp: 203°-205°C

Rf_1: 0.65, Rf_2: 0.75, Rf_3: 0.40.

ESI-MS: calcd: 1640.85; found: 1640.85 $[M+H]^+$; 820.93 $[M]^{2+}$

$[\alpha]_D^{20}$ = +27.4 (c = 0.5, MeOH).

IR (KBr): 3321, 1731, 1664, 1530, 1153 cm^{-1}.

^1H NMR (200 MHz, $CDCl_3$): δ 7.86 (d, 2H, NH Asp1), 7.41 (s, 2H, N-H Aib), 7.35 (m, 10H, Z phenyl-CH), 7.33 (s, 2H, N-H Aib), 7.10 (s, 2H, N-H Aib), 7.08 (s, 2H, N-H Aib), 6.54 (s, 2H, N-H Asp2), 5.04 (s, 4H, Z-CH_2), 4.32 (m, 4H, α-CH Asp), 3.92 (m, 4H, OC$H_2$$CH_2$), 3.62 (s, 6H, OMe), 2.88-2.75 (m, 8H, β-CH_2 Asp), 2.46 (m, 4H, $OCH_2C$$H_2$), 1.44-1.35 (m, 48H, β-$CH_3$ Aib), 1.33 (s, 18H, CH_3-*t*Bu).

Z-Aib-Asp(*t*Bu)-Aib$_2$-Asp(O)-Aib$_2$-OMe **Z-Aib-Asp(*t*Bu)-Aib$_2$-Asp(O)-Aib$_2$-OMe**

To a solution of Z-Aib-OH (605 mg, 2.6 mmol) in anhydrous CH_2Cl_2, cooled to 0°C, HOAt (348 mg, 2.6 mmol) and EDC (490 mg, 2.6 mmol) were added. After 2 min this solution was added to a solution of unprotected peptide [(**6**) **Table 4.1**, obtained from Pd-catalyzed hydrogenolysis of 1.02 g, 0.6 mmol of the corresponding Z-protected derivative] in CH_2Cl_2. To the resulting mixture DIPEA (0.44 ml, 2.6 mmol) was added. The mixture was stirred at room temperature for 96 hs while keeping the pH at 8 by addition of DIPEA. Then, the solvent was removed and the residue dissolved in EtOAc. The solution was washed with 10% $KHSO_4$, H_2O, 5% $NaHCO_3$ and H_2O, dried over Na_2SO_4, and evaporated to dryness. The product was purified by flash chromatography (eluant, EtOAc/acetone 9:1). Yield 35%.

mp: 219°-221°C

Rf_1: 0.60, Rf_2: 0.70, Rf_3: 0.40.

ESI-MS: calcd: 1808.93; found: 905.46 $[M]^{2+}$

$[\alpha]_D^{20}$ = +36.8 (c = 0.5, MeOH).

IR (KBr): 3314, 1733, 1663, 1532, 1153 cm^{-1}.

^1H NMR (200 MHz, $CDCl_3$): δ 7.83 (s, 2H, N-H Aib), 7.76 (d, 4H, NH Asp), 7.44 (s, 2H, N-H Aib), 7.33 (m, 10H, Z phenyl-CH), 7.17 (s, 2H, N-H Aib), 7.09 (s, 2H, N-H Aib), 7.08 (s, 2H, N-H Aib), 6.23 (s, 2H, NH Aib), 5.09 (s, 4H, Z-CH_2), 4.41 (m, 4H, α-CH Asp), 4.18 (m, 4H, α-CH Asp), 3.99 (m, 4H, OC$H_2$$CH_2$), 3.61 (s, 6H, OMe), 2.96-2.72 (m, 8H, β-CH_2 Asp), 1.59 (m, 4H, $OCH_2C$$H_2$), 1.48-1.37 (m, 60H, β-$CH_3$ Aib), 1.35 (s, 18H, CH_3-*t*Bu).

Z-Aib-Asp-Aib$_2$-Asp(O-CH$_2$-CH$_2$-CH$_2$-CH$_2$-O)-Aib$_2$-OMe

To a solution of Z-Aib-Asp(*t*Bu)-Aib$_2$-Asp(O-butyl tether)-Aib$_2$-OMe (previous paragraph) in anhydrous CH_2Cl_2, TFA (5 ml) was added. The mixture was stirred for 5 hs, then the volatiles were removed under vacuum. To the residue Et_2O (10 ml) was added and removed under vacuum. This operation was repeated until a white solid was obtained. Yield: 97%.

mp: 191°-194°C

Rf_1: 0.35, Rf_2: 0.55, Rf_3: 0.30.

ESI-MS: calcd: 1697.81; found: 849.90 $[M]^{2+}$

$[\alpha]_D^{20} = +11.5$ (c = 0.5, MeOH).

IR (KBr): 3309, 1710, 1657, 1532, 1147 cm^{-1}.

^{1}H NMR (200 MHz, $CDCl_3$): δ 7.85 (d, 4H, NH Asp1), 7.81 (s, 2H, N-H Aib), 7.79 (s, 2H, N-H Aib), 7.59 (s, 2H, N-H Aib), 7.35 (m, 10H, Z phenyl-CH), 7.15 (s, 2H, N-H Aib), 5.09 (s, 4H, Z-CH_2), 4.70 (m, 2H, α-CH Asp), 4.45 (m, 2H, α-CH Asp), 4.03 (m, 4H, OC*H*$_2$CH$_2$), 3.65 (s, 6H, OMe), 2.08-2.76 (m, 8H, β-CH_2 Asp), 1.63 (m, 4H, OCH$_2$C*H*$_2$), 1.66-1.45 (m, 60H, β-CH_3 Aib).

Z-Aib-Asp(OAl)-Aib$_2$-Asp(O-CH$_2$-CH$_2$-CH$_2$-CH$_2$-O)-Aib$_2$-OMe

ladder "open" [(**7**), in **Table 4.1**]

To a solution of Z-Aib-Asp-Aib$_2$-Asp(diester)-Aib$_2$-OMe (50 mg, 0.03 mmol) in anhydrous CH_2Cl_2, cooled to 0°C, DMAP (18 mg, 0.07 mmol) and EDC (26 mg, 0.07 mmol) were added. After 5 min allyl alcohol (0.200 ml, 30 mmol) was added. The mixture was stirred at room temperature for 72 hs, then the solvent was removed and the residue was purified by flash chromatography (eluant, $CHCl_3$→$CHCl_3$/EtOH 99:1→98:2). Yield 53%.

mp: 176°-178°C

Rf_1: 0.70, Rf_2: 0.85, Rf_3: 0.40.

ESI-MS: calcd: 1777.96; found: 889.95 $[M]^{2+}$

HPLC: t_r = 12.20 min; Conditions: analytical Vydac C_{18} column (particle size: 5 μm; pore size: 300 Å); gradient system, 40→80% B in 20 min; flow rate, 1 ml/min (eluant

A: H_2O/MeCN 9/1 + 0.05% TFA; eluant B: MeCN/H_2O 9/1 + 0.05% TFA); room temperature; absorbance detector at 226 nm.

$[\alpha]_D^{20}$ = -6.6 (c = 0.5, MeOH).

IR (KBr): 3316, 1735, 1667, 1524, 1147, 740 cm^{-1}.

^1H NMR (600 MHz, CD_3OH): δ 8.50 (d, 4H, NH Asp), 8.08 (s, 2H, N-H Aib), 8.03 (d, 4H, NH Asp), 7.77 (s, 2H, N-H Aib), 7.74 (s, 2H, N-H Aib), 7.70 (s, 2H, N-H Aib), 7.46 (s, 2H, N-H Aib), 7.38 (m, 10H, Z phenyl-CH), 5.95 (m, 2H, C*H*=CH_2), 5.35 (m, 2H, CH=C*H*-H), 5.21 (m, 2H, CH=C*H*-H), 5.05 (s, 4H, Z-CH_2), 4.61 (m, 2H, α-CH Asp), 4.47 (m, 1H, α-CH Asp), 4.38 (m, 1H, α-CH Asp), 4.10 (m, 4H, OCH_2CH_2), 3.67 (s, 6H, OMe), 3.06-2.85 (m, 8H, β-CH_2 Asp), 1.68 (m, 4H, OCH_2CH_2), 1.49-1.41 (m, 60H, β-CH_3 Aib).

Ladder RCM [(**8**) in **Table 4.1**]

Compound [(**7**) in **Table 4.1**] (20 mg, 0.01 mmol) was dissolved in distilled CH_2Cl_2 (3 ml, 5 mM) in a nitrogen-flushed flask equipped with a water-cooled condenser. Second generation Grubbs' catalyst (1 mg, 5 mol%) was added under an inert atmosphere. The solution was warmed at a gentle reflux for 8 hs, when the TLC revealed consumption of the starting material and formation of a new lower-Rf product. Then the reaction was quenched by adding 3 µl of ethyl vinyl ether directly to the flask after cooling. Stirring was continued for 20 min, after which the solvent was evaporated under reduced pressure and the residue purified by flash chromatography (eluant, $CHCl_3$EtOH 99:1→ $CHCl_3$/EtOH 9:1). Yield: 65%.

mp: 155°-156°C

Rf_1: 0.65, Rf_2: 0.80, Rf_3: 0.40.

ESI-MS: calcd: 1748.84; found: 875.45 $[M]^{2+}$

HPLC: t_r = 14.10 min; Conditions: analytical Vydac C_{18} column (particle size: 5 µm; pore size: 300 Å); gradient system, 40→80% B in 20 min; flow rate, 1 ml/min (eluant A: H_2O/MeCN 9/1 + 0.05% TFA; eluant B: MeCN/H_2O 9/1 + 0.05% TFA); room temperature; absorbance detector at 226 nm.

$[\alpha]_D^{20}$ = -34.2 (c = 0.5, MeOH).

IR (KBr): 3312, 1735, 1662, 1264, 1159, 732 cm^{-1}.

^{1}H NMR (600 MHz, CD_3OH): δ 8.45 (d, 4H, NH Asp), 8.11 (d, 2H, N-H Asp), 8.08 (s, 4H, NH Aib), 7.78 (s, 2H, N-H Aib), 7.77 (s, 2H, N-H Aib), 7.69 (s, 2H, N-H Aib), 7.49 (s, 2H, N-H Aib), 7.38 (m, 10H, Z phenyl-CH), 5.91-5.75 (m, 2H, C*H*=C*H*, *cis*/*trans* ratio 1:15), 4.88 (s, 4H, Z-CH_2), 4.62 (m, 6H, CH_2-CH=CH_2 and 2H, α-CH Asp), 4.49 (m, 1H, α-CH Asp), 4.34 (m, 1H, α-CH Asp), 4.11 (m, 4H, OC$H_2$$CH_2$), 3.67 (s, 6H, OMe), 3.11-2.78 (m, 8H, β-CH_2 Asp), 1.70 (m, 4H, OCH_2CH_2), 1.47-1.39 (m, 60H, β-CH_3 Aib).

Synthesis of ladder peptide: double esterification-metathesis approach

Z-Asp(OCH$_2$CH$_2$CH$_2$CH$_2$OH)-Aib$_2$-OMe

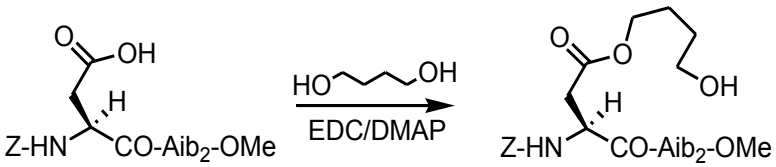

To a solution of Z-Asp-Aib$_2$-OMe (700 mg, 1.6 mmol) in anhydrous CH_2Cl_2, cooled to 0°C, DMAP (293 mg, 2.4 mmol) and EDC (460 mg, 2.4 mmol) were added. After 5 min 1,4-butanediol (0.424 ml, 7.2 mmol) was added. The mixture was stirred at room temperature for 12 hs, then the solvent was removed and the residue dissolved in EtOAc. The solution was washed with 10% $KHSO_4$, H_2O, 5% $NaHCO_3$ and H_2O, dried over Na_2SO_4, and evaporated to dryness. Yield 83%.

mp: 65°-67°C

Rf_1: 0.60, Rf_2: 0.80, Rf_3: 0.40.

ESI-MS: calcd: 524.23; found: 524.25 $[M+1]^+$

$[\alpha]_D^{20}$ = -19.8 (c = 0.5, MeOH).

IR (KBr): 3312, 1764, 1664, 1531, 1267, 1166 cm^{-1}.

^{1}H NMR (200 MHz, $CDCl_3$): δ 7.34 (m, 5H, Z phenyl-CH), 6.93 (s, 1H, N-H Aib), 6.86 (s, 1H, N-H Aib), 6.05 (d, 1H, N-H Asp), 5.11 (s, 2H, Z-CH_2), 4.45 (m, 1H, α-CH Asp), 3.64 (s, 3H, OMe), 3.61 (m, 4H, OCH_2), 2.93-2.77 (m, 2H, β-CH_2 Asp), 1.64 (m, 4H, OCH_2CH_2), 1.45 (s, 6H, β-CH_3 Aib), 1.43 (s, 6H, β-CH_3 Aib).

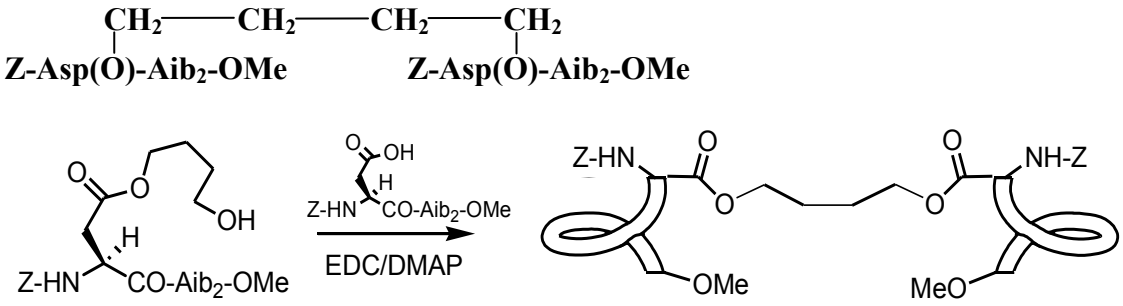

To a solution of Z-Asp-Aib_2-OMe (1 g, 2.2 mmol) in anhydrous CH_2Cl_2, cooled to 0°C, DMAP (322 mg, 2.9 mmol) and EDC (509 mg, 2.9 mmol) were added. After 5 min Z-Asp($OCH_2CH_2CH_2CH_2OH$)-Aib_2-OMe (1.42 g, 2.7 mmol) and DIPEA (0.46 ml, 2.9 mmol) were added. The mixture was stirred at room temperature for 24 hs, then the solvent was removed and the residue dissolved in EtOAc. The solution was washed with 10% $KHSO_4$, H_2O, 5% $NaHCO_3$ and H_2O, dried over Na_2SO_4, and evaporated to dryness. Yield 72%.

mp: 115°-117°C

Rf_1: 0.60, Rf_2: 0.85, Rf_3: 0.45.

ESI-MS: calcd: 957.46; found: 957.46 $[M+H]^+$

$[\alpha]_D^{20}$ = -18.1 (c = 0.5, MeOH).

IR (KBr): 3312, 1764, 1664, 1531, 1267, 1166 cm^{-1}.

^1H NMR (200 MHz, $CDCl_3$): δ 7.36 (m, 5H, Z phenyl-CH), 6.89 (s, 1H, N-H Aib), 6.81 (s, 1H, N-H Aib), 5.90 (d, 1H, N-H Asp), 5.09 (s, 2H, Z-CH_2), 4.48 (m, 1H, α-CH Asp), 4.09 (m, 4H, OCH_2), 3.70 (s, 3H, OMe), 3.09-2.69 (m, 2H, β-CH_2 Asp), 1.72 (m, 4H, OCH_2CH_2), 1.48 (m, 12H, β-CH_3 Aib).

References

1. Kotrotsiou, O., Kotti, K., Dini, E., Kammona, O. and Kiparissides, C., *J. Phys. Confer. Ser.*, 10, (**2005**).

2. Fairman, R. and Åkerfeldt, K.S., *Curr. Opin. Struct. Biol.*, *15*, 453 (**2005**).

3. Toniolo, C., Crisma, M., Formaggio, F., Peggion, C., Epand, R.F. and Epand, R.M., *Cell. Mol. Life Sci.*, 58, 1179 (**2001**).

4. Ramachandran, G.N. and Sasisekharan, V., *Adv. Protein Chem.*, 23, 283 (**1968**).

5. IUPAC-IUB, *Biochemistry*, 9, (**1970**).

6. Toniolo, C. and Benedetti, E., *Trends Biochem. Sci.*, 16, 350 (**1991**).

7. Donohue, J., *Proc. Natl. Acad. Sci. USA*, 39, 470 (**1983**).

8. Ramachandran, G.N., Venkatachalam, C.M. and Krimm, S., *Biophys. J.*, 66, 849 (**1966**).

9. Baker, E.N. and Hubbard, R.E., *Progr. Biophys. Mol. Biol.*, 44, 97 (**1984**).

10. Robbins, A.H. and C.D., S., *Protein Struct. Funct. Genet.* , 5, (**1989**).

11. Pathak, D. and Ollis, D., *J. Mol. Biol.*, *214*, *497* (**1990**).

12. Kostrikis, L.G., Liu, D.J. and Day, L.A., *Biochemistry*, 33, 1694 (**1994**).

13. Nagaraj, R. and Balaram, P., *Acc. Chem. Res.*, 14, 356 (**1981**).

14. Shea, J.E. and Brooks, C.L., *Annu. Rev. Phys. Chem.*, 52, 499 (**2001**).

15. Tirado-Rives, J. and Jorgensen, W.L., *Biochemistry*, 30, 3864 (**1991**).

16. Soman, K.V., Karimi, A. and Case, D.A., *Biopolymers*, 31, 1351 (**1991**).

17. Venkatachalam, C.*M.*, *Biopolymers*, 6, 1425 (**1968**).

18. Toniolo, C., Crisma, M., Formaggio, F., Valle, G., Cavicchioni, G., Précigoux, G., Aubry, A. and Kamphuis, J., *Biopolymers*, 33, 1061 (**1993**).

19. Toniolo, C., Crisma, M., Formaggio, F. and Peggion, C., *Biopolymers (Pept. Sci.)*, 60, 396 (**2001**).

20. Toniolo, C., Crisma, M., Formaggio, F., Peggion, C., Broxterman, Q.B. and Kaptein, B., *Biopolymers (Pept. Sci.)*, 76, (**2004**).

21. Toniolo, C., Formaggio, F., Tognon, S., Broxterman, Q.B., Kaptein, B., Huang, R., Setnicka, V., Keiderling, T.A., Mc Coll, I.H., Hecht, L. and Barron, L.D., *Biopolymers*, 75, 32 (**2004**)

22. Ramachandran, G.N. and Chandrasekaran, R., *Indian J. Biochem. Biophys.*, 9, 1 (**1972**).

23. Burgess, A.W. and Leach, S.J., *Biopolymers*, 12, 2599 (**1973**).

24. Pavone, V., Di Blasio, B., Santini, A., Benedetti, E., Pedone, C., Toniolo, C. and Crisma, M., *J. Mol. Biol.*, 214, 633 (**1990**).

25. Benedetti, E., Di Blasio, B., Pavone, V., Pedone, C., Santini, A., Crisma, M. and Toniolo, C., Indian Academy of Sciences, Bangalore (**1991**), pp.

26. Formaggio, F., Crisma, M., Rossi, P., Scrimin, P., Kaptein, B., Broxterman, Q.B., Kamphuis, J. and Toniolo, C., *Chem. Eur. J.*, 6, 4498 (**2000**).

27. Scarso, A., Scheffer, U., Göbel, M., Broxterman, Q.B., Kaptein, B., Formaggio, F., Toniolo, C. and Scrimin, P., *Proc. Natl. Acad. Sci. USA*, 99, 5144 (**2002**).

28. Demirdoeven, N., Cheatum, C.M., Chung, H.S., Khalil, M., Knoester, J. and Tokmakoff, A., *J. Am. Chem. Soc.*, 126, 7981 (**2004**).

29. Barth, A. and Zscherp, C., *Q. Rev. Biophys.*, *35*, *369* (**2002**).

30. Krimm, S. and Bandekar, J., *Adv. Protein Chem.*, 38, 181 (**1986**).

31. Hamm, P., Helbing, J. and Bredenbeck, J., *Annu. Rev. Phys. Chem.*, 59, 291 (**2008**).

32. Ganim, Z., Chung, H.S., Smith, A.W., DeFlores, L.P., Jones, K.C. and Tokmakoff, A., *Acc. Chem. Res.*, 41, 432 (**2008**).

33. Jackson, M. and Mantsch, H.H., *Crit. Rev. Biochem. Mol.* , 30, 95 (***1995***).

34. Byler, D.M. and Susi, H., *Biopolymers*, 25, 469 (**1986**).

35. Cheatum, C.M., Tokmakoff, A. and Knoester, J., *J. Chem. Phys.*, 120, 8201 (**2004**).

36. Miyazawa, T. and Blout, E.R., *J. Am. Chem. Soc.*, 83, 712 (**1961**).

37. Hamm, P., Lim, M. and Hochstrasser, R.M., *J. Phys. Chem. B*, *102*, *6123* (***1998***).

38. Woutersen, S. and Hamm, P., *J. Phys.: Condens. Matter* 14, 1035 (**2002**).

39. Zanni, M.T. and Hochstrasser, R.M., *Curr. Opin. Struct. Biol.*, 11, 516 (**2001**).

40. Scheurer, C., Piryatinski, A. and Mukamel, S., *J. Am. Chem. Soc.*, 123, 3114 (**2001**).

41. DeCamp, M.F., DeFlores, L.P., McCracken, J.M., Tokmakoff, A., Kwac, K. and Cho, M., *J. Phys. Chem. B*, 109, 11016 (**2005**).

42. Chung, H.S., Khalil, M., Smith, A.W., Ganim, Z. and Tokmakoff, A., *Proc. Natl. Acad. Sci. USA*, 102, 612 (**2005**).

43. Chung, H.S., Khalil, M. and Tokmakoff, A., *J. Phys. Chem. B*, 108, 15332 (**2004**).

44. Chung, H.S. and Tokmakoff, A., *J. Phys. Chem. B*, 110, 2888 (**2006**).

45. Ganim, Z. and Tokmakoff, A., *Biophys. J.*, 91, 2636 (***2006***).

46. Hayashi, T. and Mukamel, S., *J. Phys. Chem. B*, 111, 11032 (**2007**).

47. Jansen, T.C. and Knoester, J., *J. Phys. Chem. B*, 110, 22910 (**2006**).

48. Choi, J.-H., Lee, H., Lee, K.-K., Hahn, S. and Cho, M., *J. Chem. Phys.*, 126, 45102 (**2007**).

49. Chung, H.S., Khalil, M., Smith, A.W. and Tokmakoff, A., *Rev. Sci. Instrum.*, 78, (**2007**).

50. Tokmakoff, A., Lang, M.J., Larsen, D.S., Fleming, G.R., Chernyak, V. and Mukamel, S., *Phys. Rev. Lett.*, 79, 2702 (**1997**).

51. Mukamel, S., *Annu. Rev. Phys. Chem.*, 51, 691 (**2000**).

52. Wright, J.C., *Int. Rev. Phys. Chem.*, 21, 185 (**2002**).

53. Zhuang, W., Abramavicius, D. and Mukamel, S., *Proc. Natl. Acad. Sci. USA*, 103, 18934 (**2006**).

54. Chung, H.S., Ganim, Z., Jones, K.C. and Tokmakoff, A., *Proc. Natl. Acad. Sci. USA*, 104, 14237 (**2007**).

55. Krummel, A.T., Mukherjee, P. and Zanni, M.T., *J. Phys. Chem. B*, 107, 9165 (**2003**).

56. Kim, Y.S. and Hochstrasser, R.M., *Proc. Natl. Acad. Sci. USA*, 102, 11185 (**2005**).

57. Zheng, J.R., Kwak, K., Asbury, J., Chen, X., Piletic, I.R. and Fayer, M.D., *Science*, 309, 1338 (**2005**).

58. Asbury, J.B., Steinel, T., Stromberg, C., Corcelli, S.A., Lawrence, C.P., Skinner, J.L. and Fayer, M.D., *J. Phys. Chem. A*, 108, 1107 (**2004**).

59. Eaves, J.D., Loparo, J.J., Fecko, C.J., Roberts, S.T., Tokmakoff, A. and Geissler, P.L., *Proc. Natl. Acad. Sci. USA*, 102, 13019 (**2005**).

60. Bredenbeck, J., Helbing, J. and Hamm, P., *J. Am. Chem. Soc.*, 126, 990 (**2004**).

61. Kolano, C., Helbing, J., Kozinski, M., Sander, W. and Hamm, P., *Nature*, 444, 469 (**2006**).

62. Khalil, M., Demirdoeven, N. and Tokmakoff, A., *J. Phys. Chem. A*, 107, 5258 (**2003**).

63. Demirdoeven, N., Khalil, M. and Tokmakoff, A., *Phys. Rev. Lett.*, 89, 237401 (**2002**).

64. Sauer, K., *Methods Enzymol.* , 246, 1 (**1995**).

65. Toniolo, C., Polese, A., Formaggio, F., Crisma, M. and Kamphuis, J., *J. Am. Chem. Soc.*, 118, 2744 (**1996**).

66. Yoder, G., Polese, A., Silva, R.A.G.D., Formaggio, F., Crisma, M., Broxterman, Q.B., Kamphuis, J., Toniolo, C. and Keiderling, T.A., *J. Am. Chem. Soc.*, 119, 10278 (**1997**).

67. Mammi, S., Rainaldi, M., Bellanda, M., Schievano, E., Peggion, E., Broxterman, Q.B., Formaggio, F., Crisma, M. and Toniolo, C., *J. Am. Chem. Soc.*, 122, 11735 (**2000**).

68. Pengo, P., Pasquato, L., Moro, S., Brigo, A., Fogolari, F., Broxterman, Q.B., Kaptein, B. and Scrimin, P., *Angew. Chem. Int. Ed.*, 42, 3388 (**2003**).

69. Martinez, G. and Millhauser, G., *J. Struct. Biol.*, 114, 23 (**1995**).

70. Silva, R.A.G.D., Yasui, S.C., Kubelka, J., Formaggio, F., Crisma, M., Toniolo, C. and Keiderling, T.A., *Biopolymers*, 65, 299 (**2002**).

71. Kubelka, J., Silva, R.A.G.D. and Keiderling, T.A., *J. Am. Chem. Soc.*, 124, 5325 (**2002**).

72. Bolin, K.A. and Millhauser, G.L., *Acc. Chem. Res.*, 32, 1027 (**1999**).

73. De Guzman, R.N., Wu, Z.R., Stalling, C.C., Pappalardo, L., Borer, P.N. and Summers, M.F., *Science*, 279, 384 (**1998**).

74. Hashimoto, Y., Kohri, K., Kaneko, Y., Morisaki, H., Kato, T., Ikeda, K. and Nakanishi, M., *J. Biol. Chem.*, 273, 16544 (**1998**).

75. Matsushima, N., Enkhbayar, P., Kamiya, M., Osaki, M. and Kretsinger, R.H., *Drug Des. Rev.*, 2, 305 (**2005**).

76. Maekawa, H., Formaggio, F., Toniolo, C. and Ge, N.-H., *J. Am. Chem. Soc.*, 130, 6557 (**2008**).

77. Maekawa, H., Toniolo, C., Moretto, A., Broxterman, Q.B. and Ge, N.-H., *J. Phys. Chem. B*, 110, 5834 (**2006**).

78. Maekawa, H., Toniolo, C., Broxterman, Q.B. and Ge, N.-H., *J. Phys. Chem. B*, 111, 3222 (**2007**).

79. Polese, A., Formaggio, F., Crisma, M., Valle, G., Toniolo, C., Bonora, G.M., Broxterman, Q.B. and Kamphuis, J., *Chem. Eur. J.*, 2, 1104 (**1996**).

80. Mukherjee, P., Kass, I., Arkin, I.T. and Zanni, M.T., *Proc. Natl. Acad. Sci. USA*, 103, 3528 (**2006**).

81. Fang, C. and Hochstrasser, R.M., *J. Phys. Chem. B*, 109, 18652 (**2005**).

82. Fang, C., Senes, A., Cristian, L., DeGrado, W.F. and Hochstrasser, R.M., *Proc. Natl. Acad. Sci. USA*, 103, 16740 (**2006**).

83. Fillaux, F. and De Lozé, C., *J. Chim. Phys., Phys.-Chim. Biol.*, 73, 1004 (**1976**).

84. Smith, W.S. and Tokmakoff, A., *J. Chem. Phys.*, 126, 45109 (**2007**).

85. Konig, W. and Geiger, R., *Chem. Ber.*, 103, 788 (**1970**).

86. Carpino, L.A., *J. Am. Chem. Soc.*, 115, 4397 (**1993**).

87. Murphy, R.C. and Clay, K.C., *Methods Enzymol.* , 193, 338 (**1990**).

88. Kopple, K.D., Ohnishi, M. and Go, A., *Biochemistry*, 8, 4087 (**1969**).

89. Martin, D. and Hauthal, H.G., in "*Dimethyl Sulphoxide"*, Ed. Van Nostrand-Reinhold, Wokingham, UK, (**1975**).

90. Mizushima, S.-I., Shimanouchi, T., Tsuboi, M. and Souda, R., *J. Am. Chem. Soc.*, 74, 270 (**1952**).

91. Toniolo, C., *CRC Crit. Rev. Biochem.*, 9, 1 (**1980**).

92. Rose, G.D., Gierasch, L.M. and Smith, J.A., *Adv. Protein Chem.*, 37, 1 (**1985**).

93. Bonora, G.M., Mapelli, C., Toniolo, C., Wilkening, R.R. and Stevens, E.S., *Int. J. Biol. Macromol.*, 6, 179 (**1984**).

94. Griesinger, C., Otting, G., Wuthrich, K. and Ernst, R.R., *J. Am. Chem. Soc.*, 110, 7870 (**1988**).

95. Bothner-By, A.A., Stephens, R.L., Lee, J., Warren, R.W. and Jeanloz, R.W., *J. Am. Chem. Soc.*, 106, 811 (**1984**).

96. Kim, J.-H. and Cho, M., *Bull. Korean Chem. Soc.*, 24, 1061 (**2003**).

97. Valle, G., Crisma, M., Toniolo, C., Beisswenger, R., Rieker, A. and Jung, G., *J. Am. Chem. Soc.*, 111, 6828 (**1989**).

98. Botan, V., Backus, E.H.G., Pfister, R., Moretto, A., Crisma, M., Toniolo, C., Nguyen, P.H., Stock, G. and Hamm, P., *Proc. Natl. Acad. Sci. USA*, 104, 12749 (**2007**).

99. Schade, M., Moretto, A., Crisma, M., Toniolo, C. and Hamm, P., *J. Phys. Chem. B*, 113, 13393 (**2009**).

100. Kennedy, D.F., Crisma, M., Toniolo, C. and Chapman, D., *Biochemistry*, 30, 6541 (**1991**).

101. Toniolo, C., Bonora, G.M., Barone, V., Bavoso, A., Benedetti, E., Di Blasio, B., Grimaldi, P., Lelj, F., Pavone, V. and Pedone, C., *Macromolecules*, 18, 895 (**1985**).

102. Sul, S., Karaiskaj, D., Jiang, Y. and Ge, N.-H., *J. Phys. Chem. B*, 110, 19891 (**2006**).

103. Ge, N.-H., Zanni, M.T. and Hochstrasser, R.M., *J. Phys. Chem. A*, 106, 962 (**2002**).

104. Hamm, P. and Hochstrasser, R.M., *Ultrafast Infrared and Raman Spectroscopy*, Ed. Fayer, M. D., Dekker, New York, NY (**2001**), pp. 273-347.

105. Fang, C., Wang, J., Kim, Y.S., Charnley, A.K., Barber-Armstrong, W., Smith, A.B., III, Decatur, S.M. and Hochstrasser, R.M., *J. Phys. Chem. B*, 108, 10415 (**2004**).

106. Cowan, P.M. and McGavin, S., *Nature*, 176, 501 (**1955**).

107. Venyaminov, S.Y. and Yang, J.T., *Determination of protein secondary structure, in "Circular Dichroism and the Conformational Analysis of Biomolecules"*, Plenum Press, Ed. Fasman, G.D., New York, NY (**1996**), pp. 69-107.

108. Sreerama, N. and Woody, R.W., *Circular Dichroism of Peptides and Proteins in "Circular Dichroism: Principles and Applications"*, Wiley, Eds. Berova, N., Nakanishi, K., Woody, R.W., New York, NY (**2000**), pp. 601-620.

109. Toumadje, A., Alcorn, S.W. and Johnson, W.C., *Anal. Biochem.*, 200, 321 (**1992**).

110. Wallace, B.A. and Jans, R.W., *Curr. Opin. Chem. Biol.*, 5, 567 (**2001**).

111. Baello, B.I., Pancoska, P. and Keiderling, T.A., *Anal. Biochem.*, 280, 46 (**2000**).

112. Nafie, L.A., Yu, G.S., Qu, X. and Freedman, T.B., *Faraday Discuss.*, 99, 13 (**1994**).

113. Barron, L.D. and Hecht, L., *Vibrational Raman optical activity: from fundamentals to biochemical applications in "Circular Dichroism, Principles and Applications"*, Wiley, Eds. Berova, N., Nakanishi, K. and Woody, R.A., New York, NY (**2000**), pp. 667-701.

114. Costante, J., Hecht, L., Polavarapu, P.L., Collet, A. and Barron, L.D., *Angew. Chem. Int. Ed. Engl.*, 36, 885 (**1997**).

115. Blanch, E.W., Robinson, D.L., Hecht, L., Syme, C.D., Nielsen, K. and Barron, L.D., *J. Gen. Virol.*, 241 (**2002**).

116. Nafie, L. and Freedman, T.B., *Biological and pharmaceutical applications of vibrational optical activity in "Infrared and Raman Spectroscopy of Biological Materials"*, Dekker, Eds. Gremlich, H. and Yan, B., New York, NY (**2001**), pp. 15-54.

117. Stephens, P.J., Devlin, F.J. and Amouche, A., *Determination of the structures of chiral molecules using vibrational circular dichroism in "Chirality: Physical Chemistry"*, Ed. Hicks, J.M., Oxford University Press, Oxford, UK (**2002**), pp. 18-33.

118. Baumruk, V., Pancoska, P. and Keiderling, T.A., *J. Mol. Biol.*, 259, 774 (**1996**).

119. Keiderling, T.A., *Vibrational circular dichroism applications to conformational analysis of biomolecules in "Circular Dichroism and the Conformational Analysis of Biomolecules"*, Plenum Press, Ed. Fasman, G.D., New York, NY (**1996**), pp. 555-598.

120. Keiderling, T.A., *"Peptide and protein conformational studies with vibrational circular dichroism and related spectroscopies in "Circular Dichroism: Principles and Applications"*, Wiley, Eds. Berova, N., Nakanishi, K., Woody, R.A., New York, NY (**2000**), pp. 621-666.

121. Silva, R.A.G.D., Kubelka, J., Decatur, S.M., Bour, P. and Keiderling, T.A., *Proc. Natl. Acad. Sci. USA*, 97, 8318 (**2000**).

122. Dukor, R.K. and Keiderling, T.A., *Biopolymers*, 31, 1747 (**1991**).

123. Pancoska, P., Bitto, E., Janota, V., Urbanova, M., Gupta, V.P. and Keiderling, T.A., *Protein Sci.*, 4, 1384 (**1995**).

124. Kubelka, J., Silva, R.A.G.D., Bour, P., Decatur, S.M. and Keiderling, T.A., *Chirality in peptide vibrations. Ab initio computational studies of length, solvation, hydrogen bond, dipole coupling and isotope effects on vibrational CD in "Chirality: Physical Chemistry"*, American Chemical Society, Ed. Hicks, J.M., Washington DC (**2002**), pp. 50-64.

125. Aamouche, A., Devlin, F.J. and Stephens, P.J., *J. Am. Chem. Soc.*, 122, 2346 (**2000**).

126. Zhao, C.X. and Polavarapu, P.L., *Biopolymers*, 62, 336 (**2001**).

127. Urbanova, M., Setnicka, V. and Volka, K., *Chirality*, 12, 199 (**2000**).

128. Hilario, J., Drapcho, D., Curbelo, R. and Keiderling, T.A., *Appl. Spectrosc.*, 55, 1435 (**2001**).

129. Nafie, L., *Appl. Spectrosc.*, 54, 1634 (**2000**).

130. Baello, B.I., Pancoska, P. and Keiderling, T.A., *Anal. Biochem.*, 250, 212 (**1997**).

131. Freedman, T.B., Nafie, L.A. and Keiderling, T.A., *Biopolymers*, 37, 265 (**1995**).

132. Keiderling, T.A. and Xu, Q., *Unfolded peptides and proteins studied with infrared absorption and vibrational circular dichroism spectra in "Unfolded Proteins"*, Academic Press, New York, NY (**2002**), pp. 111-162.

133. Tanaka, T., Inoue, K., Kodama, T., Kyogoku, Y., Hayakawa, T. and Sugeta, H., *Biopolymers*, 62, 228 (**2001**).

134. Krimm, S. and Tiffany, M.L., *Isr. J. Chem.*, 12, 189 (**1974**).

135. Huang, R., Kubelka, J., Barber-Armstrong, W., Silva, R.A.G.D., Decatur, S.M. and Keiderling, T.A., *J. Am. Chem. Soc.*, 126, 2346 (**2004**).

136. Chi, H., Lakhani, A., Roy, A., Nakaema, M. and Keiderling, T.A., *J. Phys. Chem. B*, 114, 12744 (**2010**).

137. Kubelka, J. and Keiderling, T.A., *J. Am. Chem. Soc.*, 123, 6142 (**2001**).

138. Huang, R., Setnička, V., Etienne, M.A., Kim, J., Kubelka, J., Hammer, R.P. and Keiderling, T.A., *J. Am. Chem. Soc.*, 129, 13592 (**2007**).

139. Bour, P. and Keiderling, T.A., *J. Phys. Chem. B*, 109, 5348 (**2005**).

140. Huang, R., Wu, L., McElheny, D., Bour, P., Roy, A. and Keiderling, T.A., *J. Phys. Chem. B*, 113, 5661 (**2009**).

141. Hauser, K., Krejtschi, C., Huang, R., Wu, L. and Keiderling, T.A., *J. Am. Chem. Soc.*, 130, 2984 (**2008**).

142. Hauser, K., Ridderbusch, O., Roy, A., Krejtschi, C., Hellerbach, A., Huang, R. and Keiderling, T.A., *J. Phys. Chem. B*, 114, 11628 (**2010**).

143. Manning, M.C. and Woody, R.W., *Biopolymers*, 31, 569 (**1991**).

144. Moretto, A., Formaggio, F., Kaptein, B., Broxterman, Q.B., Wu, L., Keiderling, T.A. and Toniolo, C., *Biopolymers (Pept. Sci.)*, 90, 567 (**2008**).

145. Yoder, G., Pancoska, P. and Keiderling, T.A., *Biochemistry*, 36, 15123 (**1197**).

146. Yasui, S.C., Keiderling, T.A., Bonora, G.M. and Toniolo, C., *Biopolymers*, 25, 79 (**1986**).

147. Toniolo, C., Crisma, M., Formaggio, F., Peggion, C., Monaco, V., Goulard, C., Rebuffat, S. and Bodo, B., *J. Am. Chem. Soc.*, 118, 4952 (**1996**).

148. Yasui, S.C., Keiderling, T.A., Formaggio, F., Bonora, G.M. and Toniolo, C., *J. Am. Chem. Soc.*, 108, 4988 (**1986**).

149. Kepler, J., in "*Mysterium Cosmographicum"*, Tübingen, (**1596**).

150. Hill, D.J., Mio, M.J., Prince, R.B., Hughes, T.S. and Moore, J.S., *Chem. Rev.*, 101, 3893 (**2001**).

151. Gellman, S.H., *Acc. Chem. Res.*, 31, 173 (**1998**).

152. Gademann, K., Ernst, M., Hoyer, D. and Seebach, D., *Angew. Chem. Int. Ed.*, 38, 1223 (**1999**).

153. Werder, M., Hauser, H., Abele, S. and Seebach, D., *Helv. Chim. Acta*, 82, 1774 (**1999**).

154. Hamuro, Y., Schneider, J.P. and DeGrado, W.F., *J. Am. Chem. Soc.*, 121, 12200 (**1999**).

155. Gunji, H. and Vasella, A., *Helv. Chim. Acta*, 83, 1331 (**2000**).

156. Ohkita, M., Lehn, J.M., Baum, G. and Fenske, D., *Chem. Eur. J.*, 5, 3471 (**1999**).

157. Ohkita, M., Lehn, J.M., Baum, G. and Fenske, D., *Heterocycles*, 52, 103 (**2000**).

158. Creighton, T.E., in "*Proteins: Structures and Molecular Principles"*, Ed. Freeman, 2nd ed., New York, NY, (**1993**).

159. Saenger, W., in "*Principles of Nucleic Acid Structure"*, Springer-Verlag, New York, NY, (**1984**).

160. Draper, D., *Trends Biochem. Sci.*, 21, 145 (**1996**).

161. Strobel, S.A. and Doudna, J.A., *Trends Biochem. Sci.*, 22, 262 (**1997**).

162. Chan, H.S. and Dill, K.A., *Annu Rev. Biophys. Chem.*, 20, 447 (**1991**).

163. DeGrado, W.F., *Adv. Protein Chem.*, 39, 51 (**1988**).

164. DeGrado, W.F., Summa, C.M., Pavone, V., Nastri, A. and Lombardi, A., *Annu. Rev. Biochem.*, 68, 779 (**1999**).

165. Betz, S.F., Bryson, J.W. and DeGrado, W.F., *Curr. Opin. Struct. Biol.*, 5, 457 (**1995**).

166. Smith, C. and Regan, L., *Science*, 270, 980 (**1995**).

167. Tanaka, S. and Scheraga, H.A., *Proc. Natl. Acad. Sci. USA*, 72, 3802 (**1975**).

168. Zimmerman, S.S. and Scheraga, H.A., *Proc. Natl. Acad. Sci. USA*, 74, 4126 (**1977**).

169. Go, N., *Annu. Rev. Biophys. Eng.*, 12, 183 (**1983**).

170. Brown, S.C. and Fawzi, N.J., *Proc. Natl. Acad. Sci. USA*, 100, 10712 (**2003**).

171. Venkatraman, J., Shankaramma, S.C. and Balaram, P., *Chem. Rev.*, 101, 3131 (**2001**).

172. Ramirez-Alvarado, M., Blanco, F.J. and Serrano, L., *Nat. Struct. Biol.*, 7, 604 (**1996**).

173. de Alba, E., Jimenez, M.A. and Rico, M., *J. Am. Chem. Soc.*, 119, 175 (**1997**).

174. Maynard, A.J. and Searle, M.S., *Chem. Commun.*, 11297 (**1997**).

175. Maynard, A.J., Sharman, G.J. and Searle, M.S., *J. Am. Chem. Soc.*, 120, 1996 (**1998**).

176. Griffith-Jones, S.R., Sharman, G.J., Mainard, A.J. and Searle, M.S., *J. Mol. Biol.*, 284, 1597 (**1998**).

177. Stanger, H.E. and Gellman, S.H., *J. Am. Chem. Soc.*, 120, 4236 (**1998**).

178. Espinosa, J.F., Syud, F.A. and Gellman, S.H., *Protein Sci.*, 11, 1492 (**2002**).

179. Cochran, A.G., Skelton, N.J. and Starovasnik, M.A., *Proc. Natl. Acad. Sci. USA*, 98, 5578 (**2001**).

180. Kemp, D.S., Boyd, J.G. and Muendel, C.C., *Nature*, 352, 451 (**1991**).

181. Kemp, D.S., Curran, T.P., Boyd, J.G. and Allen, T.J., *J. Org. Chem.*, 56, 6638 (**1991**).

182. Job, G.E., Heitmann, B., Kennedy, R.J., Walker, S.M. and Kemp, D.S., *Angew. Chem. Int. Ed. Engl.*, 43, 5649 (**2004**).

183. Hanessian, S., Papeo, G., Fettis, K., Therrien, E. and Viet, M.T., *J. Org. Chem.*, 69, 4891 (**2004**).

184. Venkatachalpathi, Y.V. and Balaram, P., *Nature*, 281, 83 (**1979**).

185. Karle, I.L., Flippen Anderson, J.L., Sukumar, M. and Balaram, P., *Proc. Natl. Acad. Sci. USA*, 84, 5084 (**1987**).

186. Di Blasio, B., Pavone, V., Saviano, M., Lombardi, A., Nastri, F., Pedone, C., Benedetti, E., Anzolin, M. and Toniolo, C., *J. Am. Chem. Soc.*, 114, 6273 (**1992**).

187. Adzhubei, A.A. and Sternberg, M.J.E., *J. Mol. Biol.*, 229, 472 (**1993**).

188. Pawson, T. and Schlessingert, J., *Curr. Biol.*, 3, (**1993**).

189. Mayer, B. and Baltimore, D., *Trends Cell Biol.*, 3, 8 (**1993**).

190. Burgess, A., Paterson, Y. and Leach, S.J., *Peptides, Polypeptides, and Proteins*, Wiley, New York (**1974**), pp. 79-87.

191. Flippen-Anderson, J.L., Gilardi, R., Karle, I.L., Frey, M.H., Opella, S.J., Gierasch, L.M., Goodman, M., Madison, V. and Delaney, N.G., *J. Am. Chem. Soc.*, 105, 6609 (**1983**).

192. Delaney, N.G. and Madison, V., *J. Am. Chem. Soc.*, 104, 6635 (**1982**).

193. Némethy, G. and Printz, M.P., *Macromolecules*, 5, 755 (**1972**).

194. Matthews, B.W., *Macromolecules*, 5, 818 (**1972**).

195. Delaney, N.G. and Madison, V., *J. Am. Chem. Soc.*, 105, 6635 (**1982**).

196. Overberger, C.G. and Jon, Y.S., *J. Polym. Sci., Polym. Chem. Edit.*, 15, 1413 (**1977**).

197. Baures, P.W., Ojala, W.H., Gleason, W.B. and Johnson, R.L., *J. Pept. Res.*, 49, 1 (**1997**).

198. Richards, N.G.J., Hinds, M.G., Brennand, D.M., Glennie, M.J., Welsh, J.H. and Robinson, J.A., *Biochem. Pharmacol.*, 40, 119 (**1990**).

199. Hinds, M.G., Welsh, J.H., Brennand, D.M., Fisher, J., Glennie, M.J., Richards, N.G.J., Turner, D.L. and Robinson, J.A., *J. Med. Chem.*, 34, 1777 (**1991**).

200. Welsh, J.H., Zerbe, O., von Philipsborn, W. and Robinson, J.A., *FEBS Lett.*, 297, 216 (**1992**).

201. Zerbe, O., Welsh, J.H., Robinson, J.A. and von Philipsborn, W., *Magn. Reson. Chem.*, 30, 683 (**1992**).

202. Zerbe, O., Welsh, J.H., Robinson, J.A. and von Philipsborn, W., *J. Magn. Reson.*, 100, 329 (**1992**).

203. Bisang, C., Weber, C., Inglis, J., Schiffer, C.A., van Gunsteren, W.F., Jelesarov, I., Bosshard, H.R. and Robinson, J.A., *J. Am. Chem. Soc.*, 117, 7904 (**1995**).

204. Nanzer, A.P., Torda, A.E., Bisang, C., Weber, C., Robinson, J.A. and van Gunsteren, W.F., *J. Mol. Biol.*, 267, 1012 (**1997**).

205. Sem, D.S., Baker, B.L., Victoria, E.J., Jones, D.S., Marquis, D., Yu, L., Parks, J. and Coutts, S.M., *Biochemistry*, 37, 16069 (**1998**).

206. Kobayashi, S., Chikushi, A., Tougu, S., Imura, Y., Nishida, M., Yano, Y. and Matsuzaki, K., *Biochemistry*, 43, 15610 (**2004**).

207. Gani, D., Lewis, A., Rutherford, T., Wilkie, J., Stirling, I., Jenn, T. and Ryan, M.D., *Tetrahedron*, 54, 15793 (**1998**).

208. Balducci, D., Emer, E., Piccinelli, F., Porzi, G., Recanatini, M. and Sandri, S., *Tetrahedron: Asymmetry*, 16, 3785 (**2005**).

209. Balducci, D., Bottoni, A., Calvaresi, M., Porzi, G. and Sandri, S., *Tetrahedron: Asymmetry*, 17, 3723 (**2006**).

210. Jainta, M., Nieger, M. and Bräse, S., *Eur. J. Org. Chem.*, 5418 (**2008**).

211. Lummis, S.C.R., Beene, D.L., Lee, L.W., Lester, H.A., Broadhurst, R.W. and Dougherty, D.A., *Nature*, 438, 248 (**2005**).

212. Flores-Ortega, A., Jiménez, A.I., Cativiela, C., Nussinov, R., Alemán, C. and Casanovas, J., *J. Org. Chem.*, 73, 3418 (**2008**).

213. Benedetti, E., Bavoso, A., Di Blasio, B., Pavone, V., Pedone, C., Toniolo, C. and Bonora, G.M., *Biopolymers*, 22, 305 (**1983**).

214. Di Blasio, B., Pavone, V., Saviano, M., Fattorusso, R., Pedone, C., Benedetti, E., Crisma, M. and Toniolo, C., *Pept. Res.*, 7, 55 (**1994**).

215. Williams, K.A. and Deber, C.M., *Biochemistry*, 30, 8919 (**1991**).

216. MacArthur, M.W. and Thornton, J.M., *J. Mol. Biol.*, 218, 397 (**1991**).

217. Yaron, A. and Naider, F., *Crit. Rev. Biochem. Mol. Biol.*, 28, 31 (**1993**).

218. Williamson, M.P., *Biochem. J.*, 297, 249 (**1994**).

219. Pal, D. and Chakrabarti, P., *J. Mol. Biol.*, 294, 271 (**1999**).

220. Eyles, S.J. and Gierasch, L.M., *J. Mol. Biol.*, 301, 737 (**2000**).

221. Berisio, R., Loguercio, S., Simone, A.D., Zagari, A. and Vitagliano, L., *Protein Pept. Lett.*, 13, 847 (**2006**).

222. Toniolo, C., *Biopolymers*, 28, 247 (**1989**).

223. Karle, I.L. and Balaram, P., *Biochemistry*, 29, 6747 (**1990**).

224. Toniolo, C., Crisma, M., Bonora, G.M., Benedetti, E., Di Blasio, B., Pavone, V., Pedone, C. and Santini, A., *Biopolymers*, 31, 129 (**1991**).

225. Sonke, T., Kaptein, B., Boesten, W.H.J., Broxterman, Q.B., Shoemaker, H.E., Kamphuis, J., Formaggio, F., Toniolo, C. and Rutjes, F.P.J.T., *Aminoamidase-catalyzed preparation and further transformations of enantiopure α-hydrogen and α,α-disubstituted α-amino acids, in "Stereoselective Biocatalysis"*, Dekker, Ed. Patel, R.N., New York, NY (**1999**), pp. 23-58.

226. Sonke, T., Ernste, S., Tandler, R.F., Kaptein, B., Peeters, W.P.H., Assema, F.B.J.V., Wubbolts, M.G. and Schoemaker, H., *Appl. Environ. Microbiol.*, 71, 7961 (**2005**).

227. Kaptein, B., Broxterman, Q.B., Schoemaker, H.E., Rutjes, F.P.J.T., Veerman, J.J.N., Kamphuis, J., Peggion, C., Formaggio, F. and Toniolo, C., *Tetrahedron*, 57, 6567 (**2001**).

228. Moretto, A., Terrenzani, F., Crisma, M., Formaggio, F., Kaptein, B., Broxterman, Q.B. and Toniolo, C., *Biopolymers*, 89, 465 (**2008**).

229. Aubry, A., Protas, J., Boussard, M. and Marraud, M., *Acta Crystallogr. A*, 36, 2825 (**1980**).

230. Aubry, A., Protas, J., Boussard, M. and Marraud, M., *Acta Crystallogr. A*, 36, 321 (**1980**).

231. Crisma, M., Valle, G., Bianco, A., Formaggio, F. and Toniolo, C., *Zeit. Kristallogr.*, 212, 465 (**1997**).

232. Aubry, A., Protas, J., Boussard, M. and Marraud, M., *Acta Crystallogr. A*, 33, 2399 (**1977**).

233. Aubry, A., Cung, M.T. and Marraud, M., *J. Am. Chem. Soc.*, 107, 7640 (**1985**).

234. Bianco, A., Bertolini, T., Crisma, M., Valle, G., Toniolo, C., Maggini, M., Scorrano, G. and Prato, M., *J. Pept. Res.*, 50, 159 (**1997**).

235. Aubry, A., Protas, J., Boussard, M. and Marraud, M., *Acta Crystallogr. A*, 35, 694 (**1979**).

236. Venkataram Prasad, B.V. and Balaram, P., *Int. J. Biol. Macromol.*, 4, 99 (**1982**).

237. Venkataram Prasad, B.V., Shamala, N., Nagaraj, R., Chandrasekaran, R. and Balaram, P., *Biopolymers*, 18, 1635 (**1979**).

238. Aubry, A., Vitoux, B. and Marraud, M., *Biopolymers*, 24, 1089 (**1985**).

239. Görbitz, C.H., *Acta Crystallogr. A*, 45, 390 (**1989**).

240. Zimmerman, S.S., Pottle, M.S., Némethy, G. and Scheraga, H.A., *Macromolecules*, 10, 1 (**1977**).

241. Wüthrich, K., in "*NMR of Proteins and Nucleic Acids*", Wiley, New York, NY, (**1986**).

242. Siemion, I.Z., Wieland, T. and Pook, K.H., *Angew. Chem. Int. Edit.*, 14, 702 (**1975**).

243. Deber, C.M., Madison, V. and Blout, E.R., *Acc. Chem. Res.*, 9, 106 (**1976**).

244. Madalengoitia, J.S., *J. Am. Chem. Soc.*, 122, 4986 (**2000**).

245. Madison, V. and Kopple, K.D., *J. Am. Chem. Soc.*, 102, 4855 (**1980**).

246. Gierasch, L.M., Deber, C.M., Madison, V., Niu, C.-H. and Blout, E.R., *Biochemistry*, 20, 4730 (**1981**).

247. Woody, R.W., *Peptides, Polypeptides, and Proteins*, Wiley, Eds. Blout, E. R., Bovey, F. A.,Lotan, N., Goodman, M., New York, NY (**1974**), pp. 338-350.

248. Perczel, A. and Hollosi, M., *Circular Dichroism and the Conformational Analysis of Biomolecules*, Plenum Press, Ed. Fasman, G. D., New York, NY (**1996**), pp. 285-380.

249. Vass, E., Hollosi, M., Besson, F. and Buchet, R., *Chem. Rev.*, 103, 1917 (**2003**).

250. Sehgal, A., *Curr. Opin. Drug Discov. & Developm.*, 5, 245 (**2002**).

251. Bidwell, G.L. and Raucher, D., *Expert Opin. Drug Deliv.*, 10, 1033 (**2009**).

252. Raucher, D., Moktan, S., Massodi, I. and Bidwell, G.L., *Expert Opin. Drug Deliv.*, 10, 1049 (**2009**).

253. Danho, W., Swistok, J., Khan, W., Chu, X.-J., Cheung, A., Fry, D., Sun, H., Kurylko, G., Rumennik, L., Cefalu, J., Cefalu, G. and Nunn, P., *Adv. Exp. Med. Biol.*, 611, 467 (**2009**).

254. Abell, A.D., *Lett. Pept. Sci.*, 8, 267 (**2002**).

255. Smith, A.B.I., Hirschmann, R., Pasternak, A., Guzman, M.C., Yokoyama, A., Sprengeler, P.A., Darke, P.L., Emini, E.A. and Schleif, W.A., *J. Am. Chem. Soc.*, 117, 11113 (**1995**).

256. Kim, E.E., Baker, C.T., Dwyer, M.D., Murcko, M.A., Rao, B.G., Tung, R.D. and Navia, M.A., *J. Am. Chem. Soc.*, 117, 1181 (**1995**).

257. ten Brink, H.T., Rijkers, D.T.S., Kemmink, J., Hilbers, H.W. and Liskamp, R.M.J., *Org. Biomol. Chem.*, 2, 2658 (**2004**).

258. Tong, Y., Olczak, J., Zabrocki, J., Gershengorn, M.C., Marshall, G.R. and Moeller, K.D., *Tetrahedron*, 56, 9791 (**2000**).

259. Dekker, F.J., de Mol, N.J., Fischer, M.J.E., Kemmink, J. and Liskamp, R.M.J., *Org. Biomol. Chem.*, 1, 3297 (**2003**).

260. Flink, B.E., Kym, P.R. and Katzenellenbogen, J.A., *J. Am. Chem. Soc.*, 120, 4334 (**1998**).

261. Bijani, C., Varray, S., Lazaro, R., Martinez, J., Lamatya, F. and Kiefferb, N., *Tetrahedron Lett.*, 43, 3765 (**2002**).

262. Wei, Q., Harran, S. and Harran, P.G., *Tetrahedron*, 59, 8947 (**2003**).

263. Lambert, J.N., Mitchell, J.P. and Roberts, K.D., *J. Chem. Soc., Perkin Trans.*, 1, 471 (**2001**).

264. Hebach, C. and Kazmaier, U., *J. Chem. Soc., Chem. Commun.*, 596 (**2003**).

265. Scholtz, J.M., Qian, H., Robbins, V.H. and Baldwin, R.L., *Biochemistry*, 32, 9668 (**1993**).

266. Ghadiri, M.R. and Fernholz, A.K., *J. Am. Chem. Soc.*, 112, 9633 (**1990**).

267. Ruan, F., Chen, Y. and Hopkins, P.B., *J. Am. Chem. Soc.*, 112, 9403 (**1990**).

268. Camarero, J.A., Giralt, E. and Andrei, D., *Tetrahedron Lett.*, 7, 1137 (**1995**).

269. Galande, A.K., Trent, J.O. and Spatola, A.F., *Biopolymers*, 71, 534 (**2003**).

270. Fujimoto, K., Oimoto, N., K., K. and M., I., *J. Chem. Soc., Chem. Commun.*, 1280 (**2004**).

271. Grubbs, R.H., *Tetrahedron*, 60, 7117 (**2004**).

272. Grubbs, R.H. and Chang, S., *Tetrahedron*, 54, 4413 (**1998**).

273. Chatterjee, A.K., Morgan, J.P., Scholl, M. and Grubbs, R.H., *J. Am. Chem. Soc.*, 122, 3783 (**2000**).

274. Pschirer, N.G., Fu, W., Adams, R.D. and Bunz, U.H.F., *J. Chem. Soc., Chem. Commun.*, 87 (**2000**).

275. Biagini, S., Gibson, S.E. and Keen, S.P., *J. Chem. Soc., Perkin Trans.*, 1, 2485 (**1998**).

276. Gilliom, L.R. and Grubbs, R.H., *J. Am. Chem. Soc.*, 108, 733 (**1986**).

277. Hofmann, M., Puskas, J.E. and Weiss, K., *Eur. Polym. J.*, 38, 19 (**2002**).

278. Trnka, T.M., Morgan, J.P., Sanford, M.S., Wilhelm, T.E., Scholl, M., Choi, T.-L., Ding, S., Day, M.W. and Grubbs, R.H., *J. Am. Chem. Soc.*, 125, 2546 (**2003**).

279. Melis, K., De Vos, D., Jacobs, P. and Verpoort, F., *J. Mol. Catal. A: Chem.*, 169, 47 (**2001**).

280. Fürstner, A. and Ackermann, L., *J. Chem. Soc., Chem. Commun.*, 95 (**1999**).

281. Hoveyda, A.H. and Zhugralin, A.R., *Nature*, 450, 243 (**2007**).

282. Aldhart, C. and Chen, P., *J. Am. Chem. Soc.*, 126, 3496 (**2004**).

283. Yamamoto, K., Biswas, K., Gaula, C. and Danishefskya, S.J., *Tetrahedron Lett.*, 44, 3297 (**2003**).

284. Thanh, G.V. and Loupy, A., *Tetrahedron Lett.*, 44, 9091 (**2003**).

285. Kotha, S., Sreenivasachary, N., Mohanraja, K. and Durani, S., *Bioorg. Med. Chem. Lett.*, 11, 1421 (**2001**).

286. Osipov, S.N. and Dixneuf, P., *Russ. J. Org. Chem.*, 39, 1211 (**2003**).

287. Hammer, K., Romming, C. and Undheim, K., *Tetrahedron*, 54, 10837 (**1998**).

288. Tjen, K., Kinderman, S.S., Schoemaker, H.E., Hiemstra, H. and Rutjes, F.P.J.T., *J. Chem. Soc., Chem. Commun.*, 699 (**2000**).

289. Conde-Frieboes, K., Andersen, S. and Breinholt, J., *Tetrahedron*, 41, 9153 (**2000**).

290. Piscopio, A.D., Miller, J.F. and Koch, K., *Tetrahedron*, 55, 8189 (**1999**).

291. Pernerstorfer, J., Schuster, M. and Blechert, S., *J. Chem. Soc., Chem. Commun.*, 1949 (**1997**).

292. Chapman, R.N., Dimartino, G. and Arora, P.S., *J. Am. Chem. Soc.*, 126, 12252 (**2004**).

293. Qian, H. and Schellman, J.A., *J. Phys. Chem. A*, 96, 3987 (**1992**).

294. Prabhakaran, E.N., Rajesh, V., Dubey, S. and Iqbal, J., *Tetrahedron Lett.*, 42, 339 (**2001**).

295. Blackwell, H.E. and Grubbs, R.H., *Angew. Chem. Int. Ed. Engl.*, 37, 3281 (**1998**).

296. Walensky, L.D., Kung, A.L., Escher, I., Malia, T.J., Barbuto, S., Wright, R.D., Wagner, G., Verdine, G.L. and Korsmeyer, S.J., *Science*, 305, 1466 (**2004**).

297. Zhang, H., Zhao, Q., Bhattacharya, S., Waheed, A.A., Tong, X., Hong, A., Heck, S., Curreli, F., Goger, M., Cowburn, D., Freed, E.O. and Debnath, A.K., *J. Mol. Biol.*, 378, 565 (**2008**).

298. Boal, A.K., Guryanov, I., Moretto, A., Crisma, M., Lanni, E.L., Toniolo, C., Grubbs, R.H. and O'Leary, D.J., *J. Am. Chem. Soc.*, 129, 6986 (**2007**).

299. Chothia, C., Levitt, M. and Richardson, D., *Proc. Natl. Acad. Sci. USA*, 74, 4130 (**1977**).

300. Bowie, J.U., *J. Mol. Biol.*, 272, 780 (**1997**).

301. Hill, R.B., Raleigh, D.P., Lombardi, A. and DeGrado, N.F., *Acc. Chem. Res.*, 33, 745 (**2000**).

302. Hol, W.G.J., Vanduijnen, P.T. and Berendsen, H.J.C., *Nature*, 273, 443 (**1978**).

303. Karle, I.L., Flippen-Anderson, J.L., Uma, K. and Balaram, P., *Biopolymers*, 33, 827 (**1993**).

304. Marshall, G.R., Hodgkin, E.E., Lang, D.A., Smith, G.D., Zabrocki, J. and Leplawy, M.T., *Proc. Natl. Acad. Sci. USA*, 87, 487 (**1990**).

305. Fuqua, C. and Greenberg, P., *Nature Rev. Mol. Cell Biol.*, 3, 685 (**2002**).

306. Li, P., Evans, C.D., Wu, Y., Cao, B., Hamel, E. and Joullié, M.M., *J. Am. Chem. Soc.*, 130, 2351 (**2008**).

307. Kuwahara, M., Arimitsu, M. and Sisido, M., *J. Am. Chem. Soc.*, 121, 256 (**1999**).

308. Wolfe, S., Wilson, M.-C., Cheng, M.-H., Shustov, G.V. and Akuche, C.I., *Can. J. Chem.*, 81, 937 (**2003**).

309. Ozinskas, A.J. and Rosenthal, G.A., *J. Org. Chem.*, 51, 5047 (**1986**).

310. Sugano, H. and Miyoshi, M., *J. Org. Chem.*, 41, 2352 (**1976**).

311. Dale, J.A., Dull, D.L. and Mosher, H.S., *J. Org. Chem.*, 34, 2543 (**1969**).

312. Presser, A. and Hufner, A., *Monat. Chem.*, 135, 1015 (**2004**).

313. Hanessian, S., Yang, G., Rondeau, J.-M., Neumann, U., Betschart, C. and Tintelnot-Blomley, M., *J. Med. Chem.*, 49, 4544 (**2006**).

314. Honda, T., Namiki, H., Kaneda, K. and Mizutani, H., *Org. Lett.*, 6, 87 (**2004**).

315. Haight, A.R., Stoner, E.J., Peterson, M.J. and Grover, V.K., *J. Org. Chem.*, 68, 8092 (**2003**).

316. Schmidt, B. and Nave, S., *Adv. Synth. Catal.*, 348, 531 (**2006**).

317. Houlihan, F., Bouchard, F. and Fréchet, J.M.J., *Can. J. Chem.*, 63, 153 (**1985**).

318. Neises, B. and Steglich, W., *Angew. Chem. Int. Ed. Engl.*, 17, 522 (**1978**).

319. Connel, E., Dixon, G.H. and Hones, C.S., *Can. J. Biochem. Physiol.*, 33, 416 (**1985**).

320. Lakhani, A., Malon, P. and Keiderling, T.A., *Appl. Spectrosc.*, 63, 775 (**2009**).

Ringraziamenti

Ringrazio la possibilità di fare questi ringraziamenti, le opportunità ricevute, le persone vicine e le risorse impiegate per essere giunto sino ad oggi a quello che sono.
Ringrazio la Chimica e in particolar modo la Chimica Organica, che bene ha saputo incarnare la mia idea di disciplina scientifica, coniugando all'astrazione della meccanica quantistica la concreta possibilità di architettare meravigliose strutture e scoprire nuove proprietà secondo princìpi e reazioni che continuano a destare in me profondo stupore.
Ringrazio il mio relatore, prof. Claudio Toniolo, che mi ha concesso di svolgere questi tre anni nei suoi laboratori e senza il quale non avrei avuto la possibilità di fare un'esperienza all'estero che ha contribuito a cambiare la mia prospettiva sul mondo.
Ringrazio il prof. Fernando Formaggio, per gli incoraggiamenti e il vivo interesse dimostrato, mai scontato e sempre opportuno.
Un sentito ringraziamento va a tutti coloro che hanno reso incancellabile la mia esperienza negli Stati Uniti: il prof. R.H. Grubbs, che mi ha ospitato nei suoi laboratori, il prof. D.J. O'Leary, che mi ha fatto passare un periodo stupendo in California senza essere un semplice turista e il prof. W.E. Steinmetz, che mi ha ospitato dimostrando una generosità non comune.
Ringrazio il dott. Alessandro Moretto per la sua carismatica presenza; un grazie di cuore va anche alla D.ssa Marta De Zotti, per l'incredibile disponibilità nei momenti piu' difficoltosi (sia per me che per lei).
Ringrazio quanti mi sono stati d'aiuto in laboratorio, e quanti si sono dimostrati buoni compagni in questi anni rendendoli una fase indimenticabile della mia vita.
Ringrazio i miei genitori, la mia famiglia ed i miei parenti più stretti, vicini e lontani, fondamenta del mio essere e del mio carattere, per aver creduto in me e avermi formato senza mai chiedermi niente in cambio, alla quale devo così tanto che sarebbe impossibile renderne giustizia in queste poche righe. Semplicemente, grazie.
Ringrazio i miei amici per i momenti felici, la spensieratezza, la disponibilità, gli scambi di opinioni, tanto nell'apollineo quanto nel dionisiaco.